Pavol Jozef Šafárik University in Košice
Faculty of Science

Charles University
Faculty of Mathematics and Physics

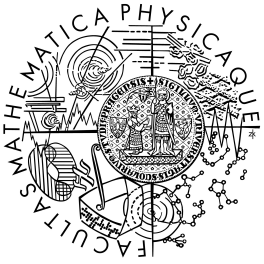

Multi-frequency research of symbiotic binaries

PhD Thesis

Prague 2022 RNDr. Jaroslav Merc

Pavol Jozef Šafárik University in Košice
Faculty of Science

Charles University
Faculty of Mathematics and Physics

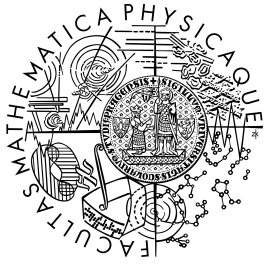

Multi-frequency research of symbiotic binaries

PhD Thesis

Field of study: Astrophysics

Supervisors: doc. RNDr. Rudolf Gális, PhD., doc. RNDr. Marek Wolf, CSc.

Prague 2022 RNDr. Jaroslav Merc

Acknowledgments

PhD is an exciting period for an early career researcher, full of new challenges. There are a few people I would like to express my gratitude to as they helped me to achieve the results presented in this thesis. Let me thank...

To both supervisors of my PhD studies, Rudolf Gális and Marek Wolf for their help, valuable advice, comments on the text of the thesis, and successful cooperation on many interesting projects. I want to emphasize at this point that thanks to their approach I have always felt like an equal colleague. This, up to my knowledge, cannot be said by all my fellow PhD students at other institutes worldwide.

To all my coauthors and collaborators for their valuable input and contribution to the projects. Especially let me thank Laurits Leedjärv and Joanna Mikołajewska who invited me to stay at their institutes and I learned a lot from them.

To the observers, professional and amateur, who contributed valuable data to this thesis. Especially I would like to thank François Teyssier for coordinating the ARAS Eruptive Star Section.

To Peter Velez, who not only observed many of my targets, and offered me to use his private telescope, but also has read the drafts of many of my papers and improved their English level.

To Tom Petit and 2SPOT team, for quick responses to my alerts for observing campaigns, sharing their observational setup with me, and for becoming my friends.

To my office mates and colleagues, especially Jan Kára and Kateřina Chrbolková, and many others for creating a good, lively working environment and making working days more enjoyable by discussing virtually everything and organizing tea parties.

To my wife Veronika, for her support, understanding, and listening to me when I needed it most. Without her and the environment she creates at home, I would never have achieved successes that I could be proud of. I realize that living with a scientist is not always easy, science is usually not done only during 'normal' working hours and sometimes one is away from home for a few days.

This work was supported by *Charles University*, project GA UK No. 890120, the internal grants VVGS-PF-2019-1047 and VVGS-PF-2021-1746 of the *Faculty of Science, P. J. Šafárik University in Košice*, and the Slovak Research and Development Agency under contracts No. APVV-15-0458 and No. APVV-20-0148.

Abstract

Symbiotic stars are among the widest interacting binaries. They consist of a late-type, cool giant and a hot component, which is typically a white dwarf or in a few cases a neutron star. The presented thesis summarizes all the relevant information on the symbiotic binaries, including both components of systems, their activity, and other manifestations of variability. Symbiotic systems are presented as unique astrophysical laboratories in the study of stellar evolution, mass transfer and its accretion, stellar winds, jets, and other physical processes.

A part of the thesis presents the New Online Database of Symbiotic Variables, a modern, complex, and most up-to-date catalog of these binaries that currently contains more than 1 000 objects in the Milky Way and another 16 galaxies. At the same time, the Database constitutes the most comprehensive collection of orbital, stellar, and observational parameters of all known symbiotic binaries. These data are studied in detail in order to better understand the symbiotic population.

From the Database, poorly characterized symbiotic candidates have been selected and studied on the basis of new and archival observational data and information from the literature. A substantial sample of 47 symbiotic candidates from the literature and 3 newly discovered objects located in our Galaxy, Large Magellanic Cloud, M31, and NGC 2403 have been analyzed. Twelve objects have been confirmed as symbiotic stars in the scope of this work, including three 'slow' symbiotic novae. Additional six are classified as possible symbiotic binaries. Notably, the discovery and characterization of the first galactic and first extragalactic symbiotic stars discovered by the *Gaia* satellite are presented. Another object is classified as the first galactic recurrent 'slow' symbiotic nova.

Keywords: binaries: symbiotic – techniques: photometric, spectroscopic – catalogs

Abstrakt

Symbiotické systémy patria medzi najrozsiahlejšie interagujúce dvojhviezdy. Tieto premenné hviezdy sa skladajú z vyvinutého chladného obra a horúcej zložky, ktorou je typicky biely trpaslík, v niekoľkých prípadoch neutrónová hviezda. Predložená práca sumarizuje všetky relevantné informácie o symbiotických dvojhviezdach, vrátane informácii o oboch zložkách systémov, ich aktivite a ďalších prejavoch premennosti. Symbiotické systémy sú predstavené ako unikátne astrofyzikálne laboratória pre štúdium hviezdnej evolúcie, prenosu a akrécie hmoty, hviezdnych vetrov, výtryskov hmoty a ďalších fyzikálnych procesov.

Časť práce predstavuje Novú online databázu symbiotických premenných hviezd, moderný, komplexný a aktuálny katalóg týchto dvojhviezd, ktorý v súčasnosti obsahuje viac ako 1000 objektov v Mliečnej ceste a ďalších 16 galaxiách. Databáza zároveň predstavuje najkomplexnejšiu kolekciu orbitálnych, stelárnych aj pozorovacích parametrov všetkých známych symbiotických hviezd. Tieto údaje sú detailne študované za účelom lepšieho porozumenia symbiotickej populácii.

Z databázy sú vybraní nedostatočne charakterizovaní symbiotickí kandidáti, ktorí sú podrobení detailnej analýze na základe nových a archívnych pozorovacích dát a informácií z literatúry. Prezentované sú výsledky štúdia významnej vzorky 47 symbiotických kandidátov a 3 novoobjavených objektov z našej Galaxie, Veľkého Magellanovho mraku a z galaxií M31 a NGC 2403. Je potvrdená symbiotická povaha 12 objektov, vrátane troch symbiotických nov. Ďalších šesť študovaných objektov je pravdepodobne symbiotických. Významným prezentovaným výsledkom je objav a charakterizácia prvej galaktickej a prvej extragalaktickej symbiotickej hviezdy objavenej satelitom *Gaia*. Ďalší objekt je klasifikovaný ako prvá galaktická rekurentná „pomalá“ symbiotická nova.

Kľúčové slová: symbiotické dvojhviezdy – fotometria, spektroskopia – katalógy

Contents

List of Figures

List of Tables

Introduction

Symbiotic stars belong to the group of widest interacting binaries in which the physical processes associated with the transfer of matter cause significant manifestations across an extensive interval of the electromagnetic spectrum. The components of these binaries are ultimately different - cool, evolved giant on one side, and very hot, luminous white dwarf or even neutron star on the other. Since the beginning of this century, a systematic search for symbiotics has begun, not only in the Milky Way but also in the Local Group of galaxies, and has already led to the discovery of many new objects. Despite the great effort of several research groups, many questions connected with various aspects of the symbiotic phenomenon remain open until now.

The present PhD thesis has three main goals. The first is to collect and summarize published information on all known symbiotic systems and candidates and process them into a comprehensive database that will replace outdated catalogs from the beginning of this century. This will allow systematic and statistical research of the symbiotic population. For this reason, the second task is to analyze the orbital, stellar and observational characteristics of known symbiotic stars in order to understand their position among other variable stars, recognize common patterns leading to the symbiotic phenomenon, and uncover the relations between the parameters of the components and their activity. Finally, on the basis of the catalog, poorly studied symbiotic systems and especially the candidates (primarily in our Galaxy and Magellanic Clouds) will be selected. These objects will be subjected to comprehensive research using archival and new multi-frequency photometric and spectroscopic data in order to confirm or reject their symbiotic nature and characterize their components. In this way, the number of confirmed symbiotic binaries will increase and a clean sample of these variable stars will be available for subsequent research.

The thesis is structured as follows. In Chapter 1, a theoretical background that summarizes all the relevant knowledge on symbiotic binaries necessary for the study of the parameters of these binaries, and for understanding their variability on vari-

ous timescales in different parts of the electromagnetic spectrum is presented. This includes a short historical overview, a detailed discussion on both stellar components and a nebula, the definition of symbiotic binaries, their quiescent and outburst variability and provides also information on the evolution of these objects. The text is supplemented by the original figures illustrating various phenomena typical for symbiotic stars.

Chapter 2 introduces the New Online Database of Symbiotic Variables, the most up-to-date catalog of symbiotic binaries. Its structure and content are described in detail. This is followed by a discussion on the size of the galactic and extragalactic symbiotic population. The catalog represents the most comprehensive collection of the orbital, stellar, and other observational parameters of the symbiotic stars ever published. Extensive analysis of the orbital periods, eccentricities of the orbits, and detection of the eclipses is presented, together with the in-depth investigation of the parameters of the cool and hot symbiotic components (their spectral types, effective temperatures, luminosities, metallicities, masses, pulsations, etc.). In addition, infrared types and X-ray emission of symbiotic stars are studied. Part of this chapter is devoted to the activity of these systems, and a model of a possible relation between various types of the symbiotic phenomenon is suggested. Finally, data on symbiotic stars presented very recently in the *Gaia* Data Release 3 are analyzed as well.

In Chapter 3, a comprehensive analysis of the symbiotic candidates selected from the New Online Database of Symbiotic Variables is presented. The first part discusses candidates on classical (Z And-type) symbiotic binaries. In the second section, objects suggested to be 'slow' symbiotic novae are studied. The final part of the chapter presents the results on all candidate symbiotic stars located in the Large Magellanic Cloud. All-together, 47 individual objects are analyzed in detail in this part of the thesis.

Chapter 4 presents the results obtained using the tools developed for the study of symbiotic candidates applied to three newly discovered objects: Gaia18aen, Hen 3-860, and DeGaPe 35. The final chapter of the thesis summarizes the accomplished outcomes and discusses their impacts on the understanding of the symbiotic population.

Chapter 1

Symbiotic binaries

Symbiotic variables are strongly interacting binary systems consisting of a cool evolved star and a hot component in which the physical mechanisms related to the transfer and accretion of matter usually cause some observable activity (e.g., Allen 1984b; Kenyon & Webbink 1984; Kenyon 1986; Mikołajewska 2007). Both the light curves and the spectra of these variable stars are complex. The investigation of these objects requires long-term monitoring as all symbiotic systems are open detached (or semi-detached) binaries with orbital periods of hundreds to thousands of days (e.g., Mürset & Schmid 1999; Belczyński et al. 2000; Gromadzki et al. 2013, Chapter 2.3). Their active stages can last for years. Moreover, several other processes can also contribute to the complexity of the light curves, such as eclipses, ellipsoidal and reflection effects, the intrinsic variation of both components, or flickering. All of these manifest on the various timescales from minutes to years (see Chapter 1.4). Thanks to their properties, symbiotic stars can serve as unique astrophysical laboratories for studying accretion processes, winds, jets, or thermonuclear outbursts. Moreover, they are important for evolutionary models as they may be one of the type Ia supernova progenitors (see Chapter 1.5).

1.1 Historical overview

A brief look at the beginning of the research on symbiotic systems is not only interesting but also important, as it results in some observational biases that persist, partly to these days. Sudden changes in the brightness (so-called outbursts) of symbiotic variable stars (not distinguished as a specific group at that time) had already been noted in the early 20^{th} century. For example, the photometrical variability of the

prototype of classical symbiotic stars with repetitive outbursts Z And was discovered in 1901 by Williamina Fleming (Pickering et al. 1901; Cannon et al. 1911).

At the beginning of 20^{th} century, several objects, later classified as symbiotic stars, were discovered in the scope of the work on the spectroscopic catalogs of stars (based on the objective prism photographic observations). While most of the observed targets showed simple stellar spectra, several stars with peculiar spectra were identified (e.g., Fleming & Pickering 1912; Cannon 1920). These were divided into several groups. For the present discussion, the most important are those, whose spectra resembled cool (red) giants, but in which the presence of emission lines (of hydrogen, helium, and unidentified nebular lines at that time) and a faint blue continuum pointed to the existence of a hotter source. The simultaneous presence of low- (demonstrated especially by TiO bands) and high-temperature sources (e.g., He II emission line at 4868 Å) gave the name to these objects – 'stars with the combination spectra'[1].

Several such objects had been discovered and analyzed in detail in the following years (e.g., R Aqr, RX Pup, RS Oph, Y CrA, CI Cyg, RW Hya, AX Per; Merrill 1919, 1933; Cannon & Shapley 1923; Merrill & Humason 1932). Z And was also very quickly included to this group of stars (Hogg 1932). These discoveries increased the interest in such objects.

It was Merrill who used the term 'symbiotic stars' for the first time while presenting his research during the American Astronomical Society meeting at Yerkes Observatory in 1941 (Merrill 1958). Later, Bidelman (1954) listed 23 'stars with the combination spectra' in his catalog, Gaposchkin (1957) included 32 objects to the group of symbiotic stars, while Boyarchuk (1969) listed 21 confirmed and 16 suspected symbiotic stars in his report. All of them were included in this group of objects based on their spectroscopic appearance (the combination spectrum; i.e., the cool continuum and strong emission lines) and/or their photometric behavior (especially prominent outbursts, nova-like activity).

Many new symbiotic stars had been identified in the seventies and eighties. Several discoveries had been made on the objective prism plates (e.g., Sanduleak & Stephenson 1973; Allen 1978). In many objects, which had been previously classified as planetary nebulae (typically due to the detection of strong emission lines), the observations in the infrared suggested the presence of cool stellar sources (e.g., Allen 1973, 1974; Allen

[1]This should not be mistaken with the stars described as showing 'composite spectra'. This denotation was originally used by Annie Jump Cannon (1863 – 1941) at Harvard Observatory to describe the spectra composed of two nearly normal separate stars (Merrill 1958).

& Glass 1974; Webster & Allen 1975). Later, higher resolution optical spectra confirmed the presence of cool giants in many of these objects with prominent emission lines (e.g., Allen 1984a; Acker et al. 1987). In addition, in several assumed planetary nebulae, strongly variable central stars had been identified (Bond 1976). Such behavior naturally marked them suspicious, which eventually led to the discovery of the symbiotic nature of some of them. As a result, the number of known symbiotic stars grew substantially. The catalog of symbiotic stars by Allen (1984a) contained 129 confirmed and 15 suspected symbiotic stars (of which 6 were extragalactic). Another one, published by Kenyon (1986) was the compilation of 133 known symbiotic stars and 20 stars suspected of being symbiotic. Vaidis (1988, 1991) included 176 objects among confirmed symbiotic stars and another 23 as possible symbiotics.

These discoveries were naturally accompanied by attempts to reveal the nature of symbiotic stars and to explain their photometric (occasional brightenings, regular variability) and spectroscopic (changes in spectral appearance during outbursts, i.e., brightening of the blue continuum, disappearance of the high excitation emission lines, P Cygni profile formation, etc.) behavior. All the advances created a renewed interest in symbiotic stars, which was further supported by the first scientific conference (Friedjung & Viotti 1982) and the first monograph (Kenyon 1986) devoted specifically to this group of variable stars.

Until 2019, the last published catalog (Belczyński et al. 2000) contained 188 confirmed symbiotic systems as well as 30 objects suspected of being symbiotic, including 17 objects beyond the Galaxy. However, over the past two decades, the number of confirmed systems has more than doubled, and many dozens of new candidates have emerged. Many of these discoveries were driven by the narrow-band Hα photometric observations. The specialized surveys searching for symbiotic stars focused not only on the galactic symbiotic stars (e.g., Corradi et al. 2008, 2010; Miszalski et al. 2013; Miszalski & Mikołajewska 2014; Rodríguez-Flores et al. 2014), but also identified new extragalactic symbiotic variables or at least promising candidates (e.g., Gonçalves et al. 2008, 2012, 2015; Kniazev et al. 2009; Mikołajewska et al. 2014a, 2017; Magrini et al. 2017; Roth et al. 2018; Ilkiewicz et al. 2018; Saeedi & Sasaki 2020, 2022).

Recently, a new census of symbiotic stars in the 2MASS, *WISE* and *Gaia* surveys was published by Akras et al. (2019a). The authors presented the list of 323 known and 87 candidate symbiotic stars. However, they did not collect all available data on individual objects, as they focused mainly on the temperatures and IR types of symbiotic binaries. They also discussed in detail the presence of the Raman-scattered

O VI lines in their spectra. At the same time, to fulfill the demand for a new full-scale catalog of symbiotic stars, we presented the New Online Database of Symbiotic Variables (Merc et al. 2019b), which is described in more detail in Chapter 2.

Symbiotic models. Already in the thirties of the 20th century, the first hypotheses trying to explain the 'combination spectra' of symbiotic stars appeared. There were basically two groups of mutually exclusive theories: binary models (e.g., Berman 1932; Kuiper 1941) and single star alternatives (e.g., Menzel 1946; Aller 1954; Sobolev 1960). The binary models consisted of a late-type, cool giant and a companion, either a faint O- or B-type star (Berman 1932), a normal main-sequence star (Kuiper 1941), a compact star with a high temperature, similar to the central stars of planetary nebulae (Boyarchuk 1969; Kenyon & Webbink 1984), or an accretion disk surrounding a low mass white dwarf or a main-sequence star (Kenyon & Webbink 1984).

Single star models were developed especially for the objects in which no periodical variations (expected for binaries) have been detected. A variety of the models was proposed, e.g., an evolved long-period variable with a condensed stellar core as a source of the emission lines and a cool atmosphere as a source of absorption features (Menzel 1946; Sobolev 1960), a very active coronal or chromospheric region surrounding a normal giant star (e.g., Aller 1954; Bruce 1955) or even a large stellar spot with the associated magnetic activity in the atmosphere of the giant (Oliversen et al. 1980).

However, subsequent observations, especially high-resolution spectra and satellite observations in UV ruled out most of these models. Nowadays, it is believed that all symbiotic stars are binaries as the single star models cannot explain the observational data of any well-examined symbiotic star. Moreover, in spite of the initial difficulties due to the long orbital periods of symbiotic binaries, at present, there are also direct pieces of evidence of the binary nature of many individual systems (e.g., the measurements of radial velocities of the components, observations of eclipses, multi-wavelength spectral energy distributions (SEDs), and in the case of R Aqr even the direct images of both components; Schmid et al. 2017).

1.2 Components of symbiotic systems

In the previous chapter, the historical development of the symbiotic model is discussed. Nowadays, the generally accepted model is a binary one, consisting of two stellar components - a cool evolved star which is a donor of the matter, and a hot component,

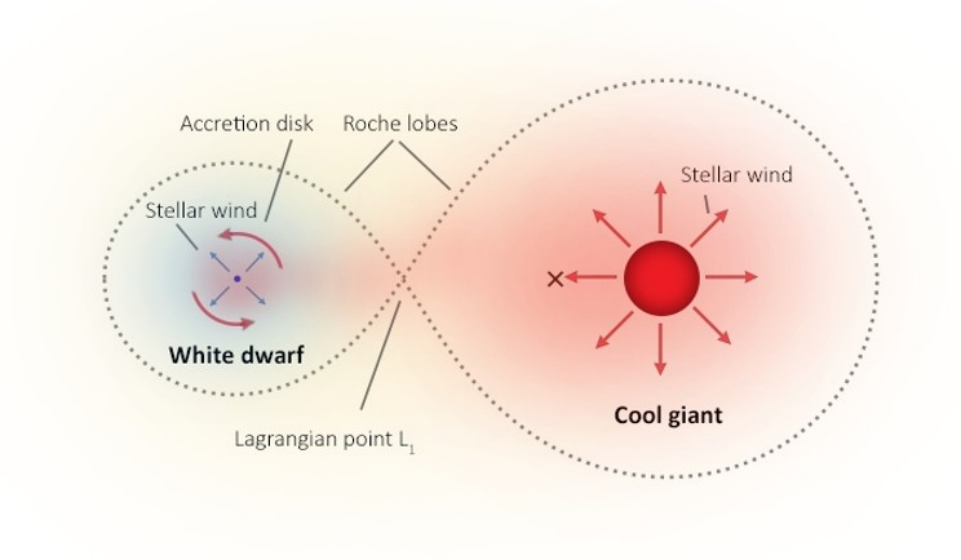

Figure 1.1: Simplified model of the symbiotic system consisting of a white dwarf as an acrretor a the cool giant as a donor of matter.

in most cases white dwarf as the accretor. The schematic model of such a binary is shown in Fig. 1.1. Long-term observations - photometrical and spectroscopical in various spectral regions - allowed to characterize the components in several symbiotic systems and the general properties are discussed in the following chapters. A factor complicating all analyses of the individual components is the fact that the observed SED is not a convolution of only two stellar components. An important contributor to the spectrum of symbiotic stars is also a dense circumbinary nebula, which is produced by mass loss of the giant and ionized by the hot component. In some symbiotic systems with more evolved cool components (Mira variables), the emission of the dust can also contribute significantly to the observed SED. The spectral regions where all the before-mentioned components dominate are shown in Fig. 1.2A.

1.2.1 Cool components

According to the generally accepted model, the cool components of symbiotic binaries are evolved stars - late-type giants (or bright giants, maybe even supergiants) of a spectral type M, with the predominant spectral types M3 – M6 and a peak at M5 in *S-type symbiotic systems* (see below) and M6 – M7 in symbiotic Miras (Mürset & Schmid 1999; Mikołajewska 2007, Chapter 2.4). There is also a small distinct group of so-called *yellow symbiotic stars*, in which K or even G giants are observed (e.g., AG Dra, LT Del).

While previously it was claimed that most of the M giants in symbiotic systems be-

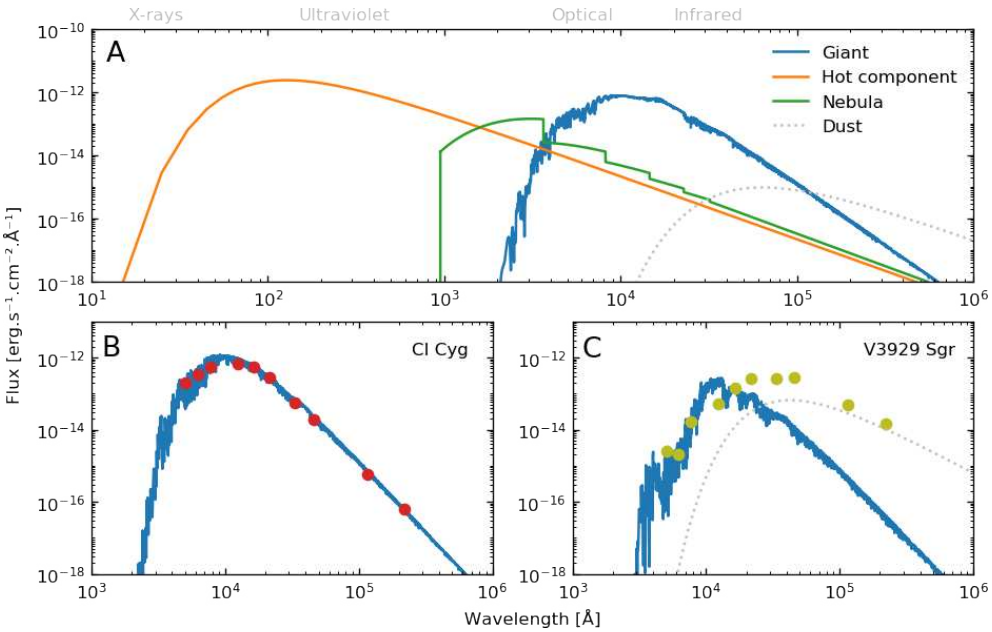

Figure 1.2: SEDs of shell-burning symbiotic stars. **A:** Radiation sources observed in the symbiotic spectrum (see Chapter 1.2). A hot component (orange line) is dominating in the X-rays and ultraviolet, a nebular radiation (shown in green) in ultraviolet and optical, and a cool giant (blue color) in optical and infrared. D-type symbiotics (see Chapter 1.2.1) show additional radiation in far-infrared caused by the warm dust (dotted gray line). **B:** Comparison of the fluxes from *Gaia* ($G_{\rm BP}$, G, $G_{\rm RP}$), 2MASS (*J, H, K*) and *WISE* (*W1, W2, W3, W4*) observations of CI Cyg (S-type symbiotic; Chapter 1.2.1) with the spectrum of normal M4 giant (Husser et al. 2013). **C:** Comparison of the fluxes from the same satellites as in panel B for D-type symbiotic star V3929 Sgr and the spectrum of normal M7 giant (Husser et al. 2013). The IR excess caused by the warm dust emission is clearly visible.

long to the metal-rich population (Whitelock & Munari 1992), more recent abundance analyses suggest that most of them are of solar or even slightly sub-solar metallicity (e.g., Mikołajewska et al. 2014b; Gałan et al. 2015, 2016, 2017, Chapter 2.4). In contrast, K giants in *yellow symbiotic binaries* are usually metal-poor (e.g., Pereira et al. 2017, and references therein; Chapter 2.4) and G giants in *D'-type symbiotic systems* (see below) are approximately of the solar metallicity (e.g., Mikolajewska et al. 2006, Chapter 2.4). Interestingly, the giants in the Magellanic Clouds are more often C-rich (carbon stars), as opposed to galactic O-rich (spectral type M) giants (e.g., Angeloni et al. 2014). This is related to the lower overall metallicity of the Magellanic Clouds. Also in our Galaxy one can find some symbiotic systems with carbon cool components or some whose cool components are classified as S stars (with an approximately equal proportion of carbon and oxygen in the photosphere and showing typical ZrO bands).

The giants dominate the spectrum of symbiotic stars at longer wavelengths, in optical and especially infrared regions (Fig. 1.2). Their presence is revealed by the prominent absorption features: molecular bands of TiO, CN, CO, VO, H_2O and

spectral lines of Ca, Na, or Fe (Fig. 1.3).

Infrared types. Different types of symbiotic binaries are distinguished depending on the giant's position in the near-infrared color-color diagram (H-K vs. J-H, see also Fig. 2.12 showing the diagram based on the up-to-date data from our New Online Database of Symbiotic Variables; Merc et al. 2019b):

- **S-type (stellar)** symbiotic stars are characterized by near-infrared temperatures of $\sim$ 3000 – 4000 K corresponding to the photosphere temperatures of normal M, K, or G giants (e.g., Webster & Allen 1975; Mikołajewska 2003). Usually, S-type symbiotic systems have a peak in their SEDs at 0.8 – 1.7 μm, with most of them being concentrated at 1.0 – 1.1 μm (Ivison et al. 1995; Akras et al. 2019a). Comparison of the optical-infrared SED of the S-type symbiotic star CI Cyg with the spectrum of M4 giant is shown in Fig. 1.2B. Typical optical spectra of four S-type symbiotic systems (two with K giants and two with M giants) are shown in Fig. 1.3A.

  The cool components of S-type symbiotic stars are usually RGB or AGB stars showing semi-regular pulsations (e.g., Gromadzki et al. 2007, Chapter 2.4), and their spectral types cluster around M3 – M6 with a peak at M5 (Mürset & Schmid 1999; Mikołajewska 2007, Chapter 2.4). Their orbital periods are typically $\leq$ 15 years, with most of them being in the interval of $\sim$ 200 – 600 days. Within the known symbiotic systems, up to 80% are of the S-type (Belczyński et al. 2000; Akras et al. 2019a, Chapter 2.4).

- **D-type (dusty)** symbiotic stars usually accommodate very evolved, pulsating variable stars of the Mira type, usually of spectral types M6 – M7 with pulsation periods $\sim$ 300 — 600 days (e.g., Whitelock 1987; Gromadzki et al. 2009, Chapter 2.4). They are surrounded by optically thick dust envelopes (e.g., Whitelock 2003; Mikołajewska 2012) causing the near-IR temperatures to be $\sim$ 700 – 1 000 K (e.g., Allen 1982). The peak in their SEDs is shifted to the longer wavelength $\sim$ 2 – 4 μm, with high occurrence between 2 and 2.5 μm (Akras et al. 2019a). Some D-types show two dust components (Angeloni et al. 2010), corresponding to two dust shells with different temperatures. Comparison of the optical-infrared SED of the D-type symbiotic star V3929 Sgr and M7 giant spectrum is shown in Fig. 1.2C. The IR excess caused by the warm

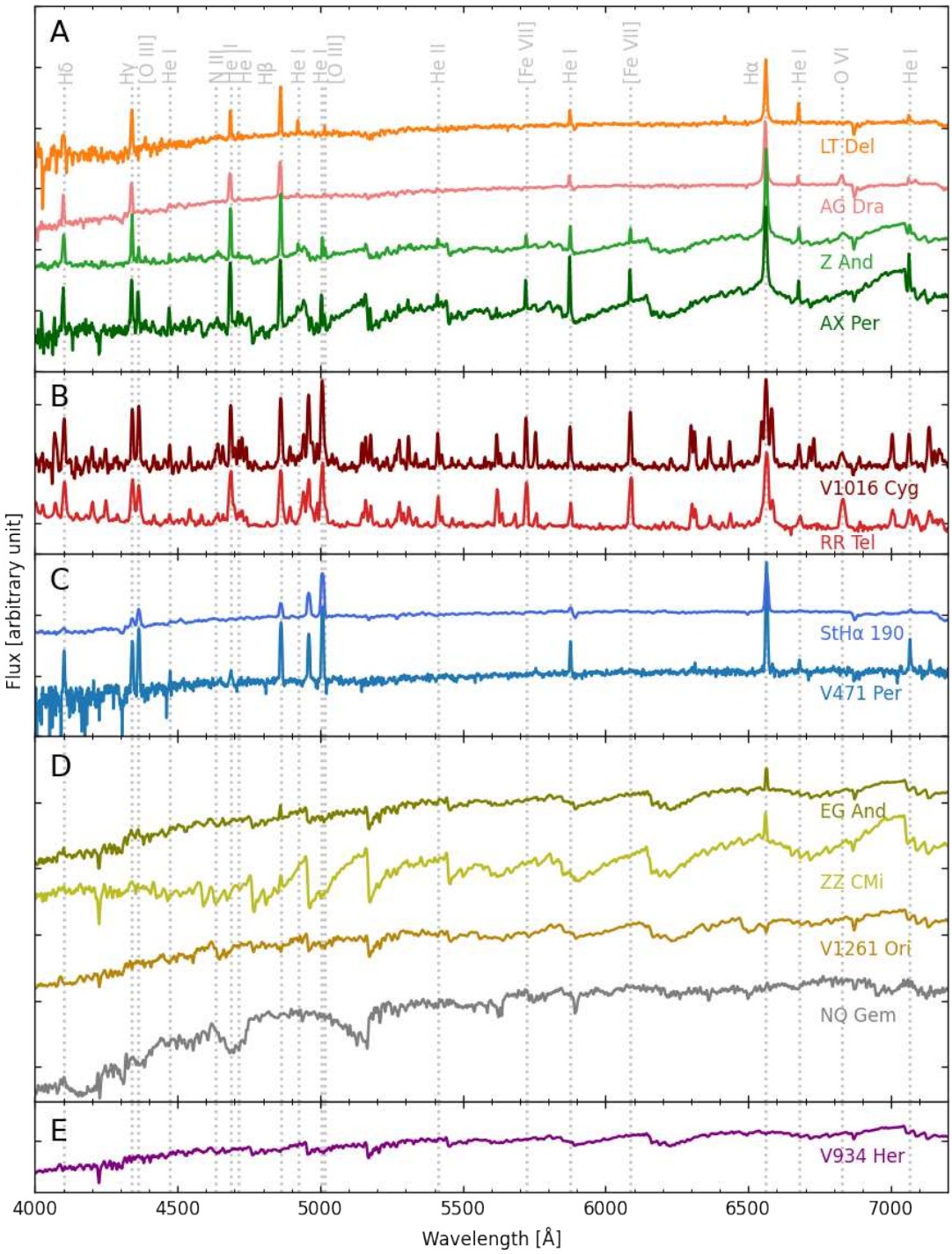

Figure 1.3: Spectra of symbiotic binaries. **A:** Quiescent spectra of shell-burning S-type symbiotic binaries - LT Del, AG Dra (yellow symbiotic stars) and Z And, AX Per (cool components are M giants). **B:** Quiescent spectra of shell-burning D-type symbiotic systems V1016 Cyg and RR Tel. **C:** Quiescent spectra of shell-burning D'-type symbiotic stars StHα 190 and V471 Per. **D:** Spectra of accreting-only white dwarf symbiotic stars - EG And, ZZ CMi (M giant cool component), V1261 Ori (S star), NQ Gem (C-rich cool component). **E:** Spectrum of accreting-only symbiotic star V934 Her hosting a neutron star accretor. Spectra were obtained from the ARAS database (see Appendix A; Teyssier 2019). Identification of prominent emission lines observed in S-type shell-burning symbiotic stars is given by the vertical dotted lines.

dust emission is clearly visible in this comparison. Typical optical spectra of two D-type symbiotics are shown in Fig. 1.3B.

In order to allow the dust formation in these systems, the separation of components should be larger than the dust formation radius (in general > 5 R_{Mira}), and therefore these symbiotic stars have much longer periods (even tens of years) than that of the S-type systems. D-types often have very extensive ionized nebulae and show strong highly-ionized emission lines. Although evolutionary models predict a larger population of D-type symbiotic stars, they are more difficult to detect in comparison with S-type ones, and therefore they make up less than 15% of all known symbiotic systems (Akras et al. 2019a).

- **D'-type** symbiotic stars, introduced by Allen (1982), show a dusty component with even lower temperatures than that of the D-type, with a peak in their SEDs at $\sim$ 20 – 30 μm. Moreover, their far-IR temperatures are similar to those of compact planetary nebulae (Kenyon et al. 1988). The spectral types of cool components in the D'-type symbiotic stars are F – G (yellow symbiotic stars). Akras et al. (2019a) classified $\approx 3.5\%$ of all known symbiotic systems as D'-types. Typical optical spectra of two D'-type symbiotic stars are shown in Fig. 1.3C.

Note that *S+IR-type symbiotic stars* were recently introduced by Akras et al. (2019a) based on the analysis of infrared data of almost all known symbiotic systems. According to the authors, the IR SEDs of these symbiotic binaries resemble those of S-type, but there is a small excess in the far-IR region. Their fluxes peak between 0.9 and 1.7 μm. Akras et al. (2019a) claimed that the observed IR spectra of these objects could be explained either by the presence of a dusty disk around a white dwarf or a cold and tenuous dusty shell around a cool component, which is less evolved (e.g., early AGB) than that in the D-type symbiotic systems (thermal-pulsating, TP-AGB)[2].

Mass transfer mechanisms. The symbiotic giants of all infrared types belong to the low-mass population. Their masses cover the interval 0.6 – 3.2 $M_\odot$ while the

[2]It is worth noting that there are important caveats to this analysis that may raise some doubts on whether this class is real. In the article, Akras et al. (2019a) addressed the issue that their analysis is based on the 2MASS and *WISE* data which were not generally obtained during the same time (and thus same orbital or pulsation phase of objects). Nevertheless, they claimed that this fact cannot significantly influence their results on the IR class. However, we have also identified other issues (discussed in detail in Chapter 2.4) and conclude that most of the objects categorized as S+IR-type symbiotic stars by Akras et al. (2019a) can be easily classified within the S/D/D' scheme.

maximum of their mass distribution is around $1.5 - 1.6\,M_\odot$ (e.g., Mikołajewska 2003, and references therein; Chapter 2.4). The key to the symbiotic activity and also to the typical symbiotic appearance is how they can lose the matter. The mass-loss rate of giants in S-type symbiotic systems is typically of the order of $10^{-7}\,M_\odot\,yr^{-1}$, which is higher as in the case of single M giants (Mikołajewska et al. 2002), and even more in the D-type symbiotic stars ($\sim 10^{-5}\,M_\odot\,yr^{-1}$; e.g., Whitelock 1987). These values confirm that the high mass-loss rate is crucial for a symbiotic star to be detectable. A portion of the matter lost by the cool giant is transferred and accreted by the hot component of the symbiotic system.

The question of the mass transfer mechanism in these strongly interacting binaries is not solved indisputably. At first, it seemed that most of the symbiotic giants do not fill their Roche lobes (their radii estimated from rotational velocities have typically values of $\sim 50 - 200\,R_\odot$, which represent 0.4 – 0.5 of their corresponding Roche lobes). Moreover, the ellipsoidal effect (caused by the tidally distorted giants; see Chapter 1.4) had been previously detected only in a small sample of symbiotic stars. For this reason, it was concluded that the matter is probably transferred by the stellar wind in most S-type and in all D-type symbiotic systems.

However, subsequent analysis of data from large photometric surveys and especially data obtained in the IR spectral region showed that there is a significantly higher proportion of the S-type symbiotic stars showing ellipsoidal light curve variations (but these are detectable only in the systems with relatively high inclination; Rutkowski et al. 2007; Mikołajewska 2012), and therefore the Roche lobe overflow is a possible mass transfer mechanism in these objects (Mikołajewska 2007). Recently, direct measurements using interferometry confirmed the presence of tidally distorted giants in several symbiotics (Hillen et al. 2013; Boffin et al. 2014). Anyway, stellar winds probably significantly contribute to the mass transfer in such objects and are dominant in D-type symbiotic stars with larger separations. Moreover, in some cases, the matter may be transferred by the so-called wind Roche lobe overflow mechanism by which the wind is contained within the Roche lobe and strongly focused toward the orbital plane (Mohamed & Podsiadlowski 2012). Note that the wind of the giant is also the source of a dense circumbinary symbiotic nebula (see Chapter 1.2.3).

Orbital parameters. As already discussed above, the cool components of symbiotic systems are giants and therefore any symbiotic binary must be large enough to accommodate such an evolved star - orbital separations are in the order of astronomi-

cal units. For this reason, symbiotic systems belong to the widest interacting binaries and unlike other such systems, have long orbital periods of hundreds to thousands of days (Belczyński et al. 2000; Gromadzki et al. 2009, 2013, Chapter 2.3). The orbital periods of S-type symbiotic stars have values of $\sim$ 300 – 600 days, and they are much longer (even tens of years) in the D-type systems with more evolved cool components. The orbital periods are known for about 40% of confirmed symbiotic stars (see Chapter 2.3). Their values were obtained using photometric measurements (periodic variations due to eclipses or reflection effect; see Chapter 1.4) or measurements of radial velocities (however, for binary systems with orbital periods $>$ 1 year, the amplitude of radial velocity variations is quite low $\sim 5 - 10\,\mathrm{km\,s^{-1}}$; Mikołajewska 2003). It is interesting to note that majority of the symbiotic systems have a circular or nearly circular orbit.

1.2.2 Hot components

In general, the hot components of symbiotic stars are responsible for the outburst activity of these interacting binaries (see Chapter 1.4). However, the process is influenced by the mass transfer from the giant (see Chapter 1.2.1). Moreover, the hot components themselves can lose some matter by the fast wind, especially during outbursts, and the balance between all these processes is shaping the observed behavior and appearance of symbiotic systems, e.g., their nebulae (see Chapter 1.2.3).

Shell-burning white dwarf symbiotic stars. Most of the known symbiotic systems show prominent emission lines in their spectra (Fig. 1.3A-C). The hot component of these interacting binaries have high temperatures $T_{\mathrm{eff}} > 10^5\,\mathrm{K}$ and luminosities $L \approx 10^2 - 10^4\,\mathrm{L_\odot}$ and reside in the same region of the Hertzsprung-Russell (HR) diagram as the central stars of planetary nebulae (Mikołajewska 2003; Skopal 2012). Given the parameters of the hot components of the shell-burning symbiotic systems, they typically dominate the UV and X-rays range of the spectrum (Fig. 1.2A).

To power such luminosities solely by accretion, furious accretion rates are required in the case of main sequence accretors (of the order of $10^{-5} - 10^{-4}\,\mathrm{M_\odot\,yr^{-1}}$; Munari 2019) and rather high accretion rates are needed also in the case of white dwarf accretors ($\sim 10^{-6}\,\mathrm{M_\odot\,yr^{-1}}$; Mikołajewska 2003; Sokoloski et al. 2017). Although the mass loss rate of the typical symbiotic giant is quite high (see Chapter 1.2.1), the expected accretion rate is not sufficient to power such energy output. For this reason,

a more probable mechanism is a quasi-steady burning of the hydrogen-rich matter in the shell on the surface of the white dwarf (Mikołajewska 2003; Luna et al. 2013; Munari 2019), since the thermonuclear reactions release 40 to 50 times more energy per nucleon compared to accretion (Mukai et al. 2016). In such a case, accretion rate of around 10^{-8} – $10^{-7}\,M_\odot\,yr^{-1}$, depending on the accretor mass, is sufficient for a typical symbiotic white dwarf (Iben 1982; Nomoto et al. 2007; Wolf et al. 2013).

The presence of the shell-burning is supported by the detection of super-soft X-ray radiation from several symbiotic binaries (e.g., Sokoloski 2003; Luna et al. 2013), although the amount of such sources is far from the number of objects which are supposed to be shell-burning symbiotic stars (see Chapter 2.5; Merc et al. 2019c). On the other hand, such a lack of detection can be easily explained by the local absorption of super-soft X-ray radiation in the dense symbiotic envelopes.

Accreting-only white dwarf symbiotic stars. At least some of the well-studied symbiotic stars, such as EG And, RT Cru or V1261 Ori, do not contain such luminous hot components. The luminosity of the hot components in these systems is powered solely by the accretion onto the white dwarf, and for this reason, it is typically in the range of 1 – $100\,L_\odot$ (e.g., Mukai et al. 2016; Munari et al. 2021, 2022). Due to the low luminosity, these objects do not ionize and excite the symbiotic nebulae to such an extent as the hot components in the shell-burning symbiotic stars. As a result, they have weaker or absent emission lines in the optical spectra (Fig. 1.3D), and if they are present, they are only of the lower ionization (e.g., Sokoloski et al. 2017; Munari 2019; Munari et al. 2021).

Only the minority of the known symbiotic systems are powered solely by accretion. This apparent bias is largely introduced by the ways, how symbiotic stars were discovered and studied in past. Especially, it is important to recall (Chapter 1.1) that most of the symbiotic binaries were detected in the framework of low-resolution objective prism photographic surveys, or were discovered as planetary nebulae candidates. This necessarily means that only objects with strong emission lines could be detected. The same argument is valid for the non-detection of accreting-only systems among the candidates selected from more recent Hα photometric surveys.

While these systems do not manifest a traditional symbiotic appearance in the optical region (Fig. 1.3D), they are active in various other spectral regions (e.g., they are hard X-rays emitters, demonstrate significant variability in UV, show prominent UV excess). Several of them were identified in the recent years thanks to the all-sky

surveys in X-rays (e.g., Luna et al. 2013; Mukai et al. 2016; Nuñez et al. 2016) or very recently in the specialized survey focusing specifically on the accreting-only symbiotic systems (Munari et al. 2021; Lucy 2021).

The mass of the vast majority of white dwarfs in both, shell-burning and accreting-only symbiotic systems is within the range $0.4 - 0.8\,M_{\odot}$. Although most of them have a mass of about $0.6\,M_{\odot}$ (Mikołajewska 2007, Chapter 2.5), there are also symbiotic systems, especially *symbiotic recurrent novae*, with more massive white dwarfs whose masses are close to the Chandrasekhar limit (e.g., Sokoloski et al. 2006b; Luna & Sokoloski 2007, see also Chapter 2.5). That is why these systems are interesting from the evolutionary point of view as they may be one of the progenitors of type Ia supernovae (see Chapter 1.5). The typical radii of the hot components (meaning white dwarfs with their pseudo-photospheres) are of the order of $0.01 - 1\,R_{\odot}$ (Muerset et al. 1991; Mikolajewska et al. 1997; Skopal 2005). However, the pseudo-photosphere of the white dwarf can expand markedly during the outbursts of symbiotic stars (e.g., Skopal et al. 2011).

Accreting-only neutron star symbiotic systems. In addition to the systems containing white dwarfs, a handful of symbiotic binaries with accreting neutron stars were identified (e.g., Masetti et al. 2007; Corbet et al. 2008; Enoto et al. 2014; Bozzo et al. 2018, 2022; Yungelson et al. 2019). These objects are usually denoted as symbiotic X-ray binaries because they are detectable in the hard X-ray spectral region. They also emit in UV, but unlike the accreting-only systems comprising white dwarfs, they are less luminous in UV than in X-rays (Mukai et al. 2016). Their X-ray emission is modulated with periods of $10^2 - 10^4$ seconds due to the slow rotation of the neutron star. Interestingly, the period of the rotation and the X-ray emission changes with the activity of these symbiotic systems (Marcu et al. 2011). The optical spectrum of the known symbiotic X-ray binary V934 Her is shown in Fig. 1.3E.

Main-sequence stars as accretors. We should add that accreting main sequence stars had been also considered as hot components in some well-known symbiotic stars (Kenyon & Webbink 1984; Mikolajewska & Kenyon 1992a, e.g., Z And, CI Cyg, YY Her, AR Pav, CL Sco, or AX Per). However, as mentioned previously, due to the fact that observed luminosities of these symbiotic systems would require extreme accretion rates, the models containing white dwarfs are preferred for these systems nowadays (Munari 2019).

On the other hand, there is a group of objects with lower luminosities, consisting of a late-type giant (a progenitor of the white dwarf) which transfers matter to an accreting main sequence companion (which will become the giant in the future). Some authors classify these objects as *symbiotic stars in their first phase of the mass transfer* (e.g., Kenyon 1986), some others consider them as *pre-symbiotic stars* (e.g., Munari 2019). A well-known example of such a system is SS Lep (Blind et al. 2011).

We should note that typical symbiotic stars are in their second episode of the mass transfer. It is crucial to distinguish between both types of objects (which are in very different evolutionary stages), for example, when comparing the known symbiotic population with the evolutionary models. In this work, we have made a decision to classify interacting binaries like SS Lep as *related objects* to symbiotic systems but not as symbiotic stars (also in the light of the adopted definition of symbiotic stars, see Chapter 1.3). One also needs to be careful with the denotation 'pre-symbiotic' as not every interacting binary consisting of a red giant and main-sequence star would eventually evolve towards a typical open symbiotic system of a red giant and a white dwarf/neutron star. Such an evolutionary scenario will strongly depend on the initial setup of the system (separation of the components, masses, etc.) and the survival or avoidance of the possible common envelope stage (e.g., Boffin & Jones 2019, see also Chapter 1.5). In a particular case of SS Lep, Blind et al. (2011) predicted that the system will evolve towards a typical symbiotic system during the second episode of the mass transfer in the future.

X-ray classification scheme. Closely related to the discussion on the hot components in symbiotic binaries is the examination of the X-ray emission observed in these interacting systems. In addition to the super-soft X-ray emission which is observed in shell-burning symbiotic stars and hard X-rays from accreting-only systems discussed in the previous two sections, other types of X-ray emission have been detected in some symbiotic stars. Muerset et al. (1997) presented a classification of X-ray emission of symbiotic systems based on the soft X-ray *ROSAT* data which was later modified and extended by Luna et al. (2013) to account for hard X-ray emission of accreting-only systems discovered especially by the *Swift* satellite. Nowadays, the classification scheme consists of four (five) classes:

- α **type**: *super-soft X-ray sources*; most of the photons have energies lower than 0.4 keV and likely originate in the quasi-steady shell burning on the surface of the

white dwarf; observability of this spectral component depends on a combination of the effective temperature and absorption;

- β **type**: *soft X-ray sources*; the majority of the photons have energies less than 2.4 keV; this unabsorbed thermal emission is interpreted as due to the shock-heated plasma emerging in the collision of winds from the symbiotic components;
- γ **type**: *symbiotics with neutron star accretors*; the photons have energies higher than 2.4 keV; the X-ray spectra of these objects can be modeled as a non-thermal, power-law type;
- δ **type**: *highly absorbed, hard X-ray sources*; the thermal emission above 2.4 keV origins in the boundary layer between the accretion disk and the white dwarf in accreting-only symbiotic stars; these objects exhibit a prominent UV flickering;
- β/δ **type**: *the sources with two thermal components* in their X-ray spectra: relatively unabsorbed soft and heavily absorbed hard emissions; these objects have properties of both β and δ types.

1.2.3 Symbiotic nebulae

The symbiotic nebula (its shape, distribution of matter, density and temperature profile, etc.) can be quite complicated, as is demonstrated by the direct observations of two close symbiotic binaries obtained by the Hubble Space Telescope (NASA/ESA) that are shown in Fig. 1.4.

These circumbinary nebulae are usually hydrogen-rich and their sources are winds of both components, especially that of the giant and the material expelled in the outbursts. They are partially or fully ionized by the radiation of the hot component (it may not be true in accreting-only symbiotic stars; see Chapter 1.2.2). In optical spectra, the presence of the nebula is manifested mainly by significant emission lines, a relatively prominent nebular continuum, and the Balmer jump at 3646 Å in emission (Fig. 1.2A and Fig. 1.3A-C). Among the most typical emission lines, the ones of H I, He I and [O III] are seen in the majority of symbiotic stars while other, high-ionization lines of He II, [Fe VII] or the Raman-scattered lines of O VI are detected in symbiotic stars comprising very hot component (see the optical spectra of symbiotic systems shown in Fig. 1.3).

The nebulae observed in symbiotic stars differ from planetary nebulae, e.g., their densities are $>$ 100 times larger (Kenyon 1986). However, their properties depend

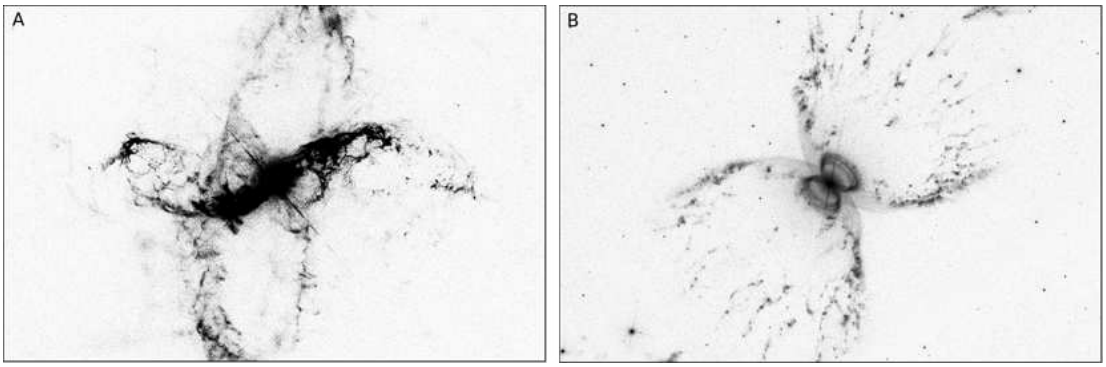

Figure 1.4: Complex structure of the symbiotic nebulae and the outflows of matter observed in two symbiotic stars. **A:** R Aquari, the closest symbiotic star. **B:** Object Hen 2-104 (Southern Crab Nebula). Images are obtained by Hubble Space Telescope. Credits: NASA and ESA.

on the IR type of the cool giant in a particular system. S-type symbiotic stars have smaller ($\sim$ few au) and denser ($n_e \sim 10^8 - 10^{12}$ cm^{-3}) nebulae while the nebulae of D-type symbiotic systems are more extended (10 – 100 au) and less dense ($n_e \sim 10^6 - 10^7$ cm^{-3}). The larger extent of nebulae of D-type systems is also the reason why the symbiotic stars with the resolved nebulae at optical and/or radio wavelengths are predominantly of this IR type (e.g., Munari & Patat 1993; Corradi & Schwarz 1993; Corradi et al. 1999). Typical electron temperatures of the symbiotic nebulae are of the order of 10^4 K (Schmid & Nussbaumer 1993; Skopal 2005; Sekeráš & Skopal 2012). Both the density and temperature are influenced by the outbursts of symbiotic binaries during their active stages.

Since the hot component directly affects the conditions in the nebula, analysis of the nebular spectrum can also provide information on changes of the hot component (its temperature, luminosity, etc.), which is usually not directly observable in the optical region (e.g., Mikolajewska et al. 1997; Leedjärv et al. 2016).

1.3 Definition of symbiotic stars

Although at first glance it might make more sense to give a definition of symbiotic stars at the beginning of the text, we decided to postpone this discussion until after describing the components of well-known symbiotic binaries (Chapter 1.2). Such an approach we consider more instructive because it reflects the evolution of views on these interacting binaries which have changed over time as new objects were gradually discovered and concepts of their nature formed (see Chapter 1.1).

The first definitions were based on the prototypes of this class of objects and new

stars were classified as symbiotic stars if their spectra resembled the ones of known representatives of the group. Merrill (1958) recognized Z And, BF Cyg, CI Cyg, RW Hya, and AX Per as such prototypes. Later, some more rigorous criteria were formulated, for example, Boyarchuk (1969) proposed to search for the absorption features of late-spectral type objects, emission lines of He II, [O III], and other, higher ionized metals, and for the presence of irregular variability. Allen (1979) suggested classifying as symbiotic stars only such objects, in which the presence of emission lines of the ions with ionization potential exceeding 55 eV is confirmed.

Kenyon (1986) summarized the following criteria for identifying symbiotic binaries:

- the presence of the absorption features of a late-type giant (e.g., molecular bands of TiO, CN, CO, VO and H_2O and absorption lines of Ca I, Ca II, Na I, Fe I, etc.) in the optical spectrum,
- bright H I and He I emission lines,
- either emission lines with an ionization potential of at least 20 eV (nowadays, at least 35 eV is generally accepted) and an equivalent width exceeding 1Å or an A- or F-type continuum with absorption lines of H I, He I and singly ionized metals (for symbiotic stars during an outburst).

Together, these three criteria require the simultaneous presence of a cool and hot component in a single object (see Fig. 1.5A for an example of the shell-burning symbiotic star CI Cyg fulfilling these criteria). Belczyński et al. (2000) added another criterion applicable also in the case when the presence of a cool giant is not evident from the observations. They considered the presence of the Raman-scattered O VI lines in spectra as a sufficient condition for classifying an object as a symbiotic star. The Raman-scattered O VI lines are broad emission features in optical spectra at 6825 and 7082 Å, which are a product of Raman-scattering of the photons of the O VI resonance lines at 1032 and 1038 Å off the atoms of neutral hydrogen (Schmid 1989). They occur (almost) exclusively in the spectra of symbiotic stars (Akras et al. 2019a), as the conditions required for their formation are very specific - the presence of a sufficient amount of neutral hydrogen in one part of the nebula and a hot source capable of ionizing oxygen five times in another part. It needs to be emphasized that the presence of O VI lines is a sufficient, but not necessary condition as only about half of stars classified as symbiotic exhibit these lines in their spectra (Allen 1984a; Belczyński et al. 2000; Akras et al. 2019a, Chapter 2.5). Typical optical spectra of the

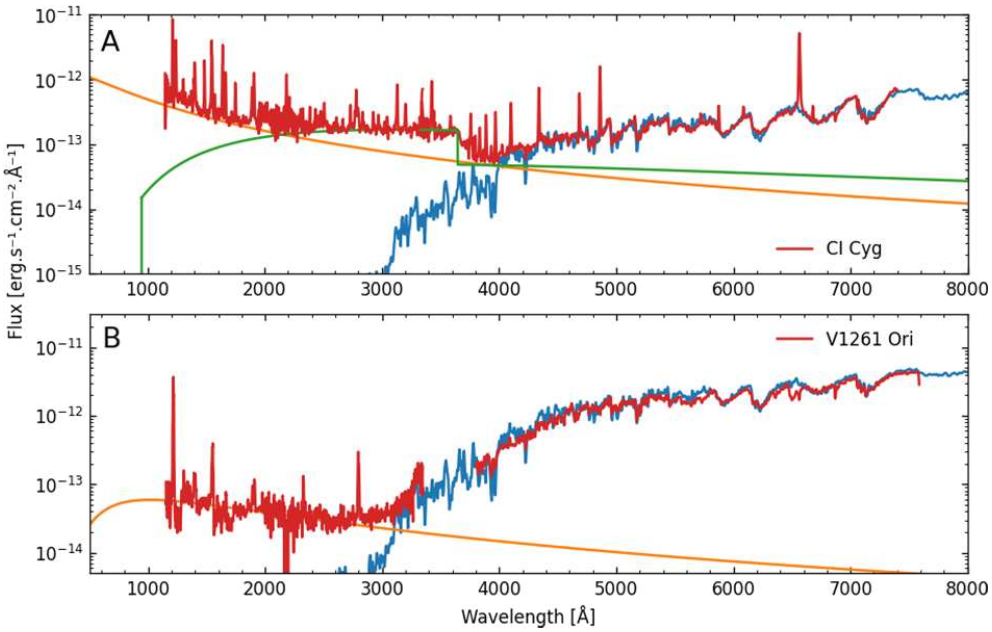

Figure 1.5: Comparison of UV-optical spectra of shell-burning (panel **A**; CI Cyg) and accreting-only (panel **B**, V1261 Ori) symbiotic stars. Observed optical spectra, shown in red, are from the ARAS database (Teyssier 2019). UV spectra (also in red) were obtained from the archive of IUE satellite (Boggess et al. 1978). The spectra of red giants (blue lines) of spectral types M4 and M3 are from the library of Pickles (1998) for CI Cyg and V1261 Ori, respectively. Nebular radiation in the shell-burning system is shown in green and hot components, approximated by the black bodies with temperatures of 150 000 and 50 000 K are shown in orange for CI Cyg and V1261 Ori, respectively.

symbiotic binaries meeting these criteria are shown in Fig. 1.3A. Spectra of symbiotic novae and symbiotic recurrent novae are shown in Fig. 1.3B.

Broader definition. The aforementioned criteria are currently the most commonly used. However, as we already mentioned, the selection of these criteria is strongly affected by the ways, how symbiotic stars were discovered and studied in past - most discoveries resulted from the optical low-resolution objective prism photographic surveys, which were capable of revealing only symbiotic stars with strong emission lines. Most of the objects fulfilling these criteria (especially the requirement for the presence of emission lines of highly ionized ions) contain shell-burning white dwarf (see Chapter 1.2.2). Only a handful of exceptions of accreting-only symbiotic stars show the emission lines of, e.g., [O III] (ionization potential of 35 eV) in quiescent optical spectra.

The requirement for emission lines in the aforementioned criteria is not limited to the optical spectrum. Several accreting-only systems have been actually confirmed as symbiotic stars only based on the observation of highly ionized ions in the UV

spectra (see Fig. 1.5B for an example). However, one should keep in mind that for many objects no UV spectra are available and optical spectra of many accreting-only symbiotic stars do not show any emission lines or only those with low ionization potential.

This is the reason why some research teams adopted alternative, usually broader definitions of symbiotic stars to account also for such systems, which consist of a giant and a hot component, but do not show any evidence of symbiotic activity in the optical region. In the physical definition of Luna et al. (2013) and Mukai et al. (2016), they consider as symbiotic systems all the binaries, in which a red giant transfers a sufficient amount of matter to a compact companion (a white dwarf or a neutron star) to produce an observable signal at any wavelength. These objects can be typically identified in short-wavelength spectral regions by their near-UV excess (Fig. 1.5B), by their UV variability, or their hard X-ray emission (Husser et al. 2013; Sokoloski et al. 2016). Mukai et al. (2016) argued that there may be a large, hidden, and still unexplored population of symbiotic stars, such as SU Lyn, NQ Gem, or 4 Dra, without prominent emission lines. The spectrum of NQ Gem is shown in Fig. 1.3D.

Finally, we should add that from the theoretical studies it seems that accreting-only symbiotic stars containing hot components with luminosities $\gtrsim$10 $L_{\odot}$ are capable of producing emission lines in their optical spectra (Mikolajewska & Kenyon 1992b; Yungelson et al. 1995). Therefore such systems pass the traditional criteria for the symbiotic classification. Iłkiewicz et al. (2022) claimed that binaries in which the hot component cannot reach this threshold should not be considered as symbiotic stars, as their components are not interacting strongly enough. They also concluded that SU Lyn should be classified as a 'transient' symbiotic system, having sufficient luminosity of the hot component only during a short period of time (when the mass accretion rate was high enough; probably during periastron passage).

1.4 Symbiotic variability

Symbiotic stars display a wide variety of interesting photometric and spectroscopic activity. The most pronounced are manifestations of the interaction between the components - outbursts during active stages. Other periodic variations are connected with the orbital motion, and apart from that, both components may exhibit their intrinsic variability influencing the brightness of the system and/or its spectroscopic appearance. These variations can occur on time scales of minutes (e.g., flickering or

quasi-periodic oscillations of the hot component), months, and years (radial pulsations or semi-regular variability of the giant), as well as decades (changes of the giant similar to the solar cycle or eclipses by the circumstellar dust).

1.4.1 Outburst activity of symbiotic stars

The most prominent changes in the light curves of symbiotic variables are outbursts. Depending on their nature, symbiotic stars can be divided into three main categories (e.g., Mikołajewska 2007). We should note that there are also objects for which no outburst has yet been detected (e.g., RW Hya or SY Mus).

Classical symbiotic stars (Z And-type). The most common group of symbiotic variables is named according to the prototypical symbiotic star Z And. In addition to the prototype, typical well-known representatives include AG Dra, AX Per, or CI Cyg. For these objects, alternations of quiescent and active stages are typical (see their light curves in Fig. 1.6A).

The active stages can last for months or even years, and classical symbiotic stars usually manifest a series of significant brightness changes (outbursts) reaching several magnitudes (2 – 5 mag in the U filter, and decline towards longer wavelengths). They are also accompanied by remarkable spectral changes like the rise of the blue continuum or the disappearance of the high ionization emission lines (Fig. 1.6B). The evolution of the system throughout the outburst may differ from one symbiotic star to another. Moreover, the morphology of the active stages of one particular system (number and shape of individual outbursts, duration, etc.) can also vary significantly over time (see Fig. 1.6A; Merc et al. 2019a). The outbursts of classical symbiotic stars are often accompanied by the outflows of matter (Fig. 1.6C), often in the form of bipolar jets (e.g., Leedjärv 2004; Skopal et al. 2018; Lucy et al. 2018; Munari 2019).

The outbursts are linked to the hot components. Thermonuclear runaways on the surface of the white dwarf, similar to classical novae, have been proposed as a possible mechanism of the outbursts activity (Kenyon & Truran 1983). However, such short recurrence time scales as observed in classical symbiotic stars are probably not possible in the thermonuclear runaway scenario for the low-mass white dwarfs typical for most symbiotic stars (Sion et al. 1979; Sokoloski et al. 2006a). On the other hand, high peak luminosities reached during some outbursts cannot be explained solely by the accretion disk instabilities similar to those in dwarf novae as proposed by some authors

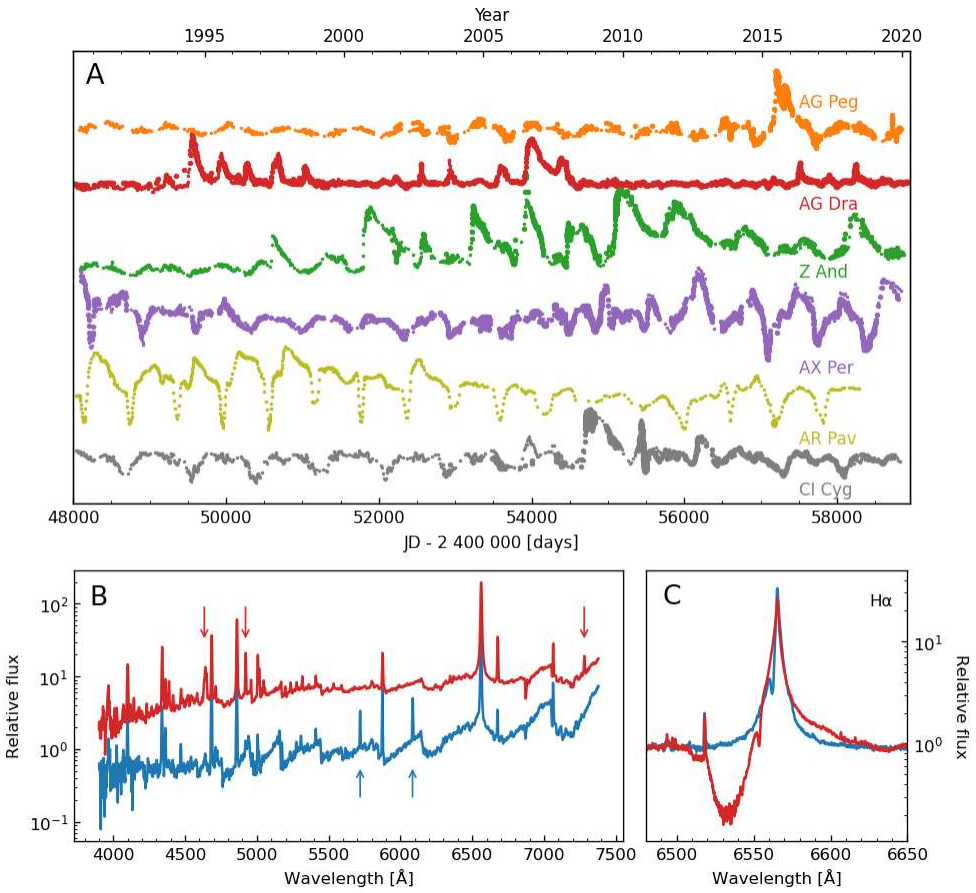

Figure 1.6: Z And-type outbursts of symbiotic stars. **A:** The long-term light curves of selected classical symbiotic stars covering an interval of 30 years. Smaller and larger dots represent visual and CCD data in V filter, respectively. **B:** Comparison of spectra of AX Per in quiescence (blue) and outburst (red). Blue arrows denote highly ionized emission lines that disappeared during the outburst. Red arrows show emission lines with low ionization potential that are observable only in outbursts. **C:** Formation of the P Cygni profile of Hα line in V694 Mon during its outburst (red) in comparison with the quiescence profile of the emission line (blue). The sources of data are summarized in the Appendix.

(Mikołajewska 2002; Sokoloski et al. 2006a; Tomov et al. 2011).

According to Munari (2019), most of the explanations currently investigated fall into two categories: the release of potential energy from extra-accreted matter (accretion event) or shift of the white dwarf emission to longer wavelengths due to its expansion in response to increased mass accretion rate. These mechanisms include increases in the mass transfer rate from the giant to the white dwarf caused by some intrinsic mechanisms of the giant or its passage through a periastron (de Val-Borro et al. 2017; Munari 2019), enhanced winds from the hot component (Skopal et al. 2011) or changes in the colliding winds from the components of symbiotic binaries (Bisikalo et al. 2006).

Moreover, it is probable that several various processes can operate in some symbi-

otic systems. The 'combination nova' model that combines the outburst mechanisms of dwarf and classical novae has been proposed to explain major and minor outbursts of Z And (Sokoloski et al. 2006a). Two types of outbursts have been detected also in the case of AG Dra (González-Riestra et al. 1999; Leedjärv et al. 2016), LT Del (Ikonnikova et al. 2019a), or StHα 169 (Munari 2019). The multi-wavelength simultaneous observations covering all the outburst phases of at least a few symbiotic stars are needed to completely understand the nature of the activity of classical symbiotic stars (Munari 2019).

Symbiotic novae. In some symbiotic variables, thermonuclear nova outbursts have been observed. Their properties strongly differ depending on the mass of the white dwarf. Symbiotic novae can be classified into two groups: *extremely slow novae*, usually referred simply as *symbiotic novae* or *'slow' symbiotic novae*, which includes the systems with low-mass white dwarfs. The second group of *very fast recurrent novae*, referred as *symbiotic recurrent novae* (most widely used in the symbiotic community), *novae within symbiotic systems* (e.g., Munari & Banerjee 2018; Munari 2019) or *embedded novae* (e.g., Chomiuk et al. 2021) occur in the systems with very massive white dwarfs (Mikołajewska 2010). Symbiotic recurrent novae are discussed in the next section.

'Slow' symbiotic novae are uncommon. Only about a dozen of such systems have been observed so far (Munari 2019, Chapter 2.6). Among the well-known examples, one can find, e.g., AG Peg, RR Tel, HM Sge, V1016 Cyg, V1329 Cyg, or PU Vul. Some of them are S-type symbiotic systems and some of them are of the D-type.

The thermonuclear burning in the case of symbiotic novae turns on upon reaching the conditions for hydrogen burning in a non-degenerate case. Therefore it is non-explosive, proceeds in thermal equilibrium, and is not accompanied by the massive mass ejections - white dwarfs retain most of the accreted mass (Fujimoto 1982a,b; Murset & Nussbaumer 1994; Mikołajewska 2007, 2010; Munari 2019). The non-degenerate envelope expands to supergiant dimensions and keeps burning under stable conditions for a long time. For this reason, the light curves of these systems are characterized by a slow rise to the maximum brightness (amplitude of $3 - 7$ magnitudes within a few years), followed by a very slow decline during several decades (lower the mass of the white dwarf, longer is the decline; see fig. 6 in Mikołajewska 2010). The light curve of symbiotic nova AG Peg is shown in Fig. 1.7 as an example.

Typically, the symbiotic novae prior to their outbursts are accreting-only symbiotic

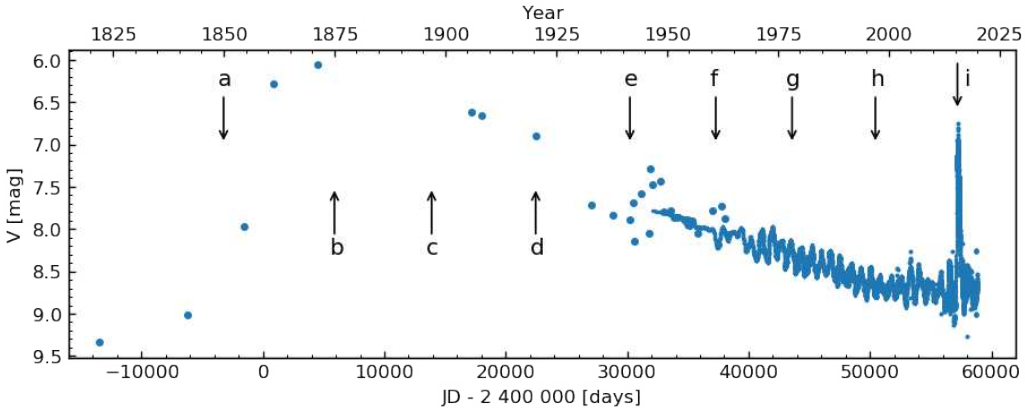

Figure 1.7: The historical light curve of AG Peg covering the period of 1821 – 2020. The photometric evolution is associated with the significant changes in spectra: a - the beginning of the nova outburst around 1850, b - the maximum of the brightness (1875), the spectrum was probably similar to an F supergiant, c - the spectrum with a Be-type continuum and Balmer hydrogen lines with P Cygni profiles (1897), d - the spectrum of a B star (1920), e - the spectrum of a Wolf-Rayet star (1941), f - sinusoidal variations typical for quiescent symbiotic stars appeared (1961), g - the spectrum of a hot sub-dwarf (1978), h - the brightness decline stopped (1997), i - the Z And-type outburst (2015). The sources of data are summarized in Appendix A.

stars. Although the pre-outburst observations of symbiotic novae are scarce, most of them were not showing prominent emission lines in their optical spectra, and they had an appearance similar to normal cool giants (e.g., Stienon et al. 1974; Mikołajewska 2010; Munari 2019; Skopal et al. 2020). At the maximum brightness, these systems usually show an A/F-type supergiant continuum with occasional emission lines (e.g., Balmer lines or Fe II lines). Later during the decline, the spectroscopic appearance can change significantly, e.g., for AG Peg the spectral appearance of a Be-type star, a Wolf-Rayet star, or a hot sub-dwarf has been reported during the decline from its nova outburst before the nebular radiation started to dominate and significant emission lines of the highly ionized elements appeared (e.g., Mikołajewska 2010; Tatarnikova et al. 2016, and references therein).

Interestingly, recent observations suggest that at least some classical symbiotic stars have gone through a symbiotic nova phase in the past. Such a transition has been undoubtedly observed in the case of AG Peg and V426 Sge, and possibly also in BF Cyg[3]. AG Peg demonstrated the Z And-type outburst in 2015, 165 years after its nova outburst (Fig. 1.7; Skopal et al. 2017; Merc et al. 2019a). V426 Sge was detected in symbiotic nova outburst in 1968 and in Z And-type outburst in 2018 (Skopal et al. 2020). BF Cyg showed a 'slow' symbiotic nova outburst from 1885 and outbursts

[3]We should note that also StHα 169 (Munari et al. 2016) shows similar photometric behavior.

similar to those in classical symbiotic stars in 1920 and 1989 (Skopal et al. 1997; Leibowitz & Formiggini 2006).

Such a scenario is also supported by the fact that many white dwarfs in classical symbiotic stars show quasi-steady hydrogen burning on their surfaces. This situation expects that the accretion rate is improbably to be very accurately set, just in the narrow interval between the minimum for shell burning and values causing expansion of the white dwarf pseudo-photosphere (e.g., Fujimoto 1982a; Iben 1982; Nomoto et al. 2007; Wolf et al. 2013). Alternatively, the shell-burning can be a residual process from a prior nova outburst (Ramsay et al. 2016; Munari 2019; Skopal et al. 2020). If the cool companion is not able to supply enough matter for the stable shell-burning at a later time, it will cease and such a symbiotic star can again switch to the accreting-only state. The white dwarf can replenish its envelope and initiate another nova cycle in the future. However, the recurrence time can be as long as 10^6 years in some symbiotic systems (e.g., Yaron et al. 2005; Wolf et al. 2013).

Symbiotic recurrent novae. In the symbiotic systems with massive white dwarfs (1.2 – 1.4 $M_\odot$), repeated, short-lasting outbursts ($\sim$ days – weeks) whose amplitudes are similar to that of normal recurrent novae are observed (up to 7 – 10 mag; see the light curve of symbiotic recurrent nova RS Oph in Fig. 1.8A-B). Their recurrence times are relatively short, in order of a few years or tens of years (Hachisu & Kato 2001; Mikołajewska 2010; Mróz et al. 2014; Munari 2019).

In contrast with 'slow' symbiotic novae, the matter in symbiotic recurrent novae is accreted under degenerate conditions. The thermonuclear outbursts are explosive and a large amount of mass is ejected at very high velocities (Starrfield et al. 2016; Munari 2019; Chomiuk et al. 2021). Contrary to the case of classical novae (with main-sequence donors) in which the ejecta expands freely into the surrounding space, in symbiotic recurrent novae, the matter expelled from the white dwarf collides with the dense slow wind of the cool component. That leads to the violent deceleration of the ejecta and the formation of the shock region. The shocked expanding gas can also give rise to the very high energy γ-ray emission (observed in the case of recent outbursts of V407 Cyg and RS Oph; e.g., Abdo et al. 2010; Zheng et al. 2022).

The high expansion velocities of the ejecta in the symbiotic recurrent novae outbursts result in very broad emission lines, which are observed together with narrow pre-existing ones (Fig. 1.8C-D). The broad lines narrow rapidly when the ejecta collides with the wind of the giant. In the initial phases, the spectrum shows only low

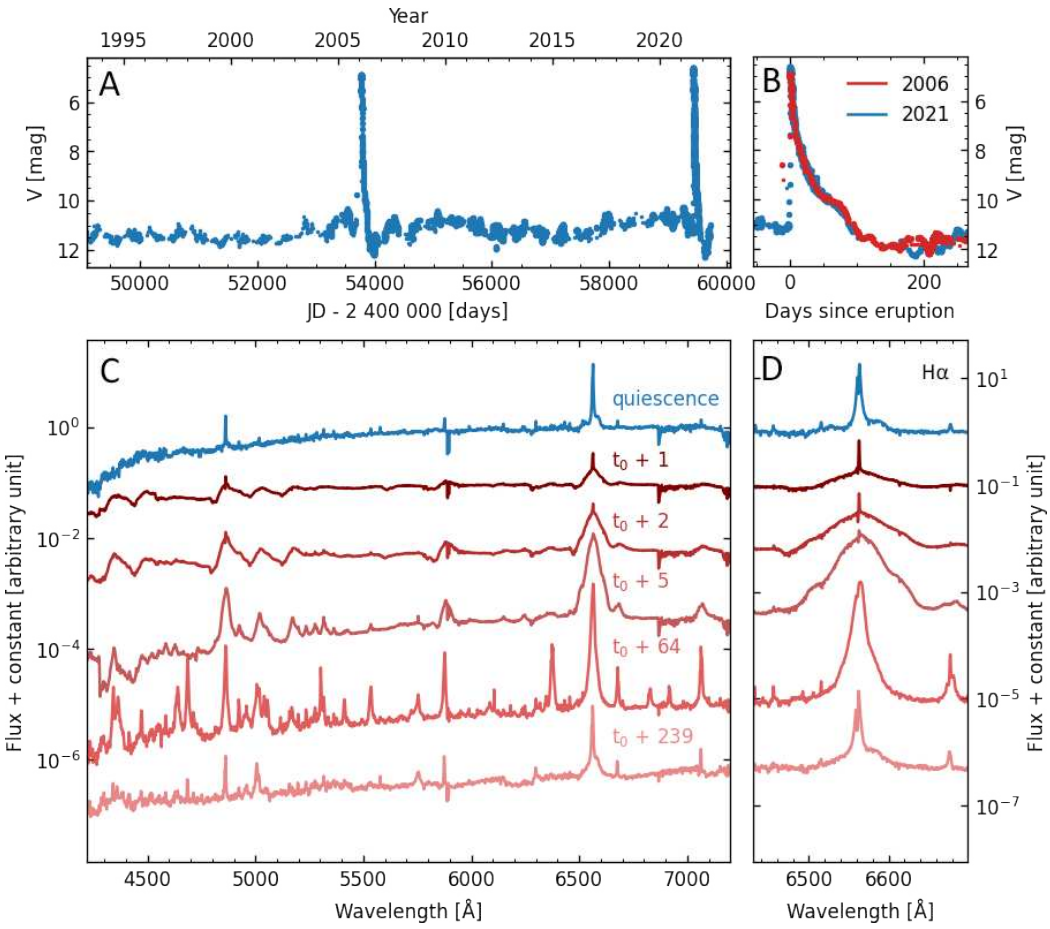

Figure 1.8: Outburst activity of the symbiotic recurrent nova RS Oph. **A:** The long-term light curve of RS Oph covering the interval of 30 years. Two outbursts in 2006 and 2021 are well visible. Smaller dots represent visual data, larger CCD data in V filter. **B:** Comparison of 2006 and 2021 outbursts of RS Oph. **C:** Evolution of low-resolution spectra of RS Oph throughout the 2021 outburst. Time from the eruption (Munari & Valisa 2021) for every spectrum is given. Quiescent spectrum from 2019 is shown for comparison (in blue). **D:** Evolution of Hα line of RS Oph throughout the 2021 outburst. The sources of data are summarized in the Appendix A.

ionization lines while later the lines with higher ionization potential emerge (e.g., He II, [Fe VII], O VI), including coronal lines ([Fe X], [Fe XI], [Fe XIV]). The high ionization emission lines start to disappear quickly after the transient thermonuclear burning on the white dwarf is switched off (accompanied by the disappearance of the super-soft X-ray emission) and the hot component begins to cool (Fig. 1.8C-D). The spectroscopic evolution of symbiotic recurrent nova RS Oph during the 2021 outburst is nicely illustrated in the atlases covering the first 18 days of the outburst until the emergence of highly ionized lines (Munari & Valisa 2021) and the days 19 – 102, until the solar conjunction of RS Oph (Munari & Valisa 2022).

Symbiotic recurrent novae are extremely rare. Only 4 such symbiotic systems have been detected in multiple outbursts: RS Oph (9 outbursts), V3890 Sgr (3 outbursts),

V745 Sco (3 outbursts), and T CrB (2 outbursts); see, e.g., Anupama & Mikołajewska (1999); Schaefer (2010); Anupama (2013), and references therein. All of them are S-type symbiotic stars.

Additionally, there are few other objects which have giant donors and have been detected in outbursts similar to that of symbiotic recurrent novae. While these objects cannot be called 'recurrent novae' yet (until their second observed outburst), the denotation of 'novae within symbiotic systems' is appropriate and these systems should be considered as members of the same group of symbiotic stars. Among them, one should consider at least V1534 Sco with an M6 III donor (Munari & Banerjee 2018), AT 2019qyl which erupted in NGC 300 and whose progenitor contained an O-rich AGB star (Jencson et al. 2021) and V407 Cyg which was classified as a wind-accreting D-type system containing a Mira-type cool component (with the second-longest pulsation period among symbiotic Miras; Tatarnikova et al. 2003), whose outburst was similar to other symbiotic recurrent novae (Iijima 2015; Iijima & Naito 2017).

Moreover, V1535 Sco is probably also a symbiotic system (hosting a K giant) showing this type of outbursts (Srivastava et al. 2015; Linford et al. 2017), and the progenitor of nova V1708 Sco was classified as pulsating red giant suggesting that it was also a nova eruption within symbiotic system (Aydi et al. 2020; Mroz & Udalski 2020). We should note that also LMC S154, a symbiotic star in the Large Magellanic Cloud with a C-rich giant donor detected probably in three outbursts, shares many similarities with the symbiotic recurrent novae, although the timescale of its outbursts is significantly longer than in the case of objects of this type (Iłkiewicz et al. 2019b).

Finally, we should also note that there might be more symbiotic recurrent novae which went unnoticed or have not been classified as members of this group. Pagnotta & Schaefer (2014) suggested that many recurrent novae are hiding among the classical novae and that several of them might have red giant donors. Mróz et al. (2015) also suggested that some of the post-novae systems observed by OGLE might have a red giant donor. It could be therefore worth obtaining deep optical/IR spectra of old novae to discover more systems belonging to the small group of symbiotic recurrent novae. However, it should be noted that, e.g., the V magnitudes of OGLE candidates are often below $V = 20\,\mathrm{mag}$.

1.4.2 Orbitally-related variations

In addition to the outburst activity, the light curves of symbiotic binaries are rich in various other changes which (with exception of flickering) are not related to the mass transfer between the components (Mikołajewska 2007). Orbitally-related variations are usually well observed during quiescent phases of symbiotic stars (Friedjung et al. 1998). Some of these effects can also influence the spectral appearance significantly.

Reflection effects. The typical orbitally-related feature of the quiescent light curves of symbiotic stars is a wave-like variability showing minima during the inferior conjunctions of the giant and maxima during the inferior conjunctions of the hot component. This effect is partly caused by the illumination and heating of that side of the giant and surrounding nebula which face the hot source and partly by the variable nebular emission due to its different optical thickness (Beliakina 1979; Friedjung et al. 1998; Skopal 2008; Munari 2012; Gromadzki et al. 2013). Consequently, these differences cause the asymmetry in the brightness of two sides of the system and an observed single minimum and maximum during one orbital revolution. The amplitude of such variations depends on the inclination of the orbital plane of the binary system.

The amplitude of these variations is more pronounced at the shorter wavelengths (e.g., in the U filter; Friedjung et al. 1998) and decreases dramatically toward longer wavelengths (in the R or I filters, this effect is almost undetectable; Skopal 2009; Munari 2012). It is worth noting that in yellow symbiotics (whose giants are hotter in comparison with symbiotic stars comprising the M giants), the giant contribution to the observed radiation dominates already at the shorter wavelengths (Skopal 2008), and therefore this variability is almost undetectable already in the V filter - see Fig. 1.9A where this effect is illustrated on the U and V data of AG Peg (M giant) and AG Dra (K giant, yellow symbiotic star).

Ellipsoidal effects. If the giant is significantly tidally distorted and the binary system is not observed pole-on, the visible area of its surface changes during the orbital motion (Munari 2012). This causes the changes in the amount of detected radiation from the giant - the observed area is the smallest during the superior and inferior conjunctions of the giant (two minima of brightness) and the largest during the quadratures (two brightness maxima). The amplitude of these variations depends on the inclination of the orbital plane. As this effect is connected with the radiation of the giant itself, it is also more pronounced at the longer wavelengths (usually in

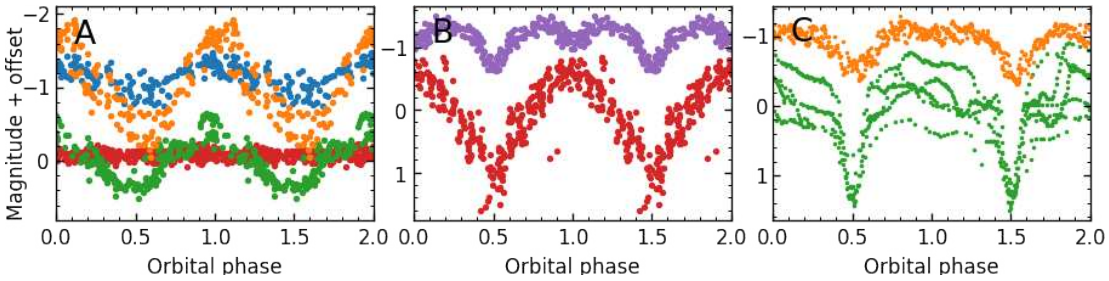

Figure 1.9: Orbitally-related variability in the light curves of symbiotic binaries. **A:** The reflection effect in AG Peg (M giant, orange in U filter, blue in V filter) and AG Dra (K giant, green in U filter, red in V filter). **B:** The reflection and ellipsoidal effects observed in LT Del (red in U filter, purple in V filter). **C:** Eclipses observed in the light curves of CI Cyg (orange) and AR Pav (green). The sources of data are summarized in the Appendix A.

the R or I filters, in some systems only in the infrared spectral region; Rutkowski et al. 2007; Mikołajewska 2012) The comparison of the U and V light curves of the yellow symbiotic star LT Del is shown in Fig. 1.9B. Reflection and ellipsoidal effects usually occur simultaneously, and the proportion between them varies depending on the particular symbiotic system and its activity.

Eclipses. As was mentioned, both reflection and ellipsoidal effects are more prominent for binary systems with higher inclinations and vanish for symbiotics seen pole-on. If the inclination of the symbiotic system is close to 90°, the eclipses of the hot component (and/or the surrounding ionized nebula) by the giant can be detected. The depth of the eclipses rises toward shorter wavelengths due to the high temperature of the eclipsed object (Munari 2012). The eclipses are usually more prominent during active stages of symbiotic stars when the radius of the hot source increases (Skopal 2008). Fig. 1.9C shows the eclipses in two symbiotic stars, CI Cyg and AR Pav. The variable shape of the eclipses can be seen for example in the long-term light curve of AX Per in Fig. 1.6A. The presence of the eclipses in light curves is usually combined with other orbitally-related effects.

1.4.3 Intrinsic variability of components

At last but not least, apart from the changes that occur on orbital period time scales and the activity of symbiotic binaries, both their components often exhibit intrinsic variability, on various time scales from minutes to years.

Pulsations. The cool components of symbiotic systems are regularly (Mira variables in D-types) or semi-regularly pulsating (in S-types). Pulsation periods of symbiotic

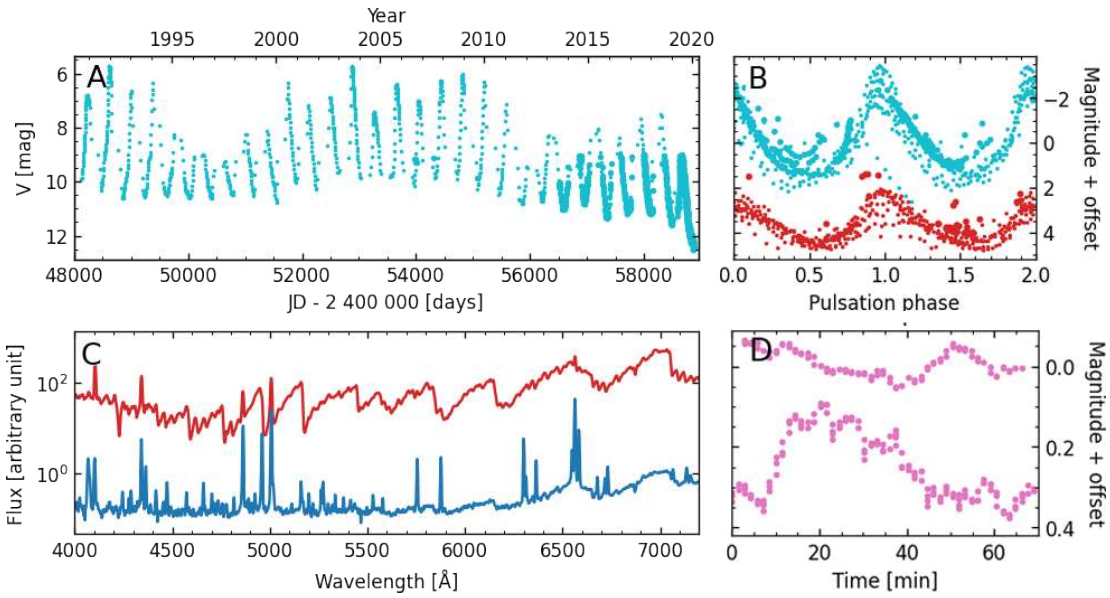

Figure 1.10: Intrinsic variability of symbiotic components. **A:** The long-term light curve of Mira pulsator R Aqr over the period of 30 years. Smaller and large dots represent visual and CCD data in the V filter, respectively. **B:** Phase diagrams of Mira pulsations of R Aqr (cyan color) and UV Aur (red). **C:** Comparison of optical spectra of R Aqr obtained near the pulsation maximum (red) and minimum (blue) of brightness. **D:** Flickering on the timescale of minutes in CH Cyg. The sources of data are summarized in the Appendix A.

Mira giants are typically longer than in the case of single stars (Whitelock 2003), usually $\sim$ 300 – 600 days (e.g., Whitelock 1987; Gromadzki et al. 2009, Chapter 2.4), and have very high amplitudes, up to several magnitudes. Fig. 1.10A shows the long-term light curve of the Mira pulsator R Aqr, Fig. 1.10B depicts the phase diagrams of light curves of R Aqr and UV Aur. The pulsations of Mira components significantly influence also the optical spectra (Fig. 1.10C). The nebular emission lines are well visible near the minimum of the light, while around the maximum, Balmer lines produced by the shocks in the atmospheres of pulsating components are visible (with Hδ being typically the strongest line).

The variations in the S-type systems are usually on the time scale of 50 – 200 days (Gromadzki et al. 2013, Chapter 2.4) and their amplitudes are smaller. Pulsations are more pronounced at the longer wavelengths at which the giants dominate.

Rotation of components. In the case of some symbiotic systems, the rotation of both components can be detected in the light curves (Munari 2012). Nevertheless, it is usually studied using spectroscopic methods. The rotational periods of the giants are typically of the same order as the orbital periods and most of the giants in the symbiotic systems with an orbital period $< 1\,000$ days are already synchronized

(i.e., their rotational periods are the same as the orbital ones; Zamanov & Stoyanov 2012). The rotation periods of the hot components are measured in minutes or hours (Sokoloski & Bildsten 1999; Zamanov & Stoyanov 2012; Munari 2012).

Flickering. The light curves of a few symbiotic systems show stochastic photometric variations (flickering) with amplitudes of several hundredths or tenths of magnitude (more prominent at shorter wavelengths) and time scales of minutes or hours (Dobrzycka et al. 1996; Sokoloski et al. 2001). This effect is probably related to the presence of accretion disks around the hot components, similarly to cataclysmic variables.

The flickering has been detected only in about twenty known symbiotic stars, all of them are accreting-only systems (Dobrzycka et al. 1996; Sokoloski et al. 2001; Gromadzki et al. 2006; Angeloni et al. 2012; Zamanov et al. 2017, 2018, 2019, 2021b). Moreover, the observations of several known flickering symbiotic systems show that it can be detectable only transiently (Stoyanov et al. 2018; Zamanov et al. 2021a, 2022). The flickering in accreting-only symbiotic stars is also very prominent in UV (Husser et al. 2013; Sokoloski et al. 2016), while both optical radiation at the short wavelengths and UV radiation of shell-burning symbiotic systems is relatively stable on short timescales (it is dominated by the radiation of the nebula and the accretion signatures are negligible). The flickering in the symbiotic star CH Cyg is shown in Fig. 1.10D.

1.5 Evolutionary perspective

The nature of symbiotic stars suggests that the symbiotic phenomenon is a special evolutionary stage of some binary systems. Since the presence of a giant is typical for all symbiotic systems, this evolutionary stage is limited by its lifetime ($\sim 10^7$ years; e.g., Kenyon 1994; de Boer & Seggewiss 2008). The evolution of binaries is not fully understood, nor is the evolution of symbiotic stars, i.e., evolutionary models predict the distribution of orbital periods for symbiotic systems rather different from the observed one (Lü et al. 2006; Podsiadlowski & Mohamed 2007; Nie et al. 2012). However, some basic facts are evident. The evolution of symbiotic systems is determined by the initial orbital periods of the progenitor binaries and the masses of their components. Typically, symbiotic stars evolve from low-mass binaries, and the initial masses should differ at least by a few percent to allow symbiotic star formation (Kenyon 1986; Lü et al. 2006).

Binary stars with orbital periods longer than 5 – 10 days can initially evolve similarly to single stars. After the main sequence stage, those systems with orbital periods shorter than $\approx$ 100 days evolve to Algol binaries when their components fill their Roche lobes. This will prevent them from evolving to the red giants observed in symbiotic stars (Kenyon 1986).

The binaries with initial orbital periods of 100 – 10 000 days can form interacting binaries (note that some authors refer to these as symbiotic stars in their first symbiotic phase or pre-symbiotic stars) when the primary ascends the red giant branch, fills its Roche lobe and starts to transfer the matter onto a low-mass main sequence companion (Webbink 1988; Iben & Tutukov 1996). An example of such a system is SS Lep (see also Chapter 1.2.2). In some cases, this phase is relatively short ($< 10^4$ years) because the systems quickly evolve into common envelope binaries and consequently into short-period cataclysmic variables (Paczynski 1976; Kenyon 1994; Hurley et al. 2002; Boffin & Jones 2019). Some systems which could escape the common envelope evolution (typically those with periods >1 000 days; e.g., Boffin & Jones 2019) can manifest the second symbiotic phase when the secondary enters the giant branch and the white dwarf companion accretes part of the matter lost by the giant via its winds (Kenyon 1986; Lü et al. 2006).

These systems are formed less frequently than the interacting binaries in the first episode of the mass transfer but they usually show typical symbiotic features, such as a rich emission spectrum, for a longer time ($\approx 10^6$ years; e.g., Webbink 1988). Moreover, in contrast with the first mass transfer phase, these binary systems are more luminous. It is worth noting that the existence of symbiotic stars containing neutron stars implicates that these systems originated in the binaries with more massive companions ($\gtrsim 8\,M_\odot$; e.g., Yungelson et al. 2019). However, there are also other evolutionary channels that need to be considered (e.g., the evolution through the accretion-induced collapse of a white dwarf in symbiotic system; Hinkle et al. 2006; Yungelson et al. 2019), and therefore the origin symbiotic systems containing neutron stars is still an open question.

The binary stars with orbital periods longer than about 10 000 days (which seems to be true for most of the binaries formed; see the period distribution in, e.g., Moe & Di Stefano 2017; Wells & Prša 2021) never enter a common envelope phase and cannot be detected as interacting binaries in the first episode of mass transfer. These objects are detected only as symbiotic stars in their second phase of the mass transfer when the secondary evolves into a giant and transfers matter to a white dwarf via

the stellar wind (Iben & Tutukov 1996; Lü et al. 2006). In order to detect such systems, very evolved giants have to be present. Such red giants often form dust in their outer atmospheres, therefore these systems can be detected as D-type symbiotic stars. According to evolutionary models, both types, evolving from longer as well as shorter initial orbital periods, should be similarly numerous (Yungelson et al. 1995; Lü et al. 2006). However, detection of D-type systems is more complicated, and therefore they only make up about 15% of known symbiotic stars (Akras et al. 2019a).

Post-symbiotic evolution The closure of the symbiotic phase of a binary is also determined by its orbital period. In short period systems (less than $\approx 1\,000$ days), the giant slowly expands and fills its Roche lobe which results in an increase in the mass-loss rate and expansion of the pseudo-photosphere of the white dwarf. Such systems form common envelope binaries resulting in the reduction of their orbital periods, and finally, in the pair of two white dwarfs surrounded by an expanding planetary nebula. Such couples may eventually be progenitors of type Ia supernovae (see below). Long-period systems (especially D-type symbiotic systems) do not experience the common envelope phase and the final stage of such a system is usually a planetary nebula in whose center binary of two white dwarfs separated by several au are detectable (Kenyon 1986; Boffin & Jones 2019).

Symbiotic stars as potential type Ia supernovae progenitors. The presence of accreting white dwarfs and giants with degenerate cores in symbiotic systems makes them promising candidates for type Ia supernovae progenitors (Munari & Renzini 1992; Branch et al. 1995; Hachisu et al. 1999). Such an evolution is possible in two ways: in a single degenerate scenario, the mass of the white dwarf exceeds the Chandrasekhar limit of 1.44 $M_\odot$, or through the merger of two white dwarfs in a double degenerate scenario (e.g., Di Stefano 2010; Mikołajewska 2013; Meng & Han 2016).

Most of the white dwarfs in symbiotic stars will probably not be able to achieve the Chandrasekhar limit as their masses are in the range of $0.4-0.8\,M_\odot$ (Mikołajewska 2007). However, in symbiotic recurrent novae (e.g., RS Oph or T CrB), the white dwarfs are more massive than the giants reaching $\sim 1-1.4\,M_\odot$. Mikołajewska & Shara (2017) provided strong evidence that RS Oph host massive ($\sim 1.3\,M_\odot$) CO white dwarf. Since the maximum mass of the CO white dwarf resulting from the stellar evolution is lower than $\sim 1-1.1\,M_\odot$ (see, e.g., Marigo 2013, and references therein), this suggests that processes connected with the mass transfer from the giant allow

the hot components of, at least, symbiotic recurrent novae, to grow in mass. Such an observational result is also supported by the theoretical predictions (e.g., Hillman et al. 2016). This makes them promising candidates to explode as type Ia supernovae (e.g., Patat et al. 2011; Mikołajewska & Shara 2017). Symbiotic nova progenitor was already proposed by Dilday et al. (2012) for PTF 11kx, the type Ia supernova discovered in 2011.

Known symbiotic recurrent novae are S-type systems. However, the single degenerate scenario can apply also in open symbiotic binary stars with massive white dwarfs and Mira donors (D-type systems), in which the wind Roche lobe overflow mechanism contributing to the mass transfer allows the white dwarf to reach the Chandrasekhar limit. Such a scenario was calculated for symbiotic star V407 Cyg (Iłkiewicz et al. 2019a). A similar symbiotic progenitor was also suggested for the Kepler's supernova (SN 1604) by Chiotellis et al. (2012).

The second possible scenario lies in the formation of the double degenerate system from classical symbiotic systems consisting of a relatively massive white dwarf (0.5– 1 $M_\odot$) and Roche lobe filling giant with a mass of 1 – 3 $M_\odot$. An example of such a system could be AR Pav in which the white dwarf has a mass of about 1 $M_\odot$ (Quiroga et al. 2002). If the system will eventually enter the common envelope phase, this could create a pair of two close white dwarfs with masses of 1 and 0.5 $M_\odot$ (Mikołajewska 2013). Their eventual merger could then lead to a type Ia supernova in the future.

Chapter 2

New Online Database of Symbiotic Variables

The rising number of symbiotic stars in recent years (Chapter 1.1) has increased the demand for a new catalog of symbiotic binaries allowing studies of the symbiotic population in detail. The last catalog was published more than 20 years ago (Belczyński et al. 2000)[1]. We have therefore decided to prepare a new, comprehensive, modern catalog - the New Online Database of Symbiotic Variables (Merc et al. 2019b). The database should serve not only as a catalog of data for all known symbiotic systems with consistent references, but we prepared also a web portal for easy access to this information (`http://astronomy.science.upjs.sk/symbiotics/`). In contrast with all the previous catalogs which became outdated virtually already at the time when their paper versions were published, our database is available online. This allows the addition of new objects as soon as they are discovered and adding or updating the data when new information becomes available. In this way, the up-to-date lists of symbiotic variables and information about particular objects can be available to the community at any time.

Classification criteria. The aim of the work was to collect all the objects which were classified as symbiotic stars or symbiotic candidates in the published literature or in the various databases. The New Online Database of Symbiotic Variables contains both types of symbiotic variables (Chapter 1.2.2): shell-burning (white dwarf accretor)

[1]At the time when we released the first version of our Database, Akras et al. (2019a) published a new census of symbiotic binaries. However, they focused especially on infrared data of symbiotic binaries collected from 2MASS and *WISE* and data from *Gaia* DR2, and have not published the full-scale catalog of symbiotic stars comparable with the previous ones.

and accreting-only (white dwarf or neutron star accretor). Interacting binaries with main-sequence accretors or whose donors are not cool evolved stars are not considered symbiotic binaries for the purpose of this work.

Following the detailed discussion on the definition of symbiotic binaries (Chapter 1.3), the objects are classified as 'Confirmed' symbiotic stars only when the observational data establish the presence of a cool evolved star (absorption features of a late-type giant in the optical or infrared; the presence of Mira pulsator, etc.) and of the degenerate hot companion, that accretes matter from its donor (interaction between the components has to be evident at some wavelengths). This can be demonstrated by the prominent emission lines in the UV-optical spectral region (especially in all shell-burning and some accreting-only symbiotic stars; bright H I and He I lines, and emission lines with the ionization potential of 35 eV and higher) or by the strong UV excess, rapid UV/optical variability (flickering), hard X-ray emission, etc. in the accreting-only systems. In the latter case, only the objects in which the observational data ruled out the possibility that the companion is a main-sequence star are classified as 'Confirmed'. Objects which spectra manifest the Raman-scattered O VI emission lines together with He II 4686 Å line[2] are also classified as 'Confirmed' symbiotic stars, even if the presence of the cool giant is not evident from the observations.

In the first version of the database published in 2019 (Merc et al. 2019b), we have classified the objects only either as confirmed symbiotic stars or candidates. However, with the growing number of objects in the Database, we have realized the need for subdivision of the group of symbiotic candidates into several categories depending on the amount of information available. Therefore, in the present version of the database, the candidates are categorized into three groups: 'Likely', 'Possible', and 'Suspected'. The objects classified as 'Likely' (= strong symbiotic candidates) do not meet all the criteria above, but several pieces of evidence point to their symbiotic nature (e.g., optical observations revealed the presence of a cool evolved star with a typical symbiotic variability, but the spectra show only emission lines with the low-ionization potential, or the accreting-only candidate shows UV excess and flickering, but it is not excluded that the hot companion is a main-sequence star with an accretion disk). The objects are classified as 'Possible', if some observational material was already

[2]Belczyński et al. (2000) suggested that the presence of Raman-scattered O VI lines is a sufficient condition for the symbiotic classification (Chapter 1.3). Akras et al. (2019a) claimed that in all known symbiotic variables in which Raman-scattered O VI lines are present, the He II 4686 Å is also detected. In the sources in which this condition is not satisfied, the detection of Raman-scattered O VI line is dubious.

collected, it does not clearly support other than symbiotic classification, but more data are needed in order to fully confirm the inclusion in the symbiotic group (e.g., optical spectra show some emission lines and the presence of a cool evolved star is supported by the infrared brightness). The category 'Suspected' is created for all the other objects classified as symbiotic candidates in the literature based on various indirect pieces of evidence (e.g., symbiotic-like variability, colors, the possible association of X-ray emission with a cool evolved star).

In addition to the aforementioned categories, we made a decision to maintain also the list of objects, which were once considered symbiotic binaries or symbiotic candidates in the literature, but were later confirmed to be of a different nature. Such stars are included in the list of 'Misclassified' objects. This is important so that objects that are once removed from the lists of symbiotic binaries are later not again considered as symbiotic stars based on older literature. An example could be Hen 2-90 which was classified as a possible symbiotic star by Sahai & Nyman (2000), later confirmed as a B[e] star by Kraus et al. (2007), but again mentioned as a possible symbiotic system by Guerrero et al. (2021). We have also listed objects which are classified as symbiotic variables in the various databases (e.g., SIMBAD; see also below) without any evidence and for which the observational data presented in the literature suggest another classification. For example, Hen 3-814 is classified as a confirmed symbiotic star in SIMBAD with the reference to Henize (1976). However, in the paper, the object is classified as a VV Cep binary which is confirmed by later analyses (e.g., Pereira et al. 2003).

2.1 Structure of the database

The database is divided into two main parts according to the location of symbiotic variables. The first part consists of 825 galactic objects, of which 290 are confirmed symbiotic stars, and 393 objects are classified in one of the candidate groups[3] and 142 objects were previously classified as symbiotic stars or symbiotic candidates, but are reclassified as something else. The second part of the database contains 179 objects (70 confirmed symbiotics, 103 candidates, and 6 misclassified objects) located in 16 galaxies (LMC, SMC, Draco Dwarf, IC 10, M31, M33, M81, M87, NGC 55, NGC 185, NGC 205, NGC 300, NGC 2403, NGC 6822, Sculptor Dwarf, Willman 1).

[3]The symbiotic candidates presented in *Gaia* DR3 (339 objects) are not included in this number. See Chapter 2.7 for a detailed discussion on symbiotic stars in the recent data release of *Gaia*.

Table 2.1: Numbers of confirmed symbiotic stars, symbiotic candidates, and misclassified objects in the current version of the New Online Database of Symbiotic Variables (as of June 30, 2022). Please refer to the online version of the database (`http://astronomy.science.upjs.sk/symbiotics/`) for the up-to-date numbers.

Galaxy	**Confirmed**	**Likely**	**Possible**	**Suspected**	**Misclassified**
Milky Way	290	45	89	259	142
Draco Dwarf	1	0	3	0	0
IC 10	1	0	0	0	0
LMC	10	0	5	22	3
M31	31	5	2	8	1
M33	12	0	0	0	1
M81	0	0	1	0	0
M87	0	0	0	9	0
NGC 55	0	0	0	3	0
NGC 185	1	0	0	0	0
NGC 205	1	0	2	0	0
NGC 300	0	1	0	8	0
NGC 2403	0	0	0	0	1
NGC 6822	1	0	11	0	0
Sculptor Dwarf	0	0	0	9	0
SMC	12	1	7	5	1
Willman 1	0	0	0	1	0
Total	360	52	120	324	148

The numbers of known symbiotic stars, candidates, and misclassified objects in particular galaxies in the present version of the Database are listed in Table 2.1.

There are two possibilities for working with the data contained in the database. Users can either download the whole database or particular tables (see the following section) to a computer, and work with the data offline, or can explore the data online, through the web portal. Moreover, on the web portal, users can choose either to work with the tabular data (Fig. 2.1) or can access the object pages of the particular symbiotic binary (Fig. 2.2).

Tables with data. The database contains data about the position of the objects, their brightness in different spectral regions and bands, and other observational properties (e.g., presence of outbursts, resolved nebulae, jets, flickering, detectable X-ray or radio emission, infrared type), as well as orbital properties (orbital period, orbital ephemeris, presence of eclipses, etc.) and parameters of the binary components (their spectral types, effective temperatures, masses, radii, luminosities, presence of pulsations, etc.). We also included the names of the objects in several other databases (SIMBAD, VSX, GCVS, etc.), their identifiers from various surveys (*Gaia* DR3, 2MASS, *WISE*, *IRAS*, etc.), and cross-identification with previous 8 catalogs of symbiotic bi-

naries (Bidelman 1954; Gaposchkin 1957; Boyarchuk 1969; Allen 1984a; Kenyon 1986; Vaidis 1988, 1991; Belczyński et al. 2000; Akras et al. 2019a).

The data of symbiotic variables are presented in the form of tables, which can be explored directly through the web portal, or can be downloaded and used offline in different formats (csv, xlsx, txt, and pdf). They are divided into seven tabs allowing the user to compare, filter, or sort them easily. From each table, by clicking on the name of the particular symbiotic binary, the user can visit its object page with the information on the object, references, notes, and links.

Object pages. For all symbiotic binaries included in the database, we have prepared their object pages covering all available information that is included in the tables. Every information and value listed is accompanied by the corresponding references which are linked directly to the SAO/NASA Astrophysics Data System[4] database allowing the user to easily and quickly find the original articles. For most of the objects, there are also some notes about interesting features added in the particular section of the page. The object pages contain also links to the portals of SIMBAD, CDS, VSX, and to the survey data such as OGLE, MACHO, and ASAS-SN.

2.2 Symbiotic population in the Database

The significant increase in the number of the confirmed symbiotic stars (360 in the current version of the New Online Database of Symbiotic Variables; 188 and 129 in the catalogs of Belczyński et al. (2000) and Allen (1984a), respectively) and especially the availability of the new estimates of several their parameters (orbital periods, spectral types, masses, etc.) allow to analyze the symbiotic population from the statistical point of view.

Size of the galactic symbiotic population. The current version of the database consists of 290 confirmed galactic symbiotics, of which less than 10 host neutron star accretor. The hot components of the rest are most probably white dwarfs. Although the number increased significantly in the last two decades, it is still deep under the estimated numbers of symbiotic stars hosting white dwarf accretors in our Galaxy, which range from 1 200 – 3 000 (Allen 1984a; Lü et al. 2006) to 15 000 – 30 000 (Kenyon et al. 1993; Lü et al. 2006) or even to 300 000 – 400 000 (Munari & Renzini 1992;

[4]https://ui.adsabs.harvard.edu/

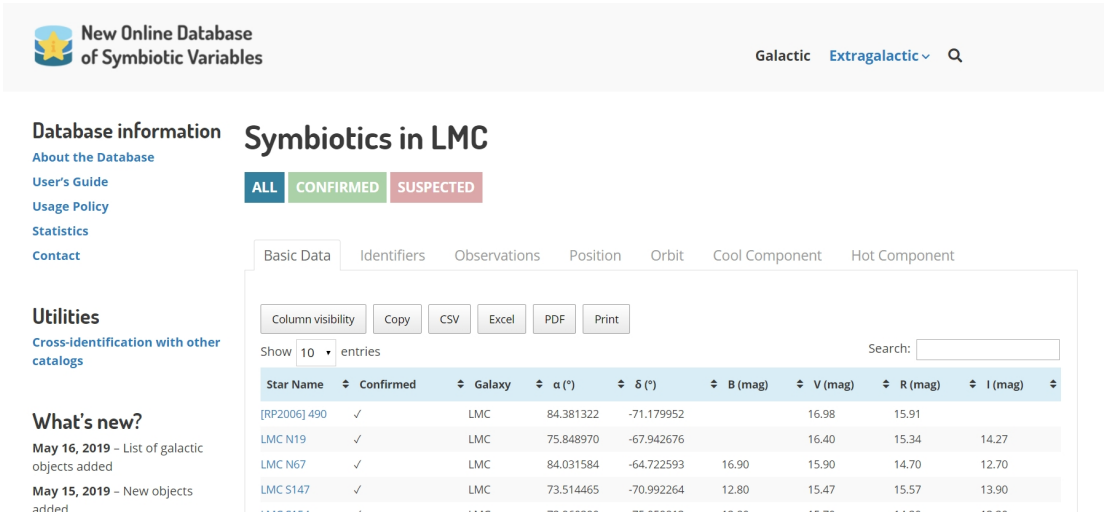

Figure 2.1: Catalog data for symbiotic stars in the LMC.

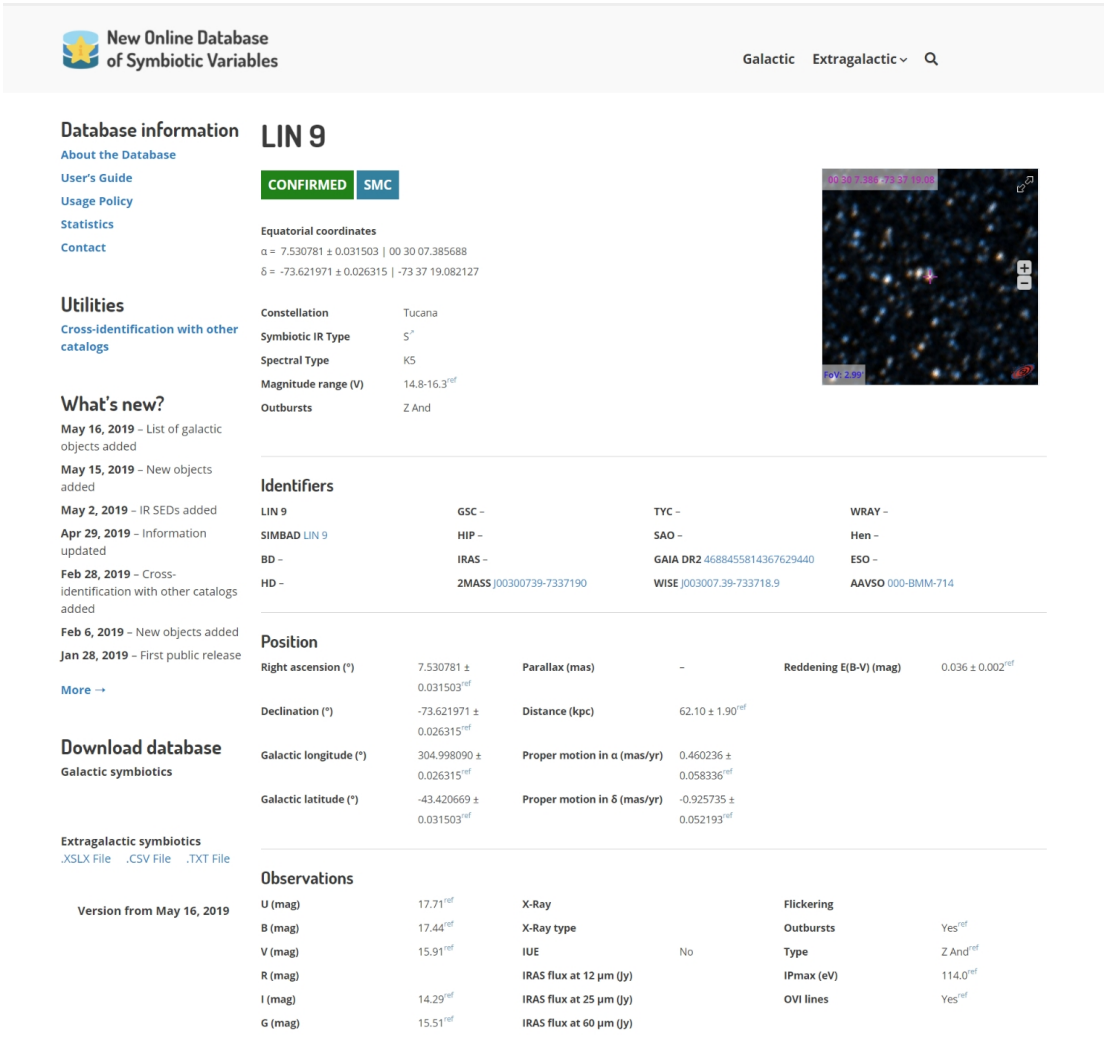

Figure 2.2: Example of the object page of the symbiotic star LIN 9.

Magrini et al. 2003). The reason for this discrepancy may be simply the overestimation of the fraction of red giant-white dwarf pairs showing symbiotic phenomenon, or that previous surveys may have missed the accreting-only symbiotic binaries (Mukai et al. 2016), which could create a significant part of the symbiotic population (see Chapter 1.2.2). When comparing with the population synthesis models, one needs to be careful because the observed sample contains also the weakly-interacting symbiotic stars (typically without emission lines in their spectra), whose hot components have luminosities $<10\,L_{\odot}$ (e.g., some objects from the sample of Munari et al. 2021), and such objects are usually not considered as symbiotic systems in the modeling (Iłkiewicz et al. 2022).

If we take into account also symbiotic candidates, the present version of the database contains 20 objects whose hot components are probably accreting neutron stars (symbiotic X-ray binaries; Chapter 1.2.2). Similarly to the case of white dwarf symbiotic stars, the number of known symbiotic systems with neutron stars is still significantly lower than what population synthesis models predict, as the estimates range from $\sim 50 - 1\,000$ (Lü et al. 2012; Kuranov & Postnov 2015; Yungelson et al. 2019). This fact probably reflects the difficulties connected with discovering such systems as they are typically not conspicuous in the optical region, are generally faint in UV and their X-ray luminosities are often lower than the sensitivity limit of the shallow X-ray surveys. Moreover, these systems are detectable as X-ray sources only for a short fraction of their binary lifetime when the accretion rate is sufficient to generate detectable X-ray luminosity. However, the number of known symbiotic X-ray binaries might increase significantly in the coming years with emerging deep all-sky hard X-rays surveys, e.g., the discovery of a new symbiotic star of this variety was recently announced based on the data from the SRG satellite launched in July 2019 (De et al. 2022). Interestingly, the donor in this system is an extremely evolved Mira-type star with the longest pulsation period among the known symbiotic Miras ($\sim 1\,500$ days).

Position of symbiotic stars in the Galaxy. The distribution of galactic symbiotic variables in the galactic coordinates is shown in Fig. 2.3. Almost all galactic symbiotic stars are located around the Milky Way equator ($|b| < 10°$). For the objects in the current version of the Database, 80% of the confirmed symbiotics and 75% of candidates are located in this sky region. The value rises to 90% for confirmed galactic symbiotic star for $|b| < 18°$. The distribution in the galactic longitude demonstrates that a significant number of symbiotic stars is located towards the galactic bulge (59%

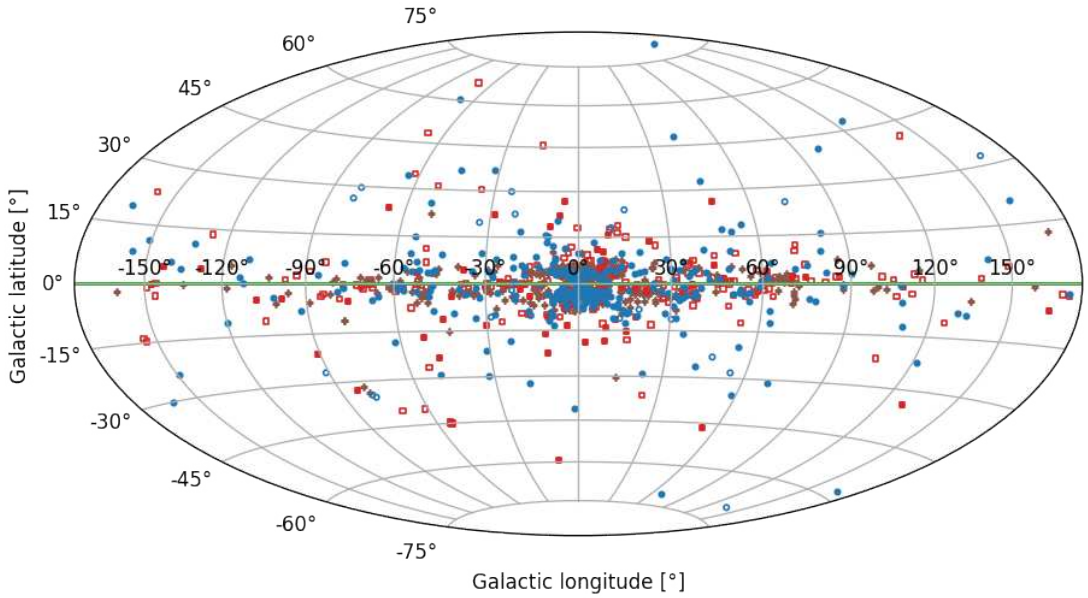

Figure 2.3: Distribution of symbiotic stars in our Galaxy. Confirmed, likely, possible and suspected symbiotic stars are denoted by blue full dots, blue empty dots, red full squares, and red empty squares, respectively. New candidates published in *Gaia* DR3 are depicted by the brown plus signs (see Chapter 2.7 for more details). Misclassified objects are not shown. The green line represents the equator of the Milky Way. The concentration towards the galactic plane/bulge is well visible.

and 57% for the confirmed symbiotic systems and candidates with $330° < l < 30°$, respectively). These ratios are though biased by the selective effect, as surveys tend to focus on the surroundings of the galactic equator. However, this would surely be also the consequence of the fact that the density of stars is higher in the galactic disk and symbiotic stars mostly belong to the old bulge/thick disk population.

Interestingly, all of the confirmed galactic symbiotic stars are isolated systems and up to now, no symbiotic stars were confirmed in the globular clusters, although some (but very few) are predicted to exist in the outskirts of less dense globular clusters (Belloni et al. 2020). Symbiotic candidate in ω Cen which was discovered as an X-ray source coincident with a carbon giant (Henleywillis et al. 2018) was later found not to be a symbiotic system but a positional coincidence of two physically unrelated sources (Belloni et al. 2020). Another object has been recently suggested to be a symbiotic system located in the globular cluster 47 Tuc (Saeedi et al. 2022), but a detailed analysis including optical spectroscopic follow-up still needs to be carried out in order to confirm or reject the symbiotic nature of this target.

It is worth noting that some of the known symbiotic stars might live in triple systems. A fraction of such systems should not be very large though, as only around

10% of the low-mass stars are found in triple system (e.g., Tokovinin 2008, 2014; Moe & Di Stefano 2017). For example, the well-known symbiotic star CH Cyg whose orbital period is suggested to be 750 days, might have a companion (possibly G-type dwarf) on a 15-year orbital trajectory (Hinkle et al. 1993; Iijima et al. 2019). On the other hand, the model in which the giant pulsates with a period of 750 days and the orbital period is one of 15 years was also proposed (Hinkle et al. 2009). In the case of accreting-only symbiotic star CQ Dra, the hot component is probably a cataclysmic variable with an orbital period of around 4 hours on a 1703-day orbital trajectory around the normal M giant (Reimers et al. 1988; Sion et al. 2017). Actually, there might be an additional star associated with CQ Dra according to *Gaia* EDR3 data which suggest the presence of the faint star at the same distance and with a similar proper motion located $\sim 9''$ away from CQ Dra. That translates to the physical distance of ~ 1600 au between the objects.

Extragalactic symbiotic stars in the Database The number of extragalactic symbiotic stars and symbiotic candidates has increased by a factor of 10 since the beginning of this century. In the recent version of our Database, there are 70 confirmed and 103 suspected extragalactic symbiotic systems. The positions of these sources within their host galaxies are shown in Fig. 2.4. For the proper description of the extragalactic symbiotic population, a systematic search for these objects is needed. Such surveys have started in recent years and focused on the galaxies M31 and M33 (Mikołajewska et al. 2014a, 2017). The analysis revealed 31 and 13 symbiotic stars in those two galaxies, respectively. The continuation of these efforts that resulted in the discovery of more than 100 further symbiotic objects in M31 will be published later (J. Mikołajewska, private communication). Symbiotic stars and candidates in other galaxies were usually discovered serendipitously, during the surveys of emission-line objects (e.g., Gonçalves et al. 2008, 2012, 2015; Kniazev et al. 2009; Sibbons et al. 2015; Magrini et al. 2017; Roth et al. 2018), thanks to their X-ray emission (e.g., Saeedi & Sasaki 2020, 2022), or variability (e.g., Shara et al. 2016).

Among the extragalactic symbiotic stars, systems located in the Magellanic Clouds, satellite galaxies of the Milky Way, have a special place, as they are bright enough to be, at least photometrically, studied using meter-class telescopes. Moreover, they evolved in an environment with a lower average metallicity than the symbiotic systems in the Galaxy, therefore the comparison of these two populations can be very useful for research of the evolution of symbiotic stars. However, the number of known

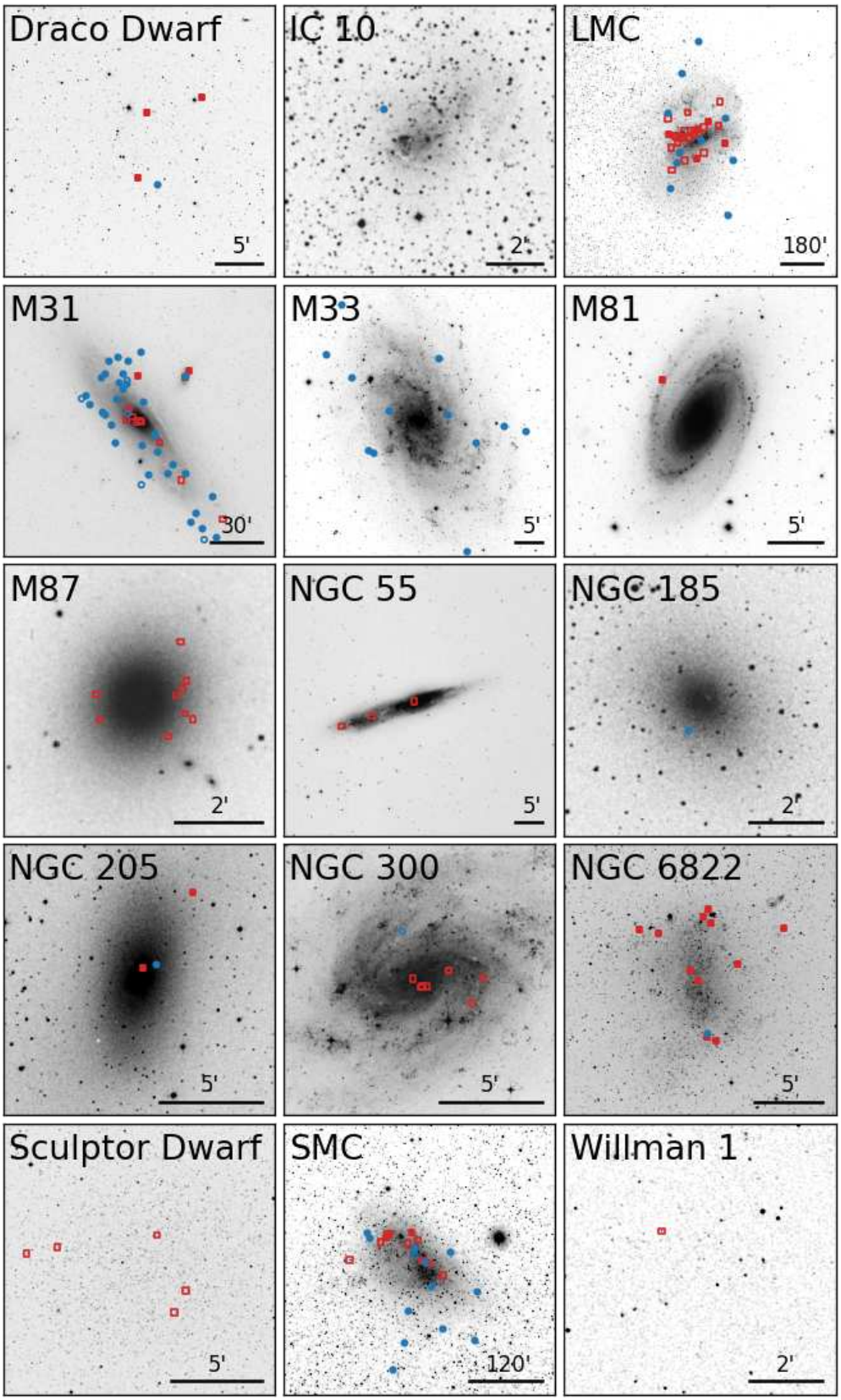

Figure 2.4: Positions of the extragalactic symbiotic stars included in the New Online Database of Symbiotic Variables within their host galaxies. Confirmed, likely, possible and suspected symbiotic stars are denoted by blue full dots, blue empty dots, red full squares, and red empty squares, respectively. Misclassified objects are not shown.

symbiotic systems in these galaxies is much lower than any estimate of the size of the Magellanic symbiotic population (similarly to the case of our Galaxy), and the specific surveys looking for these interacting binaries in the Magellanic Clouds have just started. The first paper in the presumed series by Ilkiewicz et al. (2018) presented the discovery of three new symbiotic stars in the Small Magellanic Cloud. To increase the size of the sample, we aimed to analyze the available data of the symbiotic candidates located in the Large Magellanic Cloud in this thesis (see Chapter 3.4).

The greatest advantage of studying extragalactic symbiotic systems is that their distances are usually known with good precision as they practically correspond to the ones of their parent galaxies. The distances to galaxies could be obtained using various independent methods. If the distance of the symbiotic system is known, its component luminosities and other distance-related parameters could be determined precisely, which is very useful for the comparison of observations with theoretical models.

Symbiotic stars in GCVS, VSX, SIMBAD. Having the full list of confirmed symbiotic stars, symbiotic candidates, and misclassified objects from the New Online Database of Symbiotic Variables, we have compared it with the objects classified either as symbiotic stars or possible symbiotic stars in the widely used databases, namely in the General Catalogue of Variable Stars (GCVS; Samus' et al. 2017), the International Variable Star Index maintained by AAVSO (VSX; Watson et al. 2006), and in the SIMBAD Astronomical Database (Wenger et al. 2000). The main goal of this comparison was to find out the portion of correctly classified symbiotic sources in these databases that are often used as the input data for the subsequent analyses in many studies.

In GCVS, 230 out of 1 004 objects from our Database are listed. Of the objects included in GCVS, only 58 are classified as confirmed symbiotic binaries (of which 4 are actually misclassified objects and a further 2 are candidates in our Database). Further 19 objects are classified as possible symbiotic binaries in GCVS, 11 of which are already confirmed as symbiotic stars, 3 are classified as candidates in our Database and 5 do not have symbiotic nature. Another 152 have other than symbiotic variability types attributed in GCVS (among them 51 confirmed symbiotic stars and 44 candidates) and 1 has no variability type listed (symbiotic candidate in our Database). That means that only $\sim$ 14% of the confirmed symbiotic stars are correctly identified in GCVS, and moreover, 12% of the sources classified as confirmed or possible symbiotic

stars in GCVS are not symbiotic systems.

We performed a similar analysis also for VSX which contains 579 out of 1 004 objects from our database - 232 are classified as symbiotic stars (210 correctly, 16 are candidates in our Database and 6 are misclassified), 48 as symbiotic candidates (32 correctly, 12 are confirmed symbiotic stars and 4 are misclassified), 281 have other variability types (94 of these are misclassified, 50 are confirmed symbiotic systems and 137 of them are candidates) and 18 have no classification (2 known symbiotic stars, 15 candidates and 1 misclassified object). Taken together, VSX contains 58% of all known symbiotic stars and about 3.5% of the objects classified as symbiotic stars and candidates in VSX have different nature in reality.

The SIMBAD database contains the highest number of sources from the New Online Database of Symbiotic Variables, 894 out of 1 004. From this number, 284 are classified as confirmed symbiotic stars (251 correctly, 22 candidates, 11 misclassified), 57 sources are listed as candidates (29 correctly, 24 are confirmed symbiotics, 4 are misclassified), and 552 object do not have symbiotic or possible symbiotic classification listed among main or other types in SIMBAD (130 of these are misclassified objects in our Database, 76 are confirmed symbiotic stars, 346 are candidates). To sum up, one can find $\sim$ 70% of all confirmed symbiotic stars correctly classified in SIMBAD, while this database lists among symbiotic systems and symbiotic candidates $\sim$ 4.5% incorrectly included objects.

For comparison, the census of Akras et al. (2019a) contains 323 confirmed and 87 suspected symbiotic stars. Of the confirmed objects, 3 were reclassified since the catalog was published and 6 are cataloged as candidates in our Database. That means that this catalog published in 2019 contains only 87% of the currently known symbiotic binaries. That strongly favors our decision to have an online version of the symbiotic database that can be updated regularly. Of the symbiotic candidates, 4 are confirmed and 6 were found to have different nature at present. The contamination rate in the catalog is about 2%.

2.3 Orbital parameters of known symbiotic stars

Although photometric variability of symbiotic stars had been known from the beginning of their research (Chapter 1.1), only later these changes were associated with the orbital motion of binary systems.

Orbital periods. The orbital periods of symbiotic stars were estimated either thanks to the observation of eclipses, reflection effect, or later some of them were determined from the spectroscopic measurements. At the beginning of this century, the orbital periods were known for about 20% of known symbiotic binaries - Belczyński et al. (2000) listed orbital periods for 34 confirmed symbiotic systems, among them 20 had orbital elements determined based on radial velocities. Mikołajewska (2003) presented the compilation of 27 spectroscopic orbits. In addition to estimates that have been published for some individual objects in the literature since then, the major advancement stemmed from the systematic infrared spectroscopic observations of symbiotic stars which in many cases produced the first spectroscopic orbits (Fekel et al. 2000a,b, 2001, 2007, 2008, 2010, 2015, 2017; Hinkle et al. 2006, 2009, 2019). The analysis of the light curves of symbiotic stars from the ASAS, MACHO and OGLE surveys by Gromadzki et al. (2013) resulted into the further significant increase in the number of symbiotic stars with known orbital periods. They presented the compilation of about 70 orbital periods of confirmed symbiotic stars, of which 34 were estimated for the first time.

In the New Online Database of Symbiotic Variables, the largest collection of orbital periods of known symbiotic stars ever published is presented - 140 confirmed symbiotic systems have some periods estimates ($\sim 39\%$ of the whole sample of confirmed galactic and extragalactic symbiotic stars). Only 17 of these are objects outside our Galaxy. Most of their period estimates are based on photometric measurements and their values are not certain. Solely one of the extragalactic symbiotic systems, Draco C1, has a spectroscopic orbit (Lewis et al. 2020), while this is true for almost 50 galactic objects. One should note that while for S- and D'-type symbiotic stars the periods are estimated from light curves or spectroscopic data, for very wide D-type systems, the orbital periods are usually estimated only from the approximated separations of the components or semi-major axes. The only exception is the D-type symbiotic star R Aqr, for which the radial velocity data allowed to derive a reliable spectroscopic orbit with an orbital period of 43.6 years (Gromadzki & Mikołajewska 2009). The adopted values for other D-type symbiotic stars have to be taken with caution as they are much less certain.

The distribution of the orbital periods of confirmed symbiotic systems is shown in Fig. 2.5. While this is the most extensive sample ever analyzed in the literature, it confirms the earlier results obtained from smaller samples (e.g., Mürset & Schmid 1999; Mikołajewska 2003, 2007, 2012). One can clearly see that most of the S-type

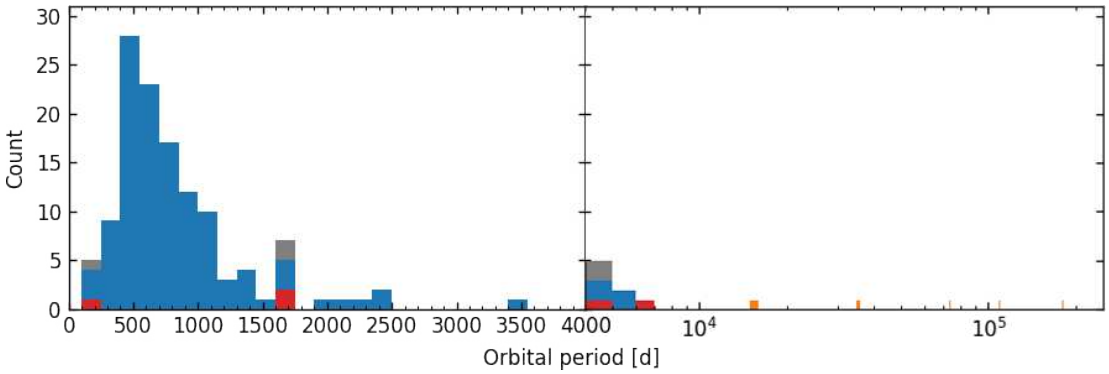

Figure 2.5: Distribution of the orbital periods of all confirmed symbiotic stars (shown in gray). The S-, D-, and D'-type symbiotic systems are shown in blue, orange, and red, respectively. Note that the scale for periods <4 000 days is linear while it is logarithmic for longer ones.

symbiotic binaries have periods in the interval of 300 – 1 100 days, with the peak between 500 and 600 days. Only about one-fifth of all characterized S-type symbiotic stars have orbital periods longer than 1 100 days, less than 5% of them lie on the shorter end with periods below 300 days, and only two are below 200 days - V483 Sct (197.6 days, but the period is quite uncertain; Munari et al. 2001a) and TX CVn (199 ± 3 days; Kenyon & Garcia 1989). The orbital periods of all D'-type symbiotic binaries are longer than 1 500 days, except for StHα 190 for which Munari et al. (2001b) suggested the orbital period of 171 ± 5 days based on the light curve and preliminary analysis of radial velocities of stellar Na I doublet, and Smith et al. (2001) proposed even shorter value of 37 – 39 days based on the subsequent observations. Open D-type systems hosting very evolved Mira pulsators have orbital periods in tens or even hundreds of years ($\sim$ few $\times$ 10^4 – 10^5 days), but they were estimated only for a very small number of systems.

The observed distribution of orbital periods is in very strong contrast with the predictions from the population synthesis models. For example, the results presented by Lü et al. (2006) predicted the peak in the distribution for the period $\sim$ 1 500 days with only $\sim$ 20% of symbiotic stars having the periods below 1 000 days, while practically the exact opposite seems to be true in reality. Moreover, Gromadzki et al. (2013) claimed that this discrepancy cannot be caused by the selection effects as was previously suggested, and concluded that the explanation of the orbital period distribution requires different, more advanced approaches to mass transfer modeling in symbiotic stars and interacting binaries with the red giant component in general.

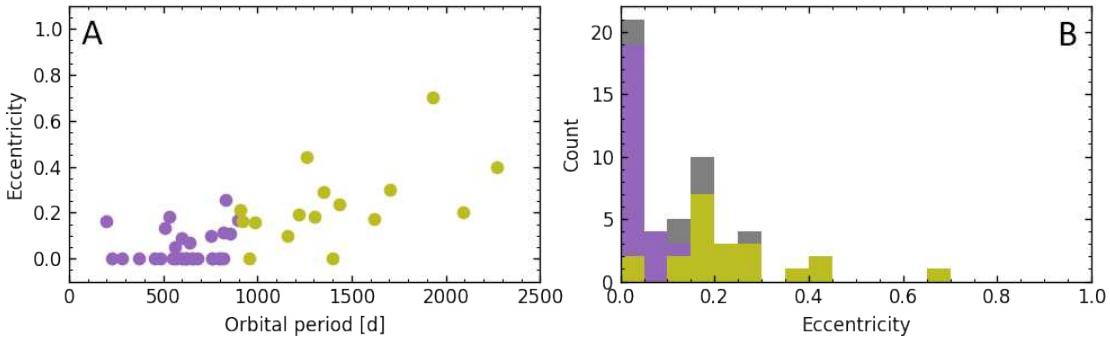

Figure 2.6: Eccentricity of symbiotic orbits. **A:** Position of confirmed symbiotic stars with known orbital elements in the e-P plane. Magenta color denotes the symbiotic stars with orbital periods below 900 days, while yellow above this value. **B:** Distribution of the eccentricities of orbits of symbiotic stars (shown in gray). Magenta and yellow color denote the same groups as in the previous panel.

Eccentricity of orbits. The distribution of eccentricities of the orbits of confirmed symbiotic binaries is shown in Fig. 2.6. It is clear that the majority ($\sim 90\%$) of symbiotic stars whose orbital periods are below 900 days (S-type systems) have circular or nearly circular orbits (i.e., $e < 0.15$). The only symbiotic star with a period below 500 days with non-zero eccentricity is TX CVn ($e \sim 0.16$; $P = 199$ days). The observed distribution strongly differs from what is observed in other binaries containing cool evolved giants, in which a significant fraction of systems with orbital periods below 900 days have eccentric orbits (see, e.g., Jorissen & Mayor 1992; Mazeh 2008; Beck et al. 2018, 2022; Hoyman et al. 2020). This suggests that in the majority of symbiotic systems mass transfer and strong tidal interaction in the prior evolutionary phases changed the orbit of a binary (Mikołajewska 2012).

Eclipses. For about 7 – 10% of confirmed symbiotic binaries in the New Online Database of Symbiotic Variables, some evidence of eclipses in the light curves has been reported in the literature. It is worth noting that for several of the confirmed systems, the long-term photometry is not available or has not yet been studied, so the real fraction of eclipsing symbiotic systems might be even larger. Moreover, in many cases, the prominent eclipses of the hot component and the surrounding ionized nebula by the cool companion are observed only during the active stages (e.g., Skopal et al. 2011; Kato et al. 2012; Merc et al. 2022b, see also Fig. 1.6).

The fraction of eclipsing symbiotic stars seems to be significantly higher than the share of eclipsing systems among the binaries with similar orbital periods in general (see, e.g., the sample from Kepler in Prša et al. 2011; Kirk et al. 2016). This can be explained by the fact that while in typical non-interacting eclipsing binaries, one stellar

source eclipses another one and the eclipses are therefore observed only for inclination very close to 90° for longer orbital periods, in symbiotic binaries, especially during outbursts, the eclipsed component is extended which allows the eclipses to be detected also for a range of lower inclinations.

2.4 Cool components of known symbiotic stars

By definition, the cool components of the symbiotic binaries are evolved giant stars (Chapter 1.2.1). The symbiotic giants are usually characterized using the optical and infrared spectra as given their temperatures, they dominate in these spectral regions.

Spectral types and effective temperatures The largest uniform sample of the spectral types of the cool components in symbiotic binaries was published by Mürset & Schmid (1999). They classified the cool components in about 100 systems based on the NIR spectra. Belczyński et al. (2000) collected the spectral types for almost all of the 188 confirmed symbiotic binaries in their catalog from the literature, though some of the classifications were limited only to distinguishing between spectral types G, K, or M. Additionally, Akras et al. (2019a) modeled infrared SEDs of almost 230 of confirmed symbiotic stars in order to obtain the effective temperatures of their cool components and to study the temperature distribution.

For the New Online Database of Symbiotic Variables, we have compiled the spectral types for 325 confirmed symbiotic binaries (90% of the whole sample) and for 178 candidates (about 36% of all candidates in the Database). Additionally, we have collected also the published effective temperatures. For this reason, the sample in the Database constitutes the largest collection of spectral types and/or effective temperatures of cool components in symbiotic stars available at present.

The distribution of spectral types of the cool components in confirmed symbiotic binaries is shown in Fig. 2.7. Our results obtained from the significantly increased sample are similar to the previous conclusions of, e.g., Medina Tanco & Steiner (1995), Mürset & Schmid (1999), and Mikołajewska (2003) - the spectral types of the S-type symbiotic binaries with M-type components cluster between spectral types M3 and M6, with the highest number classified as M5.

Interestingly, there is an apparent second peak in the distribution of spectral types of S-type symbiotic stars around K5 – M0. This is partly caused by the discoveries of new yellow symbiotic stars. However, the strong clustering around this interval might

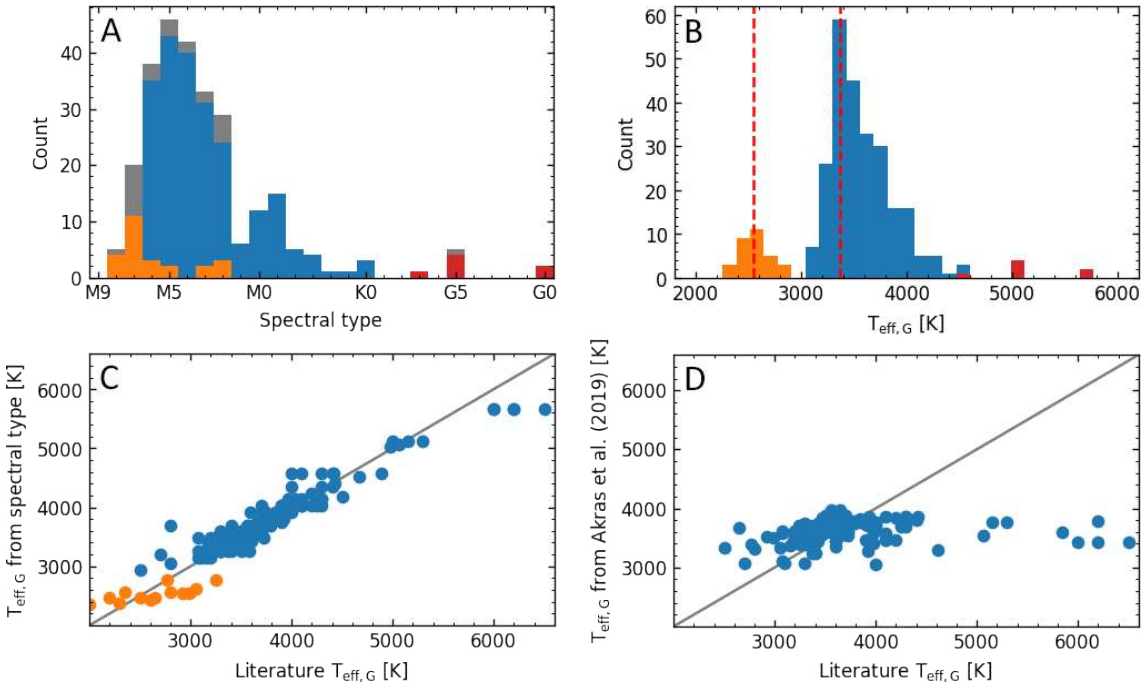

Figure 2.7: Spectral types and effective temperatures of symbiotic giants. **A:** Distribution of the spectral types (gray). S-, D-, and D'-type symbiotic stars are shown in blue, orange, and red, respectively. **B:** Distribution of effective temperatures of cool components. Temperatures of S- and D'-type symbiotic stars obtained from the spectral types using the calibration of van Belle et al. (1999) are shown in blue and red, respectively. Temperatures of symbiotic Miras with known pulsation periods are shown in orange. Vertical red dashed lines denote median values for the two groups (2 550 and 3 370 K, respectively). **C:** Comparison of the effective temperatures published in the literature with the ones obtained from the spectral types of normal giants and pulsation periods of Mira cool components. See the text for more details. **D:** Comparison of the effective temperatures from the literature with the ones obtained by Akras et al. (2019a) by modeling of the infrared SED. See the text for more details.

be, to some extent, also connected with the observational difficulties to estimate the accurate spectral types of these objects from the optical spectra as they have weak or absent TiO bands. Therefore, it is quite possible that some of the objects with the spectral types in this interval have actually earlier spectral types, which would make the distribution slightly more continuous towards higher temperatures. On the other hand, a mild overabundance of K5 – M0 symbiotic systems was already present in the sample of Medina Tanco & Steiner (1995). Symbiotic stars of D-type (symbiotic Miras) clearly peak at spectral types M7-8. The symbiotic stars of infrared type D' have, by definition, the cool components of spectral types F/G (Chapter 1.2.1), but their number is too low for reasonable statistical analysis.

Allen (1980b) and Mürset & Schmid (1999) noted the significant preference of the later spectral types of symbiotic giants in comparison with the field giants in the solar

neighborhood. While we have a larger number of yellow symbiotic stars or systems hosting earlier M-type giants in our sample, the former conclusions still hold. The giants in symbiotic stars, which are of later spectral types, are more evolved and have a larger radius, and higher mass loss, which seem to be important ingredients for the symbiotic phenomenon (Mikołajewska 2003). Whitelock & Munari (1992) suggested that while the symbiotic giants are not similar to the bright giants in the solar neighborhood, they are similar to the giant found in the Galactic Bulge and elsewhere. However, these stars have metallicities higher than solar and have low masses (~ 1 M$_\odot$; Whitelock & Munari 1992) while recent analyses of the abundances of the M giants in symbiotic binaries suggested sub-solar metallicities and the higher masses with a peak around 1.5 M$_\odot$ (see below).

It is also worth noting that in addition to O-rich giants, some symbiotic stars are hosting C-rich giants. In the galactic sample, the occurrence is very low: only 10 of 269 confirmed symbiotic stars with known spectral types contain C-rich cool components (additional 7 host S stars). This translate to about a 3.7% fraction among galactic symbiotic stars. On the other hand, among the Magellanic symbiotic systems, one can find 4 out of 8 (LMC) and 2 out of 8 (SMC) carbon giants which might be connected with the lower overall metallicity of the Magellanic Clouds (Munari 2019). In M31, no carbon symbiotic star is found, while in M33, 4 symbiotic stars have carbon giants (25% of symbiotic systems with known spectral types).

As mentioned above, we have also collected the effective temperature estimates from the literature. These are often independently derived, e.g., from the multi-frequency SEDs or from the modeling of spectra. To obtain a larger sample, we have calculated the effective temperatures of cool components of S- and D'-type O-rich symbiotic stars also from their spectral types using the calibration of van Belle et al. (1999). We excluded the objects classified as S or C giants. Such an approach should be independent of the luminosity class (e.g., de Jager & Nieuwenhuijzen 1987; van Belle et al. 2009), and gives results very consistent with the estimates published in the literature (as demonstrated by the comparison in Fig. 2.7C). The only exception is three D'-type symbiotic stars for which the spectral type G0 is reported in the literature (which we used for temperature calculation), but independently published temperatures (6 000 – 6 500 K) are more consistent with spectral types F4-7 III (e.g., Alonso et al. 1999).

The temperatures of symbiotic Miras for which their pulsation periods are known were estimated from the calibrations of Glass & Feast (1982). The obtained tempera-

tures are, within their errors, similar to ones obtained using the spectral type-effective temperature relation for Mira variables inferred by van Belle et al. (1996). Note that in the case of Mira variables, the resulting temperatures are lower in comparison with the red giants of the same spectral types (van Belle et al. 1996). The resulting distribution of the temperatures is shown in Fig. 2.7B. The temperatures of S-type symbiotic stars have a median of 3 370 K, while symbiotic Miras have a peak at 2 550 K.

A comprehensive collection of effective temperatures of cool components of symbiotic giants was inferred by Akras et al. (2019a) from the infrared SEDs. However, our comparison of their temperatures with the estimates from the literature (Fig. 2.7D) showed serious inconsistencies for some sources. We clearly see from the comparison that while for the stars with temperatures in the range from $\sim$ 3 000 – 3 900 K, their method gives more or less consistent results (given the estimated errors for their temperatures of 250 – 450 K), the inferred temperatures are severely underestimated for symbiotic stars whose cool components are K and G giants (with temperatures $>$ 3 900 K; yellow S- and D'-type systems).

In their work, Akras et al. (2019a) compared their temperatures only with a small sample of literature values (48 symbiotic stars), and due to how they decided to plot the comparison (the plot of their temperatures on the X-axis vs. difference from the literature estimates on Y-axis; Fig. 7 therein), they have not identified the issue of symbiotic systems with cool components of earlier spectral types, which is clearly visible in our Fig. 2.7D. They also compared their results with the temperatures published for 171 sources in *Gaia* DR2 catalog. However, it is necessary to note that the astrophysical parameters are inferred only from the three broad filters and are very unreliable for symbiotic giants due to the fact that the radiation of the nebulae and possibly of the hot components significantly contribute to the measured radiation in these filters (see, e.g., the comparison of the symbiotic SED with the transmission curves of the *Gaia* filters in Merc et al. 2021c).

Akras et al. (2019a) fitted the 2MASS and *WISE* data using the black-body models: one for S-type systems (for a stellar source), two or three for D- and D'-type systems (stellar source and cool dust shell/-s). The temperatures of stellar sources obtained from the black-body fits were then corrected to account for differences between the black-body and effective temperatures. Using such an approach, without putting any constraints on the temperatures of stellar sources, it is not easy to remove the degeneracy between the temperature of the star and that of the dust.

For example, in several cases of D'-type symbiotic stars, the SED can be fitted

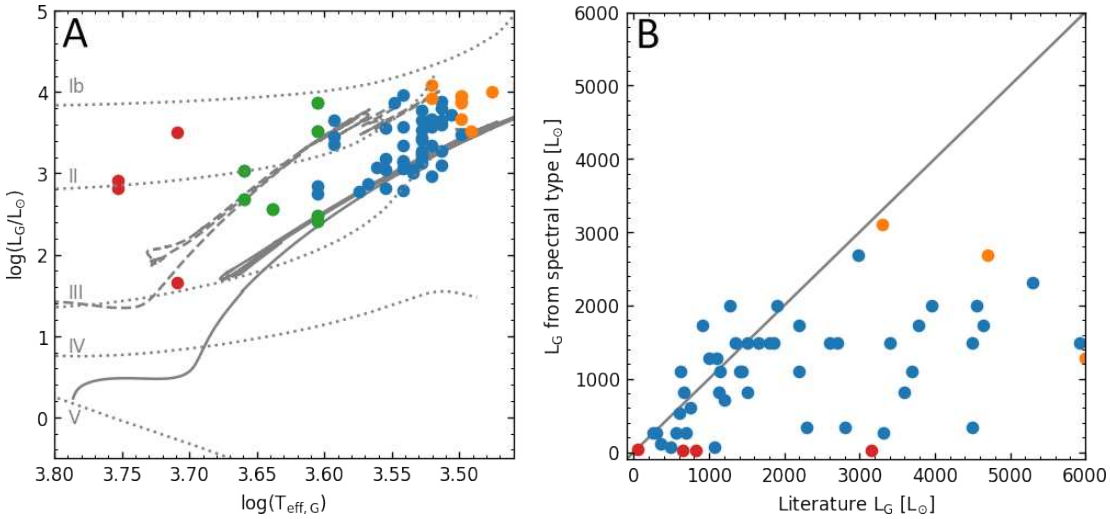

Figure 2.8: Luminosities of the symbiotic giants. **A:** Position of the symbiotic giants in the HR diagram. Temperatures are estimated from the published spectral types (see the text for details), and luminosities were collected from the literature. S-type symbiotic stars hosting M and K giants are shown in blue and green, respectively. D-type systems with Mira pulsators are depicted in orange. D'-type symbiotic stars (G giants) are shown in red. The dotted gray lines render luminosity and temperatures of the stars of various luminosity classes (Ib – V; de Jager & Nieuwenhuijzen 1987). For illustration, the MESA evolutionary tracks (Paxton et al. 2011) obtained using MIST Web Interpolator (Choi et al. 2016) for 1.5 $M_\odot$ stars with metallicities of [Fe/H] = -0.18 (median value for S-type systems with M giants), and [Fe/H] = -1.15 (yellow symbiotic stars) are shown with solid gray and dashed gray lines, respectively. **B:** Comparison of the literature luminosities of the symbiotic giants with the luminosities calculated using the Stefan–Boltzmann law from the values of effective temperatures and radii obtained from the relations for red giants (luminosity class III; van Belle et al. 1999). The used colors of points denote the same groups of symbiotic stars as in panel A.

with the hotter stellar source ($\sim$ 5 000 – 5 500 K) and two dust shells, but the same 7 photometric points used for construction of the SED can be fitted with the cooler stellar source ($\sim$ 3 000 – 3 500 K), perhaps with some additional black-body to account for the infrared excess (their S+IR type; see the discussion below). We should also note that they did not correct the data for interstellar reddening which can be non-negligible in some cases and change the temperature estimate significantly.

Luminosity classes of the cool components We have also collected the cool component luminosity estimates from the literature. These values and the temperatures discussed in the previous section are used to construct the HR diagram for symbiotic giants shown in Fig. 2.8A. In the figure, symbiotic giants are compared with the stars of various luminosity classes (Ib – V; de Jager & Nieuwenhuijzen 1987) and with the MESA evolutionary tracks (Paxton et al. 2011) obtained using MIST Web Interpolator (Choi et al. 2016) for 1.5 $M_\odot$ stars (median mass of the cool compo-

nents in symbiotic stars; see below) with metallicities of [Fe/H] = -0.18 (median value for the S-type systems with M giants) and [Fe/H] = -1.15 (yellow symbiotic stars). It is clearly seen from the comparison that typical cool components in the symbiotic stars are located in the region of the HR diagram occupied by the luminosity classes of III – II. This is consistent with the conclusion that these giants are typically either at the top of the RGB, or they are early AGB stars with some systems being among more evolved AGB stars (e.g., Mikołajewska 2007).

In Fig. 2.8B, we show the comparison of the literature luminosities with the values corresponding to the particular spectral types of symbiotic giants. These were calculated using the Stefan–Boltzmann law adopting the temperatures and radii obtained from the relations for red giants (luminosity class III; van Belle et al. 1999). It is clear from the figure, that the luminosities calculated under the assumption of luminosity class III are often underestimated (in the HR diagram, they occupy the region of luminosity class III – II). Therefore an approach of obtaining luminosity from a spectral type is not appropriate in this case, in contrast to effective temperatures (see Fig. 2.7C and the discussion above). One should keep in mind that the luminosity of the star is a distance-dependent parameter and unfortunately, the distances to symbiotic binaries are often poorly known.

Metallicities While the metallicities of some objects from the sample of yellow symbiotic stars (hosting K giants) were known since the nineties (see, e.g., Pereira et al. 2017, and references therein), the chemical abundances of the symbiotic giants of M spectral type were obtained only recently. Mikołajewska et al. (2014b) and Gałan et al. (2015, 2016, 2017) used the high-resolution near-IR spectra and employing the spectrum synthesis method, they obtained abundances for about 40 southern symbiotic giants.

The distribution of metallicities of all symbiotic giants for which these data are published in the literature is shown in Fig. 2.9. Sample collected in the New Online Database of Symbiotic Variables confirms the previous suggestions (e.g., Mikołajewska 2007; Gałan et al. 2016), that M giants in symbiotic stars have on average slightly sub-solar metallicities - the median is [Fe/H] = -0.18. This is in contrast with the suggestion of Whitelock & Munari (1992) who claimed that the symbiotic giants are similar to the metal-rich, low-mass M giants in the Galactic Bulge. Therefore Gałan et al. (2016) suggested that efficient mass loss is needed in order to explain the symbiotic activity. We should add that according to Munari (2019) all the abundances were

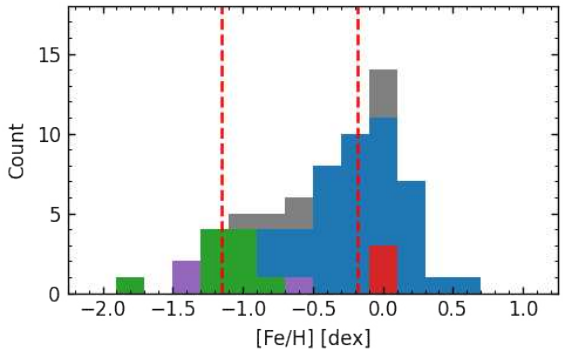

Figure 2.9: Distribution of metallicites of symbiotic giants (gray color). The symbiotic stars hosting M-type giants are shown in blue. Yellow symbiotic stars (K-type giants), D'-type systems (G giants), and symbiotic stars with C-rich giants are shown in green, red and purple, respectively. Vertical red dashed lines denote median values for the M-type giants ([Fe/H] = -0.18) and K-type giants ([Fe/H] = -1.15).

obtained adopting several simplifications (e.g., thin, plane-parallel, static, LTE atmospheres), which are, according to the authors, in strong contrast with real atmospheres of red giants, and therefore the abundances should be treated with caution.

Yet the symbiotic giants seem to have slightly higher masses in comparison with the Galactic Bulge giants (see below). To complete the discussion of the metallicities of the cool components in symbiotic binaries, we add that all the yellow symbiotic stars analyzed up to now host metal-poor (median [Fe/H] = -1.15) and s-process overabundant K giants, as already reported in the literature previously. On the other hand, all analyzed G giants in D'-type symbiotic stars have solar metallicities.

Masses The cool component mass estimates for 17 and 22 symbiotic giants were collected and presented in Mikołajewska (2007) and Mikołajewska (2010), respectively. From their data, it is clear that the symbiotic cool components belong to the low-mass population with $M_{\rm G} \leq 2$ - 3 $\rm M_{\odot}$. These results are confirmed by the significantly larger collection of cool component masses (66 confirmed symbiotic stars) in the New Online Database of Symbiotic Variables whose distribution is shown in Fig. 2.10. Most of the symbiotic giants have masses in the interval of 1 – 3 $\rm M_{\odot}$, with only a small fraction found with masses >3 $\rm M_{\odot}$ (typically found in D'-type systems). The median of our sample is 1.5 $\rm M_{\odot}$. This suggests that the symbiotic giant population is indeed different from the low-mass metal-rich giants found in the Galactic bulge which have masses $\sim$ 1 $\rm M_{\odot}$ and whose connection with the symbiotic population was suggested by Whitelock & Munari (1992).

In Fig. 2.10, we have highlighted the group of symbiotic recurrent novae (shown

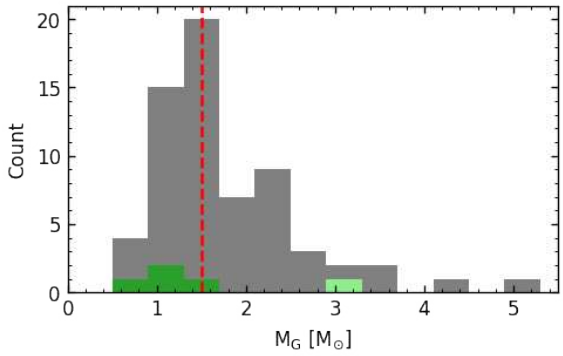

Figure 2.10: Masses of symbiotic giants (gray). The vertical dashed red line denotes the median value of 1.5 $M_\odot$. The symbiotic stars showing symbiotic recurrent nova outbursts are shown in dark green. A light green color denotes V407 Cyg showing similar outburst properties but is not included in the group of genuine recurrent novae as only one outburst was observed so far (see the text for details).

in green) whose cool components seem to have masses $\sim$ 1 $M_\odot$ and mass ratio $q = M_{\rm G}/M_{\rm h} \leq 1$ (see below). V407 Cyg (light green in the figure) showed similar outburst properties but constitutes an exception. Its cool component is more massive, it is pulsating as a Mira-type variable (D-type system), and the progenitor of the present hot component in this symbiotic system was also a more massive star ($\sim$ 4 – 8 $M_\odot$; Mikołajewska 2010). We should note that this star is not classified as a genuine recurrent nova as only one outburst was observed so far.

Variability of the cool components The long-term photometric observations, especially the systematic ones obtained by the photometric surveys covering a significant part of the sky, such as OGLE, ASAS, MACHO, ASAS-SN, or ZTF, revealed that a substantial number of symbiotic giants show pulsations. Variability of the large sample of known systems was analyzed by Gromadzki et al. (2009, 2013). Additionally, many symbiotic stars were analyzed in individual studies. S-type systems usually show semi-regular pulsations or pulsate as so-called OSARGs (OGLE small-amplitude red giants; Wray et al. 2004). D-type systems show radial pulsation of Mira-type (e.g., Gromadzki et al. 2009, 2013).

In the New Online Database of Symbiotic Variables, we have collected the pulsation properties of 86 confirmed S-type symbiotic stars and 31 confirmed symbiotic Miras (D-type systems). The distributions of the pulsation periods are shown in Fig. 2.11. The pulsation periods of S-type symbiotic systems strongly cluster in the range of 40 – 200 days, with a median value of 92.5 days. Only about 15% of known S-type symbiotic stars have pulsation periods longer than 200 days. If the exact dis-

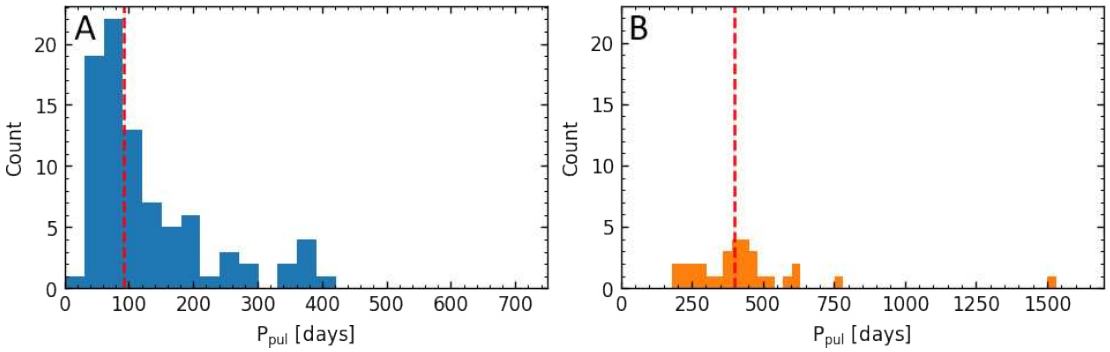

Figure 2.11: Pulsation periods of symbiotic giants. **A:** Distribution of the pulsation periods of S-type symbiotic stars (typically SR or OSARG pulsations). The median value of 92.5 days is denoted by the vertical red dashed line. **B:** Pulsation periods of D-type systems (Mira pulsators). The median value of 400 days is denoted by the vertical red dashed line. Note that the ranges of periods on the X-axis are different in the panels.

tance to these objects were known, the pulsation periods could help to distinguish between RGB and AGB cool components in the symbiotic binaries (see, e.g., the period-luminosity relations of Wood et al. 1999; Soszyński et al. 2007; Lebzelter et al. 2019). However, given the uncertainties in the distances even in the *Gaia* era, it is not possible to unambiguously identify the pulsation types in S-type systems. Still it seems that many of the systems, at least those with longer pulsation periods are on AGB (e.g., Gromadzki et al. 2013) which is consistent with their position in the HR diagram (see the discussion above).

All of the D-type symbiotic systems which contain Mira pulsators have pulsation periods longer than 200 days, with a median value of 400 days. Two systems with the longest pulsation periods (>650 days) among D-type symbiotic stars are V407 Cyg ($\sim$ 745 days; Munari et al. 1990) which also showed an outburst similar to those in symbiotic recurrent novae, and recently discovered symbiotic X-ray binary SRGA J181414.6-225604 ($\sim$ 1 502 days; De et al. 2022).

The longest pulsation periods of S-type symbiotic giants are comparable to their orbital periods (see Chapter 2.3). Moreover, in several systems, the ellipsoidal effect was detected (causing two minima in the light curve per one orbital cycle). This makes it difficult to distinguish between these two effects in the light curves, especially if observations only in one band are available. It is easier with multi-color photometry as the radiation of the giant, and therefore the pulsations (and the ellipsoidal effect) dominate on the longer wavelengths while the effects connected with the orbital motion (e.g., reflection effect or eclipses of the hot component) are more pronounced in bluer bands (Chapters 1.4.2 and 1.4.3). On the other hand, relatively long pulsation periods

(hundred of days) observed in D-type systems are still a few orders of magnitude shorter than the orbital periods of these symbiotic stars (tens of years; Chapter 2.3) and have typically also larger amplitudes in comparison with the S-type symbiotic stars. For this reason, revealing the nature of the strong variability observed in the D-type systems is more straightforward.

Infrared types The presence of the cool giants in symbiotic binaries makes them bright infrared sources that could be easily detected by all-sky ground-based or satellite surveys such as 2MASS or *WISE*. Symbiotic stars occupy a particular region in the color-color diagram (H-K vs. J-H, Fig. 2.12) and could be classified in 3 IR types (see Chapter 1.2.1). Unfortunately, as seen in the figure, infrared colors solely are not capable of distinguishing the symbiotic stars from other types of objects, which are mimicking their appearance (e.g., planetary nebulae, Be stars, T Tauri stars). On the other hand, the infrared observation can help to select promising symbiotic candidates which could then be confirmed by spectroscopic methods.

We have collected and reviewed the published IR classifications of the known symbiotic stars and supplemented them with the first IR classifications of 28 confirmed symbiotic stars whose IR types were not analyzed in the published literature. Our IR classifications are based on the IR data from the 2MASS survey (Skrutskie et al. 2006) and *WISE* satellite (Wright et al. 2010). Additionally, we have obtained 264 new IR types for the symbiotic candidates included in the New Online Database of Symbiotic Variables that supplemented the sample of 153 symbiotic candidates with IR types published in the literature. From the sample of the known symbiotic stars in the Database, $\sim$ 77%, 15%, and 3% are classified as S-, D-, and D'-type systems, respectively. The rest of the symbiotic systems (18 objects) do not have IR classification yet. Mostly they are too faint and are not included in the IR catalogs (extragalactic objects in M31, M33, IC10, and NGC 205).

The distribution of the IR types might not reproduce the real fractions of symbiotic stars of various types. More probably it reflects the observational difficulties connected with the discovery of dusty systems. They are fainter in the optical region due to high extinction caused by the circumbinary matter and moreover, they do not show typical characteristics of the giant star in the optical spectrum. Often they optical spectra resemble the spectra of planetary nebulae (see Chapter 1.2.1).

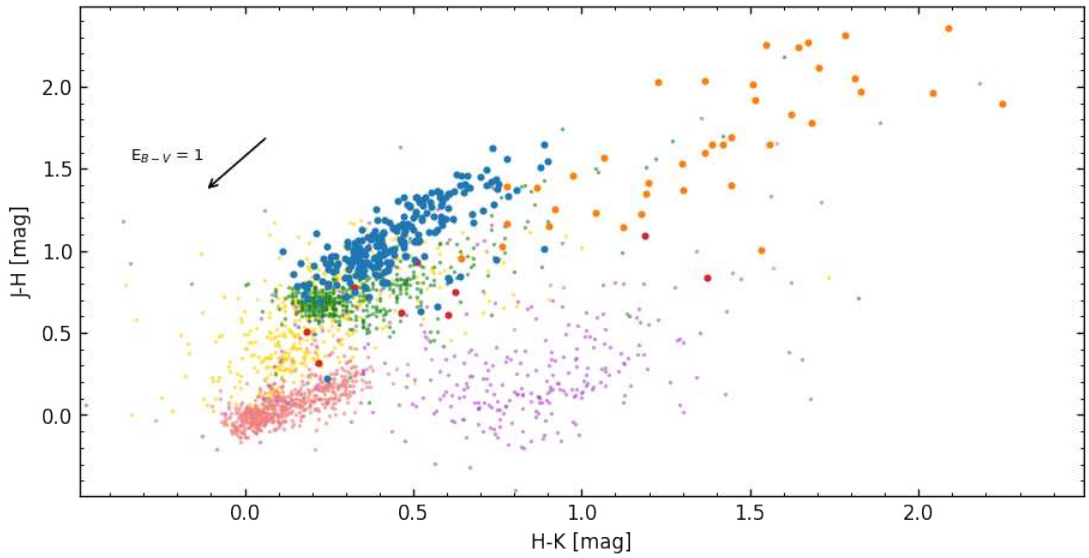

Figure 2.12: Positions of symbiotic stars of various infrared types (S, D, and D', shown in blue, orange, and red, respectively) as well as other objects in the near IR color-color diagram based on the 2MASS observations. Data for the Be stars (pink symbols) are from Zhang et al. (2005), planetary nebulae (violet symbols) from Ramos-Larios & Phillips (2005), T Tauri stars (green symbols) from Dahm & Simon (2005), and cataclysmic variables (yellow symbols) are from Downes et al. (2001).

On the existence of the S+IR infrared type As mentioned in Chapter 1.2.1, the fourth IR class was recently introduced by Akras et al. (2019a). The SEDs of such symbiotic stars should resemble S-type systems but show an additional small excess in the far-IR region. However, we have analyzed in detail all the objects classified as the S+IR type in the article of Akras et al. (2019a) and identified several important issues in the analysis. The first concern, partly addressed by Akras et al. (2019a) is that the data used for the analysis, coming from 2MASS and *WISE* surveys were not obtained at the same time. The authors claimed that this will not influence the analysis significantly which seems to be true for the S-type systems whose variability has relatively small amplitudes in the IR region.

On the other hand, at least in two cases of their S+IR objects (UV Aur, V366 Car; both Mira pulsators), it seems that the pulsations significantly affect the IR SEDs of these objects. In these particular cases, the objects saturated the detector in W1 and W2 filters, although these values are mentioned as upper limits in the *WISE* catalog and were treated as such by Akras et al. (2019a). Therefore they identified the excess only in W3 and W4 bands while in reality, the IR brightness of the objects changed between the 2MASS and *WISE* observations and the simultaneous data would allow classifying these objects either as S- or D-type symbiotic stars.

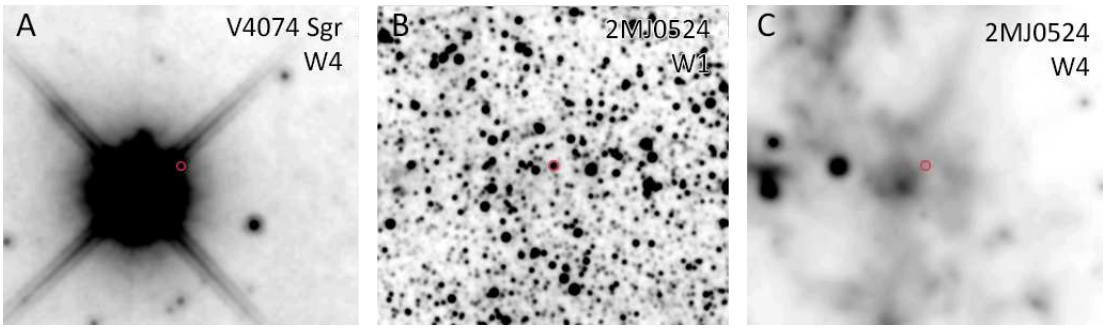

Figure 2.13: *WISE* images (Wright et al. 2010) of selected objects classified as S+IR by Akras et al. (2019a). **A**: Field of the symbiotic star V4074 Sgr (red circle) in the W4 filter. Contamination by the strong nearby source is visible. **B:** Image of the field around symbiotic candidate 2MASS J05240989-6919479 (red circle) in W1 filter. **C:** The same field as in panel B, but in W4 filter. Red circle shows the position of 2MASS J05240989-6919479. Diffuse background emission contributing to the measured flux is clearly visible.

Another caveat of the analysis presented in Akras et al. (2019a) is that the interstellar extinction was neglected. In several cases of the objects classified as the S+IR type in the mentioned article, e.g., Hen 2-87, 2MASS J17334728-2719266, 2MASSJ17463311-2419558, the dust maps suggest very significant extinction values which could seriously alter the SED of the studied object. Correcting the IR observations with a reasonable value of extinction would allow classifying these targets as S-type symbiotic stars. This particular omission also led in most of the cases to the incorrect value of the cool component temperature, typically lower by about 600 – 800 K in comparison with the literature or values obtained from the spectral types (see also the discussion on the temperature above).

Other objects classified as the S+IR type by Akras et al. (2019a) are actually the D'-type systems (e.g., WRAY 15-157, StHα 190, SMP LMC 88) which is confirmed by the optical/IR spectroscopic observations. The incorrect temperature of the cool components inferred in the mentioned study (often underestimated by 2 500 – 3 000 K; see Fig. 2.7) led to the necessity of adding the weak dust component in addition to the stellar photosphere to sufficiently model the IR SED of these objects. In reality, if a correct temperature of the cool component would be adopted (much higher than the authors used), the IR SEDs of these targets would resemble the D'-type systems with two dust shells of slightly different temperatures.

In many other cases, the *WISE* data seem to be unreliably, and therefore cannot be used for the IR type classification. They are either contaminated by the nearby sources (e.g., V4074 Sgr; Fig. 2.13A), or the detections have unreliability flags in the catalog (e.g., diffraction spikes, optical ghost images, scattered light halo coming from

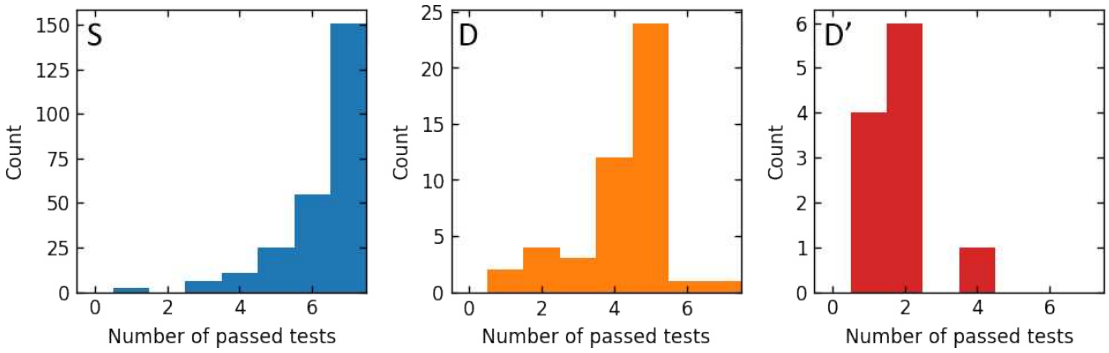

Figure 2.14: Accuracy of IR classification trees of Akras et al. (2019b). The number of passed tests (out of seven) are shown separately for S-, D-, and D'-type symbiotic systems in blue, orange and red, respectively.

a nearby bright source, data contaminated by a latent image left by a bright star) or there is a strong diffuse emission dominating the flux at the longer wavelengths (e.g., 2MASS J05240989-6919479; Fig. 2.13B, C). Especially in the case of the nearby sources, one has to keep in mind that the angular resolution of the W4 filter is about 12" in contrast with W1 – W3 having the resolution of about 6" (Wright et al. 2010), which is particularly important in the cases when the excess is detected in the W4 filter only. Finally, some candidates classified as the S+IR type by Akras et al. (2019a) simply seem not to be symbiotic stars at all (e.g., SSTISAGEMC J010336.26-720404.2, Hen 2-379), and therefore they are not relevant for the discussion of the new IR type of symbiotic systems.

Taken together, from 37 objects (confirmed symbiotic stars and candidates) classified as the S+IR type by Akras et al. (2019a), most of them (35) can be classified in the S/D/D' scheme. There are only two objects which might show real additional excess in the W3 and W4 bands (visible also in data from *AKARI* mission): V455 Sco and V3804 Sgr. Given how heterogeneous the group of symbiotic stars is, we made a decision not to create a special category for those two objects in the New Online Database of Symbiotic Variables, especially unless this would be confirmed by the simultaneous observations and a detailed analysis of the data.

Infrared criteria for symbiotic stars Given the particular difficulties in discovering the D-type symbiotic stars mentioned above, new approaches to the search for symbiotic stars have been adopted recently. For example, Akras et al. (2019b) used the machine learning algorithms trained on the 2MASS and *WISE* IR data of known symbiotic stars and identified 36 new S-type and 36 new D-type candidates.

We tested the classification criteria used in their work on the whole sample of

the confirmed symbiotic stars in the New Online Database of Symbiotic Variables. In addition to the classification trees distinguishing either between S-type symbiotic stars and 'mimics' or D-type symbiotic stars and 'mimics', Akras et al. (2019b) presented seven further classification trees to separate specific groups of objects from symbiotic stars (planetary nebulae, T Tauri stars, Be stars, Wolf-Rayet stars, single Miras, etc.).

The infrared criteria for S-type symbiotic systems are satisfied in 74% of all confirmed symbiotic stars with S-type classification in our Database. This is in contrast with the number of around 90% given by Akras et al. (2019b). The reason for this discrepancy is especially that many of the S-type systems in our Database which are not fulfilling the criteria are classified as the S+IR type in the sample of Akras et al. (2019b), and therefore are excluded from their S-type sample. As we have discussed above, the IR data from *WISE* are unreliable for some of these objects, therefore they cannot be accurately used for symbiotic classification. The fraction of S-type symbiotic stars correctly classified by the classification tree would be therefore larger, if only objects with reliable IR photometry would be taken into account, but still not as high as claimed by Akras et al. (2019b).

In the case of the classification tree to distinguish between dusty systems (D-, D'-, and S+IR-type systems in their work) and 'mimics', they found that typically only the D-type symbiotic stars pass their criteria. This classification tree has a lower success rate and higher number of contaminants in comparison with the one used for S-type systems. From our sample of confirmed D-type objects, about 53% are classified as symbiotic stars while the rest as mimics using the criteria of Akras et al. (2019b).

In Fig. 2.14 we demonstrate how many out of seven additional classification trees, the particular confirmed symbiotic star is correctly classified as a symbiotic system. It is clearly visible that these classification trees are usually reliable for the S-type systems. The majority of the systems fulfill five or more criteria, while most of the systems passing less than five criteria contain K giants (yellow symbiotic stars) or C-rich cool components. The classification trees are less reliable in the case of D-type systems and are unable to successfully distinguish between the D'-type symbiotic systems and other objects showing similar IR properties.

2.5 Hot components of known symbiotic stars

As discussed in detail in Chapter 1.2.2, the hot components of symbiotic binaries are either luminous and hot white dwarfs (in the case of shell-burning symbiotic

stars), or faint accreting white dwarfs or neutron stars (in accreting-only systems). The population of symbiotic systems hosting neutron star accretor is, at least for now, too small ($\sim$ 20 objects among confirmed systems and symbiotic candidates) for a reasonable statistical analysis. For this reason, we focus on the analysis of symbiotic stars with white dwarfs in this section. We have collected several characteristics of the hot components from the literature for the confirmed symbiotic stars and symbiotic candidates included in the New Online Database of Symbiotic Variables. It should be noted that the hot components of symbiotic stars have typically (in quiescence) almost negligible contribution to the flux observed in the optical spectral region, and the UV observations are not always available. Therefore in many cases, the parameters such as temperatures or luminosities are obtained indirectly, e.g., from the influence of the hot component on the symbiotic nebula and the appearance of prominent emission lines (see, e.g., Kenyon et al. 1991; Mikolajewska et al. 1997; Leedjärv et al. 2016).

Temperatures and luminosities The position of the symbiotic white dwarfs in the HR diagram is shown in Fig. 2.15A. While the hot components of shell-burning symbiotic stars occupy the same region of the HR diagram as central stars of planetary nebulae (see their position, e.g., in Fig. 1 of Herwig 2005), the hot components of accreting-only symbiotic variables are typically slightly cooler and significantly less luminous. The distributions of temperatures and luminosities are shown in Fig. 2.15B and Fig. 2.15C, respectively. Both need to be taken with caution. The temperatures are in some cases only the lower limits calculated from the maximal ionization potential observed in the spectrum using the method of Murset & Nussbaumer (1994). On the other hand, luminosities are distance-dependent and the distances to symbiotic stars are poorly constrained in most cases. Moreover, both, the temperature and the luminosity of the hot component change with the activity of the system, so throughout the active stage the white dwarf can occupy various parts of the HR diagram (see, e.g., Mikolajewska et al. 1995; Mikołajewska 2003, 2010; Merc et al. 2020b). In general, the temperatures of white dwarfs in the shell-burning symbiotic systems have typical temperatures of a few $\times 10^4$ – 10^5 K and luminosities of 10^2 – 10^4 $L_\odot$. The white dwarfs in accreting-only symbiotic stars have temperatures $<10^5$ K and luminosities ~ 1 – 10^2 $L_\odot$.

Masses The mass estimates for 17 and 22 white dwarfs in symbiotic binaries were collected and presented in Mikołajewska (2007) and Mikołajewska (2010), respec-

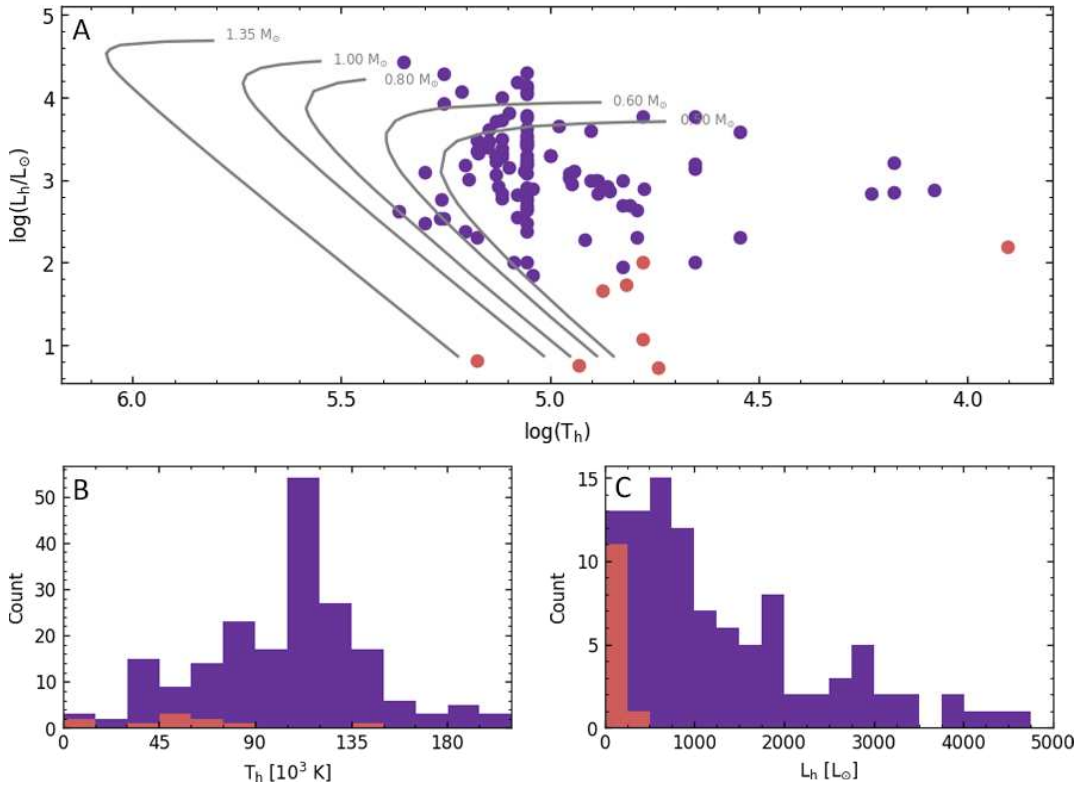

Figure 2.15: Temperatures and luminosities of symbiotic white dwarfs. Shell-burning systems and accreting-only symbiotic stars are shown in purple and red, respectively. **A:** Position of the symbiotic white dwarfs in the HR diagram. The solid gray curves are steady-state models of Nomoto et al. (2007). The white dwarf mass is shown for each model. **B:** Distribution of temperatures of symbiotic white dwarfs. **C:** Distribution of luminosities of white dwarfs in symbiotic systems.

tively. In Fig. 2.16A, we show the distribution of white dwarf masses of 50 confirmed symbiotic binaries in the New Online Database of Symbiotic Variables. Most symbiotic white dwarfs have masses between 0.4 – 0.8 $M_\odot$ in accordance with the previous results. The median mass is 0.6 $M_\odot$. Interestingly, the distribution of the masses of symbiotic dwarfs is very similar to one of the galactic disk white dwarfs (see, e.g., Catalán et al. 2008; Kleinman et al. 2013; Kepler et al. 2015, 2016).

Neglecting the growth in mass caused by the mass transfer from the cool components, one can estimate the mass of the progenitors of symbiotic white dwarfs from the initial-final mass relations. Theoretical relation of Choi et al. (2016) predicts the initial masses in the range of ∼2 – 3 $M_\odot$ for a final mass of 0.6 $M_\odot$. Unfortunately, there is a plateau in the initial-final mass relation in this part of the function preventing more exact evaluation. The progenitor mass of about 2 $M_\odot$ is also suggested by the semi-empirical relation of Catalán et al. (2008), while the more recently published semi-empirical relations of Cummings et al. (2018) gives the initial mass of ∼1.4 $M_\odot$ for a final mass of 0.6 $M_\odot$. The latter seems to be slightly underestimated given that

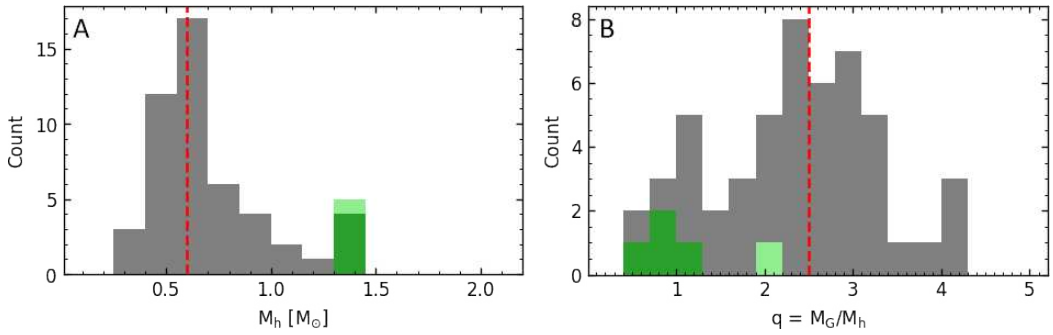

Figure 2.16: Masses and mass ratios in white dwarf symbiotic stars. **A:** Distribution of masses of symbiotic white dwarfs (gray). The vertical dashed red line denotes the median value of 0.6 $M_\odot$. The symbiotic stars showing symbiotic recurrent nova outbursts are shown in dark green. A light green color denotes V407 Cyg (see the text for details). **B:** Mass ratios in white dwarf symbiotic stars. The median value of 2.5 is shown by the vertical dashed red line. Symbiotic recurrent novae and V407 Cyg are highlighted by dark green and light green colors, respectively.

the current symbiotic white dwarf had to be initially a more massive component and the masses of current cool components (initially less massive) have a peak at about 1.5 $M_\odot$ (see above).

In contrast to the most symbiotic white dwarfs, in a small group of symbiotic binary stars showing recurrent nova outbursts, white dwarfs have higher masses ($\sim$ 1.2 – 1.4 $M_\odot$; highlighted in dark green Fig. 2.16). The white dwarf in V407 Cyg also has a similarly high mass and the system experienced at least one outburst typical for symbiotic recurrent novae. At least for RS Oph, there is evidence of the CO nature of the white dwarf (Mikołajewska & Shara 2017). The evolutionary upper limit of the masses of CO white dwarfs is $\sim$ 1 – 1.1 $M_\odot$ (see, e.g., Marigo 2013, and references therein). Therefore this constitutes the clear observational evidence, that the hot components of symbiotic binaries can grow in mass. This makes them promising progenitors of supernovae Ia (see Chapter 1.5).

In Fig. 2.16B, the distribution of mass ratios of the components in white dwarf symbiotic stars is shown. Generally, the current hot components are less massive than the cool companions with the typical mass ratio $q = M_{\rm G}/M_{\rm h}$ in the range of 2 – 3 and the median value of 2.5. In the case of symbiotic recurrent novae, the opposite is true and the hot components are more massive or at least of a similar mass as the giants in those systems ($q \leq 1$). V407 Cyg constitutes an exception in this sense, as the giant of this system is more massive than the white dwarf ($q \sim 2$). In contrast with all the other symbiotic stars showing symbiotic recurrent nova outbursts, the cool companion of V407 Cyg is an evolved Mira pulsator (D-type system).

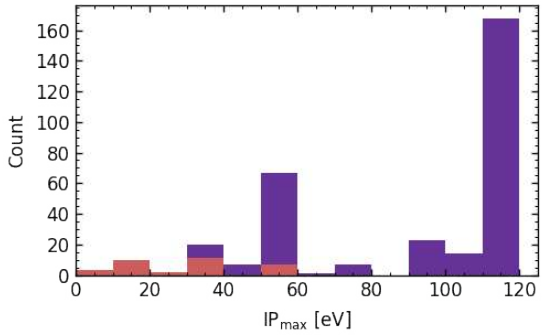

Figure 2.17: Distribution of maximal ionization potential of emission lines in the quiescent spectra of shell-burning (purple) and accreting-only symbiotic systems (red).

Observational manifestations of the hot components Given the high temperatures of the symbiotic hot components in quiescence, the maximum of their radiation is shifted toward short wavelengths (UV, X-ray; see Chapter 1.2 and Fig. 1.2). During their outbursts (discussed in more detail in Chapter 2.6), they can contribute to the flux in the optical region, too. Nevertheless, also in quiescence, their radiation influences the surrounding environment, especially the slow wind of the cool component which is the main source of the symbiotic nebula. Part of the nebula ionized by the hot companion is a source of strong emission lines which are observable in the optical and/or UV part of the spectrum.

The distribution of maximal ionization potential (IP) of emission lines observed in the optical spectra of confirmed symbiotic binaries in the New Online Database of Symbiotic Variables is shown in Fig. 2.17. In accordance with previous analyses (e.g., Allen 1984a; Belczyński et al. 2000; Akras et al. 2019a), in about 54% of the confirmed shell-burning symbiotic stars, the emission lines with the maximal IP are those of Raman-scattered O VI at 6825 Å and 7088 Å ($IP = 113.9\,\mathrm{eV}$). It is worth noting that these emission lines are observed (almost) exclusively in symbiotic binaries (e.g., Akras et al. 2019a) as their creation requires specific conditions: the presence of the source hot enough to ionize the oxygen five times and the presence of neutral hydrogen to allow the Raman-scattering of the UV lines of O VI into the optical region (Schmid 1989). These lines (at least that at 6825 Å, which is typically the stronger of the two) are observed simultaneously with other highly ionized emission lines. The He II lines (e.g., at 4686 Å; $IP = 54.4\,\mathrm{eV}$) are always present (Akras et al. 2019a), and the lines of [Fe VI] ($IP = 75.0\,\mathrm{eV}$) and/or [Fe VII] ($IP = 99\,\mathrm{eV}$) are often present together with the O VI line(s). In the shell-burning symbiotic systems which do not show the Raman-scattered O VI lines in their optical spectra, the emission lines with

the maximal IP are typically either those of He II, [Fe VII], or [O III] ($IP = 35.1\,\mathrm{eV}$).

The accreting-only symbiotic binaries usually do not present emission lines with high IP in their quiescent optical spectra (Fig. 2.17). In some of these systems, [O III] or He II have been reported, while in others only the H I and He I emission lines are seen. In reality, there are also objects that show the emission lines only in the UV part of the spectrum where the contribution of the red giant continuum is negligible (see Fig. 1.5). On the other hand, symbiotic recurrent novae, which are in accreting-only state during their quiescence, can show prominent emission lines throughout their nova outbursts (see, e.g., Munari & Valisa 2022), including the Raman-scattered O VI, or even coronal lines of [Fe X] ($IP = 233.6\,\mathrm{eV}$), [Fe XI] ($IP = 262.1\,\mathrm{eV}$), and [Fe XIV] ($IP = 361.0\,\mathrm{eV}$).

Another observational manifestation of the interaction between the components in the accreting-only symbiotic systems is prominent flickering on the timescale of a few minutes. It has been detected only in the small number of confirmed symbiotic binaries (~ 20 objects in the New Online Database of Symbiotic Variables), especially in the scope of the systematic surveys of Dobrzycka et al. (1996) and Sokoloski et al. (2001), and during the analysis of individual objects (e.g., Gromadzki et al. 2006; Angeloni et al. 2012; Zamanov et al. 2017, 2018, 2019, 2021b). The amplitude of the flickering rises towards short wavelengths and therefore can be easily detected using the satellite UV observations. It is more complicated to detect the flickering from the ground, especially at present as photoelectric photometers are no longer widely used and CCDs have much lower sensitivity at the U-band wavelengths (Munari et al. 2021). For this reason, the small size of the sample of symbiotic binaries with the detected flickering is more a result of observational difficulties and does not reflect the real fraction of symbiotic systems in which the flickering is present.

Symbiotics in X-rays A significant number of symbiotic stars are strong X-ray sources. Thanks to the abundance of observations of symbiotic systems obtained by the *ROSAT* satellite and later by *Swift*, the classification of symbiotic binaries based on their X-ray spectra is available nowadays (see Chapter 1.2.2).

For the present study, we gathered information concerning the X-ray emission of confirmed symbiotic stars and candidate objects included in the New Online Database of Symbiotic Variables. Altogether, the data on the X-ray emission of 149 confirmed symbiotic stars are available in the literature, with the most abundant collection up to now presented by Luna et al. (2013). From this number, 62 observed sources have

been detected in X-rays while the rest (87 sources) have only upper limits available. To increase the size of the sample, we have searched the updated *Swift*-XRT point-source catalog (2SXPS; Evans et al. 2020) and the fourth *XMM-Newton* serendipitous source catalog (4XMM-DR9; Webb et al. 2020) for the detections of the known symbiotic stars. If no detection was reported at the queried positions, and the region was covered by the *Swift* observations, we obtained the upper limits using the *Swift*-XRT 2SXPS Upper limit server[5]. In this way, we report on the detection of 3 additional symbiotic sources and the non-detection of further 124 confirmed symbiotic systems. We have also employed the *Swift* and *XMM-Newton* observations to provide the first X-ray classifications for 8 sources, increasing the number of symbiotic sources with this classification to 61.

In addition to confirmed symbiotic stars, 229 of the symbiotic candidates have been observed in X-rays. The information on the detection or the non-detection of 144 objects from this sample was obtained in the same way as described above, while 85 were analyzed previously in the literature. Possible X-ray classifications are now available for 51 symbiotic candidates, 15 are classified for the first time in this work.

Based on the classification scheme discussed in Chapter 1.2.2, 8 confirmed symbiotic stars are classified as α types (X-ray emission from the shell-burning), 23 as β (collision of the winds), 7 as γ (neutron star accretors), 12 as δ (accreting-only symbiotics), and 11 systems show β/δ type of X-ray emission. These results confirm that X-ray emission is not an exception for symbiotic stars and is observed with a large number of sources (currently for about 24% of observed symbiotic stars). According to our study (see the details in Merc et al. 2019c), the X-ray emission is detected preferentially from the brightest and closest sources (however, these two parameters are correlated).

The reason why not all shell-burning symbiotic stars are detected in soft X-rays could be explained by the fact that the interstellar medium is capable of the efficient absorption of energetic photons and in addition, these systems are subjected to significant local absorption in the symbiotic nebula. On the other hand, it is more difficult to detect accreting-only, hard X-ray symbiotic stars, and their number would probably rise with specialized surveys looking for such objects. We also analyzed the relationship between the IR type of symbiotic stars (i.e., the cool components) and their X-ray emission. We found out that emission in this spectral range is not exclu-

[5]https://www.swift.ac.uk/2SXPS/ulserv.php

sive to any IR type, and was detected in S-, D-, D'-type systems. The sample is still relatively small, but anyway there seems to be no relationship between a particular IR type with a particular type of X-ray spectra of symbiotic stars.

2.6 Outburst activity of symbiotic stars

The most prominent changes in the symbiotic stars are connected with their outbursts. The activity is linked to their hot components. Three different types of outbursts are observed in symbiotic systems: classical (Z And-type), 'slow' nova, and recurrent nova outbursts (see Chapter 1.4.1).

From the confirmed symbiotic binaries included in the catalog of Belczyński et al. (2000), the authors reported on the detection of outbursts in 41 systems, in the other 7 objects outbursts are not certain. We have gathered the data about the activity of the symbiotic stars in the New Online Database of Symbiotic Variables: 79 of the confirmed symbiotic systems are now firmly established as outbursting sources, while another 9 systems might have been also observed in outbursts. The most abundant is the group of classical symbiotic stars, 43 symbiotic systems have certainly or probably experienced at least one outburst of this type in their observational history. Another 13 sources have been observed in proven 'slow' symbiotic nova outbursts while another 9 confirmed symbiotic stars are suspected 'slow' symbiotic novae. Only four systems from our Database (namely, RS Oph, V3890 Sgr, V745 Sco, T CrB) could be classified as genuine symbiotic recurrent novae, as they have been observed in multiple nova outbursts. As discussed in Chapter 1.4.1, few other objects have been observed in similar outbursts (V15345 Sco, AT 2019qyl, V407 Cyg, V1535 Sco, V1708 Sco) which suggests that they also belong to the same category of symbiotic stars, but only one outburst was detected so far, and therefore these objects cannot be classified as 'recurrent' yet.

Relation between various types of symbiotic phenomenon At least two (AG Peg and V426 Sge), maybe even four symbiotic stars (possibly also BF Cyg and StHα 169) that have been detected in 'slow' symbiotic nova outbursts showed classical symbiotic outbursts later in their evolution (see Chapter 1.4.1). Based on the observations of AG Peg and V426 Sge, Skopal et al. (2020) suggested the relations of the basic types of the symbiotic stars (see their section 4.3). We expand this picture based on all data gathered for the New Online Database of Symbiotic Variables.

As all the symbiotic stars consist of a cool evolved giant and a white dwarf or a neutron star, let us assume that the binary successfully evolved towards such a system. We especially focus on the white dwarf symbiotic systems. Initially, the mass transfer rate would not be sufficient to power the symbiotic features, and the system would resemble a single giant in the optical spectral region and would not be detected as a symbiotic star. We could designate such an object as a *pre-symbiotic binary*[6]. During the subsequent evolution of the red giant, its mass loss can increase significantly. The mass transfer rate could reach a lower limit for the accretion to produce sufficient luminosity ($\gtrsim$10 $L_{\odot}$; Mikolajewska & Kenyon 1992b; Yungelson et al. 1995) for a binary to be detected as an accreting-only symbiotic system. Iłkiewicz et al. (2022) claimed that binaries in which the hot component is less luminous should not be considered as symbiotic stars. If the sufficient accretion rate is maintained only temporarily (e.g., during the periastron passage), the binary appears as an accreting-only system only for a short period of time. This seems to be the case of SU Lyn. Iłkiewicz et al. (2022) suggested to denote this object as a *'transient' symbiotic system.*

A pre-symbiotic or 'transient' symbiotic star could eventually evolve towards a persistent accreting-only system. As mentioned, this transition can be gradual as a result of the progressive evolution of the red giant and an increase in its mass loss. The mass loss of the red giant can also increase abruptly due to the helium flash (e.g., Mattsson et al. 2007). According to Iłkiewicz et al. (2022), CH Cyg is a probable example of this scenario as it started to show symbiotic features only in ∼1960s (e.g., Mikolajewski et al. 1990).

In an accreting-only symbiotic star, the accretion rate is below the stable-burning limit, and the white dwarf is accumulating mass on its surface. When enough material is accreted, the thermonuclear outburst is observed. In symbiotic stars with very massive white dwarfs (see Chapter 2.5), the outbursts are fast and explosive. For a short time during the outbursts, the white dwarfs in these symbiotic stars exhibit shell-burning on their surfaces, they are detected as soft X-ray sources and show prominent emission lines in their optical spectra (see, e.g., the evolution of RS Oph throughout its recent outburst; Munari & Valisa 2021, 2022; Page et al. 2022). Afterward, as the red giants are not capable of supplying enough matter for the continuation of the shell-burning, the white dwarfs in these systems return to the accreting-only state.

[6]Munari (2019) denoted also objects such as SS Lep as pre-symbiotic stars. However, SS Lep is an interacting binary system consisting of a cool giant and a main-sequence star, and not every analogous system would evolve toward a normal symbiotic star. Therefore, we decided not to adopt such a notation in this study (see Chapter 1.2.2 for more details)

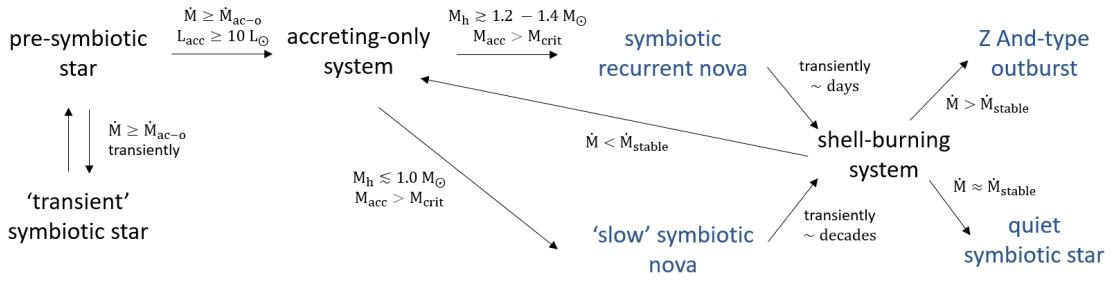

Figure 2.18: Relations between various types of symbiotic stars (pre-symbiotic, 'transient', accreting-only, shell-burning) and the activity observed in symbiotic binaries.

The outbursts can repeat when sufficient mass is accumulated again. The recurrence scale is relatively short, and therefore for some of these stars, several outbursts have been already detected (= *symbiotic recurrent novae*).

If the white dwarf in a symbiotic system is less massive, the outburst proceeds in non-degenerate conditions. Its envelope expands slowly to supergiant dimensions. This process is accompanied by the equally slow rise to the maximum brightness (= *'slow' symbiotic novae*). These systems then appear as shell-burning symbiotic stars. If the red giant is later not capable of transferring enough mass to the white dwarf to support the stable shell burning, the residual burning from the nova outburst slowly fades and the post-nova symbiotic system will become accreting-only until its next nova outburst. This might be the case of TYC 1371-69-1 (Tang et al. 2012, Chapter 3.3). The recurrence time can be as long as 10^6 years in some symbiotic systems (e.g., Yaron et al. 2005; Wolf et al. 2013), but also significantly shorter as is probably the case of LMC S154 (Iłkiewicz et al. 2019b) or V618 Sgr (this thesis).

On the other hand, if the mass transfer rate is sufficient for the stable shell-burning, a system can stay in this regime for a longer time. According to Skopal et al. (2020), the *quiet symbiotic stars* exhibiting wave-like variability in their light curves (e.g., SY Mus or RW Hya) are examples of such symbiotic stars. They have also suggested that if the accretion rate transiently exceeds the upper limit for the stable shell-burning, such systems exhibit classical Z And-type outbursts. All discussed relations between symbiotic types and their outburst activity are summarized in Fig. 2.18.

2.7 Symbiotic stars in *Gaia* DR3

The *Gaia* mission (Gaia Collaboration et al. 2016), launched in December 2013, already belongs to the most successful space probes ever built. The main goal of the

satellite is astrometry with unprecedented precision. However, the repeated quasi-simultaneous photometric measurements in three filters (G, $G_{\rm BP}$ and $G_{\rm RP}$) also serve as an all-sky photometric survey. In addition, thanks to the low-resolution spectroscopy in broad BP and RP bands (R $\sim$ 20 – 60) covering the optical-IR region, and medium-resolution spectra (R $\sim$ 11 500) in the near IR (RVS), it provides also astrophysical parameters for huge numbers of sources. The observations and data products from the satellite have already been made available in several data releases.

The most recent, *Gaia* Data Release 3 (DR3) was published on June 13, 2022 (Gaia Collaboration et al. 2022) and is based on the same dataset collected during the first 34 months of the mission (July 25, 2014 – May 28, 2017) as *Gaia* EDR3. The astrometric data in *Gaia* DR3 are the same as those of *Gaia* EDR3. However, a significant number of new data products was presented in the later release. In this section, we discuss some of the results obtained from *Gaia* DR3 for known symbiotic stars from the New Online Database of Symbiotic Variables. We focus especially on the astrophysical parameters, distances, and variability of known symbiotic stars. Additionally, we shortly describe new symbiotic candidates which were published in the scope of *Gaia* DR3.

We have cross-matched all the objects in our Database (1 004 sources) with the objects published in the DR3. Here, we will focus especially on the confirmed symbiotic stars. However, the data from *Gaia* are used also in our analysis of symbiotic candidates (see, e.g., Chapter 3.2 and 3.3). Out of 290 confirmed galactic symbiotic stars, 286 have at least some information presented in the DR3 (not necessarily the full astrometric solution). In addition, *Gaia* data are available for 36 out of 70 confirmed extragalactic objects. The rest is typically too faint.

Astrophysical parameters A major component of *Gaia* DR3, which was not present in the previous releases, are the astrophysical parameters of the sources ($T_{\rm eff}$, $\log g$, [M/H]; for subsets of sources also radii, masses, ages, chemical abundances, Hα equivalent widths, etc.). These parameters have been obtained either from the mean BP/RP spectra or using mean RVS spectra (Creevey et al. 2022). While we found out that, e.g., the detailed chemical abundances are not available for the majority of the symbiotic systems, $T_{\rm eff}$ obtained using both BP/RP and RVS spectra are inferred for a large sample of symbiotic stars.

We have therefore compared the temperatures from *Gaia* with the effective temperatures of symbiotic giants (which dominate the observed spectral region) estimated

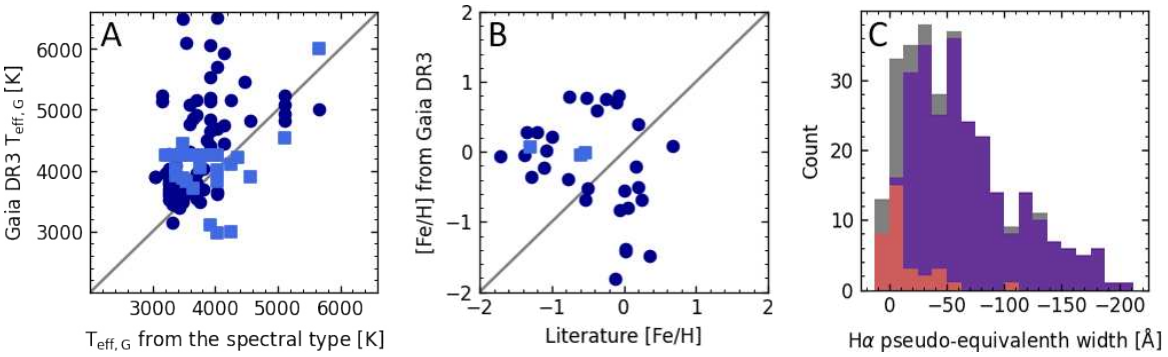

Figure 2.19: Astrophysical parameters of symbiotic stars in *Gaia* DR3. **A:** Comparison of temperatures presented for known symbiotic stars in *Gaia* DR3 with those obtained from the spectral types of the giant (see Chapter 2.4). Temperatures obtained from the mean BP/RP spectra and from fitting of RVS spectra are shown as dark blue dots and light blue squares, respectively. **B:** Comparison of metallicities from literature and *Gaia* DR3. The colors are same as in panel A. **C:** Distribution of pseudo-equivalent widths of Hα line of known symbiotic binaries (gray). Objects classified as shell-burning sources and accreting-only systems in our Database are shown in purple and red, respectively.

from their spectral types (see Chapter 2.4). Unfortunately, it seems that there is a rather large scatter in the *Gaia* temperatures that in many cases differ from the ones estimated from the spectral types of the giants by a few thousand K (Fig. 2.19A). This difference might be caused by several factors, e.g., by the fact that the measured flux in the *Gaia* filters is not solely given by the flux of the red giant, but also the nebula can contribute significantly to it. The fluxes are contaminated not only by the continuum emission of the symbiotic nebula but also by the strong emission lines, which would not be resolved with the resolution of the BP/RP spectra (with exception of the most prominent ones, such as Hα).

In addition, the fact that could complicate the analysis is also the imprecise extinction as the reddening in symbiotic binaries is often caused not only by the interstellar dust but also by the matter surrounding the binary. A procedure that will analyze the *Gaia* spectra adopting some priors based on the non-*Gaia* data (e.g., the infrared observations from 2MASS, *WISE*) may provide more consistent results in the future. Given these results and the issue with the unknown distances to many symbiotic stars (see below), we do not discuss other parameters such as luminosities or radii here at this time.

It is still an open question, if symbiotic giants belong to a metal-rich population as suggested by Whitelock & Munari (1992) or their metallicity is sub-solar, as suggested by more recent measurements (see Chapter 2.4). Only a few symbiotic stars have metallicity estimates obtained from the RVS spectra, while for most of them, only

the values inferred from the BP/RP spectra are available. In general, both samples suggest slightly sub-solar metallicities for known symbiotic stars. On the other hand, it is clear from the comparison of the metallicities of known symbiotic stars collected in the New Online Database of Symbiotic Variables from literature with the values estimated from the *Gaia* data (Fig. 2.19B) that the latter values differ significantly from the values obtained typically using the high-resolution IR spectra. Therefore, one needs to be careful when interpreting *Gaia* metallicities of symbiotic stars.

Finally, we show here the distribution of equivalent widths of Hα line measured from the mean BP/RP spectra (Fig. 2.19C). It is clear from the data that this spectral line is detected in emission (equivalent width is negative) in most of the symbiotic sources. The observations of *Gaia* confirm that Hα line is typically stronger in shell-burning symbiotic stars, in comparison with accreting-only systems. In the minority of symbiotic stars, Hα is indicated to be observed in absorption in *Gaia* DR3 (positive equivalent width). This seems to be the case, especially in some accreting-only systems (see their spectra in Fig. 1.3). It could also be that the Hα in some of these objects is just too faint to be revealed as an emission line with the low resolution of BP/RP spectra. Overall, it seems that this parameter could be a very good indicator of the symbiotic activity of an object and could be used to distinguish between single variable or non-variable giants and symbiotic stars.

Distances to symbiotic stars One of the major limiting factors in the analysis of the parameters of symbiotic components is the unknown distance. A significant improvement in this sense is expected in the *Gaia* era. However, there are important caveats that need to be taken into account in the case of symbiotic systems. First of all, according to Bailer-Jones et al. (2018, 2021), the reliable distance estimate cannot be obtained by simple inversion of the *Gaia* parallax for the sources that are too faint or distant, and consequently, their fractional parallax uncertainties are large. This would be the case for a significant fraction of the symbiotic binaries, as they are located at the distances of several kpc. As shown in the distribution of parallaxes of known symbiotic stars divided by their standard errors in Fig. 2.20A, a large fraction of them have very high relative errors and/or even negative parallax values (52 out of 316 confirmed symbiotic binaries with parallax estimate) in *Gaia* EDR3/DR3 catalog.

To overcome this problem, Bailer-Jones et al. (2021) adopted the probabilistic approach to estimate the distances using *Gaia* EDR3 parallaxes. As the prior, they used the three-dimensional model of the Galaxy (geometric model), and in the photo-

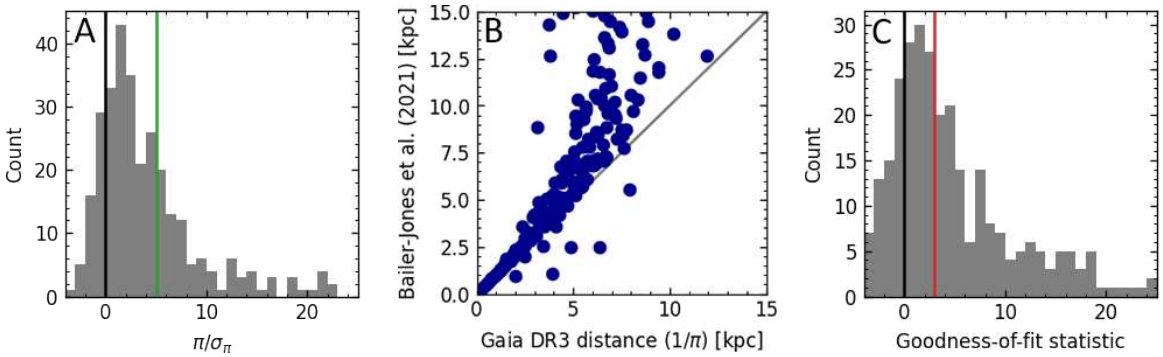

Figure 2.20: Distances to symbiotic stars in *Gaia* EDR3/DR3. **A:** Distribution of parallaxes from *Gaia* EDR3/DR3 divided by their standard errors. The value of 5 and higher denotes reliable estimate according to the *Gaia* documentation. **B:** Comparison of distances obtained as inverse of the parallaxes with the distances obtained by Bailer-Jones et al. (2021). **C:** Distribution of the goodness-of-fit statistic. The values above 3 indicate poor fit according to the *Gaia* documentation.

geometric model also the color and apparent magnitudes of a given star. The comparison of distances obtained as the inversion of the parallaxes and the photo-geometric distances inferred by Bailer-Jones et al. (2021) is shown in Fig. 2.20B. For distances greater than 3 – 4 kpc, these estimates are beginning to differ considerably. In *Gaia* DR3, a set of distances was also obtained from BP/RP spectra and parallaxes simultaneously with other astrophysical parameters. These values are consistent with the literature estimates, e.g., based on the asteroseismic analysis, for the distances up to 2.5 – 3 kpc (Fouesneau et al. 2022).

Already for *Gaia* DR2 data, several authors drew attention to the problem of the presence of the zero-point offset of parallaxes. It was shown that this offset depends on the magnitude, the color of objects, and their position in the sky (Lindegren et al. 2018). It seems that the value of the offset is slightly lower in *Gaia* EDR3/DR3 (Lindegren et al. 2021b; Stassun & Torres 2021), but still it is dependent at least on the magnitude, color and ecliptic latitude of the object in a nontrivial way (Lindegren et al. 2021a). This can be especially important if one analyzes individual objects and not a statistically significant sample (such as a cluster of stars). The severity of the zero-point offset issue is larger for distant objects, as for them the absolute value of the parallax can be of the same order as the value of the zero-point offset. The distances inferred by Bailer-Jones et al. (2018) from *Gaia* DR2 data assumed constant value of the zero-point, later for the EDR3 data Bailer-Jones et al. (2021) calculated the zero-point as a function of G, $BP - RP$ and ecliptic latitude for every source independently.

Another problem may be related to the binarity of symbiotic stars and their or-

bital motion. In such long-period binaries, the shift of the center of light caused by the orbital motion can be comparable to the effect caused by their parallax (e.g., as noted for AG Peg by Sion et al. 2019). This effect might explain the fact that a significant number of symbiotic stars have large values of the so-called 'goodness-of-fit' (gof) parameter (Fig. 2.20C). According to the *Gaia* documentation, the gof values over 3 indicate the poor fit to the data in the inference of the astrometric solution. The errors of the astrometric parameters could be probably significantly lowered by adopting the binary model.

In *Gaia* DR2 and EDR3, all sources have been considered as single stars. In *Gaia* DR3, a binary model was applied to the subset of the sources. Unfortunately, all but one confirmed symbiotic star are classified as single stars in *Gaia* DR3. The probability of being a single or binary star is inferred from the BP/RP spectra (Fouesneau et al. 2022). For most of the symbiotic sources in *Gaia* DR3, single star probability is $> 99\%$. This is understandable as the direct contribution of the symbiotic hot component is not visible in the BP/RP range and a symbiotic star would resemble a late-type star in most cases (with emission lines).

Variability of symbiotic sources in *Gaia* DR3 In *Gaia* DR3, the G and $G_{\rm BP}/G_{\rm RP}$ band mean magnitudes are available for about 1.8 and 1.5 billion sources, respectively. For a subset of almost 12 million sources, photometric time series are available (Gaia Collaboration et al. 2022). Based on the 34-month-long photometric series, RP spectra, radial velocity time series, and source astrometry, the search for variability and potential periodicity was performed (Eyer et al. 2022). The variable sources have been classified into 35 variability types (subtypes), including symbiotic stars. Out of 360 confirmed symbiotic stars in the New Online Database of Symbiotic Variables, 247 are correctly classified as symbiotic stars in *Gaia* DR3. Also, 61 candidates and 2 misclassified objects from our Database are marked as symbiotic stars in the *Gaia* catalog. In addition, 339 objects which have not been known as symbiotic stars or candidates before were classified as symbiotic stars in the scope of *Gaia* DR3 (see below).

Some of the groups of variable stars have been studied in more detail for *Gaia* DR3, including long-period variables (LPV; Lebzelter et al. 2022). For these objects, additional parameters, such as the observed periods and the amplitudes have been published. Among the objects classified as LPV in *Gaia* DR3, one can find 242 confirmed symbiotic stars. In Fig. 2.21A and B, we compared the periods published in

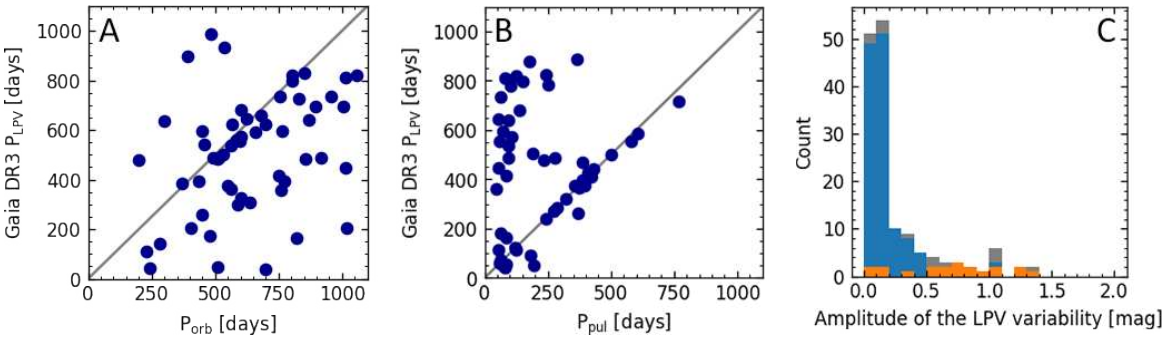

Figure 2.21: Variability of *Gaia* DR3 long-period variables. **A:** Comparison of the orbital periods of known symbiotic stars classified as long-period variables in *Gaia* DR3 with the values obtained from the *Gaia* data. **B:** Same as panel A, but for pulsation periods collected in our Database. **C:** Distribution of the variability amplitudes for known symbiotic stars (gray). The S- and D-type symbiotic stars are shown in blue and orange, respectively.

Gaia DR3 LPV sub-catalog with the known orbital and pulsation periods of particular symbiotic stars, respectively. It is clear from these comparisons that the inferred *Gaia* periods are in some cases consistent with pulsation and in others with orbital periods of known symbiotic systems.

More careful analysis of the time series would be needed to disentangle the effects in the multi-color light curves in which the orbital variability could dominate at shorter and pulsation at longer wavelengths. In any case, this result proves that the observations of the *Gaia* satellite could serve as a great resource for the analysis of the periodicities observed in symbiotic binaries, especially when a longer time base is available. The current data release is based only on 34 months of data (slightly more than 1 000 days). That means that in most of the cases of known symbiotic binaries, not even two orbital cycles have been observed (S-type symbiotic stars have periods in the range of 500 – 600 days; Chapter 2.3). In Fig. 2.21C, we show the amplitudes of the detected variability as published in *Gaia* DR3 for S- and D-type symbiotic stars. In D-types, the variability has a larger amplitude and is predominantly due to Mira pulsations as the orbital periods of these symbiotic stars are much longer than the studied timescales (tens of years; Chapter 2.3).

New symbiotic candidates from *Gaia* DR3 As mentioned above, the variable sources in *Gaia* DR3 have been classified into several categories, including symbiotic stars. In addition to 310 sources that have been previously confirmed or suspected of a symbiotic nature and are included in the New Online Database of Symbiotic Variables, another 339 objects are classified as symbiotic binaries in *Gaia* DR3 for the first time (Eyer et al. 2022). These objects are not covered in the sample discussed

in this thesis (1 004 sources in the New Online Database of Symbiotic Variables), but would be included in our Database as symbiotic candidates.

We should emphasize that the classification of the sources as symbiotic stars in *Gaia* DR3 is based on the astrometric parameters of the objects, RP spectra and especially their light curves in G, $G_{\rm BP}$, and $G_{\rm RP}$ bands. In our opinion, such an approach could produce a number of contaminants. Especially, one should keep in mind that the light curves of symbiotic binaries are very complex (e.g., the variations are caused by the orbital motion, pulsations, and outbursts). For this reason, it is hard to find a set of statistical parameters to describe the general photometric behavior of a prototypical symbiotic star.

Another major concern comes from the fact that a single pulsating red giant (semiregular, or Mira variable) can have exactly the same light curve as a quiescent symbiotic binary. It is true that 247 out of 360 confirmed symbiotic binaries from our Database are correctly classified as symbiotic stars in *Gaia* DR3. However, it is not clear for now, how many of these sources the symbiotic nature was anticipated in advance in order to train the classifiers. The discussion on the literature data sets used for classifier training should be presented by Gavras et al. according to Eyer et al. (2022), but neither the article nor the preprint was available at the time of submission of this thesis.

We have plotted the new symbiotic candidates from *Gaia* DR3 to the *Gaia* HR diagram (Fig. 2.22A) constructed on the basis of G, $G_{\rm BP}$, and $G_{\rm RP}$ mean magnitudes, the distance from Bailer-Jones et al. (2021), and the reddening values from the dust map of Schlafly & Finkbeiner (2011). The position of the sources from the New Online Database of Symbiotic Variables (excluding the misclassified objects) is shown in the figure as well. Most of the new candidates occupy the part of the HR diagram where confirmed symbiotic stars can be found (but also normal single giants). This is not unexpected as the RP spectra (which would reveal the late-type star easily) and the astrometric data (which would distinguish between close red dwarfs and distant red giants) have been used for the classification.

The majority of the candidates also share the position in the NIR color-color diagram with symbiotic stars (especially the ones of infrared S-type; Fig. 2.22B). Again, one should keep in mind that many single red giants can be found in the same region of the diagram. Still, this makes them reasonable symbiotic candidates. We have used the same diagrams as a partial source of information also in our study to classify the symbiotic candidates from the literature (Chapter 3).

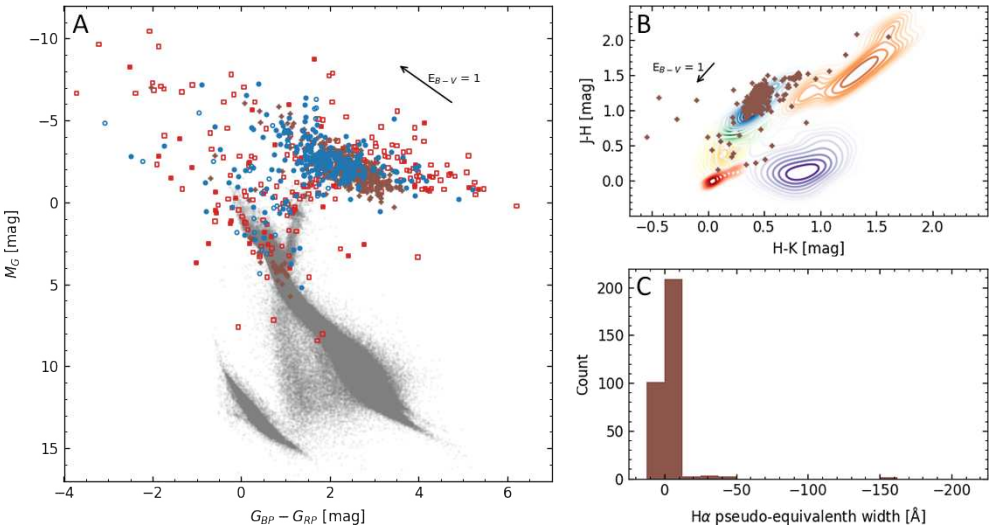

Figure 2.22: *Gaia* DR3 symbiotic candidates. **A:** Positions of the new symbiotic candidates from *Gaia* DR3 (brown plus symbols) in the *Gaia* HR diagram of a sample of stars within 200 pc (shown in gray) with reliable astrometry (Gaia Collaboration et al. 2018). Confirmed, likely, possible and suspected symbiotic stars from the New Online Database of Symbiotic Variables are denoted by blue full dots, blue empty dots, red full squares, and red empty squares, respectively. **B:** Positions of the new symbiotic candidates from *Gaia* DR3 (brown plus symbols) in the near IR color-color diagram based on the 2MASS observations (Skrutskie et al. 2006). The positions of the known S- and D-type symbiotic stars from the New Online Database of Symbiotic Variables are shown as density maps in blue and orange, respectively. Planetary nebulae (Ramos-Larios & Phillips 2005), Be stars (Zhang et al. 2005), T Tauri stars (Dahm & Simon 2005), and cataclysmic variables (Downes et al. 2001) are shown in violet, red, green and yellow, respectively. **C:** Distribution of pseudo-equivalent widths of Hα line in new symbiotic candidates from *Gaia* DR3.

Unfortunately, our concern about the possible contamination of the symbiotic candidate *Gaia* DR3 sample by single late-type long-period variables is supported by the distribution of the Hα equivalent widths observed for these candidates (Fig. 2.22C). As we have shown above, in the majority of the known symbiotic stars, Hα is detected as a rather strong emission line (its equivalent width is negative; see Fig. 2.19C). In contrast with the sample of known symbiotic binaries, the new candidates have the Hα equivalent widths close to zero (either slightly negative or slightly positive).

It might be that some of these candidates are accreting-only symbiotic stars, but some might be 'just' pulsating red giants. We should note that in pulsating giants, one can sometimes find Hα in emission as well. The detailed analysis of the symbiotic candidates from *Gaia* DR3 is beyond the scope of this thesis and will be presented elsewhere.

Chapter 3

Spectroscopic and photometric analysis of symbiotic candidates

Ongoing systematic searches for symbiotic stars in the Milky Way and in nearby galaxies have resulted in the number of known symbiotic systems growing rapidly. The present version of the New Online Database of Symbiotic Variables contains 1 004 objects (Chapter 2). Many of the known symbiotic stars are only poorly studied. Moreover, there are several objects proposed to be symbiotic stars based only on their photometric appearance or behavior. For this reason, we have decided to analyze available data on selected symbiotic candidates from our Database and supplement them with new spectroscopic and photometric data, in order to confirm or reject their symbiotic nature.

In this Chapter, we discuss the results of this project. In the first part, we focus on the candidates on classical symbiotic stars (Chapter 3.2). Some of these stars were detected in brightenings, in some cases, their variability reminds the changes observed in symbiotic stars during quiescence. In Chapter 3.3, we present the analysis of sources that have been suggested to be 'slow' symbiotic novae in the literature, or whose variability is similar to known symbiotic novae. Finally, in Chapter 3.4, the data on the candidates located in the Large Magellanic Cloud, a satellite galaxy to the Milky Way are presented.

3.1 Observational data and processing

To confirm or reject the symbiotic nature of the studied galactic candidates, we obtained new spectroscopic observations by organizing international observing cam-

paigns in cooperation with the ARAS Group[1] (*Astronomical Ring for Amateur Spectroscopy*; Teyssier 2019). For two symbiotic novae candidates (ASAS J174600-2321.3 and V5590 Sgr), further spectroscopic observations were acquired using ESO Faint Object Spectrograph and Camera mounted at the 3.58-m New Technology Telescope at La Silla, Chile (V. Schaffenroth; private communication). Optical spectra of the most symbiotic candidates located in the Large Magellanic Cloud were secured in the scope of the project searching for planetary nebulae in that galaxy (see the details in Reid & Parker 2006, 2010; Reid 2014; Reid & Parker 2012). The spectra were provided for our analysis by W. Reid (private communication). The spectra of three objects were acquired during the search for the post-AGB, post-RGB and YSO objects in the Large Magellanic Clouds (Kamath et al. 2015) and were provided for this study by D. Kamath (private communication). The data for one symbiotic candidate in the Large Magellanic Cloud were downloaded from the ESO Archive Science Portal[2]. Basic information about the spectra (JD, spectral range, observer) is summarized in the log of observations presented in Table B1 in Appendix B.

The obtained spectra were compared to the ones from empirical libraries of stellar spectra of Falcón-Barroso et al. (2011) (MILES; giants), Kesseli et al. (2017) (dwarfs, giants earlier than M0), and the library of Fluks et al. (1994) (giants). The reference spectra were down-sampled to the resolution of the observed data in order to obtain the spectral classification of the studied objects. If present, emission spectral lines have been identified in each spectrum.

For the classification of the symbiotic candidates, we have retrieved all available information on the objects from the literature and supplemented them with the data from *Gaia* EDR3/DR3 (Gaia Collaboration et al. 2021, 2022), *GALEX* (Bianchi et al. 2017), SkyMapper (Wolf et al. 2018), Pan-STARRS (Flewelling et al. 2020) APASS (Henden et al. 2015), 2MASS (Skrutskie et al. 2006), *AKARI* (Ishihara et al. 2010), and *WISE* (Wright et al. 2010). From this data, we have also constructed the multi-frequency spectral energy distributions, color-magnitude diagram, and near-infrared color-color diagram. The constructed SEDs of the symbiotic candidates were compared with the BT-Settl grid of theoretical spectra (Allard 2014) downloaded from Theoretical spectra webserver at the Spanish Virtual Observatory Theoretical Model Services[3] in order to estimate the parameters of the radiation sources. The spectral

[1]https://aras-database.github.io/database/symbiotics.html
[2]http://archive.eso.org/scienceportal/home
[3]http://svo2.cab.inta-csic.es/theory/newov2/index.php

types were estimated from the effective temperatures using the statistical relations of van Belle et al. (1999) and Malkov et al. (2020).

To study the photometric variability of the selected objects, we have employed the data obtained from the *Expérience pour la Recherche d'Objets Sombres* survey (EROS; $B_{\rm E}$ and $R_{\rm E}$ filters; Renault et al. 1998), DASCH (Digital Access to a Sky Century at Harvard) archive of digitized glass photographic plates of the Harvard College Observatory (Laycock et al. 2010), the Super Wide Angle Search for Planets (SuperWASP; Butters et al. 2010), All-Sky Automated Survey (ASAS; V filter; Pojmanski 1997), All-Sky Automated Survey for Supernovae (ASAS-SN; V and g filters; Shappee et al. 2014; Kochanek et al. 2017), the Zwicky Transient Facility (ZTF) survey (r and g filters; Masci et al. 2019), *Gaia* DR3 (G filter; Gaia Collaboration et al. 2022), and from the database of American Association of Variable Star Observers[4] (AAVSO; Kafka 2022). For symbiotic candidates in the Large Magellanic Cloud, we have also used the data from the Optical Gravitational Lensing Experiment (OGLE; V and I filters; Udalski et al. 2008) and Massive Compact Halo Objects survey (MACHO; $B_{\rm M}$ and $R_{\rm M}$ filters; Alcock et al. 1999). The photometric data were subjected to visual inspection and used for construction of the light curves of the selected candidates. Period analysis was performed using the Peranso software[5] to obtain the information on any periodic behavior of the studied symbiotic candidates.

3.2 Candidates on classical symbiotic stars

We have analyzed 11 candidates (Table 3.1) that were suggested to be classical symbiotic stars in the literature. For every particular candidate, we first introduce the literature information and then present and discuss our results and conclusions. The results presented in this Chapter were partly published in Merc et al. (2020a, 2021d) and Dubovský et al. (2021).

3.2.1 2MASS J07363415+6538548

This object was first detected by the *Chandra X-Ray Observatory* thanks to its X-ray emission (Schlegel & Pannuti 2003). Several authors attributed this source to the galaxy NGC 2403 (Schlegel & Pannuti 2003; Leonidaki et al. 2010; Yukita et al. 2010; Liu 2011; Mineo et al. 2012; Earnshaw et al. 2019), a spiral galaxy which belongs

[4]https://www.aavso.org/
[5]https://www.cbabelgium.com/peranso/

Table 3.1: List of the candidates on classical symbiotic stars analyzed in this thesis. The last column gives the reference to the study, in which the object was suspected of a symbiotic nature for the first time.

No.	Name	α_{2000} [h m s]	δ_{2000} [d m s]	Reference
1	2MASS J0736..	07 36 34.146	+65 38 54.77	Binder et al. (2015)
2	V503 Her	17 36 40.454	+23 18 11.60	Meinunger (1980)
3	V2204 Oph	18 26 01.923	+11 55 09.53	Samus' (1983)
4	V1988 Sgr	18 27 57.308	-27 37 23.11	Kenyon (1986)
5	V562 Lyr	18 31 13.817	+46 58 34.67	Guilbault et al. (2000)
6	IRAS 19050..	19 07 37.430	+00 06 09.10	Akras et al. (2019a)
7	EC 19249-7343	19 31 02.317	-73 37 07.64	O'Donoghue et al. (2013)
8	V1017 Cyg	19 56 15.815	+53 19 12.12	Szczerba et al. (2007)
9	PN K1-6	20 04 14.278	+74 25 35.93	Frew et al. (2011)
10	Hen 4-204	22 45 01.416	-44 52 38.52	Vanture & Wallerstein (2003)
11	V379 Peg	23 53 50.821	+23 09 18.09	Kopylov et al. (1988b)

to the M81 group, located at the distance of 3.3 Mpc (Karachentsev & Kashibadze 2006). It was classified as an H II region or a massive star cluster (Schlegel & Pannuti 2003), a potential supernova remnant (Leonidaki et al. 2010), a high-mass X-ray binary (Mineo et al. 2012; Sazonov & Khabibullin 2017), and finally as a possible cataclysmic variable or a symbiotic binary (Binder et al. 2015).

By analysis of available photometric data from ground-based surveys, together with high precision photometry from *TESS* (Ricker et al. 2015), astrometric measurements of the *Gaia* satellite and observations of other surveys spanning from X-rays to infrared, we have found that the object is not a symbiotic star nor a cataclysmic variable but rather an active K-type dwarf (Merc et al. 2020a). The star is located in the distance of 415 pc, has an effective temperature of 4 275 K, luminosity of $0.14\,L_\odot$, mass of $0.7\,M_\odot$, and radius of $0.7\,R_\odot$. It has a rotational period ~ 3 days and is a strong X-ray source with the X-ray luminosity of $\sim 10^{30}\,\mathrm{erg\,s^{-1}}$. Gyrochronology and isochrone fitting confirmed that the star is young. More details can be found in Merc et al. (2020a). Our spectrum of the object (presented in Dubovský et al. 2021) confirmed these results. The continuum is consistent with the K6 dwarf star. The presence and strength of the Hα emission line verified that the object is rather active.

3.2.2 V503 Her

V503 Her was first mentioned as a possible symbiotic star by Meinunger (1980). Later it was also included, as a suspected symbiotic binary, in the book by Kenyon (1986), and in the catalogs by Belczyński et al. (2000) and Akras et al. (2019a). At the

time of writing of this thesis, V503 Her was denoted as a confirmed symbiotic star in the SIMBAD database, with a reference to the General Catalogue of Variable Stars (GCVS; Samus' et al. 2017). GCVS itself listed the star as a type 'ZAND:'.

Bond (1978) obtained the spectrum of the object using the spectrograph mounted on the Kitt Peak 2.1-m telescope while searching for bright quasi-stellar objects. According to the author, the spectrum showed 'TiO bands about as well-developed as in type M2, but very weak'. In addition, he noted that the blue part of the spectrum 'appears filled in, as if by a hotter star' and suggested that the spectrum might be composite. Up to our knowledge, the only subsequent spectrum of V503 Her was published by Munari & Zwitter (2002). Their spectrum showed a continuum similar to a K-type star with a hint of TiO bands and no emission lines.

After the spectroscopic observation of a possible composite spectrum of V503 Her by Bond (1978), the photometric variability of the star was analyzed by Meinunger (1980) based on the Sonneberg plates. The author of the latter study suggested that the object showed the long-term variability similar to symbiotic stars, in addition to shorter brightness fluctuations with various amplitudes on the timescale of 80 – 100 days.

The more recent photometric observations of V503 Her obtained by the All Sky Automated Survey (ASAS) were analyzed by Gromadzki et al. (2013). They suggested that the object might be an eclipsing symbiotic star with an orbital period of around 1 575 days (based on the two detected minima at JD 2 453 145 and JD 2 454 720). Additionally, the authors of the aforementioned study detected pulsations with a period of 130 ± 2 days.

Two UV observations of V503 Her by the *Galaxy Evolution Explorer* (*GALEX*; Bianchi et al. 2017) and the *Neil Gehrels Swift Observatory* (*Swift*; Roming et al. 2005) are available. The object was detected in the NUV filter ($\lambda_{\rm eff} = 2305\,$Å), but not in FUV filter ($\lambda_{\rm eff} = 1549\,$Å) of the *GALEX* satellite . Luna et al. (2013) did not detect V503 Her in the UVM2 filter of the *Swift* satellite ($\lambda_{\rm eff} = 2246\,$Å).

We have collected 23 low-resolution optical spectra of V503 Her (in the scope of our observational campaign and from the archive of the ARAS database). Most of the spectra show the continuum of a K-type star with an occasional appearance of mild TiO bands connected with the photometric variations (pulsations and possible eclipses). The spectra obtained during the pulsation maximum and during the supposed eclipse of V503 Her are shown in Fig. 3.1A. The only emission lines detectable in our spectra are Balmer lines of H I, namely Hα and in the minority of the spectra

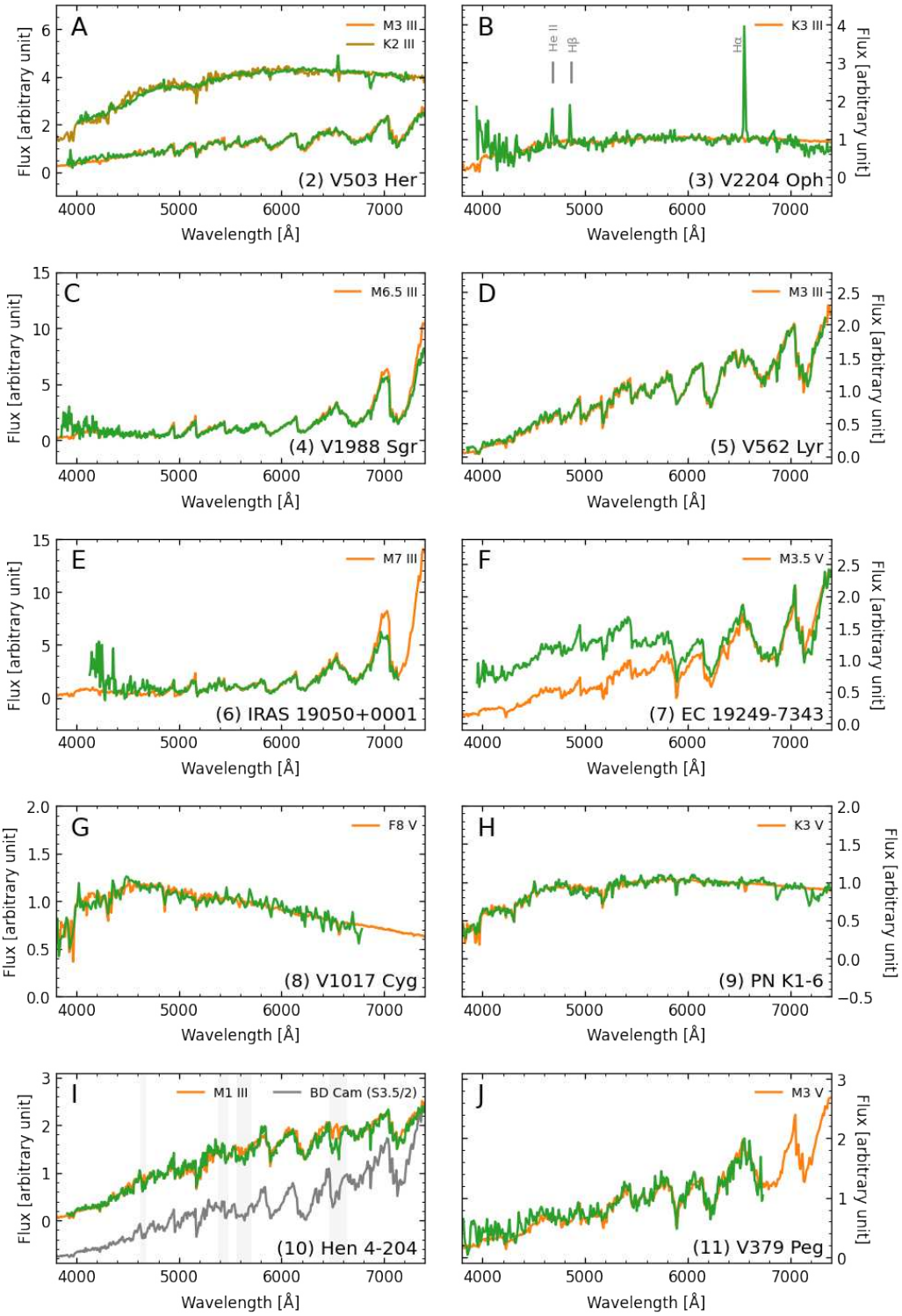

Figure 3.1: Spectra of the studied classical symbiotic candidates. The spectra obtained in the scope of our campaign and the best-fitting empirical spectra (Falcón-Barroso et al. 2011; Kesseli et al. 2017) are shown in green and orange, respectively. In the B panel, the identification of the most prominent emission lines is depicted. In panel I, the ARAS spectrum of BD Cam, the symbiotic star with an S-type star component is shown in grey. The position of the most prominent ZrO bands is depicted by shaded areas. All spectra were de-reddened by the $E_{(\mathrm{B-V})}$ values listed in Table 3.2 using the reddening law of Cardelli et al. (1989), and adopting the total to selective absorption ratio $R = 3.1$.

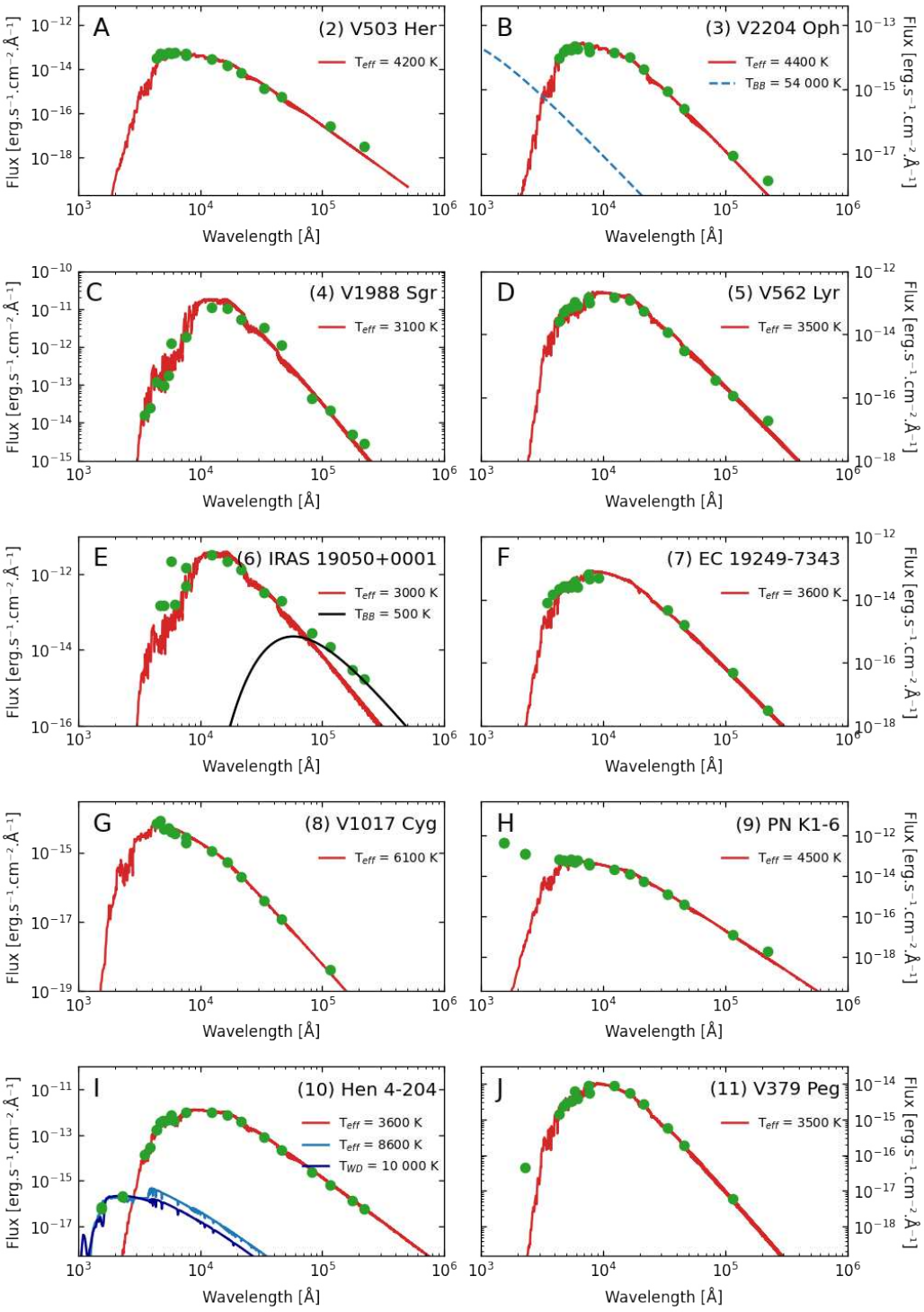

Figure 3.2: Multi-frequency SEDs of the studied classical symbiotic candidates. Measurements from *GALEX*, SkyMapper, APASS, *Gaia* EDR3, 2MASS, *AKARI*, and *WISE* are shown in green. The best fitting theoretical spectra (Allard 2014) are plotted in red. If two sources of radiation are present, the hotter is shown in blue (stellar spectra for PN K1-6 and Hen 4-204, black body of 54 000 K for V2204 Oph; see the text for details). In the case of Hen 4-204, we also show the best fitting WD spectrum in dark blue (Koester 2010). In the case of IRAS 19050+0001, the excess in IR presumably caused by a dust is modeled by the black body (shown in black). The fluxes were de-reddened by $E_{(\mathrm{B-V})}$ values listed in Table 3.2 using reddening law of Cardelli et al. (1989) and adopting the total to selective absorption ratio $R = 3.1$.

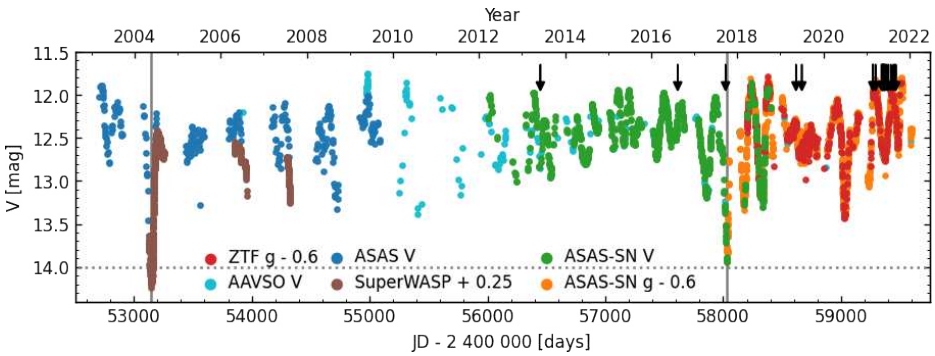

Figure 3.3: Light curve of V503 Her covering the period of the years 2002 – 2022, constructed on the basis of data from AAVSO, ASAS, SuperWASP, ASAS-SN, and ZTF. The positions of two possible eclipses are shown by vertical grey lines. The horizontal dotted line shows the level of the brightness of the system in the middle of the 2017 eclipse. Arrows denote the times when our spectra were obtained.

also Hβ. This ultimately excludes the classification of V503 Her as a shell-burning symbiotic system. K-type spectral classification of the object is supported also by the analysis of the SED (see Fig. 3.2A).

The long-term light curve of V503 Her is shown in Fig. 3.3. The ASAS-SN g and ZTF g data were simply linearly shifted to correspond to the V magnitudes. SuperWASP data are unfiltered and were shifted by +0.25 mag to correspond to ASAS V data obtained at the same time. While one needs to treat the absolute values with caution due to possible inaccuracies of these shifts and due to the fact that various filters have various effective wavelengths, this approach allows us to analyze the long-term variability of V503 Her.

The most prominent feature of the light curve are the semi-regular pulsations with a variable amplitude on a variable timescale (see Fig. 3.4A). The observed behavior fits well the description of the SRb subtype of semiregular variable stars. However, these are typically giants of late spectral types (M, C, and S). The pulsating star in V503 Her is probably hotter (spectral type K based on the optical spectra) which would place this object among the subclass SRd. According to the absolute V magnitude of this component calculated for the distance of 10.6 kpc (Bailer-Jones et al. 2021), it is more luminous than the giant of luminosity class III and lies close to the class II, at a maximum of light even between classes II and Ib (Sung et al. 2013).

In addition to pulsations, we have identified two prominent drops in brightness (JD 2 453 148 and JD 2 458 031; years 2004 and 2017) which we attribute to the possible eclipses of the pulsating component. During these eclipses, the V magnitude of the system decreases to $\sim 14 - 14.5$ mag. Gromadzki et al. (2013) analyzed solely the

ASAS data (covering the first of the mentioned eclipses) and also supposed that the decrease of brightness (to $\sim$ 13.3 mag) detected at JD 2 454 720 might be an eclipse. From this feature and the eclipse in 2004, they calculated a possible orbital period of 1 575 days. Thanks to the availability of the new data collected in this study, we were able to detect several other minima in the light curve during which the brightness decreased to the magnitude around $13.3 - 13.4$ mag in the V filter. These are apparently caused by the pulsations, as they occur on a variable timescale which cannot be expected for the orbital variability. For this reason, we consider the value of 1 575 days for the orbital period of V503 Her to be incorrect.

Considering that both deep minima detected in our light curve are primary eclipses and there has been no other eclipse between these events, we can calculate the orbital period of the system to be about 4 883 days (13.4 years). If the eclipsing nature of V503 Her and the length of the period would be confirmed by the subsequent observations (e.g., by the observations of the next eclipse in 2040), that would make V503 Her an eclipsing binary with the sixth-longest orbital period known.

The nature of the eclipsing component is not clear from the observations. We have only one spectrum which was obtained during the assumed eclipse of V503 Her in 2017 (10 days before the minimum). It shows the continuum similar to ∼M3 III star, which might be a secondary component of V503 Her. On the other hand, it is also possible that V503 Her is not an eclipsing system and that the deep minima are unusually faint pulsation minima of the K-type giant. In any case, the symbiotic nature of V503 Her seems to be contradicted by the observational data collected in this thesis.

3.2.3 V2204 Oph

The object has been observed in at least two brightenings, by Ross (1926) and by Samus' (1983). Samus' classified the star as a possible symbiotic binary. No spectrum has been obtained since then.

The continuum spectrum (Fig. 3.1B) and multi-frequency SED (Fig. 3.2B) of the object is consistent with a K3 giant. The spectral type of the cool component, the presence of the emission lines of H I, He I, and the strong line of He II 4686 Å, together with reported outbursts of the star (Ross 1926; Samus' 1983) allows us to confirm it as a yellow symbiotic binary. A spectrum of higher S/N would be needed to precisely characterize the symbiotic nebula and the hot component of the system. The lower

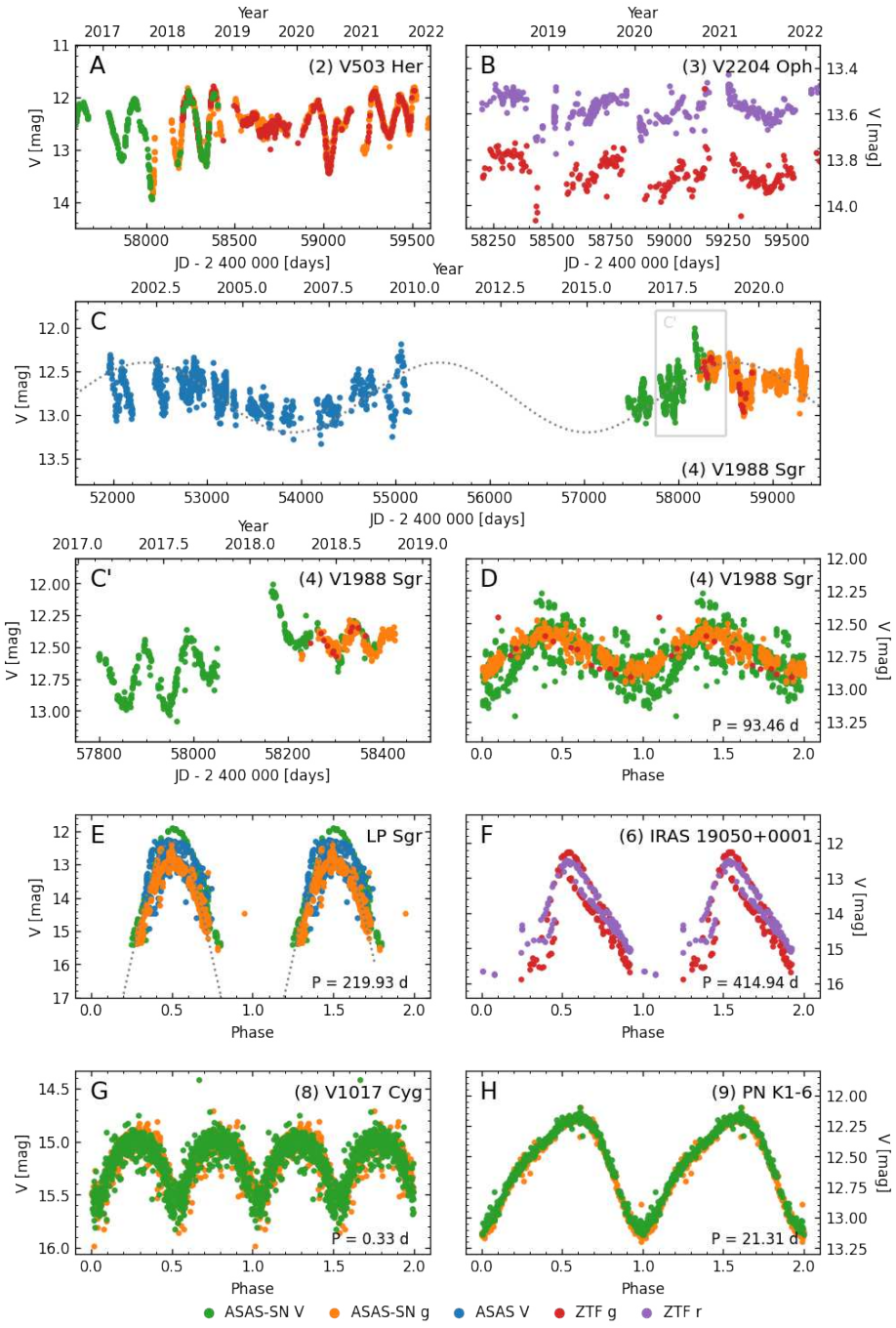

Figure 3.4: Light curves of the studied symbiotic candidates. **A**: Part of the light curve of V503 Her showing semi-regular pulsations. The g light curve was shifted by -0.6 mag to the level of V magnitudes for clarity. Full light curve is shown in Fig. 3.3. **B**: Light curves of V2204 Oph. **C**: Light curve of V1988 Sgr. ASAS V observations were shifted by +0.25 mag, ASAS-SN g and ZTF g by -0.95 mag to the level of ASAS-SN V ones. The dotted grey curve shows long-term variation with a period of 3 125 days. **C'**: Part of the light curve of V1988 Sgr showing the pulsation features. **D**: Light curves of V1988 Sgr with subtracted long-term variability, phased with the period of 93.46 days. **E**: Light curves of LP Sgr, phased with the period of 219.93 days. Data in the g filter were shifted by -0.60 mag to the level of V ones. **F**: Light curves of IRAS 19050+0001 phased with a period of 414.94 days. Data in the g filter were shifted by -3.5 mag to the level of the r filter. **G**: Light curves of V1017 Cyg phased with a period of 0.33 days. Data in the g filter were shifted by -0.22 mag to the level of V ones. **H**: Light curves of PN K1-6 phased with a period of 21.31 days. Data in the g filter were shifted by -0.44 mag to the level of V ones.

Table 3.2: Photometric properties of the studied classical symbiotic candidates. Data were obtained from *Gaia* EDR3 (G, π, $G_{\rm BP}$, $G_{\rm RP}$; Gaia Collaboration et al. 2021), and 2MASS (J, H, $K_{\rm S}$; Skrutskie et al. 2006). The values of extinction $E_{\rm (B-V)}$ used in this thesis (the last column) were taken from Schlafly & Finkbeiner (2011) and adjusted for the closest objects (as the catalog values correspond to the total Galactic extinction in the given direction): (7) EC 19249-7343, (11) V379 Peg. Higher value than given by the reddening map was adopted for (6) IRAS 19050+0001 (see the text for details).

No.	G	π	$G_{\rm BP}$	$G_{\rm RP}$	J	H	$K_{\rm S}$	$E_{\rm (B-V)}$
	[mag]	[mas]	[mag]	[mag]	[mag]	[mag]	[mag]	[mag]
1	15.41	2.43 ± 0.04	16.16	14.55	13.41	12.77	12.66	0.03
2	12.05	0.08 ± 0.01	12.77	11.20	10.24	9.76	9.57	0.07
3	13.61	0.04 ± 0.02	14.56	12.64	11.16	10.32	10.1	0.16
4	9.24	1.39 ± 0.14	12.73	7.72	3.93	2.79	2.35	0.34
5	10.90	0.28 ± 0.01	12.05	9.84	8.28	7.41	7.23	0.04
6	11.86	0.32 ± 0.12	16.28	10.12	6.16	5.02	4.30	1.50
7	12.06	51.69 ± 0.09	13.05	10.78	9.18	8.51	8.24	0.00
8	15.04	0.88 ± 0.02	15.44	14.48	13.82	13.41	13.39	0.19
9	12.30	3.86 ± 0.03	12.86	11.51	10.62	10.01	9.81	0.18
10	8.82	0.73 ± 0.02	10.03	7.74	6.26	5.42	5.12	0.01
11	14.03	9.36 ± 0.02	15.36	12.89	11.35	10.76	10.52	0.03

limit of the temperature of the hot component is 54 000 K according to the method of Murset & Nussbaumer (1994). The position of V2204 Oph in the HR diagram (Fig. 3.5) is typical for other symbiotic stars.

In the NIR color-color diagram, the object is located in the bottom-left part of the region occupied by the S-type symbiotic stars (Fig. 3.6). This very same position in the diagram is occupied by another well-known yellow symbiotic star, AG Dra. The IR properties also satisfies the criteria for S-type symbiotic stars which were proposed by Akras et al. (2019b, 2021, Chapter 2.4).

ASAS-SN and ZTF photometric observations revealed the possible presence of the period ∼450 days, which may be due to the orbital motion. However, the time interval covered by the ZTF observations (shown in Fig. 3.4B) is too short to be conclusive and there is a rather large scatter in the light curves of V2204 Oph in the ASAS-SN data. This could be because the star is close to the limit of the survey ($V \sim 14.5$ mag). On the other hand, giants in symbiotic stars often pulsate on timescales of 50 – 200 days (Chapter 2.4), which introduce additional scatter to the quiescent light curves. Only a well-sampled long-term light curve and/or radial velocity measurements would help to confirm the presence of the period and to refine its value.

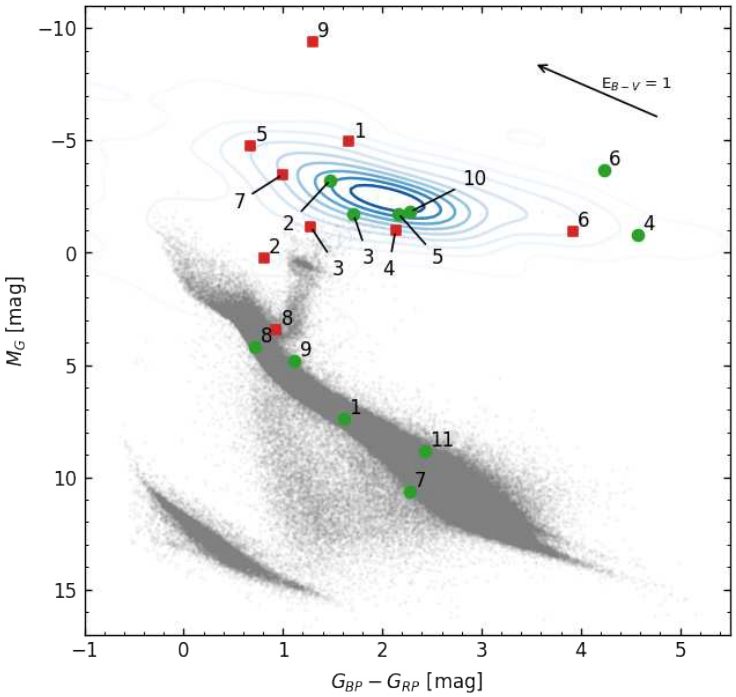

Figure 3.5: Position of the studied objects (classical symbiotic candidates and 'slow' symbiotic nova candidates are depicted by green circles and red squares, respectively; labels are according to Table 3.1 and 3.3) in the *Gaia* HR diagram of a sample of stars within 200 pc with reliable astrometry (Gaia Collaboration et al. 2018). The blue density map shows the position of the known symbiotic variables from the New Online Database of Symbiotic Variables. The photometric measurements from *Gaia* EDR3 (Gaia Collaboration et al. 2021) were used, corrected for reddening obtained using the dust map of Schlafly & Finkbeiner (2011), adjusted for the nearby targets. To calculate the absolute G magnitude of objects, distances of Bailer-Jones et al. (2021) were adopted.

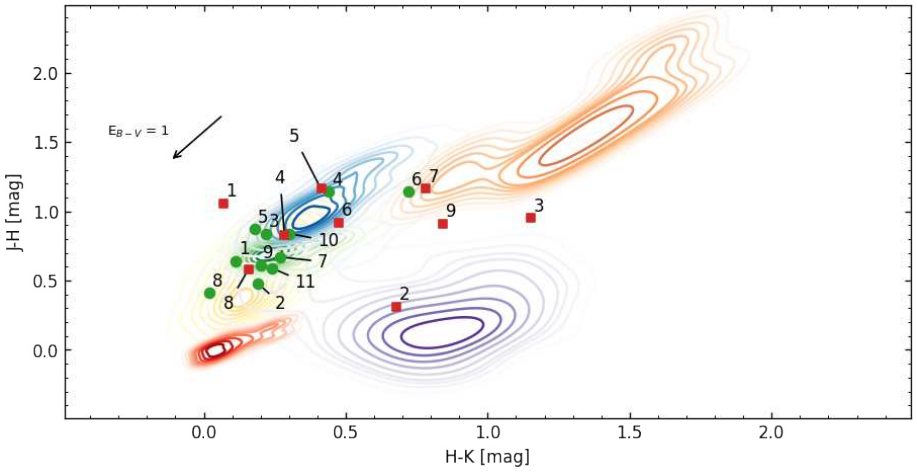

Figure 3.6: Position of the studied objects (classical symbiotic candidates and 'slow' symbiotic nova candidates are depicted by green circles and red squares, respectively; labels are according to Table 3.1 and 3.3) in the near IR color-color diagram based on 2MASS observations (Skrutskie et al. 2006). The positions of the known S- and D-type symbiotic stars from the New Online Database of Symbiotic Variables are shown as density maps in blue and orange, respectively. Planetary nebulae (Ramos-Larios & Phillips 2005), Be stars (Zhang et al. 2005), T Tauri stars (Dahm & Simon 2005), and cataclysmic variables (Downes et al. 2001) are shown in violet, red, green and yellow, respectively.

3.2.4 V1988 Sgr

The star is included in the General Catalogue of Variable Stars (GCVS) as a possible symbiotic binary (Samus' et al. 2017) based on photometric variability (possible brightening by < 1.3 mag detected on five photographic plates) identified by Hoffleit (1962). The object is also listed as a suspected symbiotic star in Kenyon (1986). We should note that GCVS and SIMBAD list IRC-30385 as a cross-identification of V1988 Sgr in the Two-Micron Sky Survey (Neugebauer & Leighton 1969). The star is classified in the survey as M7. However, in the catalog itself, IRC-30385 is identified as LP Sgr, which is a Mira variable with Me spectrum according to GCVS. No spectrum of either of the two variable stars is available in the literature. We have analyzed both objects. The field around V1988 Sgr is shown in Fig. B1 in Merc et al. (2021d).

V1988 Sgr is the most reddened of the studied symbiotic candidates (see HR diagram in Fig. 3.5) and its position in the NIR color-color diagram is typical for S-type symbiotic binaries (Fig. 3.6). The light curve of the object (Fig. 3.4C, C', and D) revealed the presence of the long-term variability with the period around 3 125 days, and the semi-regular pulsations with period $\sim$ 90 days. Such a photometric variability is often visible in the light curves of symbiotic stars (e.g., Gromadzki et al. 2013). On the other hand, the obtained spectra of V1988 Sgr (Fig. 3.1C) are consistent with an M6.5III star and do not show any emission lines nor excess in the blue part, which are typical for the shell-burning symbiotic stars. Therefore, these data do not allow us to confirm the symbiotic nature of the system. The SED of the object (Fig. 3.2C) confirms the spectral classification and these data do not indicate the presence of a hot symbiotic component.

It could be that V1988 Sgr is not a shell-burning symbiotic star but an accreting-only one. As mentioned in Chapter 1.3, such symbiotic systems do not show emission lines in the spectrum, they are bright in UV and show significant flickering in this spectral range. Unfortunately, no observations of V1988 Sgr in this part of the spectrum are available. Flickering is often detectable also at optical wavelengths, with the highest amplitudes observed at the shortest wavelengths (e.g., in the Johnson U filter). As the observations in the U filter are rather infrequent in the era of CCDs, we executed a 90-min observing run at JD 2 459 329.8 (April 25, 2021) in Johnson B filter using Danish 1.54-meter telescope at La Silla, Chile. In total, 35 frames were obtained with an exposure time of 120 s each. We have not detected any significant flickering

above the observational noise. For this reason, the data do not allow us to confirm the symbiotic status of V1988 Sgr. On the other hand, as Munari et al. (2021) pointed out, even in the case of well-known accreting-only symbiotic stars such as SU Lyn or MWC 560, flickering is not always detectable.

Based on these findings, we cannot classify V1988 Sgr as a genuine symbiotic star, but at the same time, we do not rule out its possible accreting-only symbiotic classification. It is worth noting that its IR properties satisfy the IR criteria proposed by Akras et al. (2019b, 2021) for S-type symbiotic systems, having W1-W2$\geq$0.09, similarly to MWC 560. On the other hand, it remains an open question whether the brightening in 1924 identified by Hoffleit (1962) was a symbiotic outburst, or was a consequence of the periodic photometric variability observed in the star even today. For definitive classification, new observations over time and/or in other spectral regions will be needed.

We have also analyzed the data of LP Sgr, a nearby star that is sometimes confused with V1988 Sgr in the literature. The ASAS-SN and ASAS light curves of LP Sgr phased with the period of 219.93 days are shown in Fig. 3.4E. These data are consistent with the Mira pulsations with a rather high amplitude of several magnitudes. The spectrum of LP Sgr, which we obtained together with observations of V1988 Sgr, shows an M3.5 III continuum and Hα in emission. The spectrum was obtained at phase $\sim$0.1 ($\varphi = 0$ being a brightness maximum). The data suggest that LP Sgr is a single Mira pulsator.

3.2.5 V562 Lyr

Unusual behavior of the star was first noted by Dahlmark (2000), who detected the object on three plates to be at least 3.3 mag fainter than usual. The variability was later studied by Guilbault et al. (2000). They confirmed the presence of a single long-lasting deep eclipse (1 000 – 1 200 days) or an R CrB variability and suggested that the object might be an eclipsing binary with a very long period, R CrB variable or a symbiotic star. No spectrum was available.

Although the star is generally referred to as a confirmed symbiotic binary (e.g., in SIMBAD), the obtained spectrum (Fig. 3.1D) and SED (Fig. 3.2D) are very well consistent with a single M3 giant and no emission lines are observed. The position of the object in the HR and NIR color-color diagrams (Figs. 3.5 and 3.6) is consistent with the giant classification. Moreover, the star has not been detected by *GALEX* in

UV, which would be expected for a symbiotic star (either burning or accreting-only) or a binary with a hot companion. Analysis of the photometric data from ASAS-SN and ZTF of V562 Lyr shows a possible presence of irregular variability on the timescale ∼16 days with an amplitude of < 0.2 mag in the V filter. No minima are seen in the recent light curve.

3.2.6 IRAS 19050+0001

The highly reddened object is relatively faint in the V filter, but bright in the red spectral region, and especially in IR. The star seems to be included in the lists of symbiotic stars by mistake, as there is confusion about the position of the object in the literature. Databases such as SIMBAD give NSV 11749, a known symbiotic binary (Bond & Kasliwal 2012; Rodríguez-Flores et al. 2014), at the position of IRAS 19050+0001. This object also appears on the list by Akras et al. (2019a). However, NSV 11749 is another object. For this reason, there is no spectroscopic information on IRAS 19050+0001 in the literature.

Its position in the *Gaia* HR diagram (Fig. 3.5) as well as in the NIR color-color diagram (Fig. 3.6) confirmed that the object is very red. Because of the high reddening and consequent faintness of the object in the blue part of the optical spectrum (< 20 mag in the B filter; Lasker et al. 2008), we have used only the part red-wards of 5 500 Å for the spectral classification. To obtain an appropriate fit by any of the empirical spectra, we have increased the extinction value to 1.5 (the value given by the reddening map is ∼0.6; Schlafly & Finkbeiner 2011). That part of the spectrum is well consistent with an M7 III star (Fig. 3.1E). The multi-frequency SED (Fig. 3.2E) seems to be more consistent with a slightly cooler star (M8), with the IR excess consistent with the black-body model with the temperature of ∼500 K.

The position of IRAS 19050+0001 in the NIR color-color diagram (Fig. 3.6) suggests that it might be a symbiotic star, possibly of a D-type. However, our spectroscopic observation has not shown the presence of emission lines in the spectrum preventing the classification of the object as a shell-burning symbiotic system. The analysis of the ZTF light curves of the star revealed the presence of the pulsations with a period of 414.94 days. The light curves phased with this period are shown in Fig. 3.4F.

Considering the shape of the light curves, the obtained value of the period, and the spectral type, we argue that the object is a (probably single) Mira variable. Using

the period-luminosity relation of Whitelock et al. (2008) for O-rich Miras, we have obtained the distance of 2.6 kpc for IRAS 19050+0001, which is consistent with the photo-geometric distance of 2.4 (2.0-3.1) kpc obtained by Bailer-Jones et al. (2021) using *Gaia* EDR3 data. The dust produced in the stellar atmosphere would explain the higher value of the extinction than the one (interstellar) given by the dust map. The presence of the warm dust and the Mira pulsations can also explain the IR excess in the SED of the object and the difference between the spectral type obtained from the spectrum and the SED, respectively.

3.2.7 EC 19249-7343

The object is listed as a symbiotic candidate in the catalog of O'Donoghue et al. (2013) based on the low-resolution spectrum from the Edinburgh-Cape survey. They suggested that the peculiar spectrum with molecular bands is similar to the recurrent symbiotic nova T CrB. The star was also included in the catalogs of M dwarfs (Lépine & Gaidos 2011; Frith et al. 2013).

According to *Gaia* EDR3 data, the object is a high proper motion star located at a distance of 19.3 pc (Bailer-Jones et al. 2021; Gaia Collaboration et al. 2021). At such a distance, its brightness is well consistent with a dwarf star (Fig. 3.5), which precludes the symbiotic classification of the object. The position of EC 19249-7343 in the NIR color-color diagram (Fig. 3.6) is also not consistent with the symbiotic classification and coincides with the position of typical M dwarfs.

The spectrum of the object is plotted in Fig. 3.1F. No emission lines are seen in the data. In addition to an M3-4 V continuum, excess in the blue part is detected. We have observed the object at several occasions (see Tab. B1) to confirm that the excess is not an observational artifact. This feature is present in all our spectra and seems to be variable to some extent. Slight excess in the blue optical spectral region is also confirmed by the SED of the object (Fig. 3.2F). Such a blue excess is often observed in white dwarf-M dwarf binaries (see e.g., Ren et al. 2014; Skinner et al. 2017, and references therein). However, no trace of broad hydrogen absorption features of a DA white dwarf is detectable in our data. On the other hand, some cool white dwarfs can have a featureless continuum (e.g., Fajardo-Acosta et al. 2016, their Fig. 9, and references therein). It seems that a similar excess in the spectra is detected also in some detached M dwarf-M dwarf binaries (e.g., Birkby et al. 2012, especially 19c-3-01405 shows a very similar continuum shape as EC 19249-7343). We should

also note that some cataclysmic binaries are located in a similar region of the *Gaia* HR diagram as EC 19249-7343 (Abril et al. 2020), though, most of the cataclysmic variables exhibit emission lines in their spectra due to the presence of accretion disks (e.g., Hellier 2001).

No periodic variability has been detected in the ASAS-SN light curves while there is a scatter of about 0.15 mag in the data. There are two epochs when the star was above the average brightness: at the beginning of the observations of ASAS-SN (at least for 2 months between JD 2 455 978 and JD 2 456 042; 0.3 mag in the V filter) and during the short (2 – 5 days) brightening distinguishable in the light curve between JD 2 458 489 and JD 2 458 491 (0.4 mag in the g filter). Unfortunately, the ZTF data are not available for this object. If the star is indeed a white dwarf-M dwarf binary or a cataclysmic system, the variability on the timescale of hours or days might be detected by careful well-sampled photometric and/or spectroscopic (i.e., variations of radial velocities) observations.

3.2.8 V1017 Cyg

The object was classified as a symbiotic star by Szczerba et al. (2007) during the analysis and cataloging of post-AGB stars. Their classification is based on the photometric appearance of the star. Later, the object has also been included in the catalog of RR Lyrae stars (e.g., Gavrilchenko et al. 2014). We should note that the reference to an object called V1017 Cyg appeared in table 2 of Wannier et al. (1990). However, this was only a mistyping of V1016 Cyg, a known symbiotic star, as indicated by the coordinates. Later in the paper (e.g., table 4), they used the correct identifier (V1016 Cyg). No spectrum of V1017 Cyg is available in the literature.

Our optical spectrum of V1017 Cyg (Fig. 3.1G) is consistent with a $\sim$F8-9 V star. This spectral classification is also confirmed by the multi-frequency SED of the star (Fig. 3.2G). Luminosity class V (see the position of the object in the HR diagram, Fig. 3.5) is confirmed by the absolute magnitude calculated for the distance of $\sim$1 200 pc from *Gaia* (Bailer-Jones et al. 2021; Gaia Collaboration et al. 2021). The object is the bluest of the whole examined sample (Figs. 3.5 and 3.6).

Using the ASAS-SN light curves of the object, we have detected variability with a period of 0.33 days (Fig. 3.4G). Combining the photometric variability of the star and the inferred spectral type, we can conclude that V1017 Cyg is a W UMa binary (sub-type W).

3.2.9 PN K 1-6

The object was discovered by Kohoutek (1962) and classified as a probable planetary nebula. Later, it was confirmed to be a bonafide planetary nebula with a variable central star. The appearance and photometric variability were studied in detail by Frew et al. (2011), who suggested that the central star might be a binary or even a triple system. The authors preferred the RS CVn or FK Com variable for the classification of the central star, although they also proposed a symbiotic binary.

The obtained optical spectra of the object (one is shown in Fig. 3.1H) is consistent with a K1-3 V star. The positions of the star in the HR and NIR color-color diagrams (Figs. 3.5, 3.6) also coincide with dwarf stars of such a spectral type. The apparent spectral type seems to change with the brightness of the star which varies with the period of ~ 21 days and amplitude of ~ 1 mag in the V filter (Fig. 3.4H).

The strong fluxes in the UV region detected using *GALEX* (see Fig. 3.2H) could be approximated by the second stellar source with a temperature of few tens of thousands K. As the object was confirmed to be a planetary nebula (Frew et al. 2011), a hot pre-white dwarf or white dwarf is expected. Moreover, several planetary nebulae have binary central stars (e.g., Boffin & Jones 2019). The brightness of the object is consistent with the dwarf star (see its position in the HR diagram in Fig. 3.5), if we assume the distance of 258 pc as inferred by Bailer-Jones et al. (2021) from *Gaia* EDR3 data (Gaia Collaboration et al. 2021). These results, together with the observed ~ 21 days variability in the light curves of the object, rule out the possible symbiotic classification of PN K1-6.

3.2.10 Hen 4-204

This relatively bright, southern object was proposed to be a possible yellow symbiotic system by Vanture & Wallerstein (2003) on the basis of the similarity of the abundance pattern of Hen 4-204 and HD 35155, a known symbiotic binary. Hen 4-204 is classified as a probable extrinsic S-type star (Van Eck et al. 2000).

The spectrum of the object is plotted in Fig. 3.1I. The molecular bands of TiO are similar to the ones seen in an M1 III star ($T_{\rm eff} \sim 3\,600$ K). However, it is clearly seen that there are some differences between the spectra of Hen 4-204 and M1 III star caused by ZrO molecular bands confirming that Hen 4-204 is an S-type star. The optical spectrum of the object is analogous to that of BD Cam, a known symbiotic binary with an S3.5/2 cool component (Keenan & Boeshaar 1980). The symbiotic na-

ture of BD Cam was confirmed by UV observations showing emission lines with a high ionization potential (up to 77.5 eV; Ake et al. 1988). Unfortunately, spectroscopic observations of Hen 4-204 in this spectral range are not available. The position of the object in the HR diagram (Fig. 3.5) and NIR color-color diagram (Fig. 3.6) coincide with the symbiotic stars, and its IR properties satisfy the criteria proposed by Akras et al. (2019b, 2021). However, that cannot be used as a definitive confirmation of the symbiotic nature.

The SED (Fig. 3.2I) suggests an emission excess in the near-UV spectral region compatible with the presence of another stellar object with an effective temperature of $\sim 8\,600$ K or a white dwarf with a temperature of $\sim 10\,000$ K. If the companion is a main-sequence star, the cool component of Hen 4-204 would have to be an intrinsic S star. However, the absolute magnitude of the object calculated for a distance of $\sim 1\,320$ pc from *Gaia* (Bailer-Jones et al. 2021; Gaia Collaboration et al. 2021) is consistent with the luminosity of a normal giant star. That means that the cool component of Hen 4-204 is not a thermally-pulsing asymptotic giant branch star, but rather it has been polluted by s-process matter from its companion which has evolved faster. Therefore, a white dwarf is preferred over the main-sequence star to be the hot component of Hen 4-204.

We should note that while the orbital period of 596 days and a possible pulsation period of 24.8 days was inferred for BD Cam by Griffin (1984) and Adelman (1998), respectively, we have detected the period of 19.12 days in the ASAS-SN V light curve of Hen 4-204 in addition to a bare detection of period $\sim$ 510 days. From all this, we can conclude that Hen 4-204 is an object very similar to BD Cam, but without further observations, especially spectroscopic in the UV region, we cannot definitively classify the system as a genuine symbiotic binary.

3.2.11 V379 Peg

The object has been detected in outburst as a UV-excess star with a blue continuum in the eighties (Lipovetsky & Stepanian 1981). It was proposed to be either a cataclysmic variable or symbiotic binary (based on the observations of Kopylov et al. 1988b). However, there is confusion about the position of the object in the sky. Most of the current databases (e.g., SIMBAD, where the star is listed as a confirmed symbiotic binary) point to a red, relatively bright object. The red star was studied by Kato et al. (2002) who contradicted the symbiotic or cataclysmic nature of the object based on

the photometric observations and detected proper motion. On the other hand, Henden et al. (2003) pointed out that the object originally classified as V379 Peg back in 1981 is not a reddish star, but a nearby blue object with magnitude >18 mag (denoted USNO-A2.0 1125-19982531; see Fig. B2 in Merc et al. 2021d).

We have chosen the red star for our observations as the blue one is too faint for the spectroscopic observations using small telescopes. Although the obtained spectrum has a low S/N ratio (especially in the blue part), it is consistent with an M2-3 V star (Fig. 3.1J). A similar spectral type is inferred from the SED (Fig. 3.2J). The position of the star in the NIR color-color diagram (Fig. 3.6) coincides with that of early M dwarf stars. This luminosity class is confirmed by the absolute magnitude of the object (see its position in the HR diagram, Fig. 3.5), assuming that V379 Peg is located at the distance of 106 pc, as given by *Gaia* (Bailer-Jones et al. 2021; Gaia Collaboration et al. 2021). Therefore, the object is a dwarf star rather than a symbiotic binary. Spectra with a higher signal-to-noise ratio may reveal some emission lines due to a chromospheric activity of the star.

The light curves of V379 Peg obtained from the ASAS-SN did not show any significant/periodic variability, but the brightness of the object was at the limit of the survey. In the light curves from the ZTF survey, we have just barely detected the possible period of $\sim$4.3 days. It is worth mentioning that the object was detected in the *GALEX* NUV filter on a level higher than expected for a single M dwarf. On the other hand, the star was not detected in the FUV filter. This might be a coincidence with some background source or the star might have a very faint companion of the earlier spectral type. The barely detected variability of $\sim$4.3 days in ZTF data might suggest the presence of orbital variability in the light curve of V379 Peg.

We should note that the near blue stellar object (USNO-A2.0 1125-19982531), which is probably the one detected in the outburst back in the eighties, still could be a cataclysmic variable. Its parallax in *Gaia* EDR3 is negative. However, adopting the range of distances 4.8 – 7.6 kpc obtained from Bailer-Jones et al. (2021), results in $M_{\rm G} = 4.8$ – 3.8 mag. Together with the color of the object $(G_{\rm BP}$ - $G_{\rm RP}) = 0.75$ mag, it falls in the region of the *Gaia* HR diagram occupied mainly by nova-like cataclysmic variables (see Fig. 2 of Abril et al. 2020). The symbiotic nature is improbable, given its blue colors and low luminosity.

3.3 'Slow' symbiotic novae candidates

In the New Online Database of Symbiotic Variables, we have also collected several candidates on the 'slow' symbiotic novae (see Chapter 1.4). As only about a dozen symbiotic stars showing this type of activity are currently known, we have decided to analyze the candidates from our Database in order to increase the size of the observed sample. The candidates on 'slow' symbiotic novae analyzed in this study are listed in Table 3.3. In the following section, we present the literature information on the selected objects and discuss the results of our analysis.

3.3.1 M31N 2017-05b

This target was detected in the outburst by the *Gaia* satellite and reported in the form of a *Gaia* Science Alert (GSA; Wyrzykowski & Hodgkin 2012; Hodgkin et al. 2013, 2021) on May 23, 2017 (Delgado et al. 2017). The photometric and spectroscopic follow-up observations on the 2-m Liverpool Telescope were reported by Williams et al. (2017). The authors suggested that the object might be a possible symbiotic nova in M31, based on the absolute magnitude of the outburst and the color changes throughout the brightening.

Given the faintness of the object ($G \sim 20$ mag), we have analyzed only the spectra obtained using the low-resolution SPRAT spectrograph ($R \sim 350$; Piascik et al. 2014) on the Liverpool Telescope (Steele et al. 2004) downloaded from the Liverpool Telescope Science Data Archive and the *Gaia* light curve of the object published in the *Gaia* Alerts archive[6]. The spectrum of M31N 2017-05b (Fig. 3.7A) obtained very close to the outburst maximum (June 20, 2017) shows very prominent emission lines of H I, He I, He II, and possibly [O III]. Such a spectroscopic appearance is not typical for symbiotic novae but is observed in classical symbiotic stars (e.g., Munari 2019).

The presence of the cool component is not apparent from the spectrum. This can be due to the low S/N in the continuum, but also the fact that during the outbursts of classical symbiotic stars, the radiation of the nebula and/or the hot component typically outshines the contribution of the cool giant (see an example in Fig. 1.6). On the other hand, the presence of the cool giant in M31N 2017-05b is supported by the absolute magnitude calculated for the distance to M31 (785 kpc; McConnachie et al. 2005) and by its position in the *Gaia* HR diagram (Fig. 3.5). The position of the source in the IR color-color diagram (Fig. 3.6) is also broadly consistent with

[6]http://gsaweb.ast.cam.ac.uk/alerts/alert/Gaia17bjg/

Table 3.3: List of candidates on 'slow' symbiotic novae analyzed in this study. Last column gives the reference to the study, in which the object was first suspected from the symbiotic nature.

No.	Name	α_{2000} [h m s]	δ_{2000} [d m s]	Reference
1	M31N 2017-05b	00 42 49.090	+41 42 41.62	Williams et al. (2017)
2	2MASS J0109..	01 09 34.843	-08 00 33.09	Honeycutt & Kafka (2010)
3	2MASS J0642..	06 42 22.190	-02 26 28.52	Blex et al. (2018)
4	TYC 1371-69-1	07 57 31.123	+20 17 34.78	Tang et al. (2012)
5	ASAS J1746..	17 46 00.182	-23 21 16.36	Hümmerich et al. (2015)
6	V618 Sgr	18 07 57.210	-36 29 52.30	Kilkenny (1989)
7	V5590 Sgr	18 11 03.700	-27 17 29.43	Mróz et al. (2014)
8	HH Sge	20 06 48.319	+20 41 55.48	Yudin (1987)
9	V627 Cas	22 57 40.972	+58 49 12.53	Bergner et al. (1988)

Table 3.4: Photometric properties of the studied symbiotic nova candidates. Data were obtained from *Gaia* EDR3 (G, π, $G_{\rm BP}$, $G_{\rm RP}$; Gaia Collaboration et al. 2021), and 2MASS (J, H, $K_{\rm S}$; Skrutskie et al. 2006). The values of extinction $E_{\rm (B-V)}$ used in this thesis (the last column) were taken from Schlafly & Finkbeiner (2011) and adjusted for the close object (8) HH Sge (as the catalog values correspond to the total Galactic extinction in the given direction). Slightly higher value than given by the reddening map was adopted for the object (3) TYC 1371-69-1 to fit the optical data with any empirical spectrum.

No.	G [mag]	π [mas]	$G_{\rm BP}$ [mag]	$G_{\rm RP}$ [mag]	J [mag]	H [mag]	$K_{\rm S}$ [mag]	$E_{\rm (B-V)}$ [mag]
1	19.90	0.17 ± 0.44	20.62	18.74	-	-	-	0.17
2	14.80	-0.02 ± 0.03	15.10	14.23	13.70	13.38	12.71	0.05
3	15.80	0.09 ± 0.04	17.27	14.62	15.85	14.90	13.75	1.07
4	9.86	0.67 ± 0.02	11.01	8.80	7.28	6.45	6.17	0.25
5	11.64	0.10 ± 0.02	12.44	10.73	9.93	8.76	8.35	0.81
6	12.96	0.19 ± 0.06	15.59	11.50	8.60	7.68	7.20	0.25
7	12.26	0.13 ± 0.03	12.92	11.22	9.29	8.13	7.35	0.54
8	11.36	3.70 ± 0.02	11.95	10.61	9.48	8.90	8.74	0.10
9	9.84	-0.01 ± 0.10	12.50	8.45	5.46	4.55	3.71	2.15

a symbiotic classification although the infrared data are, given the faintness of the object, less reliable than for the brighter sources.

The light curve of M31N 2017-05b (Fig. 3.9A) shows an outburst of about 1.6 mag in the G filter. The rise to the maximum took approximately four months and was followed by the decline with the duration of $\sim$ 1 year. Later, a smaller brightening of 0.4 mag was detected. After three years and three months, the object seems to return to its pre-outburst brightness. Such behavior, similarly to spectroscopic appearance, contradicts the symbiotic nova classification of the target. The photometric evolution of the outburst observed in the case of M31 N 2017-05b is typical for the classical symbiotic stars (see their light curves in Fig. 1.6).

Taken together, the limited observational material analyzed in this study allows

us to classify M31N 2017-05b as a classical symbiotic star observed during a Z And-type outburst. Interestingly, it is the second symbiotic star discovered by the *Gaia* satellite (after Gaia18aen; see Chapter 4.1) and the first extragalactic symbiotic star discovered by this European mission.

3.3.2 2MASS J01093484-0800329

This target (also known as FBS 0107-082 and Cet 7) was previously classified as a nova-like cataclysmic variable (Kopylov et al. 1988a). The photometric and spectroscopic data were studied by Honeycutt & Kafka (2010), who suggested that the object might be a symbiotic nova in a prolonged outburst (based on the 0.33 mag brightness decrease between their observations from 2005 – 2008 and the USNO-B1.0 magnitudes obtained 55 years earlier). The spectra of the object analyzed in their work showed emission lines of H I, He I, [O III], and He II and absorption features from an early-F star.

Our optical low-resolution spectrum of the target (Fig. 3.7B) confirmed the presence of the emission lines of H I, He I, He II, and [O III]. The S/N in the continuum is too low to study the absorption features, but the spectrum does not seem to show any late-type molecular bands typical for symbiotic giants. The SED of the object (Fig. 3.8A) is not conclusive as its analysis is not well constrained without further assumptions. If a cool giant is present (we assumed its temperature of 3 500 K), then a hotter source and possibly also some dust emission has to be included in order to model the UV and IR excess observed in the system.

The position of 2MASS J01093484-0800329 in the *Gaia* HR diagram (Fig. 3.5) is not relevant for the analysis of the symbiotic status, as the data were obtained in the scope of the assumed ongoing outburst. On the other hand, we should note that the position of the target in the IR color-color diagram does not support the symbiotic classification, as 2MASS J01093484-0800329 is located in the region occupied by planetary nebulae (Fig. 3.6). Moreover, the object is neither fulfilling the IR criteria of Akras et al. (2019b, 2021, Chapter 2.4), nor is classified as a symbiotic system in six out of seven classification trees (only criterion where the object is classified as a symbiotic star is to distinguish between symbiotic stars, K and M giants).

Unfortunately, there are no historical photometric measurements of the object 2MASS J01093484-0800329 available in the literature to assess, when its proposed symbiotic nova outburst might have started. If the brightness decrease of 0.33 mag

over 55 years suggested by Honeycutt & Kafka (2010) is indeed the decline from the symbiotic nova outburst, that would suggest that the evolution of the system in outburst is extremely slow (decline rate of $\sim 6{\times}10^{-3}\,\mathrm{mag\,yr^{-1}}$). Such an evolution would be very unusual even in the comparison with the slowest symbiotic nova ever observed (AG Peg; Fig. 1.7). The recent photometric data of the object from the ZTF survey are not sufficient for a proper period analysis, but still show some short-term ($\sim$ hours – days) variability with an amplitude of about 0.3 – 0.4 mag. Similar scatter is also seen in the ASAS-SN data, but the period analysis has not revealed any significant periods.

Taken together, given that there is only rather vague evidence of the long-term photometric evolution of 2MASS J01093484-0800329 which is expected for an object in a symbiotic nova outburst, and the lack of the observational proof for a presence of a giant star (necessary to confirm an object as a symbiotic binary), we do not classify this star as a symbiotic nova for now. It seems more probably that the emission lines observed in the source are from a planetary nebula or that the object is a cataclysmic variable. Further high-resolution spectroscopic observations and long-term photometry might provide hints about the nature of the object.

3.3.3 2MASS J06422218-0226285

The outburst of the object, discovered by Blex et al. (2018), started between the end of 2012 and early 2014. The authors suggested that the object might be a possible cataclysmic variable, symbiotic binary, or a FUor or EXor type young stellar object. They favored an outbursting young stellar object due to the color properties. The object was previously classified as a planetary nebula candidate (Viironen et al. 2009).

The pre-outburst SED of the object (Fig. 3.8B) seems to support the presence of the source with $T_{\mathrm{eff}} \sim 6\,000\,\mathrm{K}$, hotter than in typical symbiotic binaries. The significant infrared excess is well visible. Such a SED is quite typical for young pre-main sequence stars (see, e.g., Schütz et al. 2005; Cruz-Sáenz de Miera et al. 2022) in which the excess is caused by the dust emission. The evolution of the SED of 2MASS J06422218-0226285 throughout its outburst (see the comparison of the pre-outburst and outburst SED in Fig. 3 in Blex et al. 2018) is similar to the behavior observed in outbursting young stellar objects (see, e.g., Miller et al. 2011; Hillenbrand et al. 2018) while during the symbiotic outbursts, the stars become significantly bluer.

The spectroscopic data for this source were not obtained in this thesis, given its

faintness. The object is located in the region of giants stars in the *Gaia* HR diagram (Fig. 3.5), but the same location is also shared by some of the young stellar objects (see Marton et al. 2022). Also, the position in the IR color-color diagram (Fig. 3.6) supports the classification of the star as a young stellar object if it is compared with the sample of Marton et al. (2022).

The light curve of the source, constructed on the basis of the observations from Blex et al. (2018) and the ZTF survey, is shown in Fig. 3.9B. These data confirm that the outburst is still ongoing and the object has currently a magnitude of about 16 mag in g filter. The amplitude of the outburst was around 3 mag in this band. Such behavior is often seen in symbiotic novae but also in young stellar objects. Taken together with the colors of the object, its position in the HR diagram, and the evolution of its SED throughout the outburst, we prefer the young stellar object over the symbiotic nova classification.

3.3.4 TYC 1371-69-1

This object was classified as a possible symbiotic star by Tang et al. (2012). They analyzed the photometric data from the DASCH archive (also shown in Fig. 3.9C) and discovered the nova-like outburst of the system which started in 1942 and had an amplitude of 1.5 mag in the B band. The decrease back to the pre-outburst brightness continued from 1943 to the 1950s. Tang et al. (2012) obtained also the spectroscopic data which allowed them to classify the cool component as an M0 III giant. Based on the radial velocities of the giant, they suggested that the second component is most likely the 0.6 $M_\odot$ white dwarf on the 119 days orbit. Their spectra did not show any emission lines in the optical.

Our spectra (Fig. 3.7C) showed the presence of a giant with a slightly later spectral type (M2 III). No emission lines are seen in the optical region. In reality, neither the optical spectrum nor the SED of the object (Fig. 3.8C) is different from a single M2 giant, therefore TYC 1371-69-1 is not a shell-burning symbiotic star. It shares the position in the *Gaia* HR diagram (Fig. 3.5) and NIR color-color diagram (Fig. 3.6) with known symbiotic stars, but those parts of the diagrams are also occupied by the single red giants.

Our analysis of the photometric data from the ASAS-SN survey revealed a variability with the period of 59.43 days (Fig. 3.9D) that is exactly the half of the spectroscopic period detected by Tang et al. (2012) in the radial velocities of the giant.

That strongly suggests that the red giant is tidally-distorted and that the photometric variability is due to the ellipsoidal effect (see also Chapter 1.4.2).

TYC 1371-69-1 in its present state cannot be classified as a genuine symbiotic star. On the other hand, Tang et al. (2012) provided strong evidence that the system is consisting of a red giant and a white dwarf and that the red giant is close to filling its Roche-lobe. They calculated the Roche-lobe filling factor of ~ 0.7 for an M0 III giant. Our data suggest that the giant is of a slightly later spectral type (M2) and therefore can have a larger radius and consequently larger Roche-lobe filling factor. The mass accretion can significantly increase in the scope of the cool component evolution, and the system can become a normal persistent symbiotic binary in the future.

In the present state, it can be classified as a pre-symbiotic binary (see Chapter 2.6). As the system showed an outburst in past, it can also be categorized as a 'transient' symbiotic star, in accordance with the proposal of Iłkiewicz et al. (2022). If the outburst observed in the 1940s was an outburst of a symbiotic nova, TYC 1371-69-1 is an example of the post-symbiotic nova system in which the red giant is not capable of fueling the shell-burning on the surface of the white dwarf for a prolonged period (Chapter 2.6). On the other hand, the duration of the outburst is shorter than in the case of typical symbiotic nova outbursts. Especially, given the anti-correlation between the mass of the white dwarf and the outburst timescale, one would expect a much longer duration of the outburst for a 0.6 $M_{\odot}$ white dwarf (see Fig. 6 in Mikołajewska 2010).

3.3.5 ASAS J174600-2321.3

This object was initially suspected to be an R CrB-type star (Tisserand et al. 2008, 2013), but rejected based on the spectroscopic observations, especially due to high abundance of the hydrogen. Later, the rich observational material was analyzed by Hümmerich et al. (2015), and they suggested that this target might be an eclipsing symbiotic nova detected in a long-lasting outburst. Using the eclipses, Hambsch et al. (2015) derived the orbital period of the system to be 1012.4 days. The cool component is probably a late-M giant ($\sim$ M7). The optical spectrum obtained in 2012 exhibited the spectral features of an early F-type supergiant and Hα in emission (Hümmerich et al. 2015).

Our optical spectrum of ASAS J174600-2321.3 (Fig. 3.7D) shows the continuum shape of an F-type star, Hα and Hβ in emission and mild TiO bands at the longer

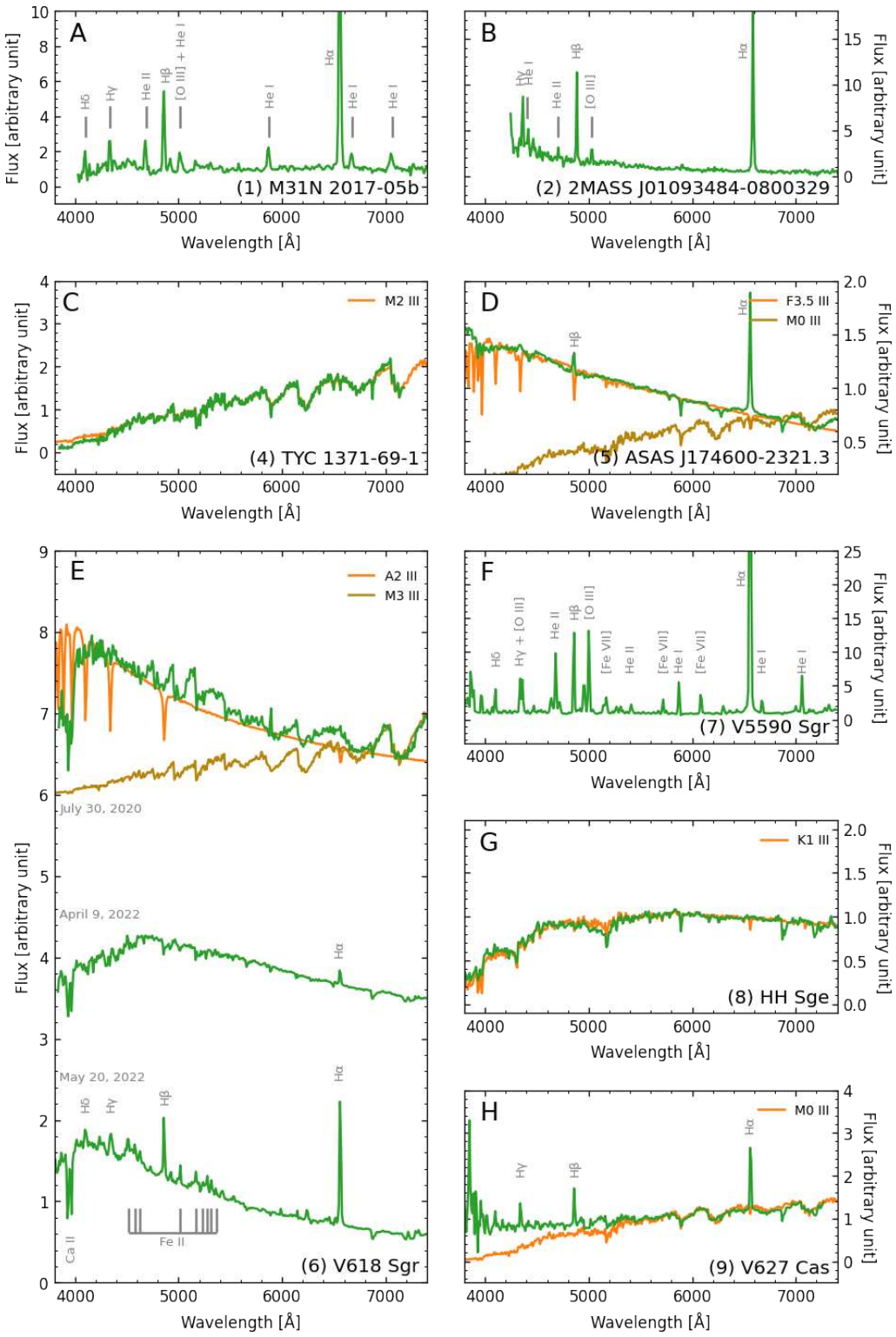

Figure 3.7: Spectra of the studied symbiotic nova candidates. The spectra obtained in the scope of our campaign and the best-fitting empirical spectra (Falcón-Barroso et al. 2011; Kesseli et al. 2017) are shown in green and orange, respectively. In panel D and E, the spectra of the cool components that contribute especially at the longer wavelengths are shown in brown. The identification of the most prominent emission lines in the particular spectra is depicted. All spectra were de-reddened by the $E_{(\mathrm{B-V})}$ values listed in Table 3.4 using the reddening law of Cardelli et al. (1989) and adopting the total to selective absorption ratio $R = 3.1$.

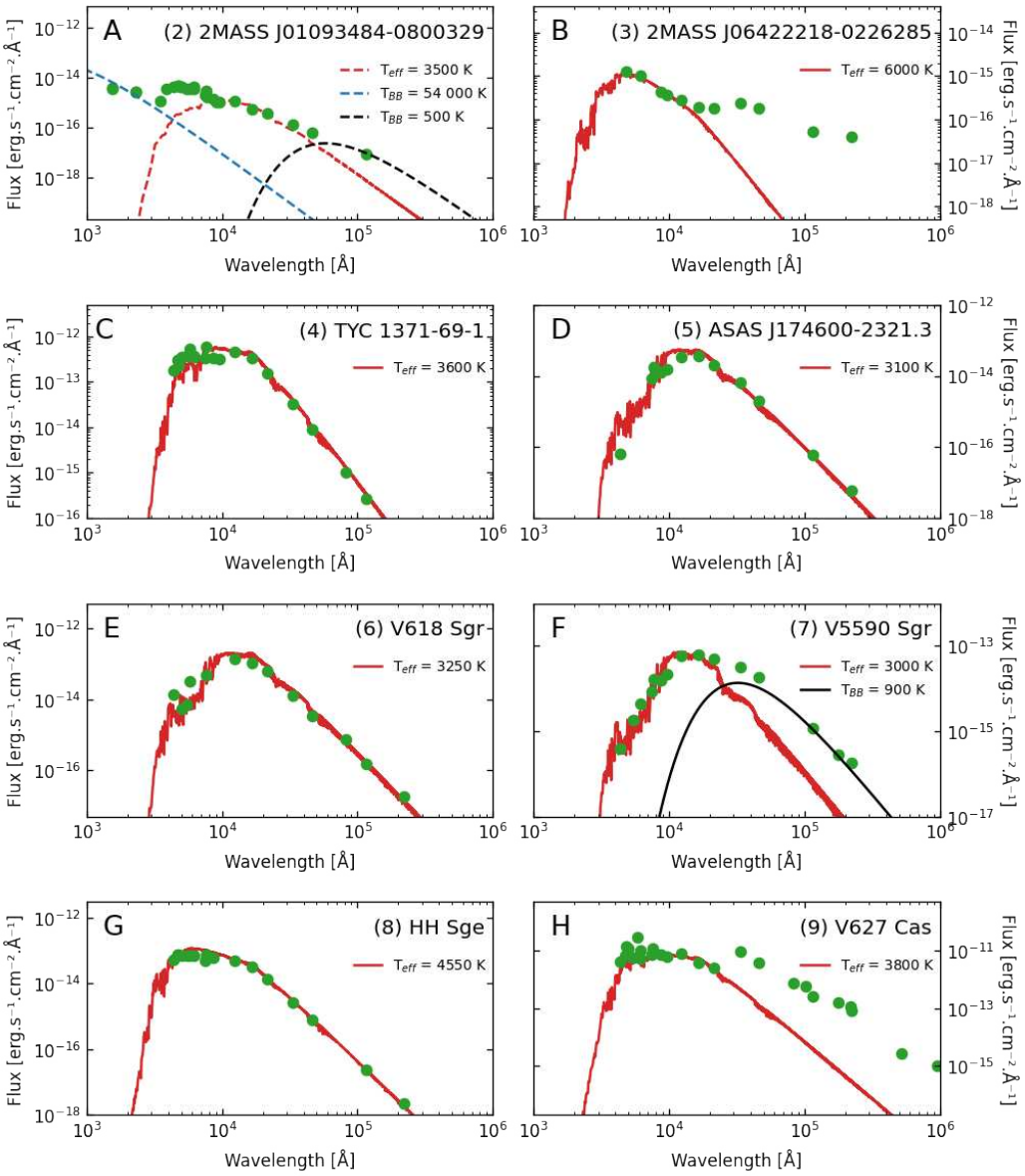

Figure 3.8: Multi-frequency SEDs of the studied symbiotic nova candidates. Measurements from *GALEX*, SkyMapper, APASS, *Gaia* EDR3, 2MASS, *AKARI*, and *WISE* are shown in green. The best fitting theoretical spectra (Allard 2014) are plotted in red. In panel A, the parameters of the assumed components are not well constrained and the model is only approximate. In the case of V5590 Sgr (panel F), the excess in IR presumably caused by a dust is modeled by the black-body (shown in black). The fluxes were de-reddened by $E_{(\mathrm{B-V})}$ values listed in Table 3.4 using reddening law of Cardelli et al. (1989) and adopting the total to selective absorption ratio $R = 3.1$.

wavelengths. That is matching the spectral appearance of the symbiotic nova after maximum (e.g., Munari 2019). Hβ was previously not seen in the spectra, confirming the slow evolution of the system. The spectral type of the red giant cannot be well constrained from the optical spectrum itself.

The pre-outburst SED of the source (Fig. 3.8D) suggests the presence of the cool source with a temperature of 3 100 K which is very well consistent with a spectral type M7 (van Belle et al. 1999) in accordance with the results of Hümmerich et al. (2015). Under the assumption that the pre-outburst brightness of ASAS J174600-2321.3 in V filter was mainly due to the cool component radiation and adopting the distance estimate of 7.6 kpc (Bailer-Jones et al. 2021), we can estimate the absolute magnitude of the star (V = -0.4 mag) that is consistent with the luminosity class III classification of the cool component in ASAS J174600-2321.3.

In the *Gaia* HR diagram (Fig. 3.5), the star is located at the blue end of the region occupied by symbiotic stars which is understandable as the *Gaia* data were acquired during the outburst of the system when it became bluer. Its position in the NIR color-color diagram (Fig. 3.6) supports the symbiotic classification. It also satisfies the IR criteria of Akras et al. (2019b, 2021), and is classified as a symbiotic system in all seven classification trees.

The light curve of ASAS J174600-2321.3 showing the brightness evolution of the system since the outburst started in 1998 is depicted in Fig. 3.9E. The rise to the maximum was rather slow, it took almost 5 years. The amplitude of the outburst was about 4.2 mag in the V filter. Such an evolution is typical for a symbiotic novae (Chapter 1.4). ASAS J174600-2321.3 is an eclipsing binary and the eclipses became more prominent during the outburst as the contribution of the hot component to the radiation in V is much more significant during such a brightening. The part of the phased light curve showing the eclipses detected while the system was in outburst is shown in Fig. 3.9F. In addition to eclipses, the period analysis of the recent ASAS-SN V and g light curves revealed the possible periods in the range of 40 – 50 days, which might be due to pulsations of the cool component. A similar value (56 days) was inferred by Hümmerich et al. (2015) from the pre-outburst EROS-2 data, while they obtained the period in the range of 80 – 90 days from the ASAS data.

To conclude, our observational data support the suggestion of Hümmerich et al. (2015) that ASAS J174600-2321.3 is an eclipsing symbiotic nova in outburst.

3.3.6 V618 Sgr

On the basis of the photometric light curve (its reconstruction from the textual description is showed in Fig. 3.9G), the object was initially classified as an R CrB variable (Swope & Shapley 1940). Spectrum covering the spectral region of 3 500 - 5 500 Å, presented by Kilkenny (1989), showed several emission lines (especially the Balmer lines of hydrogen and singly ionized iron). Due to this spectral appearance, Kilkenny contradicted the R CrB classification and suggested the symbiotic nature. On the other hand, the emission lines with higher ionization potential (e.g., He II) were missing in the observed spectrum and singly ionized helium lines were absent (or at least very weak).

Initially, we have included this object among the classical symbiotic candidates. However, the recent light curve of the system (Fig. 3.9H) showed an outburst similar to ones observed in symbiotic novae. The rise to maximal brightness took about 1.5 years and the outburst had an approximate amplitude of 5 mag in V. The star is at its maximal brightness since 2019 until now. On two occasions, significant drops in brightness have been recorded, which we attribute to the eclipses of the component in outburst.

It is very interesting to compare the recent light curve with the photometric evolution observed by Swope & Shapley (1940) and interpreted as R CrB behavior. Since no light curve was published in the paper, as mentioned above, we have reconstructed it based on the textual description (Fig. 3.9G). V618 Sgr showed two brightenings in the period of 1889 – 1933. During the latter period of increased brightness, three minima were observed which were repeated at the interval of $\sim$ 700 days. This is exactly the same period that we inferred for the eclipses observed in the recent light curve (703 days). Such an orbital period is typical for S-type symbiotic stars (see Chapter 2.3). The symbiotic classification of the source is also supported by its position in the *Gaia* HR (Fig. 3.5) and NIR color-color diagrams (Fig. 3.6) as well as by the IR criteria and classification trees of Akras et al. (2019b, 2021).

We have acquired several optical spectra of V618 Sgr in the scope of our observational campaign. By chance, the first spectrum of the object was obtained during the eclipse of the system in 2020. In the spectrum (top part of Fig. 3.7E), the presence of the red giant is well visible due to prominent TiO bands. The late-type spectral classification is confirmed by the analysis of the SED of V618 Sgr (Fig. 3.8E) constructed on the basis of pre-outburst observations. It is consistent with a cool star

with temperature $T_{\rm eff} \sim 3\,250\,{\rm K}$ ($\sim$M6 giant; van Belle et al. 1999).

Outside the eclipse, V618 Sgr has the spectroscopic appearance of a typical symbiotic nova after the optical maximum. Until middle May 2022, the spectrum showed the continuum shape of an A-F type star (typical for symbiotic novae in outbursts; Munari 2019). Only Hα was seen in emission (Fig. 3.7E, middle part). The continuation of our monitoring revealed the change in the spectral appearance that happened in May 2022 (Fig. 3.7E, bottom part). Several emission lines appeared in the spectrum (prominent Balmer lines of H I, Fe II lines). That would suggest that the symbiotic nova is slowly entering the nebular phase (see Fig. 6.5 in Munari 2019).

The data analyzed in this thesis confirms the symbiotic nova classification of V618 Sgr. This makes the object very interesting because it was already observed at least in two outbursts in past. This ultimately makes V618 Sgr the first (and only, for now) galactic recurrent 'slow' symbiotic nova (not to confuse with symbiotic recurrent novae, see Chapter 1.4). The only comparable object might be a symbiotic star LMC S154 located in the Large Magellanic Cloud. Iłkiewicz et al. (2019b) suggested that this system has experienced at least one, but more probably two or three symbiotic nova outbursts in past. However, the evidence of multiple outbursts is not as clear as in the case of V618 Sgr. Moreover, outbursts of LMC S154 might have been more similar to the ones of symbiotic recurrent novae, not 'slow' symbiotic novae.

Finally, the relatively short recurrence time of outbursts of V618 Sgr suggests that the white dwarf in this system might be quite massive (e.g., Nomoto et al. 2007; Wolf et al. 2013). Therefore, it would be interesting to follow the evolution of the system in the next years/decades, as it could be faster in comparison with typical 'slow' symbiotic novae. That makes V618 Sgr a good testbed for the study of the nova outbursts.

3.3.7 V5590 Sgr

The brightening of this object was discovered by T. Kojima from Japan and first noted in April 2012 (Nakano et al. 2012). Later it was confirmed that the object was already bright since July 2010 (Walter et al. 2012; Mróz et al. 2014). The progenitor is a Mira variable with a pulsation period of 236 days (Mróz et al. 2014). Based on the shape of the light curve and presence of the Mira pulsator, Mróz et al. suggested possible D-type symbiotic nova classification.

The data analyzed in this study support the symbiotic nova classification of

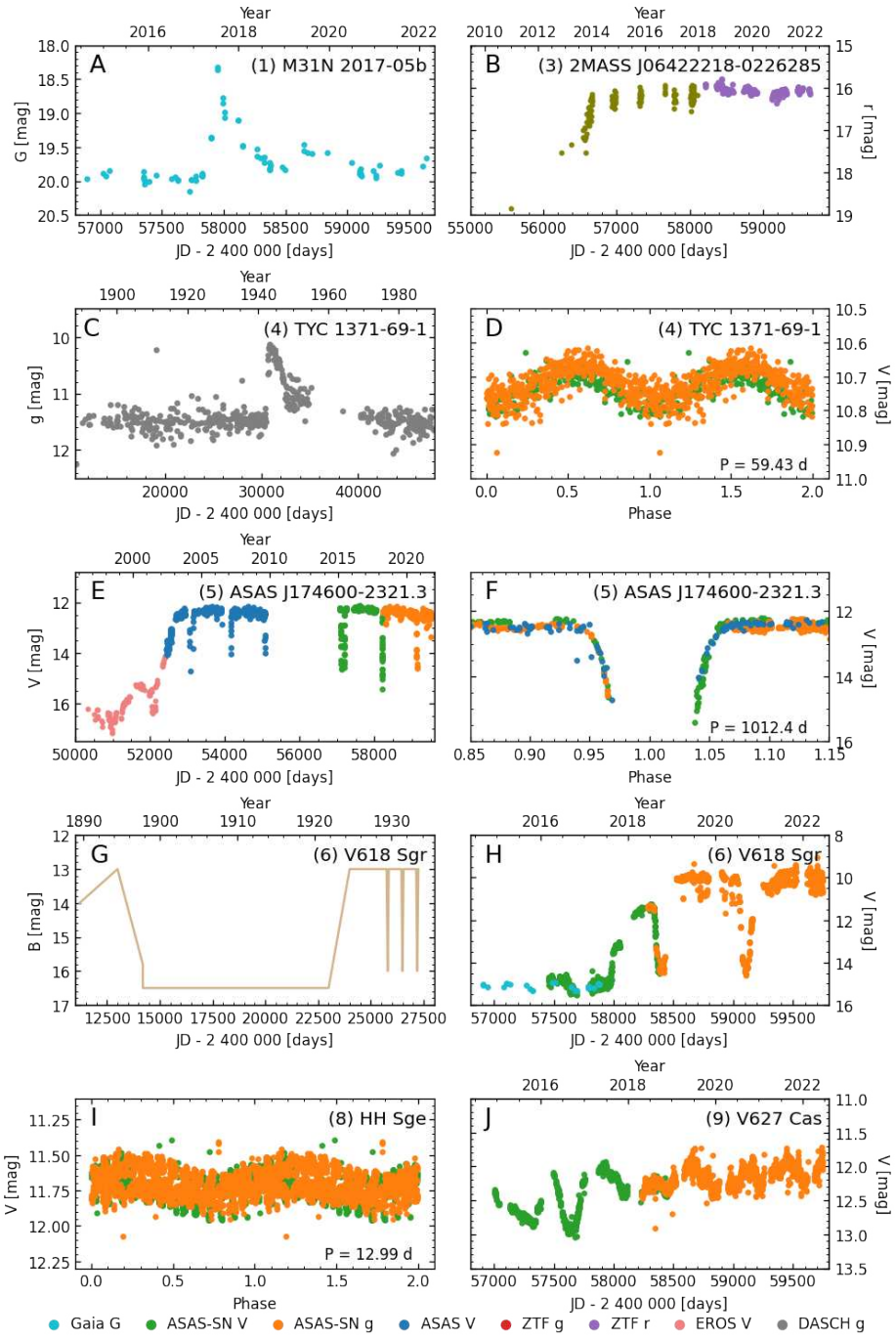

Figure 3.9: Light curves of the studied symbiotic nova candidates. **A**: *Gaia G* light curve of M31N 2017-05b. **B**: Light curve of 2MASS J06422218-0226285 in r filter constructed on the basis of data from Blex et al. (2018) and ZTF. **C**: Light curve of TYC 1371-69-1 from the DASCH archive (Laycock et al. 2010). **D**: Light curves of TYC 1371-69-1 phased with the period of 59.43 days. The g light curve was shifted by -0.75 mag to the level of V magnitudes for clarity. **E**: Light curve of ASAS J174600-2321.3. Data in the g filter were shifted by -0.55 mag to the level of V ones. EROS V light curves are as reported by Hümmerich et al. (2015). **F**: Part of the phased light curve of ASAS J174600-2321.3 showing its eclipses. **G**: Reconstruction of the light curve of V618 Sgr based on the textual description in Swope & Shapley (1940). **H**: Recent part of the V618 Sgr light curve. Data in the g filter were shifted by -0.1 mag to the level of V ones. The shift of +2.2 mag was applied to the *Gaia G* data. **I**: Light curves of HH Sge phased with the period of 12.99 days. Data in g were shifted by -0.4 mag to the level of V magnitudes. **J**: ASAS-SN light curves of V627 Cas showing irregular variability. The g light curve was shifted by -1.4 mag to the level of V magnitudes.

V5590 Sgr. Its symbiotic nova outburst had an amplitude of < 3 mag and ~ 6 mag in I and V band, respectively (Mróz et al. 2014). The brightness of the system is still declining according to recent ASAS-SN data, at the rate of about $0.2\,\mathrm{mag\,yr^{-1}}$.

In the *Gaia* HR diagram (Fig. 3.5), the object is slightly bluer than most symbiotic stars. However, one should keep in mind that *Gaia* observations were carried out when the star was already in the outburst. The position of the object in the NIR color-color diagram supports the D-type classification (Fig. 3.6). Our spectroscopic observations (Fig. 3.7F) are well consistent with a symbiotic nova in the nebular phase. Many strong emission lines, including Balmer lines of H I, He I, [O III], and highly ionized He II and [Fe VII] are visible.

The presence of the red giant is not visible in the optical spectrum (which is usual for D-type systems; Fig. 1.3), but is confirmed by the Mira pulsations and the pre-outburst SED (Fig. 3.8F). Infrared excess caused by the dust typical in D-type systems is well visible in the SED.

3.3.8 HH Sge

The object was mentioned as a symbiotic nova in the conclusion section of the paper by Yudin (1987). Although this was a clear mistyping of the name of another symbiotic nova, HM Sge, we have included the object to our list to confirm its non-symbiotic nature, as it is classified as a long-period variable in the literature. Such photometric behavior is typical for many of the known symbiotic stars.

Both the obtained spectra of this target (Fig. 3.7G) and its multi-frequency SED (Fig. 3.8G) are consistent with a single K-type star. The spectral type K1 III was obtained from the optical spectrum, the temperature corresponding to the spectral type K2 (van Belle et al. 1999) from the fit of the SED. No emission lines are seen in the optical spectrum and no UV excess is visible contradicting the possible symbiotic nature. The position of the star in the *Gaia* HR (Fig. 3.5) and NIR color-color diagram (Fig. 3.6) is also consistent with single K-type giant/subgiant. The period analysis of the ASAS-SN light curves of HH Sge revealed a variability with the period of 13 days which might be due to pulsations (Fig. 3.9I).

3.3.9 V627 Cas

The object was initially included in the catalog of young stars by Herbig & Kameswara Rao (1972). However, Gahm et al. (1975) did not detect any features typical for T Tau

stars in the spectrum and claimed that the spectrum has a well-defined molecular structure, especially TiO bands typical for red giants. Bergner et al. (1988) suggested that the object is consisting of a red giant (or supergiant) and a hot companion. Possible symbiotic nature was later suggested by Kolotilov (1988) based on the light curve showing a decrease similar to the one after a symbiotic nova-like outburst. According to Kolotilov et al. (1996), the cool component of the system might be a post-AGB cool giant. They also reported the presence of pulsations with a period of $\approx$ 466 days. The search for the short-term variability of V627 Cas by Gromadzki et al. (2006) revealed a short-lasting, flare-like brightening in the B band.

V627 Cas is placed among the most luminous objects in the *Gaia* HR diagram (see Fig. 3.5). Assuming the distance value of 6.25 kpc (Bailer-Jones et al. 2021), excess $E_{\mathrm{B-V}} = 2.15$ mag (Schlafly & Finkbeiner 2011), and brightness in V of 12.5 mag (Henden et al. 2015), it is possible to calculate the absolute V magnitude of $\sim$-8 mag. Such a value would place V627 Cas among the stars of the luminosity class Ia (Sung et al. 2013). That would exclude the possible symbiotic classification of this source and also the post-AGB nature of the giant (which are less luminous; e.g., van Winckel 2003; Kamath et al. 2022). If the distance estimate is correct, V627 Cas would be a supergiant star evolving from a more massive progenitor than the typical symbiotic or post-AGB giants.

The optical spectra of V627 Cas (Fig. 3.7H) revealed the emission lines of H I. The continuum shows mild TiO bands typical for late-type stars. The excess in blue is seen when the spectra are corrected for the extinction suggesting the presence of a secondary (hotter) component. The SED of V627 Cas (Fig. 3.8H) confirms the presence of a cool star with $T_{\mathrm{eff}} \sim 3\,800$ K (corresponding to the spectral type M2; van Belle et al. 1999). The infrared part of the SED revealed a significant excess. The recent light curves of V627 Cas from the ASAS-SN survey (Fig. 3.9J) show the irregular variability on the timescale of 400 – 450 days. In addition, the g light curve shows also some changes with a shorter period of about 260 days.

To sum up, the observations suggest that V627 Cas is a binary system. It cannot be classified as a shell-burning symbiotic star due to the lack of highly ionized emission lines, but an accreting-only system cannot be ruled out. In such a case, this object might be another example of a post-symbiotic nova in which the giant was not transferring sufficient mass to the accretor to supply the shell-burning. As a consequence, the system returned to an accreting-only state (see also Chapter 2.6).

V627 Cas shows a significant infrared excess. The infrared emission of the dust is

typically seen in D-type symbiotic binaries whose cool components are Mira pulsators. The photometric variability does not support the presence of the Mira pulsator, moreover, the inferred spectral type is much earlier than those of typical symbiotic Miras (M7-8; Chapter 2.4). Instead, the cool component might be a post-AGB star as suggested by Kolotilov et al. (1996) that often shows strong infrared excesses in their SEDs (van Winckel 2003; Kamath et al. 2015).

In such a case, the brightness decrease reported by Kolotilov (1988) and suggested to be due to the nova-like outburst might have been the consequence of the evolution of the cool component. The secondary component might then be different from the white dwarf (e.g., could be a main-sequence star) which would exclude the symbiotic classification of V627 Cas. In any case, it would be interesting to follow up on this object in the future. The radial velocity measurements might provide some further clues on the secondary component of V627 Cas.

3.4 Possible symbiotic stars in the Large Magellanic Cloud

In the current version of the New Online Database of Symbiotic Variables, 10 confirmed symbiotic stars located in the Large Magellanic Cloud are listed (Chapter 2). The systems located in the Magellanic Clouds are important for understanding the symbiotic phenomenon, especially for two main reasons. They are bright enough to be photometrically studied using small telescopes and they evolved in an environment with different chemistry (lower average metallicity) in comparison with the systems in the Milky Way. To increase the size of the sample of known symbiotic stars in the Large Magellanic Cloud, we have decided to study all 27 symbiotic candidates located in this galaxy (Table 3.5).

Given the fact that relatively precise distance to these candidates can be estimated from the distance to their host galaxy, we have adopted a slightly different approach to their study than in the case of galactic symbiotic candidates (Chapter 3.2 and 3.3). Moreover, virtually all the candidates show emission lines in their optical spectra, therefore we have employed also additional diagnostics to distinguish between symbiotic stars and mimics.

In the first step, the optical spectra of the candidate systems (available for 24 out of 27 objects) were studied (Fig. 3.10). We especially searched for the late-type

Table 3.5: List of symbiotic candidates in the Large Magellanic Cloud analyzed in this thesis. The last column gives the reference to the study, in which the object was first suspected of a symbiotic nature.

No.	Name	α_{2000} [h m s]	δ_{2000} [d m s]	Reference
1	SMP LMC 16	05 02 02.143	-69 48 56.98	Iłkiewicz & Mikołajewska (2017)
2	[RP2006] 1459	05 08 13.324	-68 36 12.69	Reid & Parker (2012)
3	HV 13055	05 08 41.580	-66 49 00.26	Hodge & Wright (1970)
4	MGPN LMC 31	05 16 29.269	-68 18 11.91	Iłkiewicz & Mikołajewska (2017)
5	[RP2006] 1192	05 19 56.725	-70 39 04.11	Reid & Parker (2010)
6	[RP2006] 1434	05 20 16.858	-68 45 09.99	Reid & Parker (2010)
7	[RP2006] 803	05 24 09.910	-69 19 48.02	Reid (2014)
8	SMP LMC 63	05 25 26.014	-68 55 53.79	Iłkiewicz & Mikołajewska (2017)
9	[BE74] 583	05 26 50.159	-71 06 35.24	Morgan et al. (1992)
10	[RP2006] 2180	05 28 04.836	-68 59 47.03	Reid (2014)
11	[RP2006] 822	05 28 06.960	-69 14 28.57	Reid & Parker (2012)
12	2MASS J0531..	05 31 16.758	-69 01 04.03	Kamath et al. (2015)
13	[RP2006] 776	05 32 39.241	-69 31 53.82	Miszalski et al. (2011)
14	[RP2006] 774	05 32 39.696	-69 30 49.48	Miszalski et al. (2011)
15	[RP2006] 977	05 32 52.293	-67 41 09.22	Reid (2014)
16	[RP2006] 883	05 35 56.897	-69 00 44.96	Miszalski et al. (2011)
17	[RP2006] 490	05 37 31.518	-71 10 47.83	Reid & Parker (2010)
18	[RP2006] 227	05 37 46.812	-69 31 55.89	Reid (2014)
19	LM 2-39	05 40 14.811	-69 28 49.14	Miszalski et al. (2011)
20	2MASS J0542..	05 42 18.206	-69 52 49.39	Kamath et al. (2015)
21	[RP2006] 264	05 43 30.378	-69 24 46.58	Miszalski et al. (2011)
22	[RP2006] 254	05 43 37.771	-69 20 10.22	Reid (2014)
23	2MASS J0545..	05 45 00.162	-69 18 19.10	Kamath et al. (2015)
24	[RP2006] 295	05 48 22.322	-67 58 53.32	Reid (2014)
25	[RP2006] 129	05 48 28.318	-70 08 48.50	Reid & Parker (2006)
26	SMP LMC 93	05 49 38.850	-69 10 00.29	Iłkiewicz & Mikołajewska (2017)
27	RX J0550.0-7151	05 49 46.235	-71 49 35.83	Schmidtke & Cowley (1995)

absorption features in the red part of the spectrum (prominent TiO bands) to provide evidence of the cool giant in the objects. As an additional indication of the giant stars in the analyzed symbiotic candidates, we have studied their position in the IR color-magnitude diagram and compared it with the location of the known evolved stars in this diagram (Fig. 3.11). Such a diagnostic can be used only if the distance to the objects is known, which is the reason why we have not used a similar approach for galactic sources with imprecise distance estimates.

The infrared observations of the symbiotic candidates from the catalog of Kato et al. (2007) were employed to analyze their position in the IR color-color diagram (Fig. 3.12). The optical spectra have been used to identify the emission lines with the highest ionization potential and to construct the [O III] diagnostic diagram (Fig. 3.13) which is very useful to distinguish between the low-density planetary nebulae, medium-

density young planetary nebulae and symbiotic stars whose nebulae are very dense (Gutierrez-Moreno et al. 1995; Iłkiewicz & Mikołajewska 2017).

Finally, we have analyzed the light curves of the targets provided by the OGLE (Udalski et al. 2008) and MACHO surveys (Alcock et al. 1999), and by the *Gaia* satellite (Gaia Collaboration et al. 2022). We have also searched for the archival data published in the DASCH archive of digitized glass photographic plates of the Harvard College Observatory (Laycock et al. 2010). In total, 6 objects have data in the OGLE database, 10 stars in the MACHO survey, and 15 light curves have been published in *Gaia* DR3. The light curves of the selected symbiotic candidates are shown in Fig. 3.14. The results on the individual objects are summarized in the next section and in Table 3.6.

3.4.1 Notes on individual objects

HV 13055, 2MASS J05311676-6901041, [RP2006] 227, and [RP2006] 295
Four objects from the sample are classified as bona-fide symbiotic stars in this study.

HV 13055 has been classified as a possible symbiotic star by Hodge & Wright (1970) based on the similarity of its brightness variations and colors to known symbiotic stars. They suggested the presence of a possible periodicity of 682 ± 90 days in the light curve. Lindsay (1971) reported further observations of the star and suggested its possible brightening in the 1940s. The spectrum obtained by Feast & Webster (1974) revealed no TiO bands and only the emission lines of H I. Due to the low ionization, Allen (1980a) excluded the object from the list of symbiotic stars. We argue that the object is most probably a symbiotic system that might have been in the accreting-only state during the observations of Feast & Webster (1974). The position of the source in the IR color-magnitude diagram (Fig. 3.11) is consistent with the presence of a giant star. Infrared colors support the symbiotic classification (Fig. 3.12).

The most conclusive evidence about the symbiotic nature of the object comes from its light curves. The outburst which started around 1940 – 1941 is well visible in the historical light curve of HV 13055 (Fig. 3.14A). The OGLE data suggest that the object might have been in the outburst also more recently (see the decline in the I light curve in Fig. 3.14B). So far, outbursts have been undoubtedly detected only in three other extragalactic symbiotic stars (see, e.g., Iłkiewicz et al. 2019b, and references therein).

The period analysis of the V band light curve revealed the presence of the period

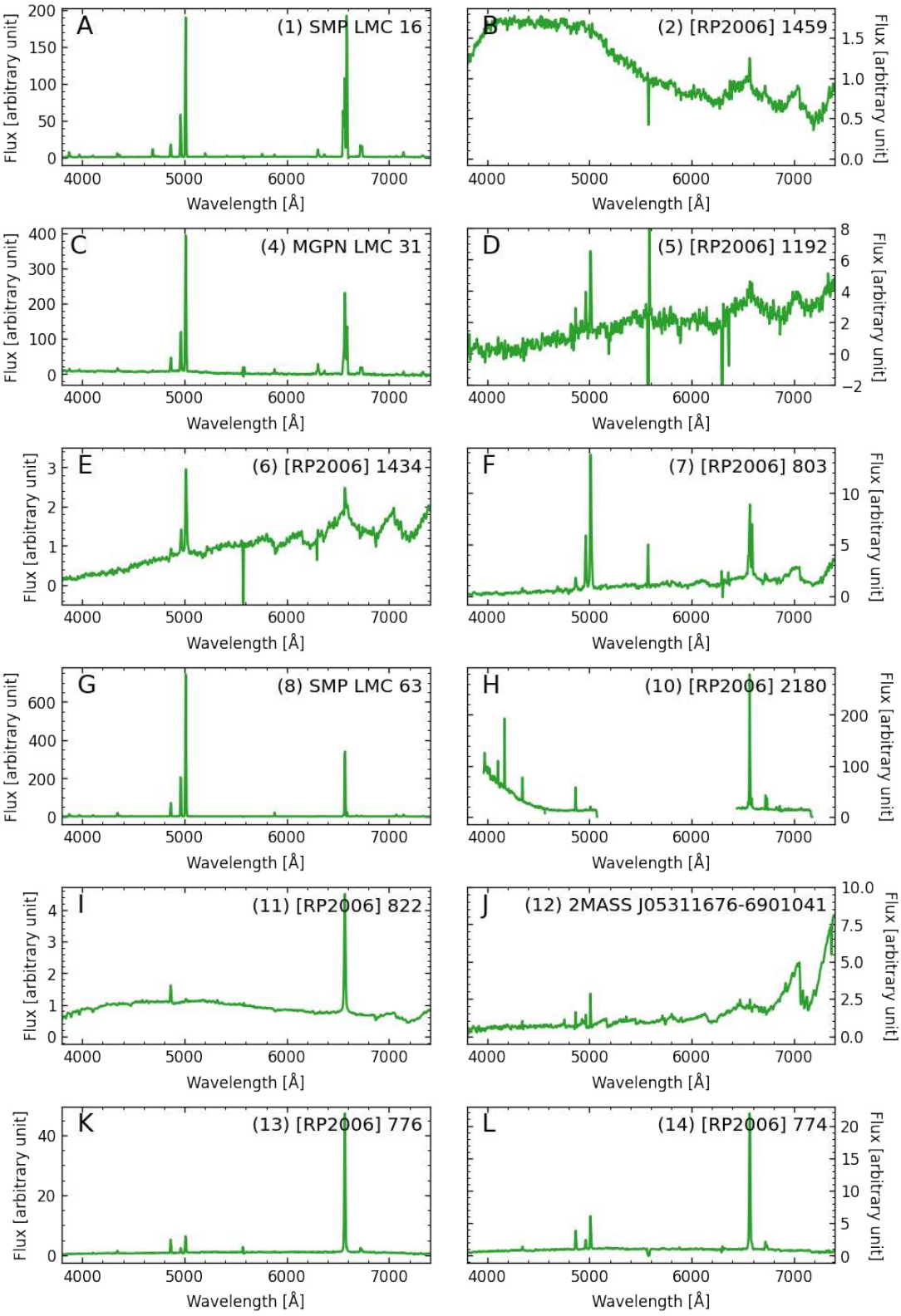

Figure 3.10: Spectra of the studied symbiotic candidates in the Large Magellanic Cloud.

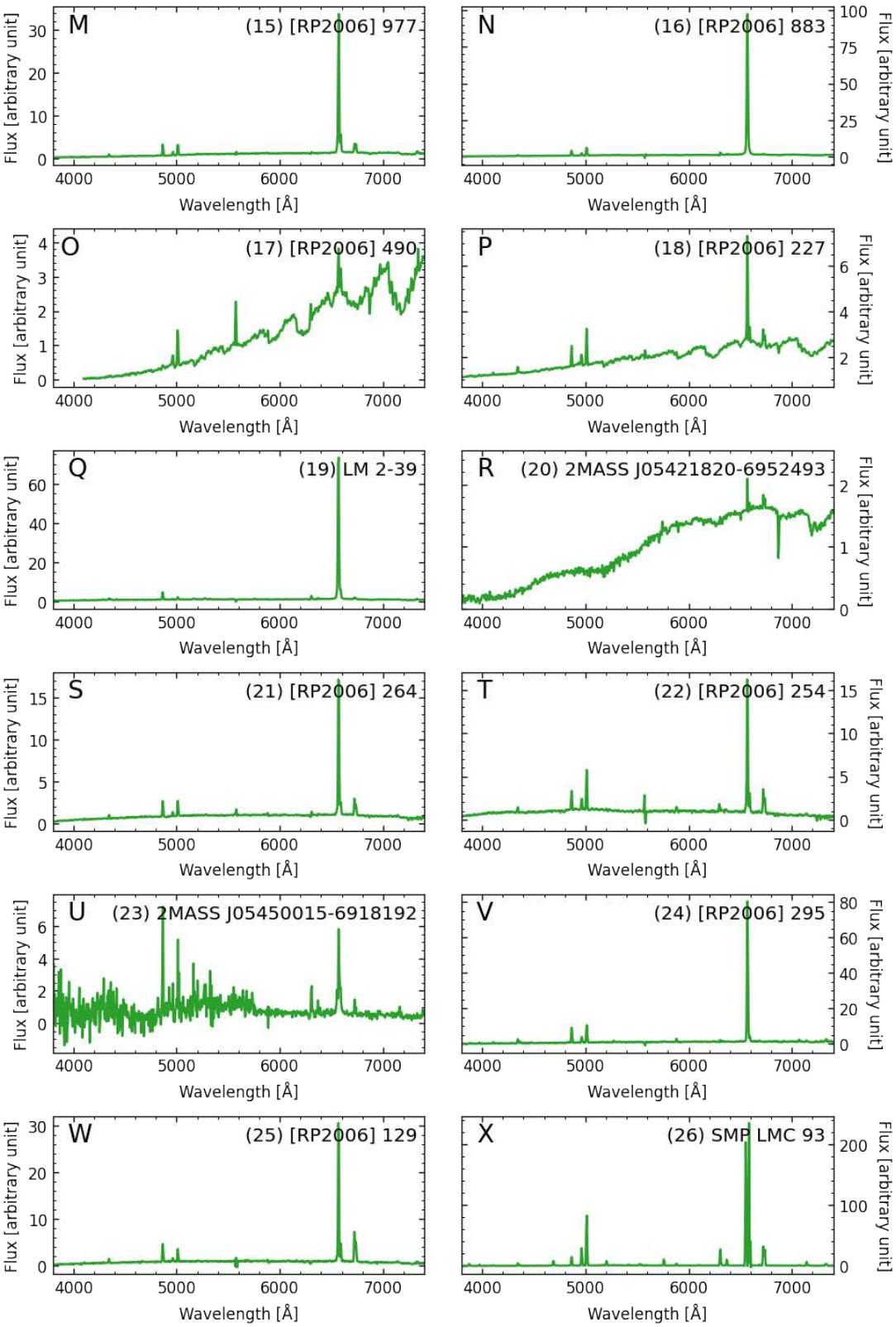

Figure 3.10: Continued.

of 661.9 days, in a good agreement with the value inferred by Hodge & Wright (1970) from very sparse observations. Interestingly, the I light curve of HV 13055 phased with this value of period shows two minima instead of one (Fig. 3.14C). This suggests that this is an orbital period of HV 13055 and that the ellipsoidal effect is responsible for the variability in the I filter (see Chapter 1.4.2). In addition, the possible pulsations of the cool component on the timescale of 40 – 60 days are detected in the I band. Both the orbital and pulsation period of HV 13055 is typical for S-type symbiotic stars (see Chapter 2.3 and 2.4).

2MASS J05311676-6901041 shows the continuum of a late-type giant (spectral type M4 suggested by the TiO indices of Kenyon & Fernandez-Castro 1987) and the emission lines of H I, He I, and [O III] (Fig. 3.10J). Hα is relatively faint suggesting that it might be an accreting-only system. The symbiotic classification is supported also by the position of the source in the IR color-magnitude diagram (Fig. 3.11), IR color-color diagram (Fig. 3.12), and [O III] diagram (Fig. 3.13), where the source is located among the symbiotic systems, but the ratio of [O III] 5006Å/Hβ is slightly higher than is typical for S-type symbiotic stars. The light curves of the object show variability with the period of 826.5 days which we attributed to the orbital period of the system (Fig. 3.14G), and with the period of 105.4 days, which is probably due to pulsations of the red giant (Fig. 3.14H).

The symbiotic nature of [RP2006] 227 is, similarly to the previous cases, supported by the optical spectrum showing late-type features (spectral type M1-2 suggested by the TiO indices of Kenyon & Fernandez-Castro 1987) and emission lines with ionization potential up to 35 eV ([O III]; Fig. 3.10P), the position in the IR color-magnitude diagram (Fig. 3.11), IR color-color diagram (Fig. 3.12), and [O III] diagram (Fig. 3.13). The star also exhibit the variability with the period of 484.7 days (attributed to the orbital motion; Fig. 3.14J) and 32 days (pulsations; Fig. 3.14K).

Finally, we classify [RP2006] 295 as a D-type symbiotic star. It does not show late-type features in the optical spectrum, but the presence of the red giant is supported by the IR color-magnitude diagram (Fig. 3.11), and the D-type symbiotic classification by the position of the star in IR color-color diagram (Fig. 3.12) and [O III] diagnostic diagram (Fig. 3.13). This object also shows the SED typical of D-type symbiotic stars. The light curve of [RP2006] 295 from the MACHO survey (Fig. 3.14L) shows a brightening which might be due to the outburst or due to the changes in the amount of the circumstellar dust in the line of sight.

[RP2006] 803, [BE74] 583, [RP2006] 883, and 2MASS J05450015-6918192
In the case of four additional candidates, there are several clues about their symbiotic nature, but definite confirmation requires further data.

[RP2006] 803 shows the continuum of a cool star (spectral type M2-4 suggested by the TiO indices of Kenyon & Fernandez-Castro 1987) and the emission lines with high ionization potential (including faint He II; Fig. 3.10F). The position of the source in the IR color-magnitude diagram (Fig. 3.11) and IR color-color diagram (Fig. 3.12) is consistent with the symbiotic classification. The light curves revealed the possible orbital variability (818.5 days; Fig. 3.14D) and pulsations (167.3 days; Fig. 3.14E). However, its position in the [O III] diagnostic diagram (Fig. 3.13) is typical for planetary nebulae with [O III] 5006 Å/Hβ being an order of magnitude higher than observed in symbiotic stars. In addition, [S II] 6717 Å/6731 Å $\sim$ 1.07 suggests a low-density environment (Osterbrock & Ferland 2006). It is possible, that the object is a symbiotic binary blended with an additional source of emission lines. However, further observations are needed to support this suggestion.

[BE74] 583 was suggested to be a symbiotic system by Morgan et al. (1992) who detected Hα, Hβ and possibly also He II 4686 Å superposed on the red stellar continuum of a G – K star. Both IR color-magnitude (Fig. 3.11) and color-color diagram (Fig. 3.12) support the possible symbiotic classification. The light curve of the system shows a clear variability with a period of 384.9 days (Fig. 3.14F). Interestingly, the light curve shows an alternation of two differently high maxima. Nevertheless, we do not have any optical spectrum of the star available, and therefore we classify the object only as a possible symbiotic star for now.

For [RP2006] 883, the available data suggest the possible D-type symbiotic classification. The position of the object in the IR color-magnitude diagram (Fig. 3.11) suggests the presence of a red giant in the system (not detected in the optical spectrum; Fig. 3.10N). Its position in the IR color-color diagram is consistent either with a reddened Be star or a D-type symbiotic star (Fig. 3.12). The position in the [O III] diagram (Fig. 3.13) is consistent with D-type classification as well. However, there is only a poor indication of possible pulsations in the MACHO $R_{\rm M}$ light curve of the system (with the suspicious period of 359 days), and no similar variability is detected in the broadband *Gaia* photometry. For this reason, [RP2006] 883 can be classified as a D-type symbiotic system only when the presence of the Mira pulsator would be verified, e.g., using the infrared time-series photometry.

2MASS J05450015-6918192 is another possible D-type symbiotic star. In the opti-

cal spectrum of the target (Fig. 3.10U), emission lines of Hα, [S II], [N II] are clearly visible. In the blue region, Hβ and [O III] lines are seen in emission and the [O III] diagram suggests the D-type classification. However, the S/N in this part of the spectrum is very low to be conclusive. The classification is also supported by the position of 2MASS J05450015-6918192 in the IR color-magnitude (Fig. 3.11) and color-color diagrams (Fig. 3.12). The *Gaia* light curves of the system show a long-term trend, but the data are not sufficient for any period analysis.

[RP2006] 977, [RP2006] 490, LM 2-39, 2MASS J05421820-6952493, and [RP2006] 264 These five sources show some characteristics of the symbiotic stars.

Optical spectra of two of these stars ([RP2006] 490, 2MASS J05421820-6952493) show the continuum of late-type giants (Fig. 3.10O, R) whose presence in the objects is supported also by the observed IR magnitudes (Fig. 3.12). Moreover, the light curves of [RP2006] 490 show the variability with the period of 32.3 days, which we attribute to the pulsations of the giant (Fig. 3.14I). The optical spectrum of [RP2006] 490 revealed the emission lines of H I, [O III] and [N II]. The ratio of [O III] 5006 Å/Hβ is much higher than observed in symbiotic stars and the position of the object in the [O III]/H I diagnostic diagram is at the border of planetary nebulae and young planetary nebulae. In 2MASS J05421820-6952493, relatively faint Hα is detected, together with [N II] and [S II] lines. The ratio of [S II] 6717 Å/6731 Å $\sim$ 1.02 suggests that the environment have a relatively low electron density of 10^2 – 10^3 cm^{-3} (Osterbrock & Ferland 2006).

[RP2006] 977 and [RP2006] 264 show continuum spectra which might be of K-type stars or of a reddened objects (Fig. 3.10M and S, respectively). Both are relatively bright in IR and in the IR color-color diagram (Fig. 3.12), they are located around the region of reddened Be stars, near the region of D-type symbiotic stars. Their position in the [O III] diagnostic diagram is at the border between S- and D-type symbiotic stars (Fig. 3.13). On the other hand, in any of these two targets, the variability has been detected expected for symbiotic Miras (D-type), and the ratios of [S II] 6717 Å/6731 Å (1.01 and 1.31, respectively) suggest in both cases very low electron density (Osterbrock & Ferland 2006). In both cases, the observations of *WISE* show the presence of diffuse emission in the part of the sky where these sources are located. Their SEDs are different from the typical D-type symbiotic star SED and resemble more the SEDs of H II regions (e.g., Stephens et al. 2014; Relaño et al. 2016).

The optical spectrum of LM 2-39 (Fig. 3.10Q) shows no continuum of the late-type star and emission lines typical for H II regions (e.g., Peimbert et al. 2017). Such

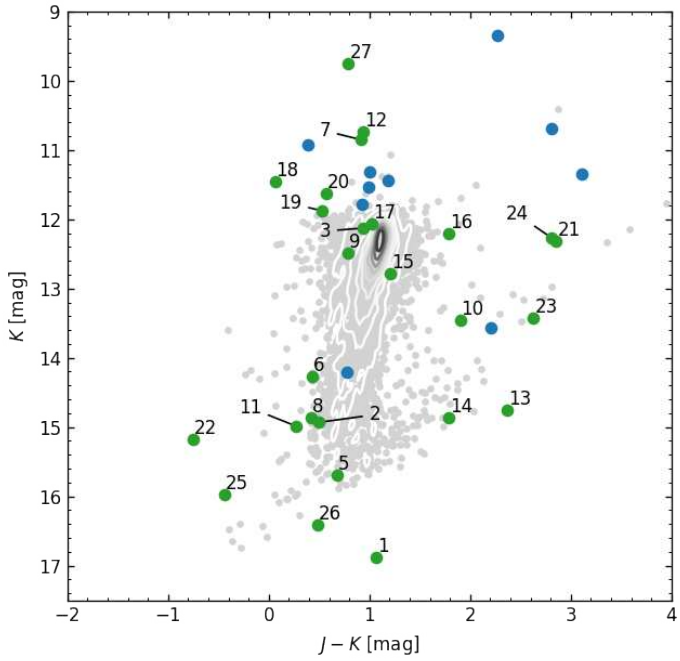

Figure 3.11: Position of the studied symbiotic candidates located in the Large Magellanic Cloud (green dots; labels are according to Table 3.5) in the IR color-magnitude diagram. The infrared magnitudes of the candidates are from Kato et al. (2007), and are corrected for the total galactic extinction taken from the dust map of Schlafly & Finkbeiner (2011). The positions of the known symbiotic stars in the Large Magellanic Cloud are shown in blue. The position of long-period variables from the Large Magellanic Cloud is shown in gray (Spano et al. 2011). The density map (gray lines) is over-plotted to guide the eye to the region in the diagram, where most of the long-period variables can be found.

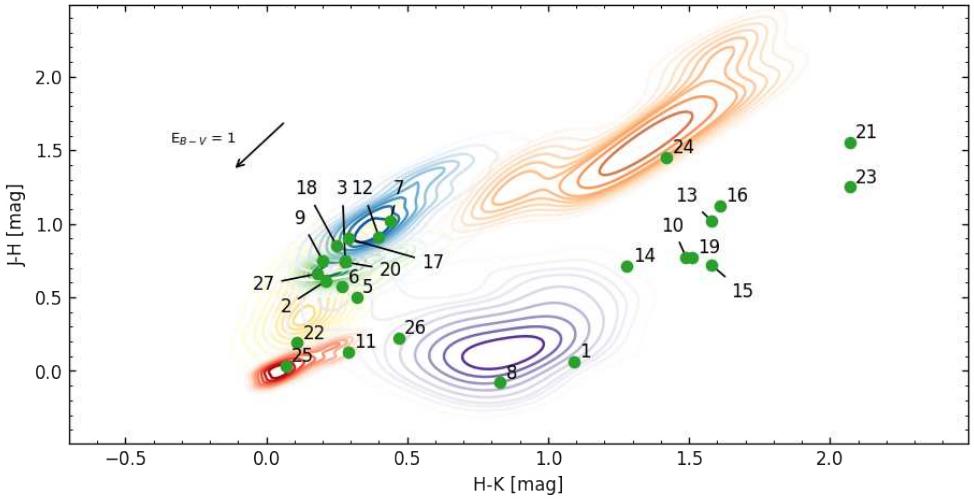

Figure 3.12: Position of the studied symbiotic candidates located in the Large Magellanic Cloud (green dots; labels are according to Table 3.5) in the near IR color-color diagram. The infrared magnitudes of the candidates are from Kato et al. (2007). The positions of the known S- and D-type symbiotic stars from the New Online Database of Symbiotic Variables are shown as density maps in blue and orange, respectively. Planetary nebulae (Ramos-Larios & Phillips 2005), Be stars (Zhang et al. 2005), T Tauri stars (Dahm & Simon 2005), and cataclysmic variables (Downes et al. 2001) are shown in violet, red, green and yellow, respectively.

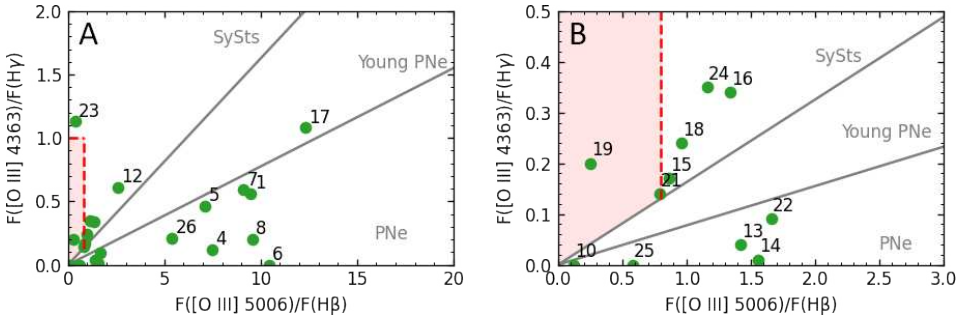

Figure 3.13: [O III] diagnostic diagram (Gutierrez-Moreno et al. 1995) for the symbiotic candidates located in the Large Magellanic Cloud (green dots; labels are according to Table 3.5). The red shaded zone indicate the region of S-type symbiotic stars (Iłkiewicz & Mikołajewska 2017). Panels A and B are the same with different axes ranges.

a classification is also supported by the SED of LM 2-39 showing an IR excess typical for H II regions. On the other hand, the position of the star in the IR color-magnitude diagram (Fig. 3.11) suggests the presence of the giant star and the MACHO $R_{\rm M}$ light curve of the system revealed the period of 360 days which might be a pulsation period of the assumed giant. However, the same period is not detected in the *Gaia* light curves of the object, and the value of close to one year leaves some doubts about the reality of such variability. If the giant is indeed present in this object, it might be just coincidentally located in the same direction as an H II region.

Taken together, these five objects cannot be readily classified as symbiotic stars. We suggest, that in reality, it might be, that the red giants in these objects are not physically connected with the environment in which the emission lines are created.

[RP2006] 1459, [RP2006] 1192, [RP2006] 1434, [RP2006] 2180, [RP2006] 822

We have classified five symbiotic candidates located in the Large Magellanic Cloud as non-symbiotic emission-line stars in this study (young stellar objects, Be stars, etc.). It is not excluded that some might be, similar to objects discussed previously, superpositions of cool stars and nebular environments.

The optical spectra of four objects ([RP2006] 1459, [RP2006] 1192, [RP2006] 1434, and [RP2006] 822) show TiO bands of an M star (Fig. 3.10B, D, E and I, respectively). In [RP2006] 1459 only the emission lines of H I and [S II] are seen. The object is relatively faint in IR and located in the region of T Tau stars in the IR color-color diagram (Fig. 3.12). In the case of [RP2006] 1192, one out of two spectra we have available shows TiO bands and relatively strong emission lines. The object is faint in IR, located in the region of T Tau stars in the IR color-color diagram (Fig. 3.12) and of planetary nebulae in the [O III] diagnostic diagram (Fig. 3.13). [RP2006] 1434

shows an M-type continuum, relatively faint Balmer lines, but strong [O III] lines that position it among planetary nebulae in the [O III] diagnostic diagram (Fig. 3.13). Its IR colors are similar to T Tau stars.

[RP2006] 2180 has a blue continuum with emission lines of H I, [N II], [S II], and faint [O III] (Fig. 3.10H). It is relatively faint in IR and in the IR color-color diagram (Fig. 3.13), it occupies the region where one can find reddened Be stars (see Fig. A2 in Miszalski et al. 2013) and a minority of planetary nebulae.

[RP2006] 822 might be a binary star consisting of a red giant and a hot main-sequence star. In addition to the continuum of the cool star, emission lines of Hα, $H\beta$, and faint [O III], the blue part of the spectrum shows excess and Balmer lines in absorption (Fig. 3.10I).

SMP LMC 16, MGPN LMC 31, SMP LMC 63, [RP2006] 776, [RP2006] 774, [RP2006] 254, [RP2006] 129, and SMP LMC 93 Eight objects from the sample are classified as planetary nebulae in this study.

While they all show emission lines with the ionization potential of at least 35 eV ([O III]; Fig. 3.10), there is no indication of the late-type star continuum in the optical spectra. The presence of the red giant is not supported by their faint infrared magnitudes (Fig. 3.11) and no variability is detected in those sources. They are not reported as variable stars in the OGLE and MACHO surveys even if they are located in the observed regions. The *Gaia* light curves of these objects do not show any period variability, only the scatter expected for the stars of this brightness. The non-variability of these objects (to the extent expected for symbiotic stars or red giants) is supported by the diagnostic index constructed from the *Gaia* flux errors using the method of Barlow et al. (2022). These objects occupy the region of planetary nebulae in both, the infrared color-color diagram (Fig. 3.12) and also in the diagnostic diagram employing fluxes of [O III] and Balmer lines (Fig. 3.13).

RX J0550.0-7151 This object was suspected to be a symbiotic system in the Large Magellanic Cloud by Schmidtke & Cowley (1995) based on the detection of the super-soft X-ray source coincident with a red star. Charles et al. (1996) reported that the spectrum of the object shows strong and narrow Balmer emission lines superposed on the cool star continuum. We should note that there is confusion about the position and the name of the object in the literature (see, e.g., Farias et al. 2020). The SIMBAD database gives a different position for this object than is reported in the

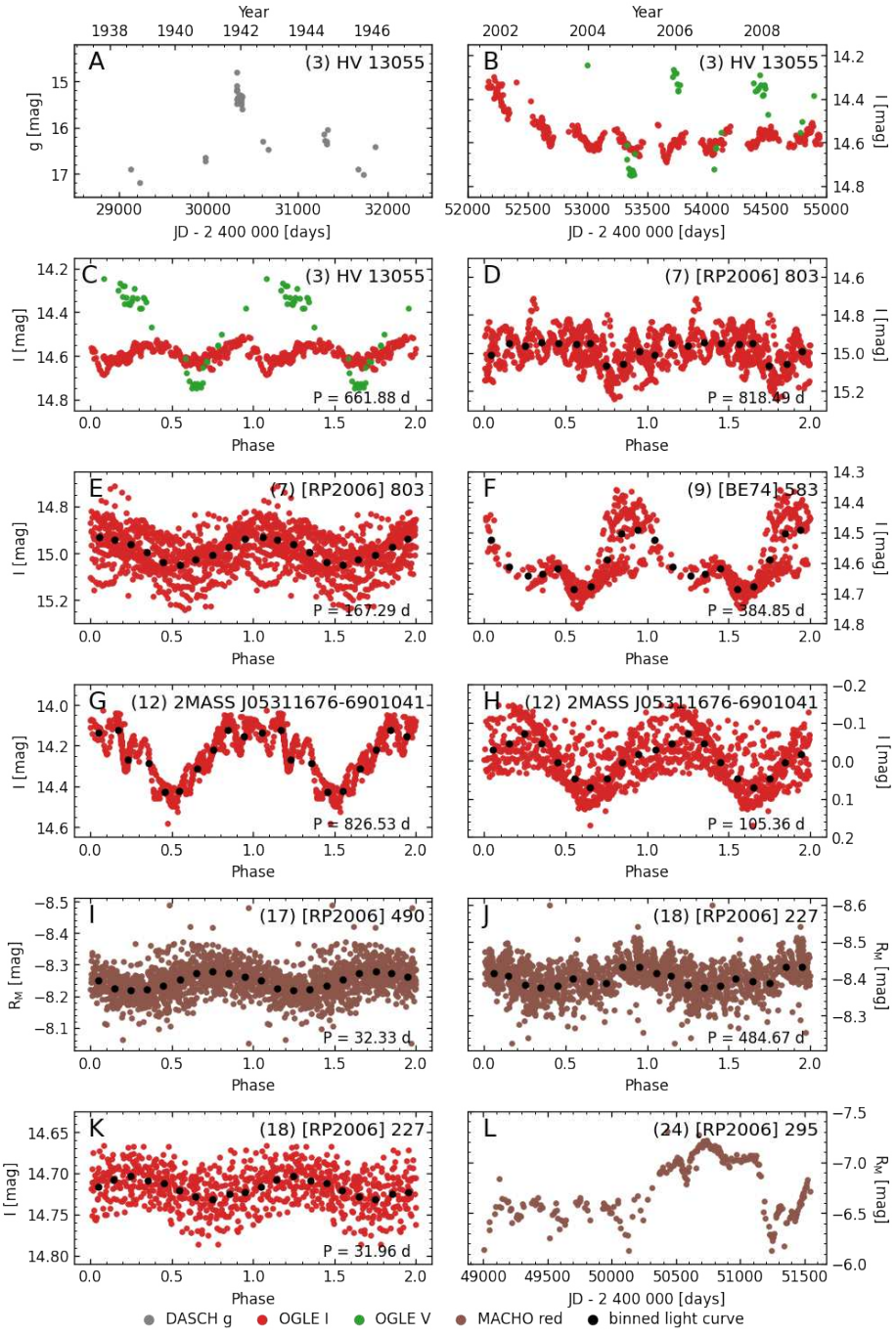

Figure 3.14: Light curves of the selected symbiotic candidates in the Large Magellanic Cloud. **A:** Historical light curve of HV 13055 from the DASCH archive showing the outburst of the system in the 1940s. **B:** Light curves of HV 13055 from OGLE survey in I and V filter. The V light curve was shifted by -1.85 mag to the level of I magnitudes for clarity. **C:** Phased light curves of HV 13055. The ellipsoidal effect is well visible. **D:** Light curve of [RP2006] 803 phased with the possible orbital period of 818.49 days. **E:** Light curve of [RP2006] 803 phased with the pulsation period of 167.29 days. **F:** Light curve of [BE74] 583 phased with the period of 384.85. Note the two maxima with different magnitudes. **G:** Light curve of 2MASS J05311676-6901041 phased with the assumed orbital period of the system (826.53 days). **H:** Light curve of 2MASS J05311676-6901041 phased with a period of 105.36 days (pulsation) after subtraction of orbital response. **I:** [RP2006] 490 light curve phased with a period of 32.33 days. The magnitudes are instrumental. **J:** Light curve of [RP2006] 227 phased with a period of 484.67 days. **K:** Light curve of [RP2006] 227 phased with a period of 31.96 days. **L:** Light curve of [RP2006] 295 in the MACHO red filter.

Table 3.6: Parameters used for classification of the symbiotic candidates in the Large Magellanic Cloud. The information on the emission lines with maximal ionization potential observed in the optical spectra, detection of TiO bands in the optical spectra, the possible presence of the red giant in the particular system according to IR magnitude-color diagram, classification suggested by IR color-color, and [O III]/H I diagram and variability of the objects are given in columns 2 – 7. In the last column, the adopted classification is given. The references to literature information for the objects without spectra in this thesis are as follows: (1) Feast & Webster (1974), (2) Morgan et al. (1992), (3) Charles et al. (1996).

No.	$IP_{\max}$	TiO	RG in IR	IR	[O III]/H I	Var.	Class.
1	He II	No	No	PN	PN		PN
2	H I	Yes	No?	T Tau			ELS
3	H I[1]	No[1]	Yes	SySt		orb, pul, outb	SySt
4	He II?	No	No		PN		PN
5	O III	Yes?	No	T Tau	PN		ELS
6	O III	Yes	Yes?	T Tau	PN		ELS
7	He II	Yes	Yes	SySt	PN	orb?, pul?	SySt?
8	O III	No	No?	PN	PN		PN
9	He II?[2]	No[2]	Yes	SySt		orb?	SySt?
10	O III	No	Yes?	Be?	PN		ELS
11	H I	Yes	No?	PN/Be?			ELS
12	O III	Yes	Yes	SySt	SySt	orb, pul	SySt
13	O III	No	No?	Be?	PN		PN
14	O III	No	No?	PN	PN		PN
15	O III	No	Yes	Be?	SySt		superposition?
16	O III	No	Yes	Be?	SySt	pul?	SySt?
17	O III	Yes	Yes	SySt	Young PN	pul	superposition?
18	O III	Yes	Yes	SySt	SySt	orb, pul	SySt
19	O III	No	Yes	Be?	SySt	pul	H II region
20	N II	Yes	Yes	SySt			superposition?
21	O III	No	Yes	Be?	SySt		superposition?
22	O III	No	No	CV/Be?	PN		PN
23	O III	No	Yes?	Be?	SySt		SySt?
24	O III	No	Yes	SySt	SySt	outb?	SySt
25	O III	No	No	Be	PN		PN
26	He II	No	No	PN	PN		PN
27	H I[3]	Yes[3]	Yes	T Tau			foreground CV

original paper of Schmidtke & Cowley (1995). The coordinates of the object we have studied (Table 3.5) are from the original paper.

While we do not have the optical spectrum of this target, we can reject the symbiotic nature of this candidate based on the available data. The parallax published in *Gaia* EDR3/DR3 of this source is 8.31 ± 0.02 mas (Gaia Collaboration et al. 2021, 2022), corresponding to the distance of ∼ 120 pc (Bailer-Jones et al. 2021). The star is therefore not located in the Large Magellanic Cloud, but it is a foreground source. At such a distance, the absolute V magnitude of ∼ 8 mag calculated from the observed $V = 13.5$ mag (Henden et al. 2015) corresponds well to the object of luminosity class V, not supporting the possible symbiotic nature of this target. The *Gaia* measurements ($M_{\rm G} = 7.5$ mag, $G_{\rm BP}$ - $G_{\rm RP} = 1.9$ mag) suggest that RX J0550.0-7151 might be a cataclysmic variable (see Fig. 2 of Abril et al. 2020).

3.5 Summary

We have presented the results of the ongoing project with the aim of characterizing the possible symbiotic stars listed in the New Online Database of Symbiotic Variables. We have employed the new spectroscopic observations of these targets, together with archival spectroscopy, available long-term light curves of the objects, multi-frequency photometric data from ground-based and space-based surveys, astrometric measurements from *Gaia* satellite, and supplemented them with information from the literature in order to confirm or reject the symbiotic nature of the candidates and to provide a clean sample of symbiotic stars for the statistical analysis.

In the first part, we have focused on 11 candidates on the classical symbiotic stars. Based on the analysis presented in this thesis, we have classified one object as a shell-burning symbiotic star (V2204 Oph). Two other objects, Hen 4-204 and V1988 Sgr definitely are not burning symbiotic stars. However, V1988 Sgr still can be an accreting-only symbiotic star and Hen 4-204 seems to be very similar to the known symbiotic star BD Cam with an S-type cool component. Subsequent long-term photometric and spectroscopic observations in various spectral regions would be needed to fully confirm or reject their symbiotic status. In addition, we have reclassified another eight symbiotic candidates as either nearby single main-sequence stars (V379 Peg, 2MASS J07363415+6538548 in the field of NGC 2403), single giants (IRAS 19050+0001), or binaries (V1017 Cyg, the MS-MS pair; PN K1-6, the system of MS star and white dwarf; EC 19249-7343, possible M dwarf-white dwarf binary

or detached M dwarf-M dwarf system; V562 Lyr, the appearance of M3 giant with a long-lasting eclipse detected in past). V503 Her is a K-type giant star showing prominent pulsations and might be a part of an eclipsing binary with a long-orbital period.

In the second part, we analyzed available archival and new data on 9 candidates on 'slow' symbiotic novae. Three objects are confirmed to be 'slow' symbiotic novae: ASAS J174600-2321.3 (S-type; eclipsing), V618 Sgr (S-type; eclipsing), and V5590 Sgr (D-type). In addition, we claim that V618 Sgr is the first galactic recurrent 'slow' symbiotic nova as it has been observed at least in three outbursts already. TYC 1371-69-1 has the appearance of a single red giant, and we classify it as a pre-symbiotic binary. It was observed in an outburst in past, therefore it can be also classified as a transient symbiotic star. If the outburst was of a nova kind, then it is a post-symbiotic nova system in which the red giant is not capable of fueling the shell-burning on the surface of the white dwarf. M31N 2017-05b is not a symbiotic nova, but a classical symbiotic star. It is the first extragalactic symbiotic star discovered by the *Gaia* satellite. 2MASS J01093484-0800329 is probably not a symbiotic nova, but a cataclysmic variable or a central star of a planetary nebula. 2MASS J06422218-0226285 is reclassified as an outbursting young stellar object. HH Sge is most probably a single K-type star. The nature of V627 Cas is still not conclusive, but the observations suggest that it might be a binary system. The shell-burning symbiotic star classification is not supported by the data, but the accreting-only system cannot be ruled out. It can also be a post-AGB star.

Finally, we have analyzed all 27 symbiotic candidates located in the Large Magellanic Cloud and listed in the New Online Database of Symbiotic Variables. We classified four objects as bona-fide symbiotic stars (2MASS J05311676-6901041, HV 13055, [RP2006] 227, [RP2006] 295) and another four ([RP2006] 803, [BE74] 583, [RP2006] 883, 2MASS J05450015-6918192) are possibly symbiotic objects too, but more data are needed for definite classification. The rest of the candidates is classified either as planetary nebulae (SMP LMC 16, MGPN LMC 31, SMP LMC 63, [RP2006] 776, [RP2006] 774, [RP2006] 254, [RP2006] 129, SMP LMC 93), other types of emission-line stars ([RP2006] 1459, [RP2006] 1192, [RP2006] 1434, [RP2006] 2180, [RP2006] 822), superposition of the giant star and an emission nebula ([RP2006] 977, [RP2006] 490, LM2-39, 2MASS J05421820-6952493, [RP2006] 264), and one target is a foreground source, most probably a cataclysmic variable (RX J0550.0-7151).

Chapter 4

Characterization of newly discovered symbiotic stars

We have used the tools developed for the characterization of the symbiotic candidates selected from the New Online Database of Symbiotic Variables also to study the objects that were neither known as symbiotic binaries nor suspected of a symbiotic nature in the literature. These objects were either identified based on the recent brightenings (by the ground- and space-based surveys) or noticed serendipitously in the scope of projects not focusing on symbiotic binaries. In many cases presented here, we followed up on the prolific collaboration with amateur observers.

In this part of the thesis, we report the discovery and characterization of Gaia18aen, an object detected in brightening by the *Gaia* satellite and confirmed in this study to be the first symbiotic star discovered by this European mission (Chapter 4.1). We also present the analysis of the photometric and spectroscopic data of the newly discovered southern eclipsing symbiotic star, Hen 3-860, detected in outburst by the ASAS-SN survey (Chapter 4.2). Finally, we report on the discovery of the southern symbiotic binary DeGaPe 35 which was discovered during the amateur observational campaign of the planetary nebula candidates (Chapter 4.3).

Other results of the ongoing project focused on the characterization of new symbiotic binaries are not presented here, but we refer the reader to the published works: discovery of the new symbiotic star, TCP J18224935-2408280, in outburst (Merc et al. 2021a); detection of the first recorded outbursts of SS73 141 (Merc et al. 2021b) and WRAY 15-1167 (Merc et al. 2022c); low-resolution observations of the recently discovered accreting-only symbiotic star THA 15-31 (Merc et al. 2022a).

4.1 Gaia18aen: First symbiotic star discovered by Gaia

Gaia18aen (= AT 2018id, WRAY 15-136; α_{2000} = 08:02:52.06, δ_{2000} = -30:18:37.19) was previously classified as an emission-line star by Wray (1966). Its outburst was detected by the *Gaia* satellite and announced by the *Gaia* Science Alert[1] (GSA; Wyrzykowski & Hodgkin 2012; Hodgkin et al. 2013, 2021) on January 17, 2018 (Delgado et al. 2018), when the star had the brightness G = 11.33 mag. In the alert, the transient was described as a bright emission-line star in the Galactic plane which brightened by 1 magnitude. Previous measurements of the *Gaia* satellite over the period from October 31, 2014 to November 3, 2017 show that the average magnitude of the star was 12.31 ± 0.10 mag with no significant changes. According to the *Gaia* data, the star started to increase its brightness at the turn of November and December 2017. The observation obtained on December 3, 2017 revealed the star with 12.07 mag, and the object continued to brighten in the following weeks. Kruszynska et al. (2018) suggested a 'nova?' classification for the object based on the spectrum obtained by VLT/X-Shooter as a part of the program focused on the spectroscopic classification of candidates for microlensing events. As is discussed in this study, the observed event was not a nova outburst, but a Z And-type outburst of a classical symbiotic star. The results presented here have been published in Merc et al. (2020b).

4.1.1 Observational data

We collected two spectroscopic observations of Gaia18aen. The first is a sequence of three low-resolution spectra obtained with the SPectrograph for the Rapid Acquisition of Transients (SPRAT) mounted on the Liverpool Telescope at La Palma (Steele et al. 2004) on January 20, 2018, under the program XOL17B02 (PI: Hodgkin). The exposure time of each spectrum is 30 s. The spectra have a wavelength range of 4 000 – 8 000 Å and a resolution $R \sim 350$. In our analysis we used averaged spectrum. Another spectroscopic observation was obtained by VLT/X-Shooter (Vernet et al. 2011). Two exposures were obtained in the A-B nodding mode on March 22, 2018, under the program 0100.D-0021 (PI: Wyrzykowski). We used slits width 1.0", 0.7", 0.6", which produced resolutions of 4 300, 11 000, 7 900. Single exposures times were 91, 120, 10s in the UV-Blue (UVB; 2 989 - 5 560 Å), Visible (VIS; 5 337 - 10 200 Å),

[1] http://gsaweb.ast.cam.ac.uk/alerts/home

and near-infrared (NIR; 9 940 - 24 790 Å) arms, respectively. The reduction of these data is described in more detail in Merc et al. (2020b).

VLT/X-Shooter spectrum of Gaia18aen is shown in Fig. 4.1. A comparison of the VLT/X-Shooter spectrum down-sampled to the resolution of the Liverpool Telescope spectrum is shown in Fig. 4.2. The identification of the most prominent emission lines visible in the spectra of Gaia18aen is also shown in this figure.

To study the photometric behavior of Gaia18aen before, during, and after its 2018 outburst, we collected all available photometric data from the databases of several surveys and from the literature to supplement the light curve in the G filter obtained by *Gaia*. The data covering the active stage of Gaia18aen are collected by various telescopes participating in the follow-up network arranged under the time-domain work package of the European Commission's Optical Infrared Coordination Network for Astronomy (OPTICON) grant[2]: Las Cumbres Observatory (LCO) 0.4 m, Panchromatic Robotic Optical Monitoring and Polarimetry Telescopes (PROMPT) 0.6 m, Terskol Observatory 0.6 m, and Physics Innovations Robotic Telescope Explorer (PIRATE) (Kolb et al. 2018). The data are available in B, V, R, i, g filters and were calibrated using the Cambridge Photometric Calibration Server (Zieliński et al. 2019, 2020). The calibration process is described in Sec 2.1 of Wyrzykowski et al. (2020).

These data are supplemented by the data from the ASAS-SN survey (V and g filters; Shappee et al. 2014; Kochanek et al. 2017) and data in V and I from the OGLE IV survey (Udalski et al. 2015), covering mainly the pre-outburst phase (they are saturated during most of the outburst); ATLAS data in non-standard orange and cyan filters (Tonry et al. 2018b); and the data from Bochum Survey of the Southern Galactic Disk (Haas et al. 2012; Hackstein et al. 2015) in r and i filters. All our photometric data are given in Table A.1. in Merc et al. (2020b). Figure 4.3 shows the individual light curves of Gaia18aen obtained in various filters. We shifted the light curves to the same level for clarity; the values of these shifts are given in the figure legend.

4.1.2 Spectral features and symbiotic classification

Spectroscopic observations of Gaia18aen revealed its symbiotic nature, satisfying the conditions of Belczyński et al. (2000), presented in Chapter 1.3. This classification is further confirmed by the presence of the O VI in the VLT/X-Shooter spectrum (see Fig. 4.2). Symbiotic classification of Gaia18aen is also supported by its position in

[2]https://www.astro-opticon.org/h2020/network/na4.html

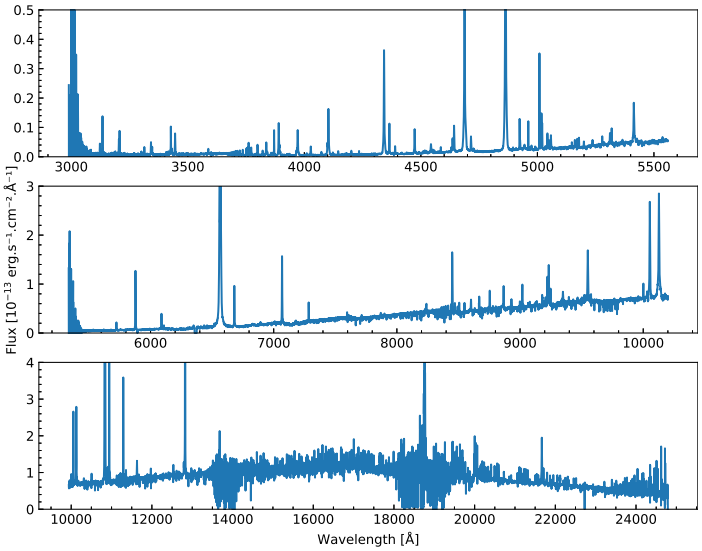

Figure 4.1: VLT/X-Shooter spectrum of Gaia18aen obtained on March 22, 2018. The upper, middle and bottom panel shows spectrum in the UBV, VIS, and NIR arm, respectively. The spectrum was corrected for the telluric features (see details in Merc et al. 2020b).

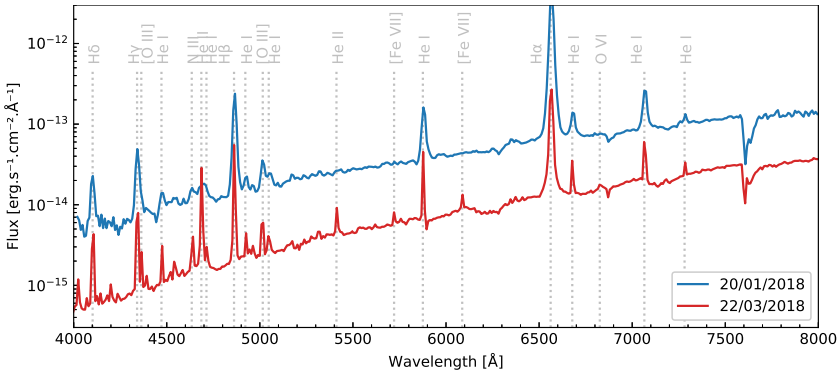

Figure 4.2: Comparison of the two spectra of Gaia18aen obtained on January 20 and March 22, 2018 together with the identification of the prominent emission lines observed.

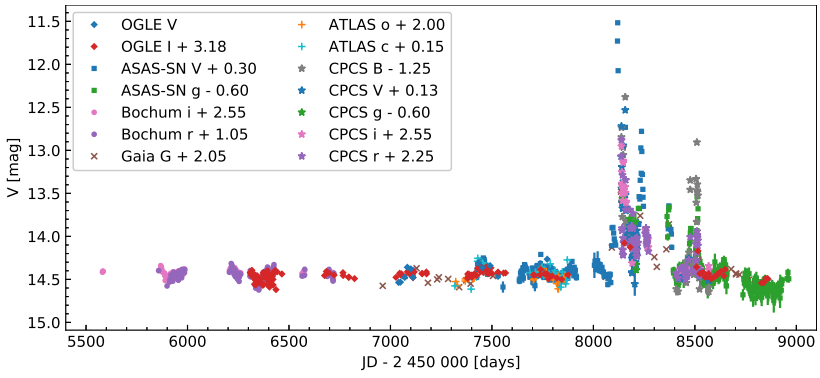

Figure 4.3: Light curves of Gaia18aen. Individual light curves in various filters were shifted to the level in the OGLE V filter for clarity; values of shifts are listed in the figure legend. Different colors denote different filters.

diagnostic diagram using [O III] and Balmer lines fluxes and in the He I diagram (for more details, see, e.g., Iłkiewicz & Mikołajewska 2017; Iłkiewicz et al. 2018). In both diagrams (see Fig. 1 and Fig. 4 in Iłkiewicz & Mikołajewska 2017), Gaia18aen is located in the region occupied solely by symbiotic stars ([O III] λ5006/Hβ = 0.04, [O III] λ4363/Hγ = 0.13; log(He I λ6678/He I λ5876) = -0.45, log(He I λ7065/He I λ5876) = -0.18).

In general, Gaia18aen shows an M-star continuum superimposed with strong emission lines, mainly of H I and He I. A comparison of both our spectra shows significant changes in the intensity of the emission lines throughout the outbursts, for example, a significant decrease in the case of the high ionization lines of He II, [O III], [Fe VII], and O VI (see Sec. 1.2.2). For clarity of the comparison of both spectra (Fig. 4.2), we down-sampled the spectrum that was obtained by VLT/X-Shooter to the resolution of the spectrum from the Liverpool Telescope (R $\approx$ 350). We also applied an absolute flux scale to the Liverpool Telescope spectrum using the average V = 12.8 mag such that convolution of the spectrum with the Johnson V filter agrees with the V mag. Table 2 in Merc et al. (2020b) gives the emission-line fluxes that were measured by fitting Gaussian profiles to the calibrated spectra.

4.1.3 Cool component

The VLT/X-Shooter spectrum of Gaia18aen was used to derive atmospheric parameters and information about the chemical composition of the atmosphere of the cool component. In order to put constraints on the physical parameters of the atmosphere of the red giant, mainly its temperature and metallicity, we used the BT-NextGen grid of the theoretical spectra (Allard et al. 2011). These spectra are calculated using the solar abundances of Asplund et al. (2009), which are available from the Theoretical spectra webserver at the SVO Theoretical Model Services[3]. Next, we used the 1D hydrostatic *MARCS* model atmospheres by Gustafsson et al. (2008) to perform a more detailed analysis of the chemical composition.

We searched among several hundreds of BT-NextGen models in the following range of parameters: $T_{\rm eff}$ = 2 900 – 4 800 K, $\log g = -0.5$ – 1.5, [M/H] = -2.5 – $+0.5$, and [α/H] = 0.0 – +0.4. All synthetic spectra were convolved with the Gaussian profile with the full width at half maximum corresponding to the velocity $v = 149\,{\rm km\,s^{-1}}$ to achieve the final resolution R$\sim$2 000. The VLT/X-Shooter spectrum of Gaia18aen

[3]http://svo2.cab.inta-csic.es/theory/newov2/index.php

was heliocentric velocity corrected by $-14.554\,\mathrm{km\,s^{-1}}$ and for the red giant velocity, $v_{\mathrm{g,hel}} = 99\ \mathrm{km\,s^{-1}}$, derived from the absorption lines in the NIR spectrum. This spectrum was consequently convolved with Gaussian profiles of $v \sin i = 145\,\mathrm{km\,s^{-1}}$ and $v \sin i = 147.5\,\mathrm{km\,s^{-1}}$ in the VIS and NIR ranges, respectively, to reduce its resolution to those adopted for the model spectra. The observed spectrum was de-reddened by $E_{\mathrm{B-V}} = 1.25\,\mathrm{mag}$ using the Cardelli et al. (1989) reddening law and adopting total-to-selective absorption ratio $R = 3.1$ with the use of the *VOSpec*[4] Virtual Observatory tool. The adopted initial value $E_{\mathrm{B-V}} = 1.20\,\mathrm{mag}$ (for more details see Merc et al. 2020b) was replaced with $E_{\mathrm{B-V}} = 1.25\,\mathrm{mag}$ to achieve better compliance in the J-band region.

Each spectrum was normalized with the flux value measured in a narrow (50 Å) range of the K-band region centered at 22 155 Å. The residuals were calculated for each pair of spectra (theoretical model and the observed spectrum) to obtain the χ^2 value that characterizes the fit quality. Only selected ranges in the NIR of the H- and K-band regions were finally used in the residual calculations to exclude the areas disturbed by some artifacts. A shorter wavelength region was not taken into account because in the case of symbiotic systems the visual range is strongly dominated by the contribution from the hot component and the nebula, and there are numerous, strong emission lines present even in the J band.

The best solutions are obtained for $T_{\mathrm{eff}} \sim 3\,500\,\mathrm{K}$. In the case of the remaining parameters, there is significant degeneration and the minimum is not clearly defined. However, in the case of metallicity, the near solar values seem to be preferred. Taking into account the values of the scale factor (generally in the range $S_f = 6.4 - 7.9 \times 10^{-19}$ in the case of the best-matching models), we can limit the value of surface gravity $\log g \approx 0.0$ because the higher value could result in a mass of the giant that is too high. The elemental abundances of the particular elements were measured through the fit of the synthetic spectrum to the observed spectrum in the K-band region. The best match was obtained for the model with a slightly super-solar metallicity value $[\mathrm{Fe/H}] = +0.25\,\mathrm{dex}$. Further results are described in detail in Merc et al. (2020b).

The NIR spectrum as well as 2MASS and *WISE* colors are all consistent with a non-dusty S-type symbiotic system. The scaling factor resulting from our best model fit combined with the adopted distance to Gaia18aen (6 kpc; Merc et al. 2020b) implies a red giant radius of $\sim 230\,\mathrm{R_\odot}$ and luminosity of $\sim 7\,400\,\mathrm{L_\odot}$, which places Gaia18aen

[4] https://www.cosmos.esa.int/web/esdc/vospec

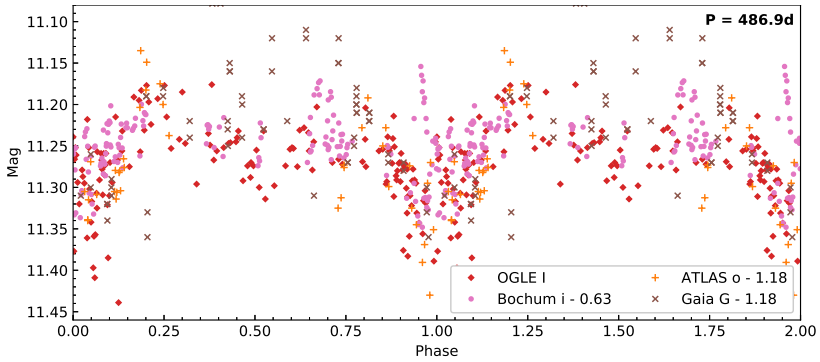

Figure 4.4: Light curves in selected filters phased with the period of $P = 486.9$ d. Individual datasets were shifted to the level in the OGLE I filter.

among the brightest symbiotic giants (e.g., Mikołajewska 2012, Chapter 2.4).

The giants in S-type symbiotic systems often exhibit pulsations, and moreover, S-type systems have orbital periods on such timescales, which should be detectable using the available data. Therefore, we used out-of-outburst data (OGLE I and *Gaia* G, with data from the period JD $\sim$ 2 458 000 - 2 458 500 excluded, ATLAS o and c, Bochum r and i) to search for any periodical changes. There are several clear minima in these quiescent light curves around JD $\sim$ 2 455 910, 2 456 355, 2 457 345, and 2 458 820, respectively. The periodicity that fits this data is written as:

$$\mathrm{Min} = (2\,457\,349.4 \pm 8.3) + (486.9 \pm 3.9) \times E. \tag{4.1}$$

ASAS-SN light curves were not used in this analysis because their coverage is insufficient (especially in g filter), or their scatter is larger than the amplitude in the best dataset (combined ATLAS o and *Gaia* G). However, the phased light curve in g seems to show the same modulation, whereas it is less obvious in V. The phased light curve in selected filters is shown in Fig. 4.4.

We tentatively attributed the 487 d modulation to the orbital period of the system. Assuming that the total mass of the system is $\sim$2 - 3 $\mathrm{M}_{\odot}$ (i.e., similar to other symbiotic stars; see, e.g., Mikołajewska 2003, Chapter 2.4 and 2.5), we estimate the binary separation to be about 1.5 - 1.7 au. The red giant with a radius of $\sim$230 $\mathrm{R}_{\odot}$ could then fill its Roche lobe. While there is some indication of a secondary minimum due to ellipsoidal variability in the phased light curve (Fig. 4.4), to fully confirm this finding and refine the period, a well-sampled, long-term light curve of Gaia18aen and measurements of radial velocities of the giant would be needed.

The large scatter in quiescent light curves may be due to additional short-term variations with timescales of 50 - 200 d caused by stellar pulsations of the red giant

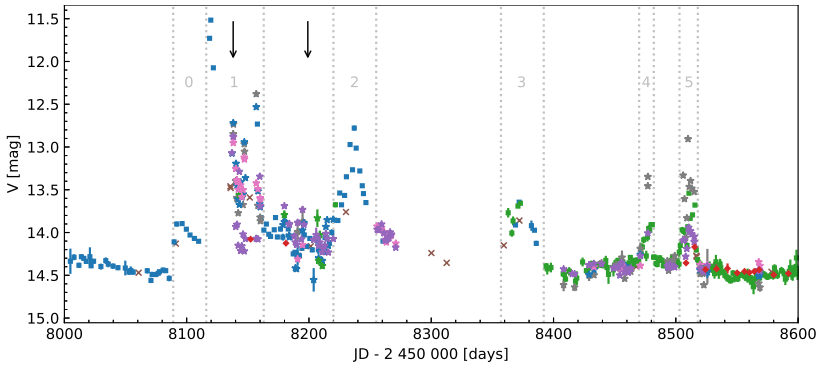

Figure 4.5: Outbursts of Gaia18aen. The colors are the same as in Fig. 4.3. The vertical dotted lines indicate the individual brightenings (denoted by numbers 0 - 5). The arrows show the times when the two spectra were obtained.

component of the binary system. This component can be either a semi-regular variable or a so-called OSARG (OGLE small-amplitude red giant). Thus, the red giant in Gaia18aen would be very similar to red giants in S-type symbiotic systems from this point of view as well (see, e.g., Gromadzki et al. 2013, and Chapter 1.4.2 and 2.4 for more details on the light curves of S-type symbiotic stars).

4.1.4 Hot component and outburst activity

The most prominent features in the light curves of Gaia18aen (Fig. 4.3) are the outbursts observed in 2018. In Fig. 4.5, the part of the light curve showing the active stage is depicted. For clarity, the light curves in various filters were shifted to the same level to study the structure of the active stage. Individual brightenings are labeled by the numbers 0 – 5.

The first small pre-outburst of about 0.5 mag in the V filter (denoted 0) was detected at JD 2 458 089. It was followed by a more prominent outburst (1) after approximately 27 d (JD 2 458 116) of gradual decline. The maximal brightness during this outburst was $\approx$ 11.2 mag in the V filter (JD 2 458 119), thus the amplitude was about 3.3 mag in comparison with the quiescent V magnitude (OGLE $V \sim 14.5$ mag). The analysis of the combined light curves constructed from the observations in various filters revealed the complex structure of this outburst with at least two another re-brightenings that followed the first maximum. Approximately 47 d (JD 2 458 163) after the first maximum Gaia18aen reached the magnitude similar to the brightness of the pre-outburst 0. The outburst denoted in this study as 2 started after 57 d of a quasi-steady period (JD 2 458 220) and lasted for 35 d (until JD 2 458 255). The maximal brightness in the V filter during this period was $\approx$ 12.5 mag.

A third, small-scale outburst was detected at JD 2 458 357. The amplitude of the outburst was much smaller than in the previous cases, but the approximate duration was similar to the outburst 2. Up to now, the last two increases in brightness (denoted 4 and 5) were detected at JD 2 458 470 and JD 2 458 503. It is worth noting that both brightenings were much shorter than the previous events, at 12 and 15 d, respectively. Moreover, the shape of at least the first event (4) looks as if it was suddenly interrupted, which may indicate that both brightenings are part of a single outburst that is apparently interrupted by some obscuration process. Since JD 2 458 518, there were no other significant brightenings detected in the case of Gaia18aen. The amplitude of the outbursts and their duration resemble the behavior of typical classical symbiotic stars (e.g., AG Dra, Z And; see, e.g., Mikolajewska et al. 1995; Mikolajewska & Kenyon 1996; Merc et al. 2019a; Munari 2019, Chapter 1.4). Multiple outbursts with timescales similar to those observed in Gaia18aen are also predicted by some nova models (Hillman et al. 2014).

In addition to the photometric evolution of the brightenings, we analyzed two spectra of Gaia18aen, obtained during its activity. The first spectrum was obtained during the decline from the outburst 1, 20 d after the optical maximum when the optical brightness dropped by about 1.5 mag, whereas the second was obtained 81 d after this maximum when the optical brightness was in the period of low state ($V \sim 14.0$ mag) between the first outburst and the re-brightening observed after approximately 100 d (see the arrows in Fig. 4.5 which are showing the times when the spectra of Gaia18aen were obtained).

The comparison of the obtained spectra of Gaia18aen is shown in Fig. 4.2. It is clear from the comparison that the outburst activity of Gaia18aen was accompanied by significant changes in its spectra. In general, the fluxes of the emission lines of H I and He I decreased by a factor of ~ 8 between the time when the first and second spectrum was obtained in the period between the outbursts, especially as a result of the decreasing continuum. At the same time, fluxes of high ionization lines are either much lower in the first spectrum of Gaia18aen (He II), or the lines are even not detectable ([O III], [Fe VII], and O VI). Such behavior indicates increasing ionization as the system declines from the outburst maximum, similar to those observed during symbiotic star outbursts (e.g., Kenyon et al. 1991; Mikolajewska & Kenyon 1992a; Mikolajewska et al. 1995; González-Riestra et al. 1999; Leedjärv et al. 2016; Merc et al. 2019a).

The maximum optical magnitude recorded for Gaia18aen was $V = 11.2$ mag on

JD 2 458 119. Assuming that most of the hot component continuum emission is shifted to the optical (a lower limit to L if not) and that during outburst $m_{\rm bol} \sim V_{hot}$, we estimate the reddening corrected $m_{\rm bol,0} \approx 7.5$ mag , and the absolute bolometric magnitude $M_{\rm bol} \sim$ -6.4 mag, which corresponds to $L \sim 28\,000$ L$_\odot$. This approach assumes that in the case of Gaia18aen, similar to other symbiotic stars, at the strong outburst maximum the optical bands are dominated by an A- or F-type photosphere ($T_{\rm eff} \sim 9\,000$ K), rather than the nebular continuum that has been confirmed by spectroscopic observations (e.g., Kenyon 1986; Mikolajewska & Kenyon 1992a).

To estimate the temperature and luminosity of the hot component during the decline, we used the emission-line fluxes. The minimum temperature is set by the maximum IP observed in the spectrum, and the relation T [10^3 K] $\sim IP_{\rm max}$ [eV] found by Murset & Nussbaumer (1994), to give $T \sim 55$ kK, and 114 kK, using the spectra obtained 20 and 81 d after the optical maximum, respectively. The upper limits for T of 80 kK and 155 kK for the first and second epoch, respectively, were derived from He II λ4 868, He I λ5 876, and Hβ emission-line ratios assuming a Case B recombination (Iijima 1981a). We estimate the luminosity of the hot component to be $L \sim 21\,000$ L$_\odot$ and 5 200 L$_\odot$, for the first and second epoch, respectively, using equation 8 of Kenyon et al. (1991). Similarly, equations 6 and 7 of Mikolajewska et al. (1997) give L(He II λ4 868) $\sim 29\,600$ L$_\odot$ and 5 890 L$_\odot$, and L(Hβ) $\sim 29\,200$ L$_\odot$ and 5 340 L$_\odot$ for the two epochs, respectively. All these estimates assume a blackbody spectrum for the hot component and case B recombination for the emission lines, and are accurate to only a factor of $\sim$ 2. These estimates also assume d = 6 kpc and $E_{\rm B-V} = 1.2$ mag.

4.1.5 Summary

We analyzed the photometric and spectroscopic observations of Gaia18aen, a transient detected by the *Gaia* satellite at the beginning of the year 2018. Our main findings are as follows: Gaia18aen is a classical symbiotic star, fulfilling the traditional criteria for symbiotic stars. Raman scattered O VI lines are observed in its spectra outside the outbursts. The system is located at the distance $\sim$ 6 kpc, 0.2 kpc from the central disk surface. The cool component of this symbiotic binary is an M giant with $T_{\rm eff} \sim 3\,500$ K of a slightly super-solar metallicity, [Fe/H] = +0.25 dex, with a radius of ~ 230 R$_\odot$. Its luminosity, $L \sim$ 7 400 L$_\odot$, makes this star one of the brightest symbiotic giants. The NIR spectrum and IR photometry from 2MASS and *WISE* are consistent with a non-

dusty S-type symbiotic star. The system experienced an outburst of about 3.3 mag in 2018, followed by re-brightening detected approximately after 100, 240, and 350 d. At least the first outburst was accompanied by the increase of the hot component luminosity ($L_{\rm h} \sim 28\,000\,{\rm L}_{\odot}$ at the optical maximum) and the decrease in temperature (A or F-type photosphere), in comparison with temperatures ~ 68 kK and ~ 135 kK, and luminosities of $\sim 26\,600$ and $5\,500\,{\rm L}_{\odot}$, corresponding to the observations obtained 20 and 81 d after the optical maximum, respectively. The outburst was accompanied by the changes in emission spectral lines typical for classical symbiotic stars. In the outburst, higher fluxes of lower ionization lines of H I and He I have been observed, together with the decrease of intensity of high ionization lines of He II, [O III], [Fe VII], and O VI. The quiescent light curves of the object are characterized by a periodicity of approximately 487 d, which we tentatively attributed to the orbital modulation. The scatter in the light curves might be caused by stellar pulsations of the red giant with a period of 50 - 200 d, which are typical for cool components in S-type symbiotic systems. These findings make Gaia18aen the first symbiotic star discovered by the *Gaia* satellite. This discovery proves the fact, that besides the astrometric mission of the *Gaia*, its repeated and high-precision observations can serve also as an photometric transient survey.

4.2 Hen 3-860: New southern eclipsing symbiotic star observed in outburst

The star Hen 3-860 (= WRAY 15-10622; α_{2000} = 13:06:12.93, δ_{2000} = -53:22:52.50) was previously classified as an Hα emitter by Wray (1966) and Henize (1976). The object was included in the International Variable Star Index database (VSX; Watson et al. 2006) as a symbiotic candidate in November 2018 by an amateur astronomer Gabriel Murawski. This classification was based on the peculiar light curve of Hen 3-860 from the ASAS-SN survey (Shappee et al. 2014; Kochanek et al. 2017), showing recent brightening (starting at the end of 2016) resembling a symbiotic outburst.

We have included the object in our observational campaign focused on never spectroscopically observed and/or very poorly studied symbiotic candidates selected from the New Online Database of Symbiotic Variables (see Chapter 3). For the selected objects, we have obtained optical spectroscopic data as well as collected the available photometry and other information from the literature in order to confirm or reject

the symbiotic nature of the objects. In this Chapter, we discuss the results of the analysis of our low- and high-resolution spectra of Hen 3-860 and provide details on its long-term photometric behavior. The results presented here have been published in Merc et al. (2022b).

4.2.1 Observational data

The low-resolution spectroscopic observations of Hen 3-860 were obtained as a part of our campaign focused on symbiotic candidates carried out in cooperation with the ARAS Group[5] (*Astronomical Ring for Amateur Spectroscopy*; Teyssier 2019). Two high-resolution spectra (R $\sim$ 25 000) were obtained with CHIRON cross-dispersed echelle spectrometer (Tokovinin et al. 2013) at the SMARTS 1.5-meter telescope located at the Cerro Tololo Inter-American Observatory, Chile. Basic information about the spectra used in this study (JD, date, resolution, spectral range, observer) is summarized in the log of observations presented in Table A1 in Merc et al. (2022b).

The spectroscopic observations of Hen 3-860 were supplemented by available photometry obtained from the All-Sky Automated Survey (ASAS; V filter; Pojmanski 1997) covering JD 2 452 032 – 2 454 836 (May 02, 2001 – January 4, 2009), and All-Sky Automated Survey for Supernovae (ASAS-SN; V and g filters; Shappee et al. 2014; Kochanek et al. 2017) covering JD 2 457 423 – 2 459 331 (February 04, 2016 – April 26, 2021). The historical data, irregularly covering the interval of JD 2 415 115 – 2 434 127 (April 5, 1900 – April 24, 1952), were obtained from the DASCH (Digital Access to a Sky Century at Harvard) archive of digitized glass photographic plates of the Harvard College Observatory (Laycock et al. 2010). Additional measurements in B, V, R_c, and I_c filters were obtained at JD 2 459 333.6 (April 29, 2021) at the Danish 1.54-meter telescope at La Silla, Chile. To construct the multi-frequency SED of Hen 3-860, we have collected the data from *Gaia* EDR3 (Gaia Collaboration et al. 2021), SkyMapper (Wolf et al. 2018), APASS (Henden et al. 2015), 2MASS (Skrutskie et al. 2006), and *WISE* (Wright et al. 2010).

4.2.2 Symbiotic classification

The possible symbiotic classification of Hen 3-860 was proposed based on the peculiar light curve of the object from the ASAS-SN survey. To definitively confirm the symbiotic nature of an object, its quiescent optical spectrum has to satisfy the

[5]https://aras-database.github.io/database/symbiotics.html

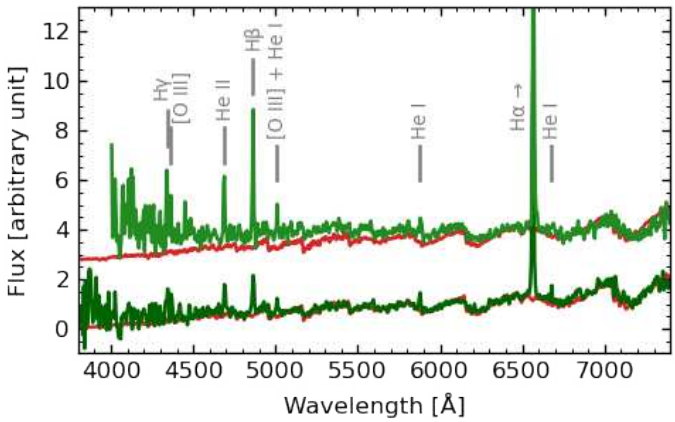

Figure 4.6: Low-resolution spectra of Hen 3-860. The spectra obtained on July 18, 2020 and July 21, 2020 are depicted by the dark and light green color, respectively. The best-fitting empirical spectrum (M3 III) from the MILES library (Falcón-Barroso et al. 2011) is shown in red (see the text for details). The identification of prominent emission lines detected in the spectra is given by the vertical lines.

spectroscopic criteria presented in Chapter 1.3. Our low-resolution optical spectra of Hen 3-860 (Fig. 4.6) satisfy the conditions in a traditional definition of a symbiotic binary. Namely, the spectra show the M2–3 III continuum and the emission lines of H I, He I, [O III], and He II. In addition, the high-resolution spectra confirmed the presence of [Fe VII] lines at 5721 Å and 6087 Å with ionization potential of 99 eV. The symbiotic classification of Hen 3-860 is further supported by its position in the diagnostic diagram employing the [O III] and Balmer lines fluxes (for more details, see Iłkiewicz & Mikołajewska 2017, and Fig. 1 therein). In the diagram, Hen 3-860 is located in the region occupied solely by symbiotic stars ([O III] $\lambda5006$ / Hβ = 0.27, [O III] $\lambda4363$ / Hγ = 0.24). The IR colors of Hen 3-860 also confirm its symbiotic classification, as they satisfy the IR criteria for symbiotic binaries presented by Akras et al. (2019b, 2021, see also Chapter 2.4). The NIR colors of Hen 3-860 are typical for S-type (stellar) symbiotic binaries.

4.2.3 Activity and long-term photometry

The historical light curve constructed on the basis of photographic observations from the DASCH archive of astronomical plates and data from the ASAS and ASAS-SN surveys is shown in Fig. 4.7. The ASAS-SN g data were simply linearly shifted to correspond to the V magnitudes. The DASCH data are calibrated using ATLAS-REFCAT2 (Tonry et al. 2018a) and correspond to the g magnitudes. For this reason,

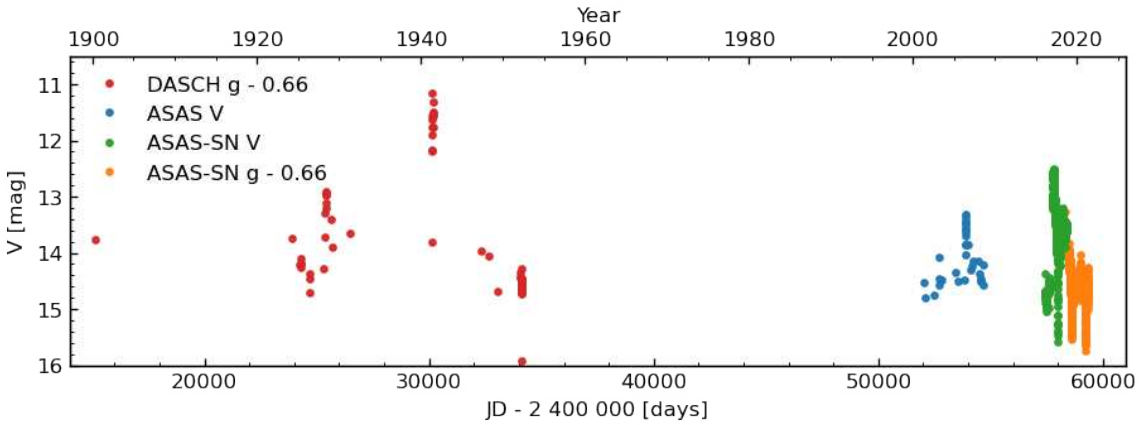

Figure 4.7: Long-term light curve of Hen 3-860 showing 121 years (1900 – 2021) of the photometric history of this symbiotic system. The light curve was constructed on the basis of photographic observations from the DASCH archive and data from the ASAS and ASAS-SN surveys.

we have applied to this dataset the same shift as for the ASAS-SN g data. Due to possible inaccuracies of these shifts, it is necessary to treat the particular historical magnitudes with caution. On the other hand, they allow us to compare the amplitudes of individual outbursts and analyze the long-term behavior of Hen 3-860.

There are four outbursts apparent in the light curve that occurred in 1928, 1941, 2006, and 2016 – 2019. For the three outbursts detected in the past, only the lower limit of duration (∼100, 100, and 150 days, respectively) could be estimated due to sparse time coverage. The recent outburst (shown in Fig. 4.8), which started in 2016 and continued until 2019, lasted at least for ∼1 000 days. Due to the seasonal gap in observations, it is not possible to determine the exact time when the outburst started. The system brightened by ∼1.6, 3.4, 1.2, and 2.1 mag in g/V during these outbursts. Interestingly, the first pair of the outbursts and the recent one repeated at about the same interval of 11 – 13 years. The amplitude, duration, and recurrence time of the outbursts are similar to the behavior of classical symbiotic binaries (see Chapter 1.4.1), and therefore we can classify the object as a symbiotic binary of Z And-type.

The quiescent orbital variability of symbiotic stars is typically well observable only at shorter wavelengths (U, B filters) and its amplitude declines significantly toward longer wavelengths. On the other hand, pulsations of cool components in symbiotic binaries (on the time scale of 50 – 200 days in S-type symbiotics; Gromadzki et al. 2013, Chapter 2.4) are usually detectable only at longer wavelengths (R, I). Both, historical data from DASCH, and ASAS survey and recent ASAS-SN data of the object were obtained only in two filters with a similar effective wavelength (g has

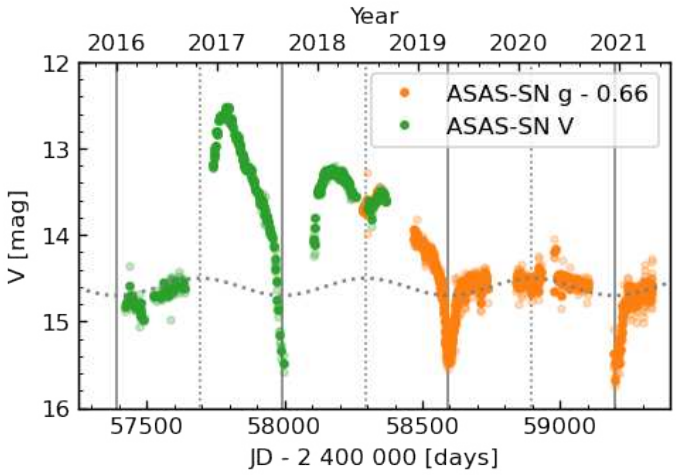

Figure 4.8: Recent light curve of Hen 3-860 covering the interval of years 2015 – 2021. The light curve was constructed on the basis of ASAS-SN V and g observations. The gray dotted sinusoidal curve fits the brightness variation of the symbiotic star during its transient and quiescent periods (outside eclipses). Vertical gray solid and dotted lines show the position of the primary and secondary eclipses, respectively. The eclipse times were calculated using the ephemeris given by eq. 4.2.

maximum efficiency between the Johnson B and V filters). Moreover, the coverage of historical data is rather sparse and the scatter is too large for reasonable analysis of quiescence variability of Hen 3-860. Although after the outburst covered by the ASAS-SN survey the optical brightness of Hen 3-860 faded nearly to the level of the quiescent phase of this symbiotic binary, the presence of eclipses in the light curve suggests that the system is in the transition period from the recent activity to the quiescence. Therefore, there are no usable quiescent data for Hen 3-860 available.

Nevertheless, in addition to the eclipses (see Chapter 4.2.4 and Fig. 4.9), the recent ASAS-SN light curve of Hen 3-860 revealed the presence of small changes in brightness. To visualize these variations, we fitted the light curve of the symbiotic system during this transition period (outside eclipses) with a sinusoidal curve (see Fig. 4.8). The mean magnitude and amplitude of these sinusoidal variations in the g filter are around 15.3 mag and 0.1 mag, respectively. Moreover, our observations secured in April 2021 ($B = 15.85\,\mathrm{mag}$, $V = 14.53\,\mathrm{mag}$) differ significantly from that from the APASS catalog ($B = 16.83\,\mathrm{mag}$, $V = 14.77\,\mathrm{mag}$) suggesting the possibility of quiescent variability with rather large amplitudes, at least at short optical wavelengths. This is further supported by the analysis of Mowlavi et al. (2021) who included Hen 3-860 in their catalog of large-amplitude variables based on the uncertainties of *Gaia* DR2 magnitudes. They obtained amplitude of 0.15 and 0.05 mag in the *Gaia* BP

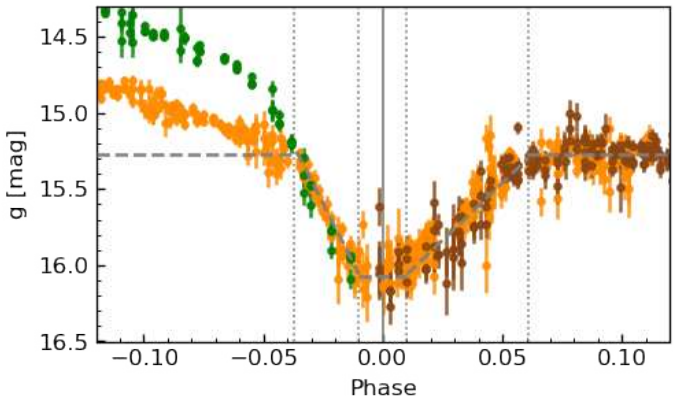

Figure 4.9: Part of the phased light curve of Hen 3-860 showing the observed eclipses. The green, orange, and brown points depict the eclipses observed in August 2017 (ASAS-SN V shifted by +0.66 mag), April 2019 (ASAS-SN g), and December 2020 (ASAS-SN g shifted by -0.14 mag), respectively. The dotted lines denote the contact times of the eclipse and the solid line marks the light minimum. The dashed line shows the simplified eclipse model. Out-of-eclipse differences are caused by the outburst.

and RP bands for Hen 3-860, respectively. These amplitudes are consistent with the amplitude we obtained for the light curve in the g filter taking into account that the *Gaia* BP filter has a lower, and RP filter has a higher effective wavelength than the g filter, and the amplitude of quiescent variability of symbiotic stars rises toward blue.

4.2.4 Binary parameters

Orbital period and the eclipses In the recent light curve of Hen 3-860 (Fig. 4.8), three primary eclipses could be detected. To evaluate the orbital period of the system, we have used the two eclipses which occurred after the recent outburst in April 2019 and December 2020. The eclipse observed during the outburst was not taken into account because there is a seasonal observational gap in the middle of the eclipse. In addition, during the outbursts of symbiotic binaries, the hot components change their size (see also the discussion below), which could distort the minimum time estimate causing the apparent changes in the O-C diagram (Skopal 1998a).

Using the two eclipses that occurred during the transition period from active to the quiescent stage in April 2019 and December 2020, we have obtained the linear ephemeris for the photometric minimum of Hen 3-860:

$$JD_{\rm min} = (2\,458\,594.8 \pm 3.2) + (602.1 \pm 4.8) \times E. \tag{4.2}$$

The derived value of the orbital period is well consistent with other S-type symbiotic stars (e.g., Gromadzki et al. 2013, Chapter 2.3). We also indicated the times of possible secondary minima in Fig. 4.8 (dotted lines), assuming a circular orbit. At least in 2018 (during the outburst), a decrease of ~ 0.2 mag is noticeable at the time of the secondary minimum.

The part of the phased light curve showing the primary eclipses of Hen 3-860 is depicted in Fig. 4.9. It is clearly seen that the shape of the eclipses is slightly asymmetric, the ingress to the eclipse taking a shorter time (t_2 - t_1 = 16.3 d) than the ascent from it (t_4 - t_3 = 30.7 d), pointing to the asymmetry of the eclipsed object (the relatively cool shell surrounding the hot component, which was created during the outburst and redistributed a fraction of the radiation of the hot component into the optical). Under the assumption of circular orbit and total mass of the system $\sim 2 - 3\,M_\odot$ (i.e., values typical for other symbiotic stars; see, e.g., Mikołajewska 2003, Chapter 2.4 and 2.5), the binary separation corresponding to the obtained orbital period would be 1.8 – 2.0 au. Using the contact times, we can then estimate the lower limits of the sizes of cool component and the eclipsed object, assuming $i = 90°$: $R_g = 57 - 63\ R_\odot$, $R_e = 33 - 36\ R_\odot$, respectively. The derived radius of the giant is well consistent with an M2 III star (van Belle et al. 1999), consistent with the spectral type estimated from our low-resolution spectra (see below). The size of the eclipsed object is similar to that of the known eclipsing symbiotic binary AX Per in the transition period (see Chapter 4.2.5).

The gap in the observations of the eclipse during the outburst precludes accurate estimates of contact times, but the eclipse duration suggests a several-fold increase in the size of the eclipsed object. This is consistent with the assumption that the hot component of symbiotic stars expands during outburst (e.g., Kenyon 1986; Skopal et al. 2011). We should note that the brightness of Hen 3-860 during the eclipse is close to the limit of the ASAS-SN survey which introduces inaccuracies in the determination of the contact times. Therefore, only precise (ideally multi-color) long-term photometric observations will help to refine the findings presented in this section.

Reddening The total Galactic extinction in the direction of Hen 3-860, given by the map of Schlafly & Finkbeiner (2011) is $E_{B-V} = 0.45$ mag. The extinction values $E_{B-V} = 0.4 - 0.5$ mag based on the interstellar Na I (Munari et al. 2005) are in agreement with the one given by the dust maps. Symbiotic stars (at least those of the D-type) are subjected to additional extinction due to circumstellar matter and

the value given by the dust maps is often an underestimation of the true reddening. We have employed other methods widely used in the case of symbiotic stars to obtain the independent reddening estimates.

Using the comparison of intrinsic (Bessell & Brett 1988) and observed $(J - K)$ colour of Hen 3-860 from the 2MASS catalog (Skrutskie et al. 2006), we have obtained $E_{\mathrm{B-V}} = 0.71$ mag and 0.62 mag for M2 and M3 giants, respectively (see below). The values from the 2MASS catalog were converted to the standard system of Bessell & Brett (1988) using the transformations of Carpenter (2001). Note that in the case of the S-type symbiotic star Gaia18aen, the extinction value based on the comparison of synthetic and observed NIR spectra of the cool giant was larger than the one from the dust maps (by about 0.2 mag, similar to Hen 3-860; Merc et al. 2020b).

We have also estimated the reddening from the emission-lines ratios following Mikolajewska et al. (1997). In S-type symbiotics, the conditions differ from the case B recombination and the reddening-free ratio of Hα / H$\beta \sim 5$ – 10 (Mikolajewska et al. 1997). Using these boundary values, we obtained $E_{\mathrm{B-V}} = 0.61$ - 1.31 mag. Another useful ratio is that of He I 7065Å / He I 5876Å which approximately equals 0.84 in S-type symbiotic stars (Proga et al. 1994). This value corresponds to the reddening $E_{\mathrm{B-V}} = 0.62$ mag in the case of Hen 3-860. Using the derived ratio of [Fe VII] emission lines ([Fe VII] 5721Å / [Fe VII] 6087Å= 0.65), which are visible only in our high-resolution spectra, we obtained $E_{\mathrm{B-V}} = 0.45$ mag. This value is lower than the other estimates but this could be caused by a low S/N ratio of the continuum in the spectra used and the consequent uncertainty in the flux measurements. All the reddening estimates assume the total-to-selective absorption ratio $R_V = 3.1$ and the reddening law of Cardelli et al. (1989). In this research, we have adopted the value $E_{\mathrm{B-V}} = 0.65$ mag.

Cool giant and the distance The presence of the cool giant in Hen 3-860 is revealed by the TiO bands well detectable in our low-resolution spectra. Using the TiO indices presented by Kenyon & Fernandez-Castro (1987, eqs. 1 and 2 therein), we have estimated the spectral type of the cool giant to be M2. We have also compared the observed spectra (Fig. 4.6) to the ones from the MILES empirical library of stellar spectra (Falcón-Barroso et al. 2011) in order to confirm this spectral classification. For calculation of χ^2, only the red part of the spectra ($> 5\,500$ Å), in which the giant dominates, was used. The empirical spectra were down-sampled to the resolution of the observed ones before the analysis. The best fit was obtained for a M3 giant. Using

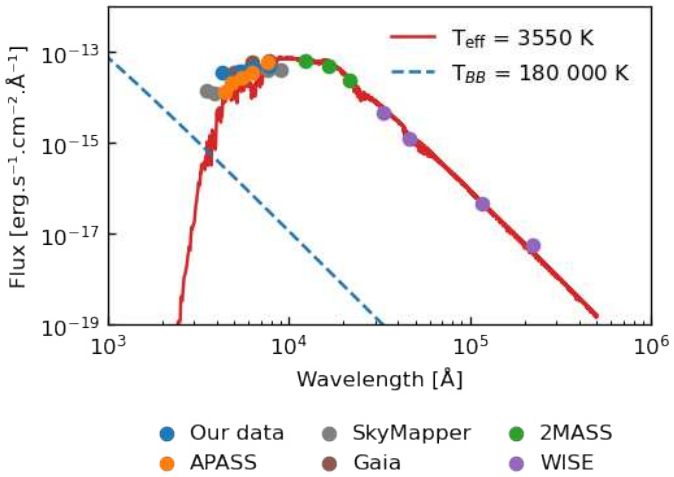

Figure 4.10: Multi-frequency SED of Hen 3-860 constructed on the basis of our data obtained with the Danish 1.54-m telescope at La Silla, Chile and data from *Gaia* EDR3, SkyMapper, APASS, 2MASS, and *WISE*. The best-fitting theoretical spectrum with $T_{\rm eff} = 3\,550\,{\rm K}$ and $\log g = 1.0$ is shown in red (Allard 2014). The dashed blue line denotes the radiation of a black-body in a distance of 5 kpc with a temperature of $1.8 \times 10^5\,{\rm K}$, and luminosity of $1\,170\,{\rm L}_\odot$ (a hot component of Hen 3-860; see the text for details). We should note that the SED represents a mean spectrum of Hen 3-860 as the individual points were obtained over a relatively long period of time covering various phases of activity of this symbiotic star.

the statistical relations of Malkov et al. (2020), we can estimate the effective temperatures corresponding to the obtained spectral types, namely 3 590 K and 3 480 K for M2 III and M3 III, respectively.

A similar temperature was obtained from the multi-frequency SED of Hen 3-860 (Fig. 4.10), which was compared with the BT-Settl grid of theoretical spectra (Allard 2014) downloaded from the Theoretical spectra webserver at the SVO Theoretical Model Services[6]. In this case, we have used only the APASS *r'* and *i'*, 2MASS, and *WISE* observations, as at shorter wavelengths the contribution of the nebular radiation and the hot component is not negligible, and would artificially increase the estimate of the temperature of the cool component. Moreover, their contribution is changing during various phases of Hen 3-860 activity covered by observations used for the construction of the SED. The best fit was obtained for the temperature of 3 550 K and $\log g = 1.0$ (corresponding to $\sim$ M2.5 giant), consistent with the estimates from the optical spectra.

The giant radius corresponding to the obtained spectral types is in the range of 60 – 75 $\rm R_\odot$ (van Belle et al. 1999), which is consistent with the lower limits from

[6]http://svo2.cab.inta-csic.es/theory/newov2/index.php

the contact times of the eclipses of Hen 3-860 assuming $i = 90°$ (57 – 63 $R_\odot$; see above). The luminosity can then be estimated directly from the Stefan-Boltzmann law. For the range of temperatures of 3 500 – 3 600 K and radii 60 – 75 $R_\odot$, one can obtain the luminosity of the giant $L_g = 540 – 760\,L_\odot$. We can use these values to estimate the distance to Hen 3-860. The range of absolute bolometric magnitudes of the symbiotic system Hen 3-860 corresponding to the obtained values of the luminosity is M_{bol} = -(2.46 – 2.09) mag. Using the relations of bolometric correction BC_K and temperature presented by Buzzoni et al. (2010), we calculated M_K = -(5.39 – 4.93) mag. The dereddened K magnitude of Hen 3-860 from the 2MASS catalog is 8.15 mag. From apparent and absolute K magnitude, we calculate a distance of 4.1 – 5.1 kpc.

The ratio of the observed and intrinsic flux values can be used to determine the angular radius of the giant. For the measured bolometric flux of the giant corrected for interstellar extinction $F_g^{obs} = 9.3 \times 10^{-10}$ erg s^{-1} cm^{-2} (red line in Fig. 4.10) and intrinsic bolometric flux of 7.2×10^9 erg s^{-1} cm^{-2} obtained from the BT-Settl theoretical spectrum (Allard 2014) with $T_{eff} = 3\,550$ K and $\log g = 1.0$ we get the angular radius of the giant $\theta = 3.6 \times 10^{-10} = 7.4 \times 10^{-5}$ arcsec. Under the assumption that the giant radius is according its derived spectral type in the interval of 60 – 75 $R_\odot$ we get its distance in the interval 3.7 – 4.7 kpc.

We have also employed the empirical relation between the observed bolometric flux and the distance presented by Skopal (2005). Using the relation for red giants (eq. 27 in Skopal 2005), we then obtained the distance range of 6.9 – 7.8 kpc. Note that this relation is based on rather a small number of values. Therefore, its statistical significance is low, which can only give us a rough estimate.

The independent distance estimate can be obtained from the astrometric data published in *Gaia* DR2 and EDR3. There are some limitations due to the presence of the zero-point offset in parallaxes, which is a nontrivial function of the magnitude, color, and ecliptic latitude of the object (Lindegren et al. 2021b; Stassun & Torres 2021), due to the orbital motion of the long-period binaries (Sion et al. 2019), and due to the fact that the reliable distance cannot be obtained by simple inversion of the parallax (Luri et al. 2018). The parallax of (0.119 ± 0.076) mas and (0.104 ± 0.03) mas was published for Hen 3-860 in *Gaia* DR2 and EDR3, respectively. The goodness-of-fit of 20.6 and 27.7 indicate a very poor fit to the data in both cases. Bailer-Jones et al. (2018, 2021) adopted the probabilistic approach with prior constructed from a 3D model of the Galaxy and obtained a distance of 5.1 kpc (with the uncertainty of 3.8 – 7.0 kpc) and 6.4 kpc (5.7 – 7.4 kpc) from the DR2 and EDR3 data, respectively.

Anders et al. (2019) obtained the photo-astrometric distance of 5.4 kpc (3.6 – 7.1 kpc) using the StarHorse code and the data from *Gaia* DR2 and photometric catalogs of Pan-STARRS1, 2MASS, and *WISE*.

All the employed methods resulted in more or less consistent results. In this research, we have adopted a distance of 5.0 kpc for the symbiotic system Hen 3-860.

Hot component The hot components in the shell-burning symbiotic stars are typically too hot to be observable at optical wavelengths at which the giant and nebular emissions dominate (Skopal 2005, Chapter 1.2.2). To estimate the parameters of the hot component (the white dwarf with its pseudo-photosphere) in Hen 3-860, we have used indirect methods for assessment of the parameters of the central source of ionizing photons based on the nebular emission line fluxes. Under the assumption of case B recombination and a black-body spectrum of the hot component, we can estimate the $T_{\rm h}$ and $L_{\rm h}$ using the fluxes of Hβ, He I 5876Å, and He II 4686Å (Iijima 1981b; Mikolajewska et al. 1997).

For the calculation, we have used the fluxes obtained from two low-resolution spectra calibrated to the ASAS-SN g magnitude from the same time ($g = 14.6$ mag). Below, we list the resulting average values of parameters as the individual values obtained from these two spectra were very similar (the time difference between the two spectra is only 2 days).

The temperature $T_{\rm h} \sim 1.8 \times 10^5$ K was obtained using the equation 2 of Leedjärv et al. (2016). The value estimated in this way is an upper limit and might be overestimated by 15 – 20% (see the discussion for AG Dra in Merc et al. 2017). The lower limit can be obtained from the maximum ionization potential IP derived from the spectrum and using the relation $T_{\rm h}$ [10^3 K] $\sim IP_{\rm max}$ [eV] (Murset & Nussbaumer 1994). In the case of Hen 3-860, the lines with the maximum IP are that of [Fe VII] (the upper panels of Fig. 4.11), and the lower limit of the hot component temperature is $T_{\rm h} \sim 1 \times 10^5$ K. We should note that these emission lines were detected only in our high-resolution spectra, and the spectra from 2020 were obtained with a lower resolution which could prevent them from being detected in the noise. Another possibility is that the emission lines [Fe VII] had not yet recovered after the outburst at the time of the 2020 observations, as during the outbursts of symbiotic stars the highly ionized elements typically disappear from the spectra in response to the expansion and decrease of the hot component temperature.

The luminosities of the hot component $L_{\rm h}$(HeII λ4686, HeI λ5876, Hβ) $\sim 1\,080\,{\rm L}_\odot$,

$L_{\rm h}$(HeII λ4686) $\sim$ 1 260 $L_\odot$, and $L_{\rm h}(\mathrm{H}\beta) \sim 550\,L_\odot$ were calculated using equation 8 of Kenyon et al. (1991) and equations 6 and 7 given in Mikolajewska et al. (1997), respectively. We should note that the method of Kenyon et al. (1991) is a proxy only of the radiation emitted shortwards of 1200 Å, but is well applicable in our case (as was used for other symbiotic stars, see, e.g., Miszalski et al. 2014; Gałan et al. 2019) as the hot component, given its high temperature, radiates mostly in this part of the electromagnetic spectrum. The numbers of H^0 and He^+ ionizing photons entering these equations, corresponding to $T_{\rm h} \sim 1.8 \times 10^5$ K, were obtained from Nussbaumer & Vogel (1987). Note that the low luminosity derived from the Hβ flux is a result of significant central absorption of this emission line (visible in the high-resolution spectra in Fig. 4.11). Due to the fact that the part of the high-resolution spectrum covering Hβ was rather noisy and the spectral line seems to be significantly underexposed, we have not used these data for analysis. At the same time, the central absorption of Hβ is not detectable in the used spectra due to their low resolution and consequently, it was not possible to make a reliable correction for the central absorption. Moreover, it is not possible to estimate the correction for the low-resolution spectra from the high-resolution spectra as they were obtained at different times and in different phases of the recovery from the outburst.

Although according to Mikolajewska et al. (1997), these estimates have accuracies of a factor of ~ 2, mostly due to uncertainties in reddening and distance, they allow us to compare the hot component of Hen 3-860 with the ones in other symbiotic systems (e.g., to distinguish between systems powered by thermonuclear burning or accretion only). Obtained temperatures ($> 10^5$ K) and luminosities ($\sim 10^2 - 10^3\,L_\odot$) are typical for quiescent shell-burning symbiotic stars (see Fig. 4 in Mikołajewska 2003 and also Muerset et al. 1991; Shen & Bildsten 2007; Munari 2019; Chapter 2.5).

4.2.5 Comparison with AX Persei

As confirmed by the analysis presented here, Hen 3-860 belongs to the group of eclipsing symbiotic binaries. It is therefore tempting to compare it with another well-known eclipsing symbiotic star, AX Per. The components of AX Per are an M4.5 giant and a white dwarf on 680-d orbit (e.g., Skopal et al. 2011, and references therein). Although the giant in AX Per is of a slightly later spectral type than that in Hen 3-860 (and therefore its radius is larger), both systems have very similar eclipsed objects - the radii obtained from the contact times are 33 – 36 $R_\odot$ (Chapter 4.2.4) and 27 – 36 $R_\odot$

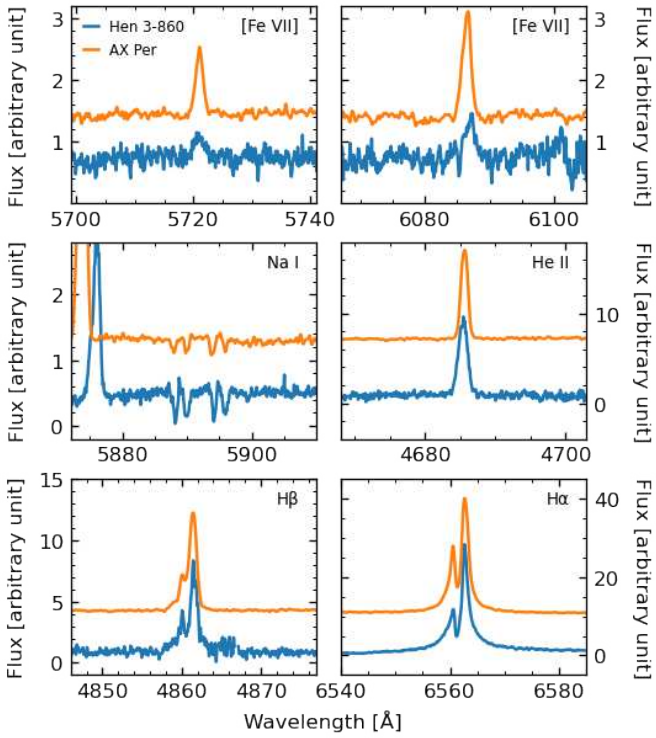

Figure 4.11: Comparison of the profiles of selected spectral lines in our high-resolution spectrum of Hen 3-860 (blue; February 4, 2021) and in the spectrum of well-known symbiotic star AX Per (orange; November 5, 2020). The spectrum of AX Per was downloaded from the ARAS database (Teyssier 2019).

(Skopal et al. 2011) in the case of Hen 3-860 and AX Per, respectively.

Both stars manifest [Fe VII] emission lines in their quiescent spectra, but do not show the Raman-scattered O VI lines. They share a similar Hα line profile showing the blue-shifted absorption component, which probably originates in the wind of the cool giant (the lower right panel of Fig. 4.11). Furthermore, there is another noteworthy similarity between the spectra of Hen 3-860 and AX Per. Both symbiotic systems show two pairs of Na I lines in their spectra (the middle left panel of Fig. 4.11). One pair has supposedly an interstellar origin and its velocity is used to put the lower limit on the distance to some symbiotic stars (see, e.g., Merc et al. 2020b; Mikołajewska et al. 2021). Our preliminary analysis of the spectroscopic data of AX Per confirmed that the other pair arises in the symbiotic system. During the active stages of AX Per, the emission doublet is sometimes observed instead of the absorption one. Interestingly, in our ongoing research, we have detected similar behavior in other symbiotic stars, suggesting that the Na I doublet in these objects originates within these interacting binaries (e.g., BF Cyg, CI Cyg, V1413 Aql; see their spectra in the ARAS database).

In addition to the aforementioned, there is a striking similarity between the light

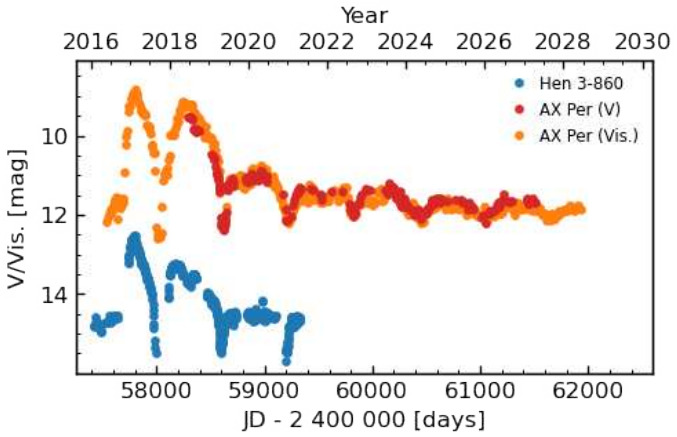

Figure 4.12: Comparison of light curves of AX Per and Hen 3-860. The light curve of AX Per, covering the time interval of 1987 – 2001, is constructed on a basis of visual observations (smoothed within 10-day bins) from AAVSO database (Kafka 2022) and V data from Skopal et al. (2001). The light curve of AX Per was shifted in time and re-scaled to match the orbital period of Hen 3-860.

curve of Hen 3-860 covering its recent outburst (2017 – 2019), and that of AX Per during its outburst in 1987 – 1990. This may indicate a similarity in the geometry and location of the main source of the optical continuum in the post-outburst (transition) stage of both symbiotic stars. In Fig. 4.12, we plotted both light curves together. Since AX Per has a slightly longer orbital period (680 d) than Hen 3-860 (602 d), we re-scaled the light curve of AX Per to match the orbital period of Hen 3-860. The light curve was then shifted in JD so that the eclipse times of both stars match. This comparison not only allows us to notice similarities in evolution during the outburst and shortly after it, but it also allows us to predict the evolution of Hen 3-860 in the coming years. On the AX Per light curve, we can clearly see that during several orbital cycles after the outburst, the narrow eclipses (well observable in 1992, 1994) gradually changed into a sinusoidal variation typical for the quiescent periods of symbiotic binaries. Hen 3-860 is now in the transition period from the outburst and if there is no further unexpected activity, we can assume that it will also continuously enter the quiescence and wave-like variability will be observable in its light curve.

4.2.6 Summary

We have analyzed spectroscopic and multi-frequency photometric data of Hen 3-860, the object observed in the recent brightening and proposed to be a symbiotic star. Our analysis confirmed that Hen 3-860 is a classical symbiotic star of the S-type. The

cool component is an M2-3 giant with $T_{\rm eff} \sim 3\,550\,{\rm K}$, $\log g \sim 1.0$, radius 60 – 75 $\mathrm{R}_{\odot}$ and luminosity of 540 – 760 $\mathrm{L}_{\odot}$. The second component is a shell-burning white dwarf possessing a high temperature of $1 - 2 \times 10^5\,{\rm K}$ and luminosity of $\approx 10^3\,\mathrm{L}_{\odot}$. The recent light curve of Hen 3-860 confirmed that the object is a representative of a group of eclipsing symbiotic binaries. The presence of eclipses allowed to obtain the orbital period of the system of 602 days. The symbiotic system experienced at least 4 outbursts in the last 120 years (1928, 1941, 2006, 2016 – 2019). Hen 3-860 is now in the transition period from the active stage to the quiescence. Based on its similarity to AX Per, a well-known eclipsing symbiotic binary, we can assume that after a few orbital cycles, the narrow eclipses in the light curve of Hen 3-860 will gradually change into wave-like variability typically observable in quiescent symbiotic stars. Therefore it is worth monitoring the system in order to document in detail the recovery of the system from the recent outburst during the transition into quiescence.

4.3 DeGaPe 35: Amateur discovery of a new southern symbiotic star

DeGaPe 35 (= 2MASS J15211785-5900339; α_{2000} = 15:21:17.86, δ_{2000} = -59:00:33.90) was identified as a possible emission-line object in the scope of an amateur survey searching for planetary nebulae. This survey is operated as a supplementary program at the amateur-built, remotely-operated Atacama Photographic Observatory located in San Pedro de Atacama, Chile. The Takahashi TOA 15-cm refractor telescope is equipped with the *LRGB* broadband filters, narrow-band Hα, S II, and O III filters and the Apogée Alta U16M cooled camera. The main goal of the observatory is the astrophotography of the southern deep-sky objects. However, the field of view of four square degrees makes the obtained data excellent to search for conspicuous objects in the vicinity of the photographed targets.

DeGaPe 35 was discovered in the field of the well-known Wolf-Rayet star WR 68 during the observations in 2017. The final discovery image is the combination of Hα, S II, and O III observations with total exposure times of 800, 600, and 600 minutes, respectively. DeGaPe 35 was identified thanks to its green appearance on the image (Fig. 4.13). Such an appearance is typical for stellar-sized planetary nebulae and other emission-line objects which have strong emission lines in their optical spectra, especially [O III] and Hα lines. Objects with such an appearance are identified on

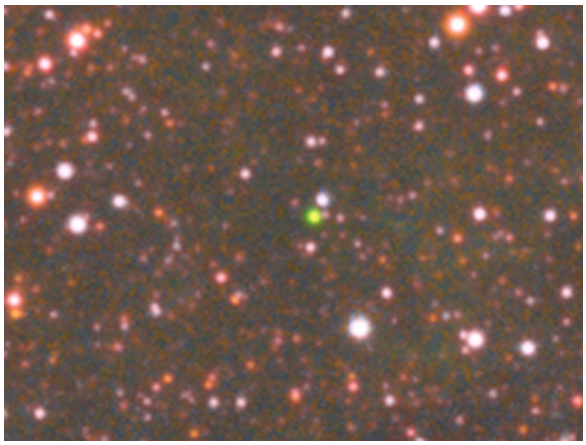

Figure 4.13: Discovery image of DeGaPe 35. The target is the conspicuous green object in the middle. See the text for more details.

the images and included in the HASH database of planetary nebulae (Parker et al. 2016) and the French amateur planetary nebulae catalog[7] as possible new planetary nebulae. The candidates are subjected to spectroscopic follow-up to confirm the planetary nebula nature or reclassify them as mimics. In the case of DeGaPe 35, a follow-up in June 2021 (see below) contradicted the planetary nebula nature of the source, and the object was reclassified as an emission-line star in the aforementioned databases. We reviewed the observations in the scope of the study on the symbiotic candidates and claim, that the object is not only an emission-line star but can be classified as a symbiotic star.

4.3.1 Observational data

Two low-resolution spectra of DeGaPe 35 obtained by the Southern Spectroscopic Project Observatory Team are used in this work. They were obtained using the remotely-operated RC12" telescope located at the Deep Sky Chile facilities, equipped with an Alpy600 spectrograph and Atik 414EX cooled camera. The first spectroscopic data were obtained on June 11, 2021 (JD 2 459 376.6), and the second dataset was acquired on May 10, 2022 (JD 2 459 709.8). In both cases, a total of 6 exposures of 1 200 s was summed to produce the final spectra (see Fig. 4.14).

For the analysis of SED of DeGaPe 35, we have collected the data from *Gaia* EDR3 ($G_{\rm BP}$*, G,* $G_{\rm RP}$; Gaia Collaboration et al. 2021), SkyMapper Southern Survey (*g, r*; Wolf et al. 2018), Two Micron All-Sky Survey (2MASS; *J, H, K*; Skrutskie et al. 2006), *Midcourse Space Experiment* (*MSX*; *A* band; Price et al. 2001), and *Wide-field*

[7] http://planetarynebulae.net/EN/index.php

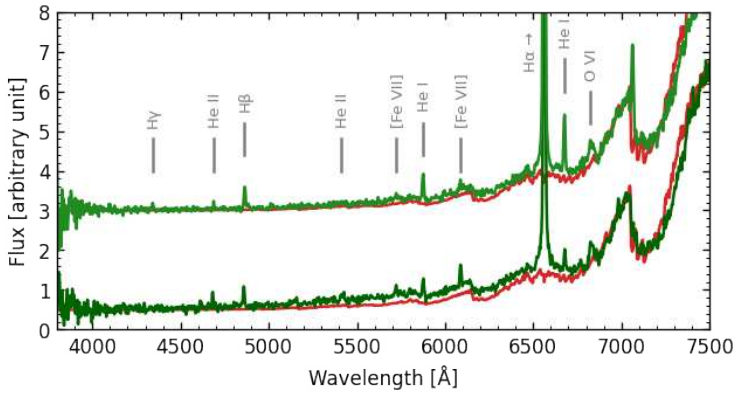

Figure 4.14: Low-resolution spectra of DeGaPe 35. The spectra obtained on June 11, 2021 and May 10, 2022 are depicted by the dark and light green color, respectively. Spectra are separated by the arbitrary constant. The intrinsic spectrum of M5 III star (Fluks et al. 1994) is shown in red. The spectrum was reddened by the value of $E(B-V) = 2.34$ mag (see the text for details). The identification of prominent emission lines detected in the spectra is given by the vertical lines.

Infrared Survey Explorer (*WISE*; *W1, W2, W3, W4*; Wright et al. 2010).

We have also searched for the time-resolved photometric observation of the target to analyze the possible variability of the target. Unfortunately, the photometry of DeGaPe 35 from the ASAS-SN survey (Shappee et al. 2014; Kochanek et al. 2017) is contaminated by the nearby bright sources, and the target is located in the southern part of the sky not covered by the ZTF survey (Masci et al. 2019). The brightness of the star seems to be close to or below the sensitivity limit of the ASAS survey (Pojmanski 1997). The only usable photometric measurements are those obtained by the *Gaia* satellite in the $G_{\rm BP}$, G, $G_{\rm RP}$ filter and published in *Gaia* DR3 (Gaia Collaboration et al. 2022). However, these cover only the interval shorter than 3 years, which might not be sufficient to study the orbital variability of symbiotic stars (Chapter 2.3).

4.3.2 Symbiotic nature

The studied object was classified as an emission-line star (without any further specification) in the HASH database and the French amateur planetary nebulae catalog. However, already at the time when the object was added to the later catalog, the possible presence of the Raman-scattered O VI lines was noted in the optical spectra. Our analysis of the low-resolution optical spectra of DeGaPe 35 (Fig. 4.14) confirmed the presence of the Raman-scattered O VI emission lines, which is a sufficient condition for the symbiotic classification of an object (see Chapter 1.3 for more details). Moreover, other highly ionized emission lines have been detected in the spectrum, including the

prominent emission lines of He II, and [Fe VII], in addition to strong emission lines of H I and He I. The continuum can be well-fitted by the spectrum of a cool M-type giant (M5 III, see below). Taken together, the optical spectra of DeGaPe 35 satisfy the symbiotic criteria of Belczyński et al. (2000), presented in Chapter 1.3.

The symbiotic classification is further supported by the IR colors of DeGaPe 35 that satisfy the IR criteria for S-type symbiotic binaries (Akras et al. 2019b, 2021, see also Chapter 2.4). Moreover, the object is classified as a symbiotic binary in all seven classification trees suggested by Akras et al. (2019b) to distinguish between symbiotic stars and common mimics (see Chapter 2.4). The lack of [O III] lines in the spectra of DeGaPe 35 precludes the use of diagnostic diagrams based on the [O III] and Balmer lines fluxes (e.g., Iłkiewicz & Mikołajewska 2017; Iłkiewicz et al. 2018) as we used them for Gaia18aen and Hen 3-860 (see Chapter 4.1.2 and 4.2.2). We have employed the He I diagram (Fig. 4 in Iłkiewicz & Mikołajewska 2017) in which DeGaPe 35 is located in the region occupied solely by symbiotic stars (for the spectrum obtained in May 2022: log(He I λ6678/He I λ5876) = -0.10, log(He I λ7065/He I λ5876) = -0.12; spectrum from 2021 was not used as the He I λ7065 was faint).

Variability The unavailability of the long-term photometric data does not allow the detailed analysis of the variability of DeGaPe 35. The light curves from *Gaia* DR3 (Fig. 4.15) suggest the variability on the timescale of 700 – 800 days, but the covered time interval is too short for a proper period analysis. The amplitude of these changes is larger in $G_{\rm BP}$ compared to the $G_{\rm RP}$ filter and is about 1 and 0.2 mag, respectively. The timescale and the color dependence of the changes are similar to the orbital variability observed in other S-type symbiotic binaries (e.g., Gromadzki et al. 2013, Chapter 2.3). Therefore, we tentatively attribute these brightness changes to the orbital motion of the symbiotic binary.

Also the spectroscopic data obtained eleven months apart show some changes in the strengths of the emission lines. Namely, the intensity of H I and He I lines increased while the He II lines are weaker in the later spectrum. Such changes are often detected in the symbiotic binaries and are generally caused by the orbital motion or the changes in the ionization structure of the nebula.

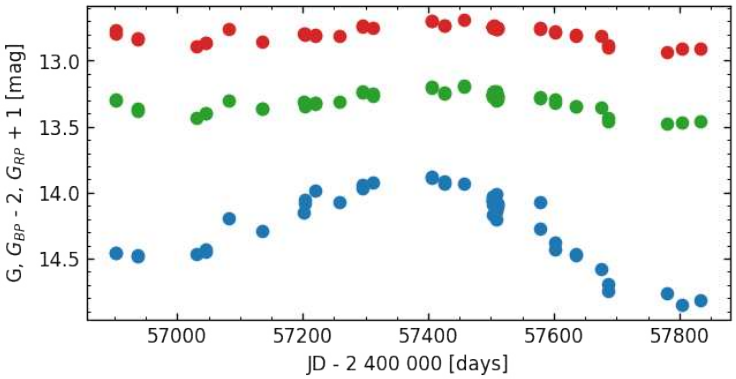

Figure 4.15: *Gaia* DR3 light curves of DeGaPe 35. The observations in $G_{\rm BP}$, $G_{\rm RP}$, and G filters are shown in blue, green, and red, respectively. For clarity, the data in $G_{\rm BP}$ and $G_{\rm RP}$ were shifted by constants of -2 and +1 mag, respectively.

4.3.3 Components of the binary

Cool component and the distance In the optical spectra (Fig. 4.14), the contribution of the red giant is well visible thanks to the prominent molecular bands of the TiO. We have employed the method of Kenyon & Fernandez-Castro (1987, equations 1 and 2) to estimate the spectral type of the cool component using the strengths of TiO bands. For the two low-resolution spectra, we have obtained the spectral type $\sim$M4. In addition, we have compared the observed spectra with the ones from the library of Fluks et al. (1994). The reference spectra were down-sampled to match the resolution of the observed spectra (R $\sim$ 550). They were also reddened by the value of $E_{\rm B-V} = 2.34$ mag corresponding to the total Galactic reddening in the direction of DeGaPe 35, estimated from the dust map of Schlafly & Finkbeiner (2011). For calculation of χ^2, only the red part of the spectra ($> 5\,500$ Å) was used, as the fluxes at the shorter wavelengths are typically contaminated by the strong nebular radiation and/or the hot component. The best fit was obtained for an M5 giant. The effective temperatures corresponding to the obtained spectral types are 3 476 K and 3 367 K for M4 and M5 giants, respectively (van Belle et al. 1999).

A similar temperature is suggested by the fitting of multi-frequency SED (Fig. 4.16) with the BT-Settl grid of theoretical spectra (Allard 2014) downloaded from the Theoretical spectra webserver at the SVO Theoretical Model Services[8]. In the fitting procedure, only 2MASS, *MSX* and *WISE* observations were used, as the radiation at shorter wavelengths is strongly contaminated by the nebular emission and the hot component (the optical/near-UV excess is visible in the figure). We should note that

[8]http://svo2.cab.inta-csic.es/theory/newov2/index.php

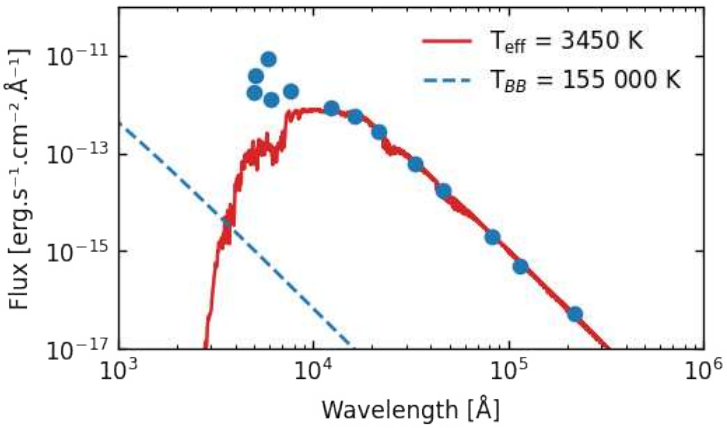

Figure 4.16: Multi-frequency SED of DeGaPe 35 constructed on the basis of data from *Gaia* EDR3, SkyMapper, 2MASS, *MSX*, and *WISE*. The best-fitting theoretical spectrum with $T_{\rm eff} = 3\,450$ K and $\log g = 0.0$ is shown in red (Allard 2014). The dashed blue line denotes the radiation of a black-body in a distance of 3 kpc with a temperature of 1.55×10^5 K, and luminosity of $1\,550\,L_\odot$ (a hot component of DeGaPe 35). The SED represents only a mean spectrum of DeGaPe 35 as the individual points were obtained over a relatively long period of time.

this procedure is only very weakly dependent on the $\log g$ value, therefore we fixed the value on $\log g = 0$, which is a typical value for symbiotic giants with late spectral types (e.g., Gałan et al. 2016, 2017).

Assuming the luminosity class III, we can estimate the radius and luminosity of the cool component in DeGaPe 35. For M4 – M5 III stars, one can obtain the radii of 92 – 114 $R_\odot$ using the calibrations of van Belle et al. (1999). Luminosity in the range of 1 100 – 1 500 $L_\odot$ is then calculated using the Stefan–Boltzmann law. We should note that the assumption of the luminosity class III might not be true for all symbiotic stars as demonstrated in Chapter 2.4.

The range of absolute bolometric magnitudes corresponding to the obtained values of the luminosity is $M_{\rm bol}$ = -(3.20 – 2.86) mag. Using the relations of bolometric correction $BC_{\rm K}$ and effective temperature (Buzzoni et al. 2010), we calculated $M_{\rm K}$ = -(6.24 – 5.81) mag. The dereddened K magnitude of DeGaPe 35 from the 2MASS catalog is 5.41 mag. From apparent and absolute K magnitude, one can get the distance estimate of 1.8 – 2.1 kpc. This value is lower than the distance estimated independently using *Gaia* EDR3 data by Bailer-Jones et al. (2021). They obtained geometric distance in the range of 3.5 – 5.3 kpc and photogeometric distance of 3.1 – 4.3 kpc. This might suggest that the real luminosity of the cool component in DeGaPe 35 is higher than the luminosity calculated under the assumption of luminosity class III. On the other hand, the goodness-of-fit of the astrometric solution

presented in *Gaia* EDR3 has a value of 3.37, which is higher than the limiting value of 3. Such solutions are suggested to be considered unreliable in the *Gaia* documentation. It is worth noting that only a single star model was adopted for the astrometric solution in *Gaia* DR3 and the binarity might influence the astrometric parameters in such a long-period system (see, e.g., Sion et al. 2019). We have adopted the compromise value of 3 kpc as a distance to DeGaPe 35 in the rest of this work. That translates to the cool component luminosity of 2 970 – 3 220 $L_\odot$ and radius 150 – 167 $R_\odot$.

Hot component We have used the indirect methods to estimate the parameters of the hot component in DeGaPe 35, as the contribution of the symbiotic white dwarfs to the observed continuum in the optical range of SED is negligible. Under the assumption of a black-body spectrum of the hot component and case B recombination, one can estimate the T_h and L_h using the fluxes of Hβ, He I 5876Å, and He II 4686Å (Iijima 1981b; Mikolajewska et al. 1997), which are directly influenced by the high energy photons of the hot component.

For the spectrum obtained in June 2021, we have obtained the temperature of the hot component of $T_\mathrm{h} \sim 1.71 \times 10^5$ K using the equation 2 of Leedjärv et al. (2016). The luminosities $L_\mathrm{h}(\mathrm{HeII}\,\lambda4686, \mathrm{HeI}\,\lambda5876, \mathrm{H}\beta) \sim 72\,L_\odot$, $L_\mathrm{h}(\mathrm{HeII}\,\lambda4686) \sim 100\ L_\odot$, and $L_\mathrm{h}(\mathrm{H}\beta) \sim 70\,L_\odot$ for the hot component of DeGaPe 35 were calculated using equation 8 of Kenyon et al. (1991) and equations 6 and 7 given in Mikolajewska et al. (1997), respectively. The same analysis for the spectrum acquired in 2022 resulted in the values $T_\mathrm{h} \sim 1.38\times10^5$ K and $L_\mathrm{h}(\mathrm{HeII}\,\lambda4686, \mathrm{HeI}\,\lambda5876, \mathrm{H}\beta) \sim 2\,830\,L_\odot$, $L_\mathrm{h}(\mathrm{HeII}\,\lambda4686) \sim 3\,500\ L_\odot$, and $L_\mathrm{h}(\mathrm{H}\beta) \sim 3\,050\,L_\odot$

The temperature estimate is independent of the absolute flux calibration of the used spectra, but it should be considered only as the upper limit. The value should not be overestimated by more than 15 – 20% (see Merc et al. 2017). The lower limit is given by the presence of Raman-scattered of O VI lines in both spectra that requires the temperature of $\sim$ 114 000 K (see Murset & Nussbaumer 1994). The luminosities presented in the previous paragraph are obtained from the flux-calibrated spectra. Given the lack of simultaneous photometry, we have calibrated both low-resolution spectra to the *Gaia* G median magnitude (G = 13.3 mag). Therefore, the luminosity should be considered only as a rough estimate as the real brightness during the spectroscopic observations might have been different from the adopted value. To some extent, that might explain the order of magnitude difference between the luminosities obtained from the 2021 and 2022 spectra. Moreover, these estimates

depend on the adopted distance and reddening values. At the same time, there might be some real variability present. The outburst activity of DeGaPe 35 is not supported by the ASAS-SN observations, but as already mentioned, the measured fluxes are contaminated by the nearby bright sources so any conclusions based on these observations are unreliable. In any case, the obtained parameters are similar to the ones observed in other shell-burning symbiotic systems (see Fig. 4 in Mikołajewska 2003 and also Muerset et al. 1991; Shen & Bildsten 2007; Munari 2019; Chapter 2.5).

4.3.4 Summary

We have presented the analysis of low-resolution spectroscopic observations, supplemented by the photometry from *Gaia* DR3 and multi-frequency SED of DeGaPe 35. This object was previously classified as an emission-line star in the scope of an amateur survey searching for new planetary nebula candidates. Our results confirm that this source is a symbiotic star whose optical spectrum shows prominent emission lines, including highly ionized [Fe VII] and O VI lines. The cool component of this symbiotic binary is an M4-5 giant with $T_{\rm eff} \sim 3\,380$ – $3\,470\,{\rm K}$ and luminosity $\sim 3 \times 10^3\,{\rm L}_\odot$ (for the adopted distance of 3 kpc). The inferred parameters of the hot component (temperature of $1 - 2 \times 10^5\,{\rm K}$ and luminosity of $\sim 10^{2-3}\,{\rm L}_\odot$) confirmed that it is a shell-burning white dwarf. The infrared data of DeGaPe 35 allowed us to classify it as an S-type symbiotic star. The photometric observations of the *Gaia* satellite, published recently in *Gaia* DR3 suggested the variability with the period of about 700 – 800 days, which we tentatively attributed to the orbital motion of the binary.

Conclusions

Symbiotic stars are among the most interesting objects that a huge variety of interacting binaries has to offer. Due to their nature and thanks to the diversity of phenomena observed in them, these systems are unique astrophysical laboratories in the study of stellar evolution, mass transfer and accretion processes, stellar winds and processes connected with their collision, thermonuclear outbursts, formation and collimation of jets, dust formation, and destruction or even variable X-ray emission.

In this thesis, we have presented the New Online Database of Symbiotic Variables, which is a modern, complex, and most up-to-date catalog of symbiotic binaries. The recent version of the New Online Database of Symbiotic Variables contains 290 confirmed symbiotic stars in our Galaxy and another 393 symbiotic candidates. The data of 70 confirmed and 103 suspected objects in 16 other galaxies are presented as well. In addition, we maintain the list of objects, which had been considered as symbiotic systems in past but are now reclassified as something else. This list of misclassified objects now contains 148 objects. The Database is published online which allows us to update the information when they become available and include the new objects as soon as they are discovered. At the same time, the Database constitutes the most comprehensive collection of orbital, stellar, and observational parameters of all known symbiotic binaries.

Several symbiotic systems are now relatively well characterized, including the parameters of both stellar components. Based on the data collected for the New Online Database of Symbiotic Variables and analyzed in this thesis, we can summarize the typical parameters of known symbiotic binaries. One should still keep in mind that the symbiotic group is quite heterogeneous and some objects differ significantly from any 'prototype'.

A typical S-type symbiotic binary ($\sim$ 77% of all symbiotic stars) would have an orbital period of 300 – 800 days, orbit close to circular, and would consist of:

- a normal giant or bright giant of a spectral type M3 – M6, semi-regularly pul-

sating with a period of 50 – 200 days, with a mass in the interval of 1 – 2.5 $M_\odot$, slightly sub-solar metallicity, loosing its mass at rate $\sim 10^{-7}\,M_\odot\,yr^{-1}$,

- a hot white dwarf with $T_{\rm eff} > 10^5$ K, luminosity $L \approx 10^2$ – $10^4\,L_\odot$, a mass in the range 0.4 – 0.8 $M_\odot$ on whose surface the shell-burning of hydrogen-rich matter accreted from the giant is present, or an accreting-only white dwarf with a similar temperature and mass but much lower luminosity $L \approx 10^1$ – $10^2\,L_\odot$,
- a circumbinary nebula formed from the matter lost by winds of the components, especially that of the giant with a size of few au, a temperature of 10^4 K, and an electron density $n_e \sim 10^8 - 10^{12}$ cm^{-3}.

There are some specific groups of S-type symbiotic systems not fitting into the picture above. In yellow symbiotic stars, a metal-poor K-type giant is found instead of the M giant. In symbiotic recurrent novae, there is a more massive white dwarf present (with a mass of 1.1 – 1.3 $M_\odot$). Moreover, a few symbiotic stars with accreting-only neutron stars have been detected. These do not manifest a typical symbiotic optical spectrum (i.e., do not have prominent emission lines in their spectra).

A typical D-type symbiotic binary has a much longer orbital period (tens of years) and its components are:

- a very evolved Mira giant of spectral type M7 – M8 with a pulsation period of 250 – 600 days surrounded by an optically thick dust envelope, the mass transfer rate of the cool component is at $10^{-5}\,M_\odot\,yr^{-1}$,
- a low mass white dwarf as in S-type systems, accreting the matter from the wind of the giant,
- a more extended (10 – 100 au) and less dense ($n_e \sim 10^6 - 10^7$ cm^{-3}) nebula.

There are also a few dusty systems whose cool component is a warmer G-type giant, these are denoted as D'-type systems and constitute about 3% of known symbiotic stars. In this thesis, we have also analyzed the symbiotic objects, which were claimed to be of a new infrared type (S+IR). Our results suggested that this class is not real and that all the objects can be easily classified in the former S/D/D' scheme.

Symbiotic systems also represent a significant population of X-ray sources. As a part of this thesis, we have evaluated the X-ray observations of the objects, which have not been analyzed in the literature before. We report on the detection or non-detection of 271 objects from the New Online Database of Symbiotic Variables, more than doubling the sample of the objects for which this information is available (from

the number of 234). The first X-ray classification is provided for 8 confirmed symbiotic binaries.

In the Database, we have collected the information on the outburst activity of symbiotic stars: 79 of the confirmed symbiotic systems are firmly established as outbursting sources, while another 9 systems might have been also observed in outbursts. Based on the data in the New Online Database of Symbiotic Variables and the literature information on individual objects, we have also suggested the model which provides possible relations between accreting-only and shell-burning symbiotic stars and all types of outbursts observed in these binaries (classical, Z And-type; 'slow' symbiotic nova; symbiotic recurrent nova), and also quiet symbiotic stars.

Our analysis confirmed many previous suggestions based on the significantly smaller samples. We have provided strong evidence that some of the stellar and orbital parameters (or their combination) are preferred for the symbiotic phenomenon to occur. This leaves several open questions, e.g., there is a clear peak in the distribution of the orbital periods of S-type symbiotic stars around 500 – 700 days, while the population synthesis models predict that most of the symbiotic stars should have orbital periods longer than 1 000 days with a maximum around 1 500 days. This discrepancy suggests that the mass transfer mechanisms in play are not fully understood and well incorporated in the models. It is still not completely clear in what fraction of symbiotic stars the mass is transferred by the Roche-lobe overflow and by the wind.

The demand for a larger sample and a better understanding of these objects is a driving force of surveys looking for them in our Galaxy and in the galaxies of the Local Group. Numerous symbiotic candidates have been discovered in recent years. Unfortunately, many of them are only poorly characterized. Moreover, the symbiotic nature of some of these candidates was suggested only based on the indistinct indications. However, many objects are not symbiotic in reality which is sometimes not reflected in the commonly used databases such as SIMBAD.

To provide a 'clean' sample of symbiotic stars which can be used for subsequent research and to increase the number of confirmed systems, we have initiated the observational campaign in order to collect sufficient material for the characterization of these objects. We have supplemented new, primarily spectroscopic data, with the available long-term light curves of the objects, multi-frequency photometric data from ground- and space-based surveys, astrometric measurements from *Gaia* satellite, and information from the literature. In this way, we subjected a substantial sample of 47 symbiotic candidates to a thorough analysis. Out of 11 classical symbiotic star

candidates, one object was confirmed to be a yellow shell-burning symbiotic system (V2204 Oph). Two other objects, Hen 4-204 and V1988 Sgr are classified as possible accreting-only symbiotic binaries. The rest of the studied symbiotic candidates was reclassified as non-symbiotic single or binary stars.

In addition, 9 symbiotic nova candidates were analyzed in detail. Three objects are confirmed as genuine 'slow' symbiotic novae: ASAS J174600-2321.3 (S-type; eclipsing), V618 Sgr (S-type; eclipsing), and V5590 Sgr (D-type). Moreover, our data showed that V618 Sgr is the first galactic 'slow' symbiotic nova that has been observed in more than one nova outburst. Our data have proved that M31N 2017-05b is not a symbiotic nova, but a classical symbiotic star. It is the first extragalactic symbiotic star discovered by the *Gaia* satellite. TYC 1371-69-1 has the appearance of a single red giant, and we classified it as a pre-symbiotic binary or possible post-symbiotic nova system. Four other studied objects were reclassified as non-symbiotic stars.

Finally, we have analyzed all 27 symbiotic candidates located in the Large Magellanic Cloud and listed in the New Online Database of Symbiotic Variables. We classified four objects as bonafide symbiotic stars (2MASS J05311676-6901041, HV 13055, [RP2006] 227, [RP2006] 295) and another four ([RP2006] 803, [BE74] 583, [RP2006] 883, 2MASS J05450015-6918192) are also possibly symbiotic objects, but more data are needed for definite classification. The rest of the candidates are classified either as planetary nebulae, other types of emission-line stars or their symbiotic-like appearance is caused by the superposition of the giant star and an emission nebula. One target is a foreground source, most probably a cataclysmic variable (RX J0550.0-7151).

We have used the tools developed for the characterization of the symbiotic candidates selected from the New Online Database of Symbiotic Variables also to study the objects that were neither known as symbiotic binaries nor suspected of a symbiotic nature in the literature. We presented the discovery and characterization of Gaia18aen, an object detected in brightening by the *Gaia* satellite and confirmed to be the first symbiotic star discovered by this European mission. We also analyzed the photometric and spectroscopic data of the new southern eclipsing symbiotic star, Hen 3-860, detected in outbursts by the ASAS-SN survey. Finally, we reported on the discovery of the southern symbiotic binary DeGaPe 35 which was identified during the amateur observational campaign of the planetary nebula candidates.

We plan to continue studying these interesting astrophysical objects in the future to reveal other properties of symbiotic systems.

Bibliography

Abdo, A. A., Ackermann, M., Ajello, M., et al. 2010, Science, 329, 817

Abril, J., Schmidtobreick, L., Ederoclite, A., & López-Sanjuan, C. 2020, MNRAS, 492, L40

Acker, A., Chopinet, M., Pottasch, S. R., & Stenholm, B. 1987, A&AS, 71, 163

Adelman, S. J. 1998, A&A, 333, 952

Ake, Thomas B., I., Johnson, H. R., & Perry, Benjamin F., J. 1988, in ESA Special Publication, Vol. 1, ESA Special Publication, ed. N. Longdon, E. J. Rolfe, Y. Kondo, & J. Sahade, 245–248

Akras, S., Gonçalves, D. R., Alvarez-Candal, A., & Pereira, C. B. 2021, MNRAS, 502, 2513

Akras, S., Guzman-Ramirez, L., Leal-Ferreira, M. L., & Ramos-Larios, G. 2019a, ApJS, 240, 21

Akras, S., Leal-Ferreira, M. L., Guzman-Ramirez, L., & Ramos-Larios, G. 2019b, MNRAS, 483, 5077

Alcock, C., Allsman, R. A., Alves, D. R., et al. 1999, PASP, 111, 1539

Allard, F. 2014, in Exploring the Formation and Evolution of Planetary Systems, ed. M. Booth, B. C. Matthews, & J. R. Graham, Vol. 299, 271–272

Allard, F., Homeier, D., & Freytag, B. 2011, in Astronomical Society of the Pacific Conference Series, Vol. 448, 16th Cambridge Workshop on Cool Stars, Stellar Systems, and the Sun, ed. C. Johns-Krull, M. K. Browning, & A. A. West, 91

Allen, D. A. 1973, MNRAS, 161, 145

Allen, D. A. 1974, MNRAS, 168, 1

Allen, D. A. 1978, MNRAS, 184, 601

Allen, D. A. 1979, in IAU Colloq. 46: Changing Trends in Variable Star Research, ed. F. M. Bateson, J. Smak, & I. H. Urch, 125

Allen, D. A. 1980a, Astrophysical Letters, 20, 131

Allen, D. A. 1980b, MNRAS, 192, 521

Allen, D. A. 1982, in Astrophysics and Space Science Library, Vol. 95, IAU Colloq. 70: The Nature of Symbiotic Stars, ed. M. Friedjung & R. Viotti, 27–42

Allen, D. A. 1984a, Proceedings of the Astronomical Society of Australia, 5, 369

Allen, D. A. 1984b, Ap&SS, 99, 101

Allen, D. A. & Glass, I. S. 1974, MNRAS, 167, 337

Aller, L. H. 1954, Astrophysics. Nuclear transformations, stellar interiors, and nebulae

Alonso, A., Arribas, S., & Martínez-Roger, C. 1999, A&AS, 140, 261

Anders, F., Khalatyan, A., Chiappini, C., et al. 2019, A&A, 628, A94

Angeloni, R., Contini, M., Ciroi, S., & Rafanelli, P. 2010, MNRAS, 402, 2075

Angeloni, R., Di Mille, F., Ferreira Lopes, C. E., & Masetti, N. 2012, ApJ, 756, L21

Angeloni, R., Ferreira Lopes, C. E., Masetti, N., et al. 2014, MNRAS, 438, 35

Anupama, G. C. 2013, in Binary Paths to Type Ia Supernovae Explosions, ed. R. Di Stefano, M. Orio, & M. Moe, Vol. 281, 154–161

Anupama, G. C. & Mikołajewska, J. 1999, A&A, 344, 177

Arkhipova, V. P., Esipov, V. F., Ikonnikova, N. P., Komissarova, G. V., & Noskova, R. I. 2011, Astronomy Letters, 37, 343

Asplund, M., Grevesse, N., Sauval, A. J., & Scott, P. 2009, ARA&A, 47, 481

Aydi, E., Buckley, D. A. H., Mikolajewska, J., et al. 2020, ATel, 14015, 1

Bailer-Jones, C. A. L., Rybizki, J., Fouesneau, M., Demleitner, M., & Andrae, R. 2021, AJ, 161, 147

Bailer-Jones, C. A. L., Rybizki, J., Fouesneau, M., Mantelet, G., & Andrae, R. 2018, AJ, 156, 58

Barlow, B. N., Corcoran, K. A., Parker, I. M., et al. 2022, ApJ, 928, 20

Beck, P. G., Mathis, S., Gallet, F., et al. 2018, MNRAS, 479, L123

Beck, P. G., Mathur, S., Hambleton, K., et al. 2022, arXiv e-prints, arXiv:2202.02373

Belczyński, K., Mikołajewska, J., Munari, U., Ivison, R. J., & Friedjung, M. 2000, A&A Sup. Ser., 146, 407

Beliakina, T. S. 1979, Izvestiya Ordena Trudovogo Krasnogo Znameni Krymskoj Astrofizicheskoj Observatorii, 59, 133

Belloni, D., Mikołajewska, J., Iłkiewicz, K., et al. 2020, MNRAS, 496, 3436

Belyakina, T. S. 1968, Soviet Ast., 12, 110

Bergner, Y. K., Miroshnichenko, A. S., Yudin, R. V., et al. 1988, Soviet Astronomy Letters, 14, 262

Berman, L. 1932, PASP, 44, 318

Bessell, M. S. & Brett, J. M. 1988, PASP, 100, 1134

Bianchi, L., Shiao, B., & Thilker, D. 2017, ApJS, 230, 24

Bidelman, W. P. 1954, ApJS, 1, 175

Binder, B., Williams, B. F., Eracleous, M., et al. 2015, AJ, 150, 94

Birkby, J., Nefs, B., Hodgkin, S., et al. 2012, MNRAS, 426, 1507

Bisikalo, D. V., Boyarchuk, A. A., Kilpio, E. Y., Tomov, N. A., & Tomova, M. T. 2006, Astronomy Reports, 50, 722

Blex, S., Hackstein, M., Haas, M., et al. 2018, IBVS, 6240, 1

Blind, N., Boffin, H. M. J., Berger, J. P., et al. 2011, A&A, 536, A55

Boffin, H. M. J., Hillen, M., Berger, J. P., et al. 2014, A&A, 564, A1

Boffin, H. M. J. & Jones, D. 2019, The Importance of Binaries in the Formation and Evolution of Planetary Nebulae

Boggess, A., Carr, F. A., Evans, D. C., et al. 1978, Nature, 275, 372

Bond, H. E. 1976, PASP, 88, 192

Bond, H. E. 1978, PASP, 90, 526

Bond, H. E. & Kasliwal, M. M. 2012, PASP, 124, 1262

Boyarchuk, A. A. 1969, Commmunications of the Konkoly Observatory Hungary, 65, 395

Bozzo, E., Bahramian, A., Ferrigno, C., et al. 2018, A&A, 613, A22

Bozzo, E., Romano, P., Ferrigno, C., & Oskinova, L. 2022, MNRAS, 513, 42

Branch, D., Livio, M., Yungelson, L. R., Boffi, F. R., & Baron, E. 1995, PASP, 107, 1019

Bruce, C. E. R. 1955, The Observatory, 75, 82

Butters, O. W., West, R. G., Anderson, D. R., et al. 2010, A&A, 520, L10

Buzzoni, A., Patelli, L., Bellazzini, M., Pecci, F. F., & Oliva, E. 2010, MNRAS, 403, 1592

Cannon, A. J. 1920, Harvard College Observatory Circular, 221, 1

Cannon, A. J., Fleming, W., & Pickering, E. C. 1911, Harvard College Observatory Circular, 168, 1

Cannon, A. J. & Shapley, H. 1923, Annals of Harvard College Observatory, 81, 179

Cardelli, J. A., Clayton, G. C., & Mathis, J. S. 1989, ApJ, 345, 245

Carpenter, J. M. 2001, AJ, 121, 2851

Catalán, S., Isern, J., García-Berro, E., & Ribas, I. 2008, MNRAS, 387, 1693

Charles, P. A., Southwell, K. A., & O'Donoghue, D. 1996, IAU Circ., 6305, 2

Chiotellis, A., Schure, K. M., & Vink, J. 2012, A&A, 537, A139

Choi, J., Dotter, A., Conroy, C., et al. 2016, ApJ, 823, 102

Chomiuk, L., Metzger, B. D., & Shen, K. J. 2021, ARA&A, 59

Corbet, R. H. D., Sokoloski, J. L., Mukai, K., Markwardt, C. B., & Tueller, J. 2008, ApJ, 675, 1424

Corradi, R. L. M., Brandi, E., Ferrer, O. E., & Schwarz, H. E. 1999, A&A, 343, 841

Corradi, R. L. M., Rodríguez-Flores, E. R., Mampaso, A., et al. 2008, A&A, 480, 409

Corradi, R. L. M. & Schwarz, H. E. 1993, A&A, 268, 714

Corradi, R. L. M., Valentini, M., Munari, U., et al. 2010, A&A, 509, A41

Creevey, O. L., Sordo, R., Pailler, F., et al. 2022, arXiv e-prints, arXiv:2206.05864

Cruz-Sáenz de Miera, F., Kóspál, Á., Ábrahám, P., et al. 2022, ApJ, 927, 125

Cummings, J. D., Kalirai, J. S., Tremblay, P. E., Ramirez-Ruiz, E., & Choi, J. 2018, ApJ, 866, 21

Dahlmark, L. 2000, IBVS, 4898, 1

Dahm, S. E. & Simon, T. 2005, AJ, 129, 829

De, K., Mereminskiy, I., Soria, R., et al. 2022, arXiv e-prints, arXiv:2205.09139

de Boer, K. & Seggewiss, W. 2008, Stars and Stellar Evolution

de Jager, C. & Nieuwenhuijzen, H. 1987, A&A, 177, 217

de Val-Borro, M., Karovska, M., Sasselov, D. D., & Stone, J. M. 2017, MNRAS, 468, 3408

Delgado, A., Harrison, D., Hodgkin, S., et al. 2017, TNS Discovery Report, 2017-591, 1

Delgado, A., Harrison, D., Hodgkin, S., et al. 2018, TNS Discovery Report, 2018-84, 1

Di Stefano, R. 2010, ApJ, 719, 474

Dilday, B., Howell, D. A., Cenko, S. B., et al. 2012, Science, 337, 942

Dobrzycka, D., Kenyon, S. J., & Milone, A. A. E. 1996, AJ, 111, 414

Downes, R. A., Webbink, R. F., Shara, M. M., et al. 2001, PASP, 113, 764

Dubovský, P. A., Merc, J., Gális, R., & Wolf, M. 2021, RNAAS, 5, 11

Earnshaw, H. P., Roberts, T. P., Middleton, M. J., Walton, D. J., & Mateos, S. 2019, MNRAS, 483, 5554

Enoto, T., Sasano, M., Yamada, S., et al. 2014, ApJ, 786, 127

Evans, P. A., Page, K. L., Osborne, J. P., et al. 2020, ApJS, 247, 54

Eyer, L., Audard, M., Holl, B., et al. 2022, arXiv e-prints, arXiv:2206.06416

Fajardo-Acosta, S. B., Kirkpatrick, J. D., Schneider, A. C., et al. 2016, ApJ, 832, 62

Falcón-Barroso, J., Sánchez-Blázquez, P., Vazdekis, A., et al. 2011, A&A, 532, A95

Farias, D. A., Clocchiatti, A., Woods, T. E., & Rest, A. 2020, MNRAS, 497, 3234

Feast, M. W. & Webster, B. L. 1974, MNRAS, 168, 31P

Fekel, F. C., Hinkle, K. H., Joyce, R. R., & Skrutskie, M. F. 2000a, AJ, 120, 3255

Fekel, F. C., Hinkle, K. H., Joyce, R. R., & Skrutskie, M. F. 2001, AJ, 121, 2219

Fekel, F. C., Hinkle, K. H., Joyce, R. R., & Wood, P. R. 2010, AJ, 139, 1315

Fekel, F. C., Hinkle, K. H., Joyce, R. R., & Wood, P. R. 2015, AJ, 150, 48

Fekel, F. C., Hinkle, K. H., Joyce, R. R., & Wood, P. R. 2017, AJ, 153, 35

Fekel, F. C., Hinkle, K. H., Joyce, R. R., Wood, P. R., & Howarth, I. D. 2008, AJ, 136, 146

Fekel, F. C., Hinkle, K. H., Joyce, R. R., Wood, P. R., & Lebzelter, T. 2007, AJ, 133, 17

Fekel, F. C., Joyce, R. R., Hinkle, K. H., & Skrutskie, M. F. 2000b, AJ, 119, 1375

Fleming, W. P. S. & Pickering, E. C. 1912, Annals of Harvard College Observatory, 56, 165

Flewelling, H. A., Magnier, E. A., Chambers, K. C., et al. 2020, ApJS, 251, 7

Fluks, M. A., Plez, B., The, P. S., et al. 1994, A&AS, 105, 311

Fouesneau, M., Frémat, Y., Andrae, R., et al. 2022, arXiv e-prints, arXiv:2206.05992

Frew, D. J., Stanger, J., Fitzgerald, M., et al. 2011, PASA, 28, 83

Friedjung, M., Hric, L., Petrik, K., & Gális, R. 1998, A&A, 335, 545

Friedjung, M. & Viotti, R. 1982, The nature of symbiotic stars; Proceedings of the Seventieth

Colloquium, Saint-Michel-l'Observatoire, Alpes-de-Haute-Provence, France, August 26-28, 1981, Vol. 95

Frith, J., Pinfield, D. J., Jones, H. R. A., et al. 2013, MNRAS, 435, 2161

Fujimoto, M. Y. 1982a, ApJ, 257, 767

Fujimoto, M. Y. 1982b, ApJ, 257, 752

Gahm, G. F., Kolotilov, E. A., Petrov, P. P., Shcherbakov, A. G., & Shanin, G. I. 1975, Astronomicheskij Tsirkulyar, 852, 5

Gaia Collaboration, Babusiaux, C., van Leeuwen, F., et al. 2018, A&A, 616, A10

Gaia Collaboration, Brown, A. G. A., Vallenari, A., et al. 2021, A&A, 649, A1

Gaia Collaboration, Prusti, T., de Bruijne, J. H. J., et al. 2016, A&A, 595, A1

Gaia Collaboration, Vallenari, A., Brown, A. G. A., Prusti, T., & et al. 2022, A&A

Gałan, C., Mikołajewska, J., & Hinkle, K. H. 2015, MNRAS, 447, 492

Gałan, C., Mikołajewska, J., Hinkle, K. H., & Joyce, R. R. 2016, MNRAS, 455, 1282

Gałan, C., Mikołajewska, J., Hinkle, K. H., & Joyce, R. R. 2017, MNRAS, 466, 2194

Gałan, C., Mikołajewska, J., Monard, B., et al. 2019, Acta Astron., 69, 25

Gális, R., Hric, L., Friedjung, M., & Petrík, K. 1999, A&A, 348, 533

Gaposchkin, C. H. P. 1957, The Galactic Novae

Gavrilchenko, T., Klein, C. R., Bloom, J. S., & Richards, J. W. 2014, MNRAS, 441, 715

Glass, I. S. & Feast, M. W. 1982, MNRAS, 199, 245

Gonçalves, D. R., Magrini, L., de la Rosa, I. G., & Akras, S. 2015, MNRAS, 447, 993

Gonçalves, D. R., Magrini, L., Martins, L. P., Teodorescu, A. M., & Quireza, C. 2012, MNRAS, 419, 854

Gonçalves, D. R., Magrini, L., Munari, U., Corradi, R. L. M., & Costa, R. D. D. 2008, MNRAS, 391, L84

González-Riestra, R., Viotti, R., Iijima, T., & Greiner, J. 1999, A&A, 347, 478

Griffin, R. F. 1984, The Observatory, 104, 224

Gromadzki, M. & Mikołajewska, J. 2009, A&A, 495, 931

Gromadzki, M., Mikołajewska, J., Borawska, M., & Lednicka, A. 2007, Baltic Astronomy, 16, 37

Gromadzki, M., Mikołajewska, J., & Soszyński, I. 2013, Acta Astron., 63, 405

Gromadzki, M., Mikołajewska, J., Whitelock, P., & Marang, F. 2009, Acta Astron., 59, 169

Gromadzki, M., Mikolajewski, M., Tomov, T., et al. 2006, Acta Astron., 56, 97

Guerrero, M. A., Cazzoli, S., Rechy-García, J. S., et al. 2021, ApJ, 909, 44

Guilbault, P. R., Hager, T., Henden, A., et al. 2000, IBVS, 4926, 1

Gustafsson, B., Edvardsson, B., Eriksson, K., et al. 2008, A&A, 486, 951

Gutierrez-Moreno, A., Moreno, H., & Cortes, G. 1995, PASP, 107, 462

Haas, M., Hackstein, M., Ramolla, M., et al. 2012, AN, 333, 706

Hachisu, I. & Kato, M. 2001, ApJ, 558, 323

Hachisu, I., Kato, M., & Nomoto, K. 1999, ApJ, 522, 487

Hackstein, M., Fein, C., Haas, M., et al. 2015, AN, 336, 590

Hambsch, F. J., Hümmerich, S., Bernhard, K., & Otero, S. 2015, JAAVSO, 43, 213

Hellier, C. 2001, Cataclysmic Variable Stars

Henden, A., Simonsen, M., & Sumner, B. 2003, IBVS, 5368, 1

Henden, A. A., Levine, S., Terrell, D., & Welch, D. L. 2015, in American Astronomical Society Meeting Abstracts, Vol. 225, American Astronomical Society Meeting Abstracts #225, 336.16

Henize, K. G. 1976, ApJS, 30, 491

Henleywillis, S., Cool, A. M., Haggard, D., et al. 2018, MNRAS, 479, 2834

Herbig, G. H. & Kameswara Rao, N. 1972, ApJ, 174, 401

Herwig, F. 2005, ARA&A, 43, 435

Hillen, M., Verhoelst, T., Van Winckel, H., et al. 2013, A&A, 559, A111

Hillenbrand, L. A., Contreras Peña, C., Morrell, S., et al. 2018, ApJ, 869, 146

Hillman, Y., Prialnik, D., Kovetz, A., & Shara, M. M. 2016, ApJ, 819, 168

Hillman, Y., Prialnik, D., Kovetz, A., Shara, M. M., & Neill, J. D. 2014, MNRAS, 437, 1962

Hinkle, K. H., Fekel, F. C., Johnson, D. S., & Scharlach, W. W. G. 1993, AJ, 105, 1074

Hinkle, K. H., Fekel, F. C., & Joyce, R. R. 2009, ApJ, 692, 1360

Hinkle, K. H., Fekel, F. C., Joyce, R. R., et al. 2019, ApJ, 872, 43

Hinkle, K. H., Fekel, F. C., Joyce, R. R., et al. 2006, ApJ, 641, 479

Hodge, P. W. & Wright, F. W. 1970, PASP, 82, 135

Hodgkin, S. T., Harrison, D. L., Breedt, E., et al. 2021, A&A, 652, A76

Hodgkin, S. T., Wyrzykowski, L., Blagorodnova, N., & Koposov, S. 2013, Philosophical Transactions of the Royal Society of London Series A, 371, 20120239

Hoffleit, D. 1962, AJ, 67, 228

Hogg, F. S. 1932, PASP, 44, 328

Honeycutt, R. K. & Kafka, S. 2010, AJ, 139, 2706

Hoyman, B., Bulut, S., Özdarcan, O., & Çakırlı, Ö. 2020, MNRAS, 496, 550

Hric, L., Gális, R., Leedjärv, L., Burmeister, M., & Kundra, E. 2014, MNRAS, 443, 1103

Hric, L., Skopal, A., Chochol, D., et al. 1994, CAOSP, 24, 31

Hric, L., Skopal, A., Urban, Z., et al. 1991, CAOSP, 21, 303

Hric, L., Skopal, A., Urban, Z., et al. 1996, CAOSP, 26, 121

Hric, V., Skopal, A., Urban, Z., et al. 1993, CAOSP, 23, 73

Hümmerich, S., Otero, S., Tisserand, P., & Bernhard, K. 2015, JAAVSO, 43, 14

Hurley, J. R., Tout, C. A., & Pols, O. R. 2002, MNRAS, 329, 897

Husser, T. O., Wende-von Berg, S., Dreizler, S., et al. 2013, A&A, 553, A6

Iben, I., J. 1982, ApJ, 259, 244

Iben, Icko, J. & Tutukov, A. V. 1996, ApJS, 105, 145

Iijima, T. 1981a, in Photometric and Spectroscopic Binary Systems, 517

Iijima, T. 1981b, in NATO Advanced Study Institute (ASI) Series C, Vol. 69, Photometric and Spectroscopic Binary Systems, 517

Iijima, T. 2015, AJ, 150, 20

Iijima, T. & Naito, H. 2017, A&A, 600, A96

Iijima, T., Naito, H., & Narusawa, S. 2019, A&A, 622, A45

Ikonnikova, N. P., Burlak, M. A., Arkhipova, V. P., & Esipov, V. F. 2019a, Astronomy Letters, 45, 217

Ikonnikova, N. P., Komissarova, G. V., & Arkhipova, V. P. 2019b, Astronomy Letters, 45, 361

Iłkiewicz, K. & Mikołajewska, J. 2017, A&A, 606, A110

Iłkiewicz, K., Mikołajewska, J., Belczyński, K., Wiktorowicz, G., & Karczmarek, P. 2019a, MNRAS, 485, 5468

Iłkiewicz, K., Mikołajewska, J., Miszalski, B., et al. 2019b, A&A, 624, A133

Iłkiewicz, K., Mikołajewska, J., Miszalski, B., Kozłowski, S., & Udalski, A. 2018, MNRAS, 476, 2605

Iłkiewicz, K., Mikołajewska, J., Scaringi, S., et al. 2022, MNRAS, 510, 2707

Ilkiewicz, K., Mikolajewska, J., Shara, M. M., et al. 2018, arXiv e-prints, arXiv:1811.06696

Ishihara, D., Onaka, T., Kataza, H., et al. 2010, A&A, 514, A1

Ivison, R. J., Seaquist, E. R., Schwarz, H. E., Hughes, D. H., & Bode, M. F. 1995, MNRAS, 273, 517

Jencson, J. E., Andrews, J. E., Bond, H. E., et al. 2021, ApJ, 920, 127

Jorissen, A. & Mayor, M. 1992, A&A, 260, 115

Kafka, S. 2022, Observations from the AAVSO International Database

Kamath, D., Van Winckel, H., Ventura, P., et al. 2022, ApJ, 927, L13

Kamath, D., Wood, P. R., & Van Winckel, H. 2015, MNRAS, 454, 1468

Karachentsev, I. D. & Kashibadze, O. G. 2006, Astrophysics, 49, 3

Kato, D., Nagashima, C., Nagayama, T., et al. 2007, PASJ, 59, 615

Kato, M., Mikołajewska, J., & Hachisu, I. 2012, ApJ, 750, 5

Kato, T., Yamaoka, H., Torii, K., Ishioka, R., & Uemura, M. 2002, IBVS, 5342, 1

Keenan, P. C. & Boeshaar, P. C. 1980, ApJS, 43, 379

Kenyon, S. J. 1986, The symbiotic stars (Cambridge: University Press)

Kenyon, S. J. 1994, Mem. Soc. Astron. Italiana, 65, 135

Kenyon, S. J. & Fernandez-Castro, T. 1987, AJ, 93, 938

Kenyon, S. J., Fernandez-Castro, T., & Stencel, R. E. 1988, AJ, 95, 1817

Kenyon, S. J. & Garcia, M. R. 1989, AJ, 97, 194

Kenyon, S. J., Livio, M., Mikolajewska, J., & Tout, C. A. 1993, ApJ, 407, L81

Kenyon, S. J., Oliversen, N. A., Mikolajewska, J., et al. 1991, AJ, 101, 637

Kenyon, S. J. & Truran, J. W. 1983, ApJ, 273, 280

Kenyon, S. J. & Webbink, R. F. 1984, ApJ, 279, 252

Kepler, S. O., Pelisoli, I., Koester, D., et al. 2015, MNRAS, 446, 4078

Kepler, S. O., Pelisoli, I., Koester, D., et al. 2016, MNRAS, 455, 3413

Kesseli, A. Y., West, A. A., Veyette, M., et al. 2017, ApJS, 230, 16

Kilkenny, D. 1989, The Observatory, 109, 229

Kirk, B., Conroy, K., Prša, A., et al. 2016, AJ, 151, 68

Kleinman, S. J., Kepler, S. O., Koester, D., et al. 2013, ApJS, 204, 5

Kniazev, A. Y., Väisänen, P., Whitelock, P. A., et al. 2009, MNRAS, 395, 1121

Kochanek, C. S., Shappee, B. J., Stanek, K. Z., et al. 2017, PASP, 129, 104502

Koester, D. 2010, Mem. Soc. Astron. Italiana, 81, 921

Kohoutek, L. 1962, Bulletin of the Astronomical Institutes of Czechoslovakia, 13, 120

Kolb, U., Brodeur, M., Braithwaite, N., & Minocha, S. 2018, Robotic Telescope, Student Research and Education Proceedings, 1, 127

Kolotilov, E. A. 1988, Astrofizika, 29, 458

Kolotilov, E. A., Munari, U., Yudin, B. F., & Tatarnikov, A. M. 1996, Astronomy Reports, 40, 812

Kondratyeva, L. & Rspaev, F. 2013, IBVS, 6056, 1

Kopylov, I. M., Lipovetskii, V. A., Somov, N. N., Somova, T. A., & Stepanyan, D. A. 1988a, Astrophysics, 28, 168

Kopylov, I. M., Lipovetsky, V. A., Somov, N. N., Somova, T. A., & Stepanian, J. A. 1988b, Astrofizika, 28, 287

Kraus, M., Borges Fernandes, M., & de Araujo, F. X. 2007, in Astronomical Society of the Pacific Conference Series, Vol. 367, Massive Stars in Interactive Binaries, ed. N. St. -Louis & A. F. J. Moffat, 349

Kruszynska, K., Gromadzki, M., Wyrzykowski, L., et al. 2018, ATel, 11634, 1

Kuiper, G. P. 1941, ApJ, 93, 133

Kuranov, A. G. & Postnov, K. A. 2015, Astronomy Letters, 41, 114

Lasker, B. M., Lattanzi, M. G., McLean, B. J., et al. 2008, AJ, 136, 735

Laycock, S., Tang, S., Grindlay, J., et al. 2010, AJ, 140, 1062

Lebzelter, T., Mowlavi, N., Lecoeur-Taibi, I., et al. 2022, arXiv e-prints, arXiv:2206.05745

Lebzelter, T., Trabucchi, M., Mowlavi, N., et al. 2019, A&A, 631, A24

Leedjärv, L. 2004, Baltic Astronomy, 13, 109

Leedjärv, L., Burmeister, M., Mikołajewski, M., et al. 2004, A&A, 415, 273

Leedjärv, L., Gális, R., Hric, L., Merc, J., & Burmeister, M. 2016, MNRAS, 456, 2558
Leibowitz, E. M. & Formiggini, L. 2006, MNRAS, 366, 675
Leonidaki, I., Zezas, A., & Boumis, P. 2010, ApJ, 725, 842
Lépine, S. & Gaidos, E. 2011, AJ, 142, 138
Lewis, H. M., Anguiano, B., Stassun, K. G., et al. 2020, ApJ, 900, L43
Lindegren, L., Bastian, U., Biermann, M., et al. 2021a, A&A, 649, A4
Lindegren, L., Hernández, J., Bombrun, A., et al. 2018, A&A, 616, A2
Lindegren, L., Klioner, S. A., Hernández, J., et al. 2021b, A&A, 649, A2
Lindsay, E. M. 1971, Irish Astronomical Journal, 10, 141
Linford, J. D., Chomiuk, L., Nelson, T., et al. 2017, ApJ, 842, 73
Lipovetsky, V. A. & Stepanian, J. A. 1981, Astrofizika, 17, 573
Liu, J. 2011, ApJS, 192, 10
Lü, G., Yungelson, L., & Han, Z. 2006, MNRAS, 372, 1389
Lü, G. L., Zhu, C. H., Postnov, K. A., et al. 2012, MNRAS, 424, 2265
Lucy, A. B. 2021, PhD thesis, Columbia University, New York
Lucy, A. B., Knigge, C., & Sokoloski, J. L. 2018, MNRAS, 478, 568
Luna, G. J. M. & Sokoloski, J. L. 2007, ApJ, 671, 741
Luna, G. J. M., Sokoloski, J. L., Mukai, K., & Nelson, T. 2013, A&A, 559, A6
Luri, X., Brown, A. G. A., Sarro, L. M., et al. 2018, A&A, 616, A9
Magrini, L., Corradi, R. L. M., & Munari, U. 2003, Astronomical Society of the Pacific Conference Series, Vol. 303, A Search for Symbiotic Stars in the Local Group, ed. R. L. M. Corradi, J. Mikolajewska, & T. J. Mahoney, 539
Magrini, L., Gonçalves, D. R., & Vajgel, B. 2017, MNRAS, 464, 739
Malkov, O., Kovaleva, D., Sichevsky, S., & Zhao, G. 2020, Research in A&A, 20, 139
Marcu, D. M., Fürst, F., Pottschmidt, K., et al. 2011, ApJ, 742, L11
Marigo, P. 2013, in Binary Paths to Type Ia Supernovae Explosions, ed. R. Di Stefano, M. Orio, & M. Moe, Vol. 281, 36–43
Marton, G., Ábrahám, P., Rimoldini, L., et al. 2022, arXiv e-prints, arXiv:2206.05796
Masci, F. J., Laher, R. R., Rusholme, B., et al. 2019, PASP, 131, 018003
Masetti, N., Landi, R., Pretorius, M. L., et al. 2007, A&A, 470, 331
Mattsson, L., Höfner, S., & Herwig, F. 2007, A&A, 470, 339
Mazeh, T. 2008, in EAS Publications Series, Vol. 29, EAS Publications Series, ed. M. J. Goupil & J. P. Zahn, 1–65
McConnachie, A. W., Irwin, M. J., Ferguson, A. M. N., et al. 2005, MNRAS, 356, 979
Medina Tanco, G. A. & Steiner, J. E. 1995, AJ, 109, 1770
Meinunger, I. 1980, Veroeffentlichungen der Sternwarte Sonneberg, 9, 197
Meng, X. & Han, Z. 2016, A&A, 588, A88

Menzel, D. 1946, Physica, 12, 769

Merc, J., Charbonnel, S., Garde, O., et al. 2022a, RNAAS, 6, 54

Merc, J., Galis, R., Charbonnel, S., et al. 2021a, ATel, 14691, 1

Merc, J., Gális, R., Kára, J., Wolf, M., & Vrašťák, M. 2020a, MNRAS, 499, 2116

Merc, J., Gális, R., & Leedjärv, L. 2017, in The Golden Age of Cataclysmic Variables and Related Objects IV, 60

Merc, J., Gális, R., & Teyssier, F. 2019a, CAOSP, 49, 228

Merc, J., Galis, R., Velez, P., et al. 2021b, ATel, 14874, 1

Merc, J., Gális, R., & Wolf, M. 2019b, RNAAS, 3, 28

Merc, J., Gális, R., & Wolf, M. 2019c, AN, 340, 598

Merc, J., Gális, R., & Wolf, M. 2021c, in The 20.5th Cambridge Workshop on Cool Stars, Stellar Systems, and the Sun (CS20.5), Cambridge Workshop on Cool Stars, Stellar Systems, and the Sun, 158

Merc, J., Gális, R., Wolf, M., et al. 2022b, MNRAS, 510, 1404

Merc, J., Gális, R., Wolf, M., et al. 2021d, MNRAS, 506, 4151

Merc, J., Mikołajewska, J., Gromadzki, M., et al. 2020b, A&A, 644, A49

Merc, J., Velez, P., Barker, H., et al. 2022c, ATel, 15340, 1

Merrill, P. W. 1919, PASP, 31, 305

Merrill, P. W. 1933, ApJ, 77, 44

Merrill, P. W. 1958, in Liege International Astrophysical Colloquia, Vol. 8, Liege International Astrophysical Colloquia, 436–448

Merrill, P. W. & Humason, M. L. 1932, PASP, 44, 56

Mikołajewska, J. 2002, MNRAS, 335, L33

Mikołajewska, J. 2003, in Astronomical Society of the Pacific Conference Series, Vol. 303, Symbiotic Stars Probing Stellar Evolution, ed. R. L. M. Corradi, J. Mikolajewska, & T. J. Mahoney, 9

Mikołajewska, J. 2007, Baltic Astronomy, 16, 1

Mikołajewska, J. 2010, arXiv e-prints, arXiv:1011.5657

Mikołajewska, J. 2012, Baltic Astronomy, 21, 5

Mikołajewska, J. 2013, in IAU Symposium, Vol. 281, Binary Paths to Type Ia Supernovae Explosions, ed. R. Di Stefano, M. Orio, & M. Moe, 162–165

Mikolajewska, J., Acker, A., & Stenholm, B. 1997, A&A, 327, 191

Mikołajewska, J., Caldwell, N., & Shara, M. M. 2014a, MNRAS, 444, 586

Mikołajewska, J., Gałan, C., Hinkle, K. H., Gromadzki, M., & Schmidt, M. R. 2014b, MNRAS, 440, 3016

Mikolajewska, J., Gromadzki, M., & Hinkle, K. H. 2006, in IAU Symposium, Vol. 232, The Scientific Requirements for Extremely Large Telescopes, ed. P. Whitelock, M. Dennefeld,

& B. Leibundgut, 278–280
Mikołajewska, J., Iłkiewicz, K., Gałan, C., et al. 2021, MNRAS, 504, 2122
Mikołajewska, J., Ivison, R. J., & Omont, A. 2002, Advances in Space Research, 30, 2045
Mikolajewska, J. & Kenyon, S. J. 1992a, AJ, 103, 579
Mikolajewska, J. & Kenyon, S. J. 1992b, MNRAS, 256, 177
Mikolajewska, J. & Kenyon, S. J. 1996, AJ, 112, 1659
Mikolajewska, J., Kenyon, S. J., Mikolajewski, M., Garcia, M. R., & Polidan, R. S. 1995, AJ, 109, 1289
Mikołajewska, J. & Shara, M. M. 2017, ApJ, 847, 99
Mikołajewska, J., Shara, M. M., Caldwell, N., Iłkiewicz, K., & Zurek, D. 2017, MNRAS, 465, 1699
Mikolajewski, M., Mikolajewska, J., & Khudiakova, T. N. 1990, A&A, 235, 219
Miller, A. A., Hillenbrand, L. A., Covey, K. R., et al. 2011, ApJ, 730, 80
Mineo, S., Gilfanov, M., & Sunyaev, R. 2012, MNRAS, 419, 2095
Miszalski, B. & Mikołajewska, J. 2014, MNRAS, 440, 1410
Miszalski, B., Mikołajewska, J., & Udalski, A. 2013, MNRAS, 432, 3186
Miszalski, B., Mikolajewska, J., & Udalski, A. 2014, MNRAS, 444, L11
Miszalski, B., Napiwotzki, R., Cioni, M. R. L., et al. 2011, A&A, 531, A157
Moe, M. & Di Stefano, R. 2017, ApJS, 230, 15
Mohamed, S. & Podsiadlowski, P. 2012, Baltic Astronomy, 21, 88
Morgan, D. H., Watson, F. G., & Parker, Q. A. 1992, A&AS, 93, 495
Mowlavi, N., Rimoldini, L., Evans, D. W., et al. 2021, A&A, 648, A44
Mróz, P., Poleski, R., Udalski, A., et al. 2014, MNRAS, 443, 784
Mroz, P. & Udalski, A. 2020, ATel, 14017, 1
Mróz, P., Udalski, A., Poleski, R., et al. 2015, ApJS, 219, 26
Muerset, U., Nussbaumer, H., Schmid, H. M., & Vogel, M. 1991, A&A, 248, 458
Muerset, U., Wolff, B., & Jordan, S. 1997, A&A, 319, 201
Mukai, K., Luna, G. J. M., Cusumano, G., et al. 2016, MNRAS, 461, L1
Munari, U. 2012, JAAVSO, 40, 572
Munari, U. 2019, The Impact of Binary Stars on Stellar Evolution, 54, 77
Munari, U., Alcalà, J. K., Frasca, A., et al. 2022, arXiv e-prints, arXiv:2203.05453
Munari, U. & Banerjee, D. P. K. 2018, MNRAS, 475, 508
Munari, U., Dallaporta, S., Righetti, G. L., Castellani, F., & Cherini, G. 2014, ATel, 6382, 1
Munari, U., Graziani, M., & Jurdana-Sepic, R. 2016, IBVS, 6176, 1
Munari, U., Henden, A., Vallenari, A., et al. 2005, A&A, 434, 1107
Munari, U., Jurdana-Šepić, R., & Moro, D. 2001a, A&A, 370, 503

Munari, U., Margoni, R., & Stagni, R. 1990, MNRAS, 242, 653

Munari, U., Ochner, P., Dallaporta, S., et al. 2012, ATel, 4265, 1

Munari, U. & Patat, F. 1993, A&A, 277, 195

Munari, U. & Renzini, A. 1992, ApJ, 397, L87

Munari, U. & Righetti, G. L. 2016, ATel, 8975, 1

Munari, U., Righetti, G. L., Sollecchia, U., & Castellani, F. 2015, ATel, 7582, 1

Munari, U., Righetti, G. L., Valisa, P., Buzzi, L., & Moretti, S. 2017, ATel, 10390, 1

Munari, U., Siviero, A., Corradi, R. L. M., et al. 2010, CBET, 2555, 1

Munari, U., Siviero, A., Dallaporta, S., et al. 2009a, CBET, 1757, 1

Munari, U., Siviero, A., Ochner, P., et al. 2009b, PASP, 121, 1070

Munari, U., Tomov, T., Yudin, B. F., et al. 2001b, A&A, 369, L1

Munari, U., Traven, G., Masetti, N., et al. 2021, MNRAS, 505, 6121

Munari, U. & Valisa, P. 2021, arXiv e-prints, arXiv:2109.01101

Munari, U. & Valisa, P. 2022, arXiv e-prints, arXiv:2203.01378

Munari, U. & Zwitter, T. 2002, A&A, 383, 188

Murset, U. & Nussbaumer, H. 1994, A&A, 282, 586

Mürset, U. & Schmid, H. M. 1999, A&AS, 137, 473

Nakano, S., Itagaki, K., Kaneda, H., et al. 2012, CBET, 3140, 1

Neugebauer, G. & Leighton, R. B. 1969, Two-micron sky survey. A preliminary catalogue

Nie, J. D., Wood, P. R., & Nicholls, C. P. 2012, MNRAS, 423, 2764

Nomoto, K., Saio, H., Kato, M., & Hachisu, I. 2007, ApJ, 663, 1269

Nuñez, N. E., Nelson, T., Mukai, K., Sokoloski, J. L., & Luna, G. J. M. 2016, ApJ, 824, 23

Nussbaumer, H. & Vogel, M. 1987, A&A, 182, 51

O'Donoghue, D., Kilkenny, D., Koen, C., et al. 2013, MNRAS, 431, 240

Oliversen, N. A., Anderson, C. M., Cassinelli, J. P., Sand ers, W. T., & Kaler, J. B. 1980, in BAAS, Vol. 12, 819

Osterbrock, D. E. & Ferland, G. J. 2006, Astrophysics of gaseous nebulae and active galactic nuclei

Paczynski, B. 1976, in IAU Symposium, Vol. 73, Structure and Evolution of Close Binary Systems, ed. P. Eggleton, S. Mitton, & J. Whelan, 75

Page, K. L., Beardmore, A. P., Osborne, J. P., et al. 2022, arXiv e-prints, arXiv:2205.03232

Pagnotta, A. & Schaefer, B. E. 2014, ApJ, 788, 164

Parker, Q. A., Bojičić, I. S., & Frew, D. J. 2016, in Journal of Physics Conference Series, Vol. 728, Journal of Physics Conference Series, 032008

Patat, F., Chugai, N. N., Podsiadlowski, P., et al. 2011, A&A, 530, A63

Paxton, B., Bildsten, L., Dotter, A., et al. 2011, ApJS, 192, 3

Peimbert, M., Peimbert, A., & Delgado-Inglada, G. 2017, PASP, 129, 082001

Pereira, C. B., Baella, N. O., Drake, N. A., Miranda, L. F., & Roig, F. 2017, ApJ, 841, 50
Pereira, C. B., Franco, C. S., & de Araújo, F. X. 2003, A&A, 397, 927
Piascik, A. S., Steele, I. A., Bates, S. D., et al. 2014, in Society of Photo-Optical Instrumentation Engineers (SPIE) Conference Series, Vol. 9147, Ground-based and Airborne Instrumentation for Astronomy V, ed. S. K. Ramsay, I. S. McLean, & H. Takami, 91478H
Pickering, E. C., Colson, H. R., Fleming, W. P., & Wells, L. D. 1901, ApJ, 13, 226
Pickles, A. J. 1998, PASP, 110, 863
Podsiadlowski, P. & Mohamed, S. 2007, Baltic Astronomy, 16, 26
Pojmanski, G. 1997, Acta Astron., 47, 467
Price, S. D., Egan, M. P., Carey, S. J., Mizuno, D. R., & Kuchar, T. A. 2001, AJ, 121, 2819
Proga, D., Mikolajewska, J., & Kenyon, S. J. 1994, MNRAS, 268, 213
Prša, A., Batalha, N., Slawson, R. W., et al. 2011, AJ, 141, 83
Quiroga, C., Mikołajewska, J., Brandi, E., Ferrer, O., & García, L. 2002, A&A, 387, 139
Ramos-Larios, G. & Phillips, J. P. 2005, MNRAS, 357, 732
Ramsay, G., Sokoloski, J. L., Luna, G. J. M., & Nuñez, N. E. 2016, MNRAS, 461, 3599
Reid, W. A. 2014, MNRAS, 438, 2642
Reid, W. A. & Parker, Q. A. 2006, MNRAS, 373, 521
Reid, W. A. & Parker, Q. A. 2010, MNRAS, 405, 1349
Reid, W. A. & Parker, Q. A. 2012, MNRAS, 425, 355
Reimers, D., Griffin, R. F., & Brown, A. 1988, A&A, 193, 180
Relaño, M., Kennicutt, R., Lisenfeld, U., et al. 2016, A&A, 595, A43
Ren, J. J., Rebassa-Mansergas, A., Luo, A. L., et al. 2014, A&A, 570, A107
Renault, C., Aubourg, E., Bareyre, P., et al. 1998, A&A, 329, 522
Ricker, G. R., Winn, J. N., Vanderspek, R., et al. 2015, Journal of Astronomical Telescopes, Instruments, and Systems, 1, 014003
Rigollet, R. 1947, L'Astronomie, 61, 247
Rodríguez-Flores, E. R., Corradi, R. L. M., Mampaso, A., et al. 2014, A&A, 567, A49
Roming, P. W. A., Kennedy, T. E., Mason, K. O., et al. 2005, Space Sci. Rev., 120, 95
Ross, F. E. 1926, AJ, 36, 122
Roth, M. M., Sandin, C., Kamann, S., et al. 2018, A&A, 618, A3
Rutkowski, A., Mikołajewska, J., & Whitelock, P. A. 2007, Baltic Astronomy, 16, 49
Saeedi, S., Liu, T., Knies, J., et al. 2022, arXiv e-prints, arXiv:2106.14535
Saeedi, S. & Sasaki, M. 2020, MNRAS, 499, 3111
Saeedi, S. & Sasaki, M. 2022, MNRAS, 512, 5481
Sahai, R. & Nyman, L.-Å. 2000, ApJ, 538, L145
Samus', N. N. 1983, Zentralinstitut fuer Astrophysik Sternwarte Sonneberg Mitteilungen ueber Veraenderliche Sterne, 9, 87

Samus', N. N., Kazarovets, E. V., Durlevich, O. V., Kireeva, N. N., & Pastukhova, E. N. 2017, Astronomy Reports, 61, 80

Sanduleak, N. & Stephenson, C. B. 1973, ApJ, 185, 899

Sazonov, S. & Khabibullin, I. 2017, MNRAS, 466, 1019

Schaefer, B. E. 2010, ApJS, 187, 275

Schlafly, E. F. & Finkbeiner, D. P. 2011, ApJ, 737, 103

Schlegel, E. M. & Pannuti, T. G. 2003, AJ, 125, 3025

Schmid, H. M. 1989, A&A, 211, L31

Schmid, H. M., Bazzon, A., Milli, J., et al. 2017, A&A, 602, A53

Schmid, H. M. & Nussbaumer, H. 1993, A&A, 268, 159

Schmidtke, P. C. & Cowley, A. P. 1995, IAU Circ., 6278, 2

Schütz, O., Meeus, G., & Sterzik, M. F. 2005, A&A, 431, 165

Sekeráš, M. & Skopal, A. 2012, MNRAS, 427, 979

Sekeráš, M., Skopal, A., Shugarov, S., et al. 2019, CAOSP, 49, 19

Shappee, B. J., Prieto, J. L., Grupe, D., et al. 2014, ApJ, 788, 48

Shara, M. M., Doyle, T. F., Lauer, T. R., et al. 2016, ApJS, 227, 1

Shen, K. J. & Bildsten, L. 2007, ApJ, 660, 1444

Sibbons, L. F., Ryan, S. G., Napiwotzki, R., & Thompson, G. P. 2015, A&A, 574, A102

Sion, E. M., Acierno, M. J., & Tomczyk, S. 1979, ApJ, 230, 832

Sion, E. M., Godon, P., Mikolajewska, J., & Katynski, M. 2019, ApJ, 874, 178

Sion, E. M., Godon, P., Mikolajewska, J., Sabra, B., & Kolobow, C. 2017, AJ, 153, 160

Skinner, J. N., Morgan, D. P., West, A. A., Lépine, S., & Thorstensen, J. R. 2017, AJ, 154, 118

Skopal, A. 1998a, A&A, 338, 599

Skopal, A. 1998b, CAOSP, 28, 87

Skopal, A. 2005, A&A, 440, 995

Skopal, A. 2008, JAAVSO, 36, 9

Skopal, A. 2009, New A, 14, 336

Skopal, A. 2012, Baltic Astronomy, 21, 97

Skopal, A., Hric, L., Chochol, D., et al. 1995, CAOSP, 25, 53

Skopal, A., Hric, L., Urban, Z., et al. 1992, CAOSP, 22, 131

Skopal, A., Pribulla, T., Vaňko, M., et al. 2004, CAOSP, 34, 45

Skopal, A., Pribulla, T., Wolf, M., Shugarov, S. Y., & Jones, A. 2000, CAOSP, 30, 29

Skopal, A., Shugarov, S., Vaňko, M., et al. 2012, AN, 333, 242

Skopal, A., Shugarov, S. Y., Munari, U., et al. 2020, A&A, 636, A77

Skopal, A., Shugarov, S. Y., Sekeráš, M., et al. 2017, A&A, 604, A48

Skopal, A., Tarasova, T. N., Cariková, Z., et al. 2011, A&A, 536, A27

Skopal, A., Tarasova, T. N., Wolf, M., Dubovský, P. A., & Kudzej, I. 2018, ApJ, 858, 120

Skopal, A., Teodorani, M., Errico, L., et al. 2001, A&A, 367, 199

Skopal, A., Vanko, M., Pribulla, T., et al. 2002, CAOSP, 32, 62

Skopal, A., Vaňko, M., Pribulla, T., et al. 2007, AN, 328, 909

Skopal, A., Vittone, A., Errico, L., et al. 1997, MNRAS, 292, 703

Skrutskie, M. F., Cutri, R. M., Stiening, R., et al. 2006, AJ, 131, 1163

Smith, V. V., Pereira, C. B., & Cunha, K. 2001, ApJ, 556, L55

Sobolev, V. V. 1960, Moving envelopes of stars

Sokoloski, J., Lawrence, S., Crotts, A. P. S., & Mukai, K. 2016, in Proceedings of Accretion Processes in Cosmic Sources. 5-10 September 2016 Saint Petersburg, 21

Sokoloski, J. L. 2003, Astronomical Society of the Pacific Conference Series, Vol. 303, Rapid Variability as a Diagnostic of Accretion and Nuclear Burning in Symbiotic Stars and Supersoft X-Ray Sources (invited review talks), ed. R. L. M. Corradi, J. Mikolajewska, & T. J. Mahoney, 202

Sokoloski, J. L. & Bildsten, L. 1999, ApJ, 517, 919

Sokoloski, J. L., Bildsten, L., & Ho, W. C. G. 2001, MNRAS, 326, 553

Sokoloski, J. L., Kenyon, S. J., Espey, B. R., et al. 2006a, ApJ, 636, 1002

Sokoloski, J. L., Lawrence, S., Crotts, A. P. S., & Mukai, K. 2017, arXiv e-prints, arXiv:1702.05898

Sokoloski, J. L., Luna, G. J. M., Mukai, K., & Kenyon, S. J. 2006b, Nature, 442, 276

Soszyński, I., Dziembowski, W. A., Udalski, A., et al. 2007, Acta Astron., 57, 201

Spano, M., Mowlavi, N., Eyer, L., et al. 2011, A&A, 536, A60

Srivastava, M. K., Ashok, N. M., Banerjee, D. P. K., & Sand, D. 2015, MNRAS, 454, 1297

Starrfield, S., Iliadis, C., & Hix, W. R. 2016, PASP, 128, 051001

Stassun, K. G. & Torres, G. 2021, ApJ, 907, L33

Steele, I. A., Smith, R. J., Rees, P. C., et al. 2004, in Society of Photo-Optical Instrumentation Engineers (SPIE) Conference Series, Vol. 5489, Ground-based Telescopes, ed. J. Oschmann, Jacobus M., 679–692

Stephens, I. W., Evans, J. M., Xue, R., et al. 2014, ApJ, 784, 147

Stienon, F. M., Chartrand, M. R., I., & Shao, C. Y. 1974, AJ, 79, 47

Stoyanov, K. A., Martí, J., Zamanov, R., et al. 2018, Bulgarian Astronomical Journal, 28, 42

Sung, H., Lim, B., Bessell, M. S., et al. 2013, Journal of Korean Astronomical Society, 46, 103

Swope, H. H. & Shapley, H. 1940, Annals of Harvard College Observatory, 90, 207

Szczerba, R., Siódmiak, N., Stasińska, G., & Borkowski, J. 2007, A&A, 469, 799

Tang, S., Grindlay, J. E., Moe, M., et al. 2012, ApJ, 751, 99

Tatarnikova, A. A., Burlak, M. A., Popolitova, D. V., Tarasova, T. N., & Tatarnikov, A. M. 2016, Baltic Astronomy, 25, 317

Tatarnikova, A. A., Marrese, P. M., Munari, U., et al. 2003, MNRAS, 344, 1233

Teyssier, F. 2019, CAOSP, 49, 217

Tisserand, P., Clayton, G. C., Welch, D. L., et al. 2013, A&A, 551, A77

Tisserand, P., Marquette, J. B., Wood, P. R., et al. 2008, A&A, 481, 673

Tokovinin, A. 2008, MNRAS, 389, 925

Tokovinin, A. 2014, AJ, 147, 87

Tokovinin, A., Fischer, D. A., Bonati, M., et al. 2013, PASP, 125, 1336

Tomov, N. A., Bisikalo, D. V., Tomova, M. T., & Kil'Pio, E. Y. 2011, in American Institute of Physics Conference Series, Vol. 1356, American Institute of Physics Conference Series, ed. I. Zhelyazkov & T. Mishonov, 35–44

Tonry, J. L., Denneau, L., Flewelling, H., et al. 2018a, ApJ, 867, 105

Tonry, J. L., Denneau, L., Heinze, A. N., et al. 2018b, PASP, 130, 064505

Udalski, A., Szymanski, M. K., Soszynski, I., & Poleski, R. 2008, Acta Astron., 58, 69

Udalski, A., Szymański, M. K., & Szymański, G. 2015, Acta Astron., 65, 1

Vaidis, J. P. 1988, Bulletin Association Fran. Obs. Etoiles Variables, 45, 13

Vaidis, J. P. 1991, Bulletin Association Fran. Obs. Etoiles Variables, 55, 21

van Belle, G. T., Creech-Eakman, M. J., & Hart, A. 2009, MNRAS, 394, 1925

van Belle, G. T., Dyck, H. M., Benson, J. A., & Lacasse, M. G. 1996, AJ, 112, 2147

van Belle, G. T., Lane, B. F., Thompson, R. R., et al. 1999, AJ, 117, 521

Van Eck, S., Jorissen, A., Udry, S., et al. 2000, A&AS, 145, 51

van Winckel, H. 2003, ARA&A, 41, 391

Vanture, A. D. & Wallerstein, G. 2003, PASP, 115, 1367

Vernet, J., Dekker, H., D'Odorico, S., et al. 2011, A&A, 536, A105

Viironen, K., Mampaso, A., Corradi, R. L. M., et al. 2009, A&A, 502, 113

Walter, F. M., Battisti, A., Towers, S. E., Bond, H. E., & Stringfellow, G. S. 2012, PASP, 124, 1057

Wannier, P. G., Sahai, R., Andersson, B. G., & Johnson, H. R. 1990, ApJ, 358, 251

Watson, C. L., Henden, A. A., & Price, A. 2006, Society for Astronomical Sciences Annual Symposium, 25, 47

Webb, N. A., Coriat, M., Traulsen, I., et al. 2020, A&A, 641, A136

Webbink, R. F. 1988, Astrophysics and Space Science Library, Vol. 145, The Formation and Evolution of Symbiotic Stars, ed. J. Mikolajewska, M. Friedjung, S. J. Kenyon, & R. Viotti, 311

Webster, B. L. & Allen, D. A. 1975, MNRAS, 171, 171

Wells, M. A. & Prša, A. 2021, ApJS, 253, 32

Wenger, M., Ochsenbein, F., Egret, D., et al. 2000, A&AS, 143, 9

Whitelock, P. A. 1987, PASP, 99, 573

Whitelock, P. A. 2003, Astronomical Society of the Pacific Conference Series, Vol. 303, A Comparison of Symbiotic and Normal Miras (invited review talks), ed. R. L. M. Corradi, J. Mikolajewska, & T. J. Mahoney, 41

Whitelock, P. A., Feast, M. W., & Van Leeuwen, F. 2008, MNRAS, 386, 313

Whitelock, P. A. & Munari, U. 1992, A&A, 255, 171

Williams, S. C., Darnley, M. J., Hornoch, K., & Shafter, A. W. 2017, ATel, 10520, 1

Wolf, C., Onken, C. A., Luvaul, L. C., et al. 2018, PASA, 35, e010

Wolf, W. M., Bildsten, L., Brooks, J., & Paxton, B. 2013, ApJ, 777, 136

Wood, P. R., Alcock, C., Allsman, R. A., et al. 1999, in Asymptotic Giant Branch Stars, ed. T. Le Bertre, A. Lebre, & C. Waelkens, Vol. 191, 151

Wray, J. D. 1966, PhD thesis, Northwestern University

Wray, J. J., Eyer, L., & Paczyński, B. 2004, MNRAS, 349, 1059

Wright, E. L., Eisenhardt, P. R. M., Mainzer, A. K., et al. 2010, AJ, 140, 1868

Wyrzykowski, Ł. & Hodgkin, S. 2012, in New Horizons in Time Domain Astronomy, ed. E. Griffin, R. Hanisch, & R. Seaman, Vol. 285, 425–428

Wyrzykowski, Ł., Mróz, P., Rybicki, K. A., et al. 2020, A&A, 633, A98

Yaron, O., Prialnik, D., Shara, M. M., & Kovetz, A. 2005, ApJ, 623, 398

Yudin, B. F. 1987, Ap&SS, 135, 143

Yukita, M., Swartz, D. A., Tennant, A. F., & Soria, R. 2010, AJ, 139, 1066

Yungelson, L., Livio, M., Tutukov, A., & Kenyon, S. J. 1995, ApJ, 447, 656

Yungelson, L. R., Kuranov, A. G., & Postnov, K. A. 2019, MNRAS, 485, 851

Zamanov, R., Boeva, S., Spassov, B., et al. 2019, Bulgarian Astronomical Journal, 31, 110

Zamanov, R., Marchev, V., Marchev, D., Atanasova, T., & Pavlova, N. 2022, ATel, 15330, 1

Zamanov, R., Stoyanov, K., Marchev, V., et al. 2021a, ATel, 14988, 1

Zamanov, R. K., Boeva, S., Latev, G. Y., et al. 2018, MNRAS, 480, 1363

Zamanov, R. K., Boeva, S., Nikolov, Y. M., et al. 2017, AN, 338, 680

Zamanov, R. K. & Stoyanov, K. A. 2012, Bulgarian Astronomical Journal, 18, 41

Zamanov, R. K., Stoyanov, K. A., Kostov, A., et al. 2021b, AN, 342, 952

Zhang, P., Chen, P. S., & Yang, H. T. 2005, New A, 10, 325

Zheng, J.-H., Huang, Y.-Y., Zhang, Z.-L., et al. 2022, arXiv e-prints, arXiv:2203.16404

Zieliński, P., Wyrzykowski, ł., Mikołajczyk, P., Rybicki, K., & Kołaczkowski, Z. 2020, in XXXIX Polish Astronomical Society Meeting, ed. K. Małek, M. Polińska, A. Majczyna, G. Stachowski, R. Poleski, Ł. Wyrzykowski, & A. Różańska, Vol. 10, 190–193

Zieliński, P., Wyrzykowski, Ł., Rybicki, K., et al. 2019, CAOSP, 49, 125

Appendices

A. Observational data used for figures in Chapter 1

Optical spectroscopic data of symbiotic stars used in this thesis in Fig. 1.3, 1.5, 1.6, 1.8, and 1.10 were downloaded from the database of Astronomical Ring for Amateur Spectroscopy (ARAS)[9], an initiative dedicated to the promotion of amateur astronomical spectroscopy and pro/am collaborations (Teyssier 2019). Observations of the group focus on novae and symbiotic binaries. Moreover, selected Be stars, cataclysmic variables, supernovae, and other objects are observed. The network consists of observers equipped with small telescopes (20 to 60 cm) with spectrographs of different resolutions (500 to 15000), covering the range from 3500 to nearly 8000 Å.

Photometric observations shown in Fig. 1.6, 1.7, 1.8, 1.9, and 1.10 come mainly from the database of the American Association of Variable Stars Observers (AAVSO; Kafka 2022)[10]. For the present study, we have used CCD observations in the V filter which are supplemented by visual observations. We should note that the running average has been applied to the visual data. These data are supplemented by the photometric observation of Rigollet (1947); Belyakina (1968); Hric et al. (1991, 1993, 1994, 1996, 2014); Skopal et al. (1992, 1995, 2000, 2002, 2004, 2007, 2012); Skopal (1998b); Gális et al. (1999); Leedjärv et al. (2004); Munari et al. (2009a,b, 2010, 2012, 2014, 2015, 2017); Munari & Righetti (2016); Arkhipova et al. (2011); Kondratyeva & Rspaev (2013); Ikonnikova et al. (2019b); Sekeráš et al. (2019).

[9]The current online version of the ARAS Database was designed and programmed by the author of this thesis and can be found at the address: https://aras-database.github.io/database/index.html.
[10]https://www.aavso.org/

B. Log of spectroscopic observations

Table B1: Log of spectroscopic observations used in Chapter 3. Asterisk (*) denotes the spectra shown in the figures. Observer codes: 2SPOT = Southern Spectroscopic Observatory Team (S. Charbonnel, O. Garde, P. Le Dû, L. Mulato, T. Petit), BHQ = T. Bohlsen, BUI = C. Buil, CBO = C. Boussin, FAS = F. Sims, HBO = H. Boussier, IBR = I. Diarrasouba, JCO = J. P. Coffin, JMO = J. Montier, JRF = J. R. Foster, MAV = Martin Vrašťák, PAD = P. A. Dubovský, PCA = P. Cazzato, TME = T. Medulka, VLZ = P. Velez. Spectra denoted with KAM, REI, and SCH are provided by D. Kamath, W. Reid, and V. Schaffenroth, respectively (private communication). These data are not available in the ARAS Database. The spectra of M31N 2017-05b are from the Liverpool Telescope Archive and were obtained in the scope of the proposal JL17A07 (PI: Williams). The spectrum of [RP2006] 2180 is from ESO Science Archive and was acquired under the program 074.D-0518 (PI: Parker).

Object	JD 2 459 ..	λ_{min}-λ_{max}	Observer
*2MASS J07363415+6538548	190.38	4000-7590	PAD
V503 Her	-2550.62	3856-7391	BUI
V503 Her	-1385.52	3911-7396	JMO
*V503 Her	-979.26	3901-7400	JRF
V503 Her	-746.16	3727-7289	FAS
V503 Her	-381.56	4101-7350	DBO
V503 Her	-332.14	3720-7391	JRF
V503 Her	-329.15	6305-9446	JRF
*V503 Her	271.03	4001-7251	FAS
V503 Her	272.69	4000-7500	JCO
V503 Her	293.67	3750-7566	CBO
V503 Her	344.46	3950-7550	PAD
V503 Her	349.76	4000-7296	FAS
V503 Her	350.80	4000-7295	FAS
V503 Her	355.41	4000-7550	PAD
V503 Her	357.77	3850-7251	FAS
V503 Her	359.74	3851-7250	FAS
V503 Her	367.42	3900-7550	TMEPAD
V503 Her	369.40	4000-7550	TMEPAD
V503 Her	374.43	3950-7550	PAD
V503 Her	387.82	3651-7400	JRF
V503 Her	402.50	4000-7500	PAD
V503 Her	423.48	4000-7500	PAD
V503 Her	445.37	4000-7500	PAD
V503 Her	465.39	4000-7550	PAD
V2204 Oph	061.39	3871-7380	HBO
*V2204 Oph	066.96	3851-7501	VLZ
V1988 Sgr	125.938	3801-7401	VLZ
V1988 Sgr	347.115	3765-5753	VLZ
*V1988 Sgr	347.116	3737-5805	VLZ
*V1988 Sgr	351.048	5503-7586	VLZ
V1988 Sgr	416.694	3701-7806	2SPOT
LP Sgr	347.144	3765-5754	VLZ
LP Sgr	351.089	5522-7567	VLZ
*IRAS 19050+0001	058.86	4000-7276	FAS

Table B1: Continued.

Object	JD 2 459 ..	λ_{min}-λ_{max}	Observer
EC 19249-7343	60.91	3801-7500	VLZ
EC 19249-7343	60.97	3800-8000	BHQ
EC 19249-7343	352.03	5518-7560	VLZ
EC 19249-7343	354.01	3930-5968	VLZ
*EC 19249-7343	360.02	3900-8200	BHQ
EC 19249-7343	410.74	3751-7806	2SPOT
*V1017 Cyg	040.51	3700-6799	BUI
V1017 Cyg	040.75	4001-7276	FAS
PN K1-6	039.80	3825-7249	FAS
PN K1-6	040.42	3700-6799	BUI
PN K1-6	051.50	3802-7300	PCA
*PN K1-6	069.51	3400-8499	MAV
Hen 4-204	060.99	3801-7500	VLZ
*Hen 4-204	357.30	3906-5982	VLZ
Hen 4-204	359.28	5564-7580	VLZ
*Hen 4-204	359.28	5581-7613	VLZ
Hen 4-204	410.83	3801-7807	2SPOT
Hen 4-204	465.85	3800-7803	2SPOT
*V379 Peg	039.60	3745-6797	BUI
M31N 2017-05b	-1093.31	4020-7994	LT Archive
*M31N 2017-05b	-1074.34	4020-7994	LT Archive
M31N 2017-05b	-1067.36	4020-7994	LT Archive
2MASS J0109..	183.95	3800-7501	VLZ
2MASS J0109..	191.96	3801-7501	VLZ
2MASS J0109..	193.33	4200-7590	PAD
2MASS J0109..	196.27	4000-7590	PAD
TYC 1371-69-1	549.53	4001-7001	HBO
*TYC 1371-69-1	613.68	3719-7309	FAS
TYC 1371-69-1	623.42	3700-7566	CBO
TYC 1371-69-1	646.53	3900-7500	JCO
ASAS J174600-2321.3	128.94	3801-7500	VLZ
*ASAS J174600-2321.3	358.68	3382-7459	SCH
*V618 Sgr	061.01	3800-8000	BHQ
V618 Sgr	523.92	4754-6788	VLZ
*V618 Sgr	678.80	3750-7807	2SPOT

Table B1: Continued.

Object	JD 2 459 ..	λ_{min}-λ_{max}	Observer
V618 Sgr	680.23	4658-6835	VLZ
V618 Sgr	705.19	4705-6764	VLZ
*V618 Sgr	719.71	3603-7809	2SPOT
V5590 Sgr	126.93	3801-7500	VLZ
*V5590 Sgr	359.68	3382-7459	SCH
V5590 Sgr	511.93	4733-6800	VLZ
HH Sge	043.50	3380-6039	IBR
*HH Sge	051.57	3750-7566	CBO
*V627 Cas	549.66	3695-7286	FAS
*SMP LMC 16	-5644.90	3472-7880	REI
*[RP2006] 1459	-5646.00	3682-8056	REI
*MGPN LMC 31	-5646.00	3682-8091	REI
[RP2006] 1192	-5644.84	3670-7966	REI
*[RP2006] 1192	-5645.86	3670-7966	REI
*[RP2006] 1434	-5643.86	3500-7880	REI
*[RP2006] 803	-5645.81	3670-7966	REI
*SMP LMC 63	-5646.06	3682-8091	REI
*[RP2006] 2180	-5654.13	3960-7183	ESO Archive
*[RP2006] 822	-5643.90	3670-7966	REI
*2MASS J05311676-6901041	-2734.97	3733-8857	KAM
*[RP2006] 776	-5643.90	3670-7966	REI
*[RP2006] 774	-5643.90	3670-7966	REI
*[RP2006] 977	-5644.05	3670-7966	REI
*[RP2006] 883	-5644.95	3670-7966	REI
*[RP2006] 490	-5646.82	4093-8845	REI
*[RP2006] 227	-5645.92	3700-8080	REI
*LM 2-39	-5644.95	3670-7990	REI
*2MASS J05421820-6952493	-3500.85	3733-8857	KAM
*[RP2006] 264	-5644.95	3500-7880	REI
*[RP2006] 254	-5644.95	3500-7880	REI
*2MASS J05450015-6918192	-3500.85	3733-8857	KAM
*[RP2006] 295	-5644.79	3670-7966	REI
*[RP2006] 129	-5645.00	3472-7850	REI
*SMP LMC 93	-6029.79	3588-7998	REI